Pregnancy-Induced Remodeling of Heart Valves

by

H Caitlin M Pierlot

Submitted in partial fulfilment of the requirements
for the degree of Doctor of Philosophy

at

Dalhousie University
Halifax, Nova Scotia
July 2014

For my parents…
I would not be who I am today,
But for your love, encouragement, and endless support.

TABLE OF CONTENTS

LIST OF TABLES

LIST OF FIGURES

ABSTRACT

Although many cardiovascular tissues have been shown to remodel when exposed to chronic changes in hemodynamic stresses, little is known about the capacity of heart valves to adapt in a non-disease state such as pregnancy. In this context, pregnancy is an ideal in vivo model, producing dramatic hemodynamic changes to the maternal circulation and resulting in enlargement of the heart and valve orifices.

The aim of the following work was to (i) investigate pregnancy-induced alterations in valve leaflet biomechanics, and (ii) perform detailed structural studies defining the material basis for these changes. Using a bovine pregnancy model, leaflets from all four heart valves were harvested from non-pregnant and pregnant cows, from a local abattoir. Gross leaflet structure was characterized by leaflet dimensions. Small-angle light scattering was used to assess changes in internal fiber architecture. ECM composition was determined using standard biochemical assays. Histological studies assessed changes in cellular and ECM components. Leaflet mechanical properties were assessed using equibiaxial mechanical testing. Collagen thermal stability and crosslinking state was assessed using denaturation and hydrothermal isometric tension tests.

We have reported rapid and extensive remodeling in pregnancy, similar across all of the maternal valves: alterations to leaflet geometry, fiber architecture, composition, biomechanics, and cellularity. All the valves expanded in pregnancy, via an increase in the production of collagen, with associated changes in the biochemical makeup of the ECM and the structure of the collagen network (i.e. loss of crimp, crosslink maturation, and reduction in thermal stability).

This thesis is the first to present a comprehensive investigation of physiological heart valve remodeling. Taken together, these studies provide irrefutable evidence of physiological remodeling of bovine heart valve leaflets. This work has expanded our understanding of maternal cardiovascular physiology as well as providing valuable insight into the structure/function relationships at play in these tissues. The ability of the heart to adapt to pregnancy, a non-disease state, without failure is remarkable. Understanding the valvular adaptations to pregnancy may be fundamental both to developing interventions and treatments for valve disease and heart failure, as well as recognizing the implications of pregnancies on maternal long-term vascular risk.

LIST OF ABBREVIATIONS AND SYMBOLS USED

α-SMA	Alpha smooth muscle actin
AJP	American Journal of Physiology
A/D	Analog to digital
ANOVA	Analysis of variance
ABME	Annals of Biomedical Engineering
ASD	Atrial-septal-defect
ATV	Atrioventricular
AV	Aortic valve
aVIC	Activated valvular interstitial cell
°C	Celcius
CFIA	Canadian Food Inspection Agency
CHF	Congestive heart failure
cm	Centimeter
°	Fiber angle
D/A	Digital to analog
DISP	Dalhousie Integrated Science Program
DAQ	Data acquisition
DHLNL	Dihydroxylysinonorleucine
DDT	Denaturation temperature testing
DNA	Deoxyribonucleic acid
DSC	Differential scanning calorimetry
EC	Endothelial cell
ECM	Extracellular matrix
EMT	Endothelial-mesenchymal transformation
EP	Early pregnant
FE	Finite element
FEA	Finite element analysis
GAG	Glycosaminoglycan
Gly	Glycine

h	Hour
HeNe	Helium-neon
HHL	Histidinohydroxlysinonorleucine
HIER	Heat-induced epitope retreival
HIT	Hydrothermal isometric tension testing
HLNL	Hydroxylysinonorleucine
HPLC	High performance liquid chromatography
HRP	Horseradish peroxidase
Hsp47	Heat shock protein-47
$I(\phi)$	Light intensity distribution
IHC	Immunohistochemistry
k	Relaxation constant
λ_C	Circumferential extensibility
λ_C^{peak}	Peak circumferential extensibility
λ_R	Radial extensibility
λ_R^{peak}	Peak radial extensibility
L	Liter
L_o	Initial load
L(t)	Load at time t
LP	Late pregnant
LV	Left ventricular
MANOVA	Multivariate analysis of variance
MASc	Master of Applied Science
mg	Milligram
min	Minute
mL	Milliliter
mm	Millimeter
mmHg	Millimeter of mercury
MMP	Matrix metalloproteinase
mRNA	Messenger ribonucleic acid
µg	Microgram

µL	Microliter
µm	Micrometer
MV	Mitral valve
N-	Nitrogen
$NaBH_4$	Sodium borohydride
nm	Nanometer
NOI	Normalized orientation index
NP	Non-pregnant
NSERC	National Science and Engineering Research Council
NSHRF	Nova Scotia Health Research Foundation
obVIC	Osteoblastic valvular interstitial cell
OFT	Outflow tract
OI	Orientation index
% dry wt.	Percentage of dry weight
% wet wt.	Percentage of wet weight
P	Pregnant
PG	Proteoglycan
PhD	Doctor of Philosophy
p_{MAX}	Maximum pressure
ϕ_c	Fiber distribution centroid
ϕ_p	Preferred fiber direction
PR	Picrosirius red
PV	Pulmonary valve
pVIC	Progenitor valvular interstitial cell
PYD	Pyridinoline
$\dot{Q}$	Cardiac output
qVIC	Quiescent valvular interstitial cell
RT-PCR	Reverse transcription – polymerase chain reaction
s	Second
SALS	Small-angle light scattering
SE	Standard error

sGAG	Sulfated glycosaminoglycan
SLRP	Small leucine-rich proteoglycan
SMC	Smooth muscle cell
SL	Semilunar valve
T	Temperature
t	Time
$t_{1/2}$	Halftime of load decay
T_d	Denaturation temperature
TGF-β	Transforming growth factor-beta
TIMP	Tissue inhibitor of matrix metalloproteinase
TV	Tricuspid valve
TVP	Transvalvular pressure
UCLA	University Committee on Laboratory Animals
VEC	Valvular endothelial cell
VIC	Valvular interstitial cell
VVG	Verhoeff-van Gieson

ACKNOWLEDGEMENTS

I would like to first acknowledge the contributions of my thesis supervisory committee, but particularly co-supervisors Sarah M Wells and J Michael Lee, who guided this thesis from conception to completion. This thesis was developed as a continuation of Andrew D Moeller's MASc research, both studies with strong conceptual contributions of SMW. Both SMW and JML provided important guidance and significant intellectual contributions to the data interpretation, editing, and revision of all manuscripts (chapters) included in this thesis.

Many further acknowledgements are needed for the experimental and intellectual contributions that others have had to this thesis, particularly due to the drafting of each chapter as separate, multi-authored manuscripts. These contributions are noted at the end of each chapter.

I would like to thank the School of Biomedical Engineering at Dalhousie University, including the support, guidance, and teamwork of faculty, staff, students, and labmates. In particular, a special thanks goes out to Marianne Ariganello for her assistance and advice in my early research, Maxine Langman and Ellen Brennan-Pierce for providing biochemical technical expertise, Stephen Whitefield for microscopy expertise, and Patricia Colp for sharing her extensive expertise in histological staining techniques as well as many entertaining afternoons full of much-needed laughs. Thank you as well to O.H. Armstrong for the supply of bovine tissues that made this research possible.

I would like to thank Dalhousie Integrated Science Program (DISP) students Mariya Turchin, Jessi Bak, Leah Johnston, Jimena Prado, and Chantell Cleversey for their assistance with histological analysis and I commend their early enthusiasm for research.

Lastly, thank you to Sandy Mansfield for her continued encouragement, even after retirement, to Karen O'Malley for all the value that comes from a great collegue to a lifelong friendship, and a special appreciation to my many friends and family (more than I can name) for their unwavering support.

CHAPTER 1

Introduction

1.1 Cardiac Physiology

On its most basic level, the heart is a pair of pumps comprised of two thin-walled atria, two thick-walled muscular ventricles, two inflow valves, and two outflow valves [1]. The atria are filling chambers that receive blood from the veins as it enters the heart. The ventricles are pumping chambers that drive blood into the arteries leaving the heart. In the demanding mechanical environment of the cardiovascular system, blood flow is controlled by the hearts valves. Once referred to simply as static, passive structures, heart valves are in fact complex and dynamic biological structures that play an elaborate role in functional heart efficiency, ensuring unidirectional blood flow by opening and closing more than three billion times in a lifetime [2, 3]. Efficient valve operation is aided by expansion and contraction of the valve orifice during the cardiac cycle.

1.1.1 Cardiac Development

The heart is arguably the most vital organ to the sustenance of life of all vertebrates. As such, it is not surprising that it is the first organ to develop and function during embryonic development. Interestingly in this developmental process, the inflow and outflow valves possess marked differences in embryological origins, ultimately resulting in dissimilarity of leaflet structure and likely remodeling potential as well.

The bilateral cardiogenic heart field, derived from the ventral splanchnic mesoderm of the early embryo, defines a spatial area occupied by early cardiac progenitor cells fated to form the heart [4-6]. This field is actually patterned into two heart fields – primary and secondary – together forming a horseshoe or crescent shape of the primordial heart [4]. The secondary heart field is a relatively recent discovery of a group of cells derived from outside of the primary heart field. These cells are thought to originate in the pharyngeal mesoderm and appear to act as sources for myocardial progenitor cells for later development [6-17].

Based on secreted factors from the pluripotent stem cells of the cardiac mesoderm, the cardiogenic field subdivides with cells of the heart differentiating into either endocardium which lines the chambers and valves of the heart, or myocardium which forms the musculature of the chambers. As this flat sheet of mesodermal cells expands, the first

indicator of cardiac morphological development is the formation of two endocardial-lined channels, constituting the emergence of the primary heart tube. The linear tube begins to beat immediately, generally around embryonic day 20 [4, 18, 19].

As development continues through the subsequent 4-5 weeks, the heart tube undergoes rightward asymmetric looping resulting in caudal (inflow)-cranial (outflow) convergence, distinct chamber appearance – first with the emergence of the left and right ventricle, and later with the ballooning out of the atria – and the formation of cardiac cushions through endothelial-mesenchymal transformation (EMT). During this time, as the name implies, the layer of endothelial cells covering the endocardial cushions transforms into mesenchymal cells, which then migrate into the interior of the cushions and proliferate [20]. The cardiac jelly, situated between the endocardium of the inner heart wall and the myocardium of the outer wall, becomes populated by mesenchymal cells from the endocardium of the atrioventricular (ATV) canal and outflow tract (OFT) [21, 22]. As the cell numbers increase, the localized regions bulge outward into the lumen of the tube, forming the cardiac cushions. Inflow cardiac cushions are formed early in development, while outflow cushions are formed much later. Both contribute to left-right separation of the heart, but most importantly these cardiac cushions serve as rudimentary valves by facilitating the forward movement of blood [4].

1.1.2 Heart Valve Development

The inflow or ATV valves have very different origins from the outflow or semilunar (SL) valves. Anatomically, the inflow and outflow valves arise at opposite ends in the developing heart tube and are thought to have derived from vastly different populations of cells [18]. The cellular origins of the inflow valves (mitral and tricuspid) are better understood, arising solely from tissues of the endocardial cushions. Outflow valves on the other hand, like much of the outflow region, may be derived both from endocardial cells as well as immigrating neural crest cells. This hypothesis is widely controversial [18, 23-25]: the presence of the neural crest cell population is not disputed but their role in development is largely unknown. Furthermore, the cells of the ATV canal and the OFT may be derived from distinctly different heart fields. Much research points to the role of the primary field in linear heart tube, inflow valve, and left

ventricular development, and the secondary field in later right ventricular, OFT, outflow valve, and atrial formation [6, 7, 11, 26].

During chamber emergence, septation, and OFT formation, several subpopulations of cells exterior to the heart, in particular neural crest cells, migrate into the heart to begin the formation of the epicardium [5, 24, 26, 27]. The cardiac neural crest cells take up close proximity to the second heart field cells and are believed to play an important role in valve maturation [26].

The formation of mature heart valves is one of the last steps in the process of cardiac development. Until this point, the endocardial cushions have served the function of the mature valves at the atrioventricular (inflow) and ventriculoarterial (outflow) junctions [7, 28]. The cushions protrude outward to form a thin layer of endothelial cells and extracellular matrix (collagen, elastin, glycosaminoglycans), free at the body of the leaflet but fixed to the myocardium at the distal edges. The myocardium remains attached to the inflow leaflets to form papillary muscles and chordae tendineae. The specific mechanism by which this process occurs is not well understood [26].

Communication between the cardiac neural crest, the second heart field, and the native mesenchyme likely mediates many of the processes essential both to OFT development as well as valve maturation [26]. Few derivatives of neural crest cells are actually found in mature outflow valves [25]. However, neural crest cell deficiency has been shown to lead to increased ECM secretion and decreased mesenchymal apoptosis in late stage outflow valve remodeling [26]; two processes ultimately resulting in abnormal valve development. In addition to their role in heart valve remodeling, neural crest cells differentiate into vascular smooth muscle cells also populating the aorta and other outflow vessels [24-26]. Defects or deficiency in this cell population (or its related signaling proteins and receptors) may thus explain the higher propensity for abnormalities and disease in the pulmonary valve and, more commonly, the aortic valve and its associated vessel structure [26, 27].

The growth of the chordae tendineae begins early in development via the formation of gaps in the atrioventricular cushions, and expanding into interchordal spaces [29, 30]. Branching of the chordae becomes evident at birth, and has been shown to continue

postnatally [29]. While this process is reported to be highly dependent on protein periostin (at least during fetal development [31]), the exact mechanisms behind the development process and division of the chordae is not known.

1.1.3 Valve Anatomy

Valves exist between the atria and ventricles, as well as between the ventricles and their great arteries. Mature heart valve leaflets are composed of a layer of valvular endothelial cells (VECs) overlying a complex network of connective tissue, with some bordered by papillary muscles and supported by chordae tendineae [2, 32-34]. The connective tissue, like any other biological tissue, is composed of cells integrated into a non-cellular, amorphous, hydrated network of extracellular matrix (ECM). The cells found within the connective tissue of heart valves are referred to as valvular interstitial cells (VICs).

In the right side of the heart, the tricuspid valve guides flow from the right atrium to the right ventricle and, in the left side of the heart, the mitral valve guides flow from the left atrium to the left ventricle. These valves are referred to as the atrioventricular, or inflow valves. Chordae tendineae are cord-like tendons that connect and anchor these valves to the papillary muscles at the base of each ventricle. The chordae prevent prolapse of the valves into the atria, but do not play a significant role in the opening and closing of the valves [1]. Hemodynamics of the two inflow valves are similar except that the velocities experienced by the tricuspid valve are reduced due to its larger orifice area: the orifice area of the tricuspid valve is the largest of all the four valves [2]. Furthermore, the tricuspid valve closes just after the mitral valve because stimulation of the left ventricle occurs before the right [2]. Each leaflet of the inflow valves is comprised of a layer of endocardium encasing a primarily collagenous core, which is divided into three regions: rough (chordae attachments), clear, and basal (vascularised and innervated region) [33].

The pulmonary valve regulates flow from the right ventricle into the pulmonary trunk, where it then separates into the right and left pulmonary arteries to supply the lungs with de-oxygenated blood. On the left side, the aortic valve governs the flow from the left ventricle into the aorta to supply circulation to the heart and the rest of the body. These valves are referred to as the semilunar, or outflow valves, and unlike the inflow valves,

they contain no anchoring chordae tendineae. The aortic valve is similar to the pulmonary but much more robust, and exposed to higher flow velocities [2] and mechanical stresses [35]. Both the aortic and pulmonary valves display similar non-linear mechanical properties, although these are different in the circumferential and radial directions [36]. The similarity in structure and mechanical properties is the fundamental rationalization behind the Ross procedure where a damaged aortic valve is replaced with an autologous pulmonary valve. The outflow valve leaflets are formed by a layer of endocardium surrounding a central fibrous core, with the arterial surface being rougher than the ventricular surface [33]. The aortic valve leaflets are significantly thicker than those of the pulmonary valve [36].

1.1.4 Cardiac Cycle and Valve Hemodynamics

The cardiac cycle is divided into two phases: diastole (filling phase) and systole (pumping phase), and governed by pressure gradients between the sides of the valves (Fig. 1.1). During diastole, the ventricles are relaxed, filling under a low venous pressure, and the inflow valves (mitral and tricuspid) hang open. The outflow valves are closed due to the high downstream pressure of the pulmonary trunk and aorta. The ventricle is passively expanded until the back-pressure due to tension in the wall matches atrial filling pressure. The ability of the heart wall to expand in such a manner is known as distensibility [1]. The end of diastole is marked by an occurrence called atrial kick, characterized by atrial contraction, which injects a small quantity of additional blood into the ventricle, raising its pressure above the initial venous filling pressure. Subsequently, during systole, the ventricle actively contracts in a twisting motion from apex to base. As its pressure mounts, there is a slight regurgitant flow into the atria, and the inflow valves close. The heart then undergoes isovolumetric systole – all valves are closed and the ventricular volume is maintained constant. Once ventricular pressure exceeds that of the downstream arteries, the outflow valves open, allowing blood to eject out from the heart. Valve openings expand until maximum ventricular contraction, and hence peak ventricular pressure, is reached, followed by the plummeting of ventricular pressure down almost to zero (~ 4 mmHg). As soon as the downstream pressure of the pulmonary trunk or aortic exceeds that of their respective ventricle, another slight regurgitant flow

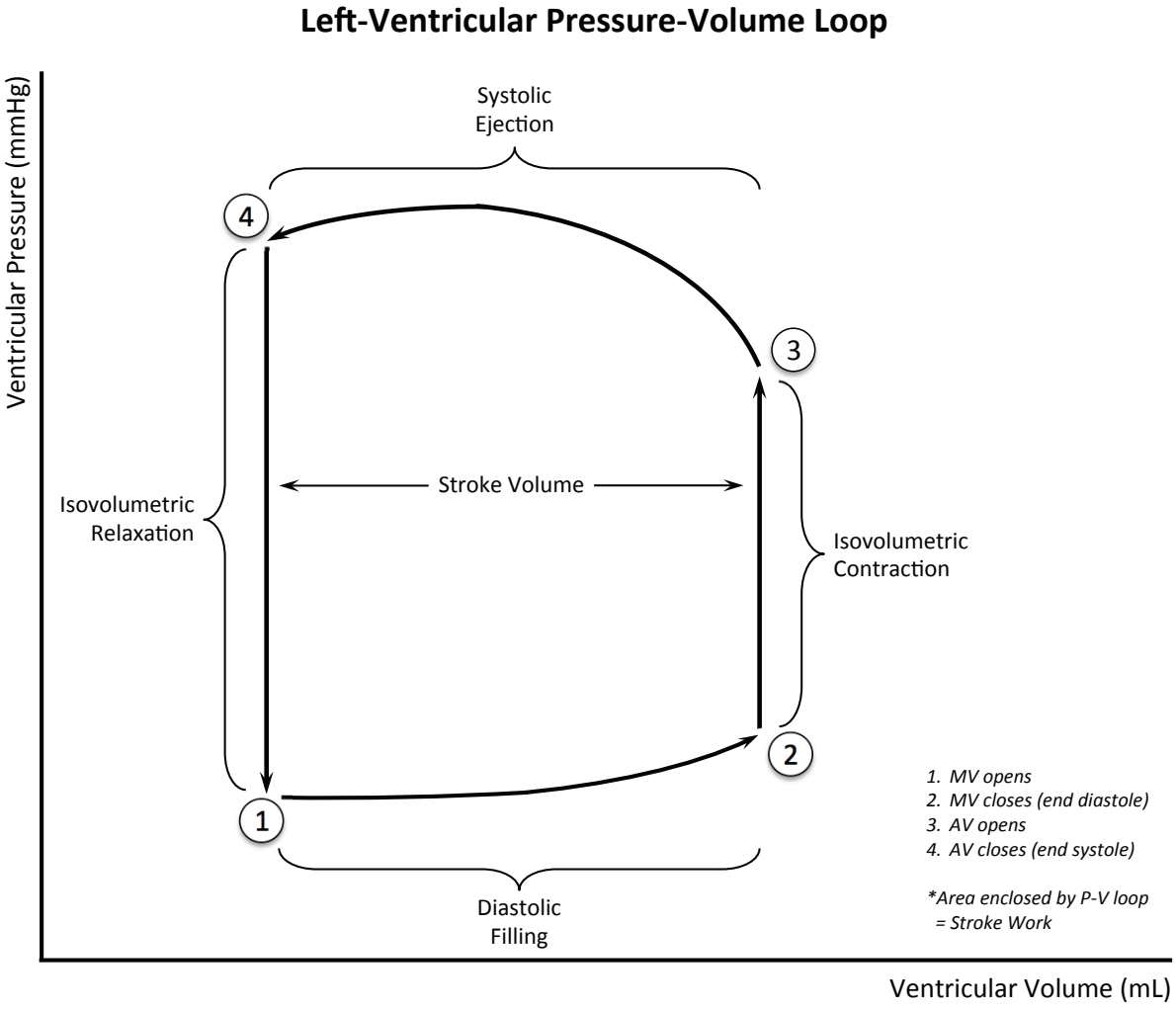

Figure 1.1 Left-ventricular pressure volume loop

Pressure volume loop of the left ventricle, dividing the cardiac cycle into two phases: i) diastole (isovolumetric relaxation and filling), and ii) systole (isovolumetric contraction and ejection). 1. The mitral valve (MV) opens at low ventricular pressure (4-8 mmHg). 2. The mitral valve closes following a slight regurgitant flow as ventricular pressure slightly surpasses atrial pressures, marking the end of diastole. 3. The aortic valve opens after ventricular pressure surpasses aortic pressure (80 mmHg). 4. Ventricular pressure continues to rise while blood is ejected from the heart, until the aortic valve closes, marking the end of systole. Ventricular pressure plummets back down to 6-8 mmHg and the cardiac cycle begins again.

occurs resulting in the closing of the outflow valves. When venous and atrial pressure is re-established, diastole recommences.

Blood flow through the heart depends on the formation of a pressure gradient across the heart valve leaflets. Healthy heart valve operation therefore ensures the development of increased pressures at arterial outlets necessary for efficient hemodynamic circulation [33]. The flow conditions differ tremendously between the left and right side of the heart, and as a result, the cells and tissues of the heart are directly affected. Understanding how the mechanical environment differs between valves may provide valuable information regarding triggering of physiological remodeling both in development and adulthood, as well as the possibility of valve-specific remodeling potential.

1.2 The Role of the Mechanical Environment

The presence of mechanical forces is not simply a consequence of the physiological environment, but is vital to connective tissue homeostasis [37]. Adaptation of cardiac valve structure results in rapid changes in hemodynamics directly downstream from the valve location. Changes in hemodynamic loading imposed on the valves, particularly when maintained for extended periods of time, leads to gradual remodeling of leaflet tissues and ultimately to macroscopic structural changes. Interestingly, however, heart valve remodeling has only been documented during fetal development and under pathological conditions – until recently, valvular remodeling in a non-pathological setting was widely considered to be impossible.

1.2.1 Mechanical Loading Alterations During Development

During development, the foraman ovale allows the flow of blood between the left and right atrium of the heart. The ductus arteriosus forms a similar shunt between the aorta and pulmonary artery to allow blood to bypass the lungs. Both of these shunts result in equal pressures in the right and left ventricles, and thus equal pressures across the outflow valves. Aikawa *et al.* performed several studies on human outflow valves throughout development [21, 38]. They found that in the second trimester of fetal development, when blood pressure in the fetal pulmonary artery and aorta is approximately 50/15 mmHg, the aortic and pulmonary valves are structurally similar, both lacking elastin content and collagen organization. At birth, the shunts rapidly close

and pressures are changed drastically – decreasing to 30/15 mmHg in the pulmonary artery and increasing to 70/40 mmHg in the aorta.

Postnatal flow conditions differ tremendously between the left and right side of the heart and, as a result, the cells and tissues of the heart are directly affected. The outcome is an increase in collagen fiber alignment and thickness along with an overall thickening of aortic valve [21, 39]. This finding agrees with a porcine aortic valve study performed by Xing *et al.* [40] examining changes in collagen synthesis under elevated pressures. Valvular endothelium is directly exposed to blood flow, and thus VECs react to changes in flow conditions and resultant shear stresses, aligning perpendicular to the direction of flow – a behavior which is completely the opposite of aortic endothelial cells [41]. VICs however, are not in direct contact with blood flow, but instead findings suggest that VICs govern remodeling in response to local tissue stress development, regulating protein synthesis and degradation of the valvular ECM [2].

1.2.2 Mechanical Loading in Adulthood

The left side of the heart has significantly increased blood pressure and transvalvular pressure (TVP). In humans, the maximum pressure experienced by the right side of the heart, which serves the lungs, is p_{MAX} ~25 mmHg [3]. The left side of the heart, which serves the entire body excluding the lungs but including the heart, experiences a maximum TVP of p_{MAX} ~120 mmHg [3]. Hence, while the shear stress and load duration are similar between all four valves, the mitral and aortic valves encounter more strenuous loading conditions due to TVP. There is evidence that the pulmonary valve tissue remodeling ability is much slower compared to that of aortic valve tissues [42], based on studies comparing VIC stiffness and phenotype [2, 3, 42]. The aortic valve is subject to extremely high pressures *in vivo* and can tolerate the least regurgitation of all the heart valves. It is therefore the most symptomatic in valve failure [43]. For this reason, most research into heart valves to date has been focused on the aortic valve, but there is still great value in examining the structure-function relationship of the other valves.

As the mechanical loading environment changes from fetal development into adulthood, there are many changes that occur in the heart valves, in terms of mechanical properties,

structure, and composition. That is, among other things, development and growth results in increased stiffness, reduced extensibility, altered tension-strain transition region behaviors, leaflet and layer thickening, increased collagen content, marbling of PGs and GAGs into the fibrosa layer, decreased cell density and increased type III collagen [44, 45]. The changes to the collagen network are also associated with an increase in crimp period [46] and overall collagen alignment [21]. It is not known if the mechanisms of response to alterations in physiological stimuli by the heart valves are fundamentally different at different ages, from fetal development through to adulthood.

1.3 Leaflet Structure and Composition

From a biomechanical perspective, heart valve leaflets are soft tissues, governed by complex and nonlinear stress-strain relationships, viscoelasticity, and deformation profiles [2]. In many instances this can be attributed to their intricate internal structure – during the closing of a valve, each leaflet undergoes a multifaceted extension stretch process involving the uncrimping (straightening and extension) and subsequent rotation of collagen fibers toward the principal strain direction [47].

1.3.1 Tri-layer Structure

All four valves are organized in a similar but not identical highly ordered tri-layer structure (Fig. 1.2): ventricularis; spongiosa; and, fibrosa. However, the arrangement of these layers differs between the inflow (ATV) and outflow (SL) valves. Moreover, the inflow valves also possess a fourth layer, the atrialis [48]. Although each layer is morphologically and functionally unique from its neighboring layers, structural-mechanical interactions between them are complex and significant [39, 49].

The ventricularis is the thinnest layer of the valve, and faces toward the ventricle. It is composed primarily of a dense network of elastin, supplemented by collagen fibers [48, 50]. The spongiosa is the cushioning layer of loosely organized collagen and elastin fibers, but high in proteoglycans (PGs), glycosaminoglycans (GAGs), and VICs [2, 48, 50-54]. The atrialis is composed mainly of elastin, important in the elastic recoil of the inflow valves during the onset of systole [48]. It is often considered together with the spongiosa. Lastly, the fibrosa is formed by a dense network of mainly circumferentially

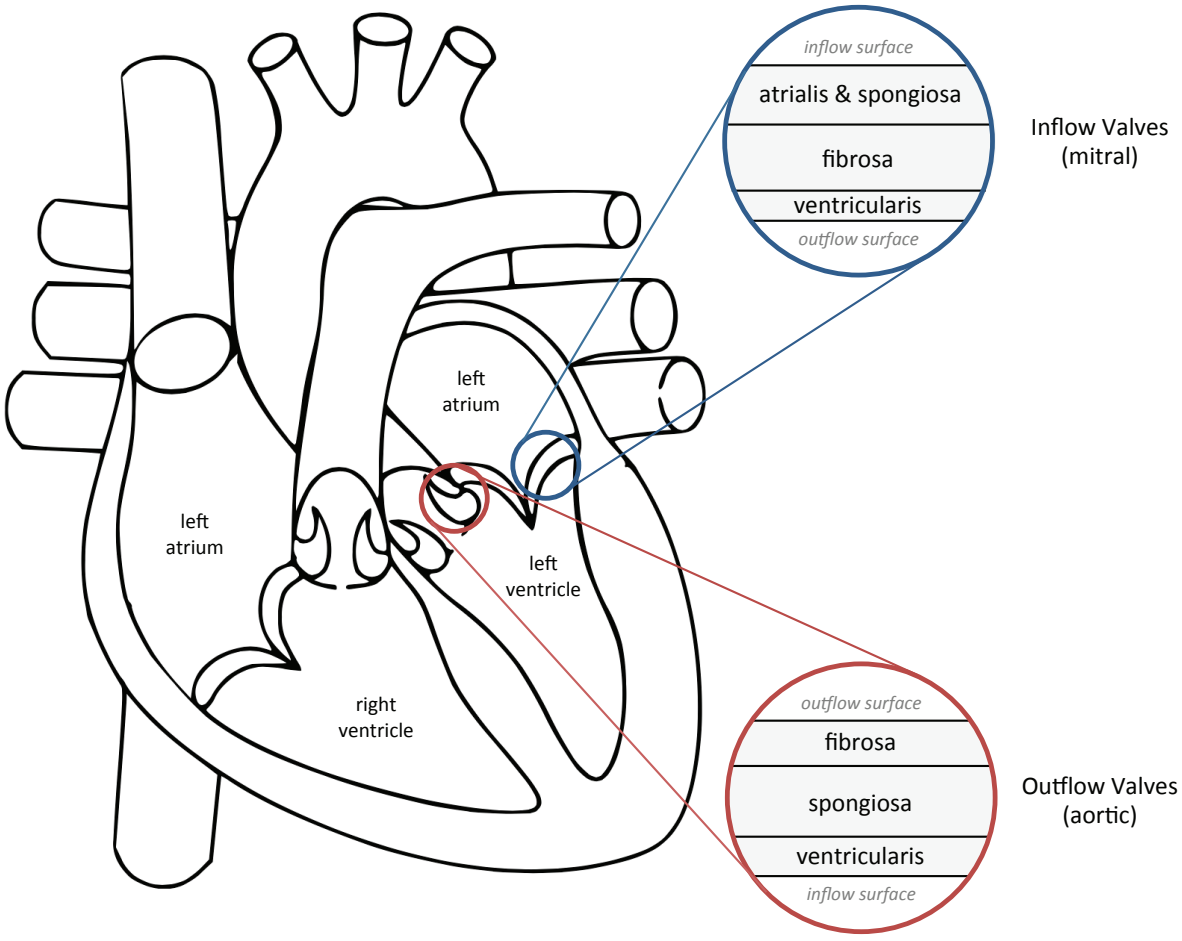

Figure 1.2 Heart valve leaflet layer structure

Schematic diagram of the heart demonstrating the differing structural architecture of the inflow and outflow valves.

aligned, wavy collagen fibers, found at or near the outflow surface of both types of valves [48, 55].

The fibrosa provides nearly all of the high stress-bearing characteristics of the leaflet, while the ventricularis aids in low stress load-bearing [2, 50, 52, 53, 56, 57]. It has been suggested that the elastic fibers of the ventricularis may provide compressive forces acting on the fibrosa that help to maintain the wavy fiber state and for the elastic recoil during valve closure when the applied stress is removed [48, 56, 58]. Forces must be transmitted between the outer leaflet layers by attachments through the spongiosa. Interestingly, this structural organization is highly conserved across species [34].

In all four valves, increased collagen type I content and decreased elastin content are found in the outflow layer (fibrosa for outflow valves, ventricularis for inflow valves) as compared to the inflow layer (ventricularis for outflow valves, atrialis for inflow valves) [55]. In all cases, the high elastin side, which is in contact with the blood flow, is more extensible and flexible than the opposite-facing high collagen layer that provides strength and toughness. Furthermore, Christie *et al.* [39] found higher load-bearing collagen content, as measured by comparing biaxial load-extension curves, in the outflow surface layer of aortic compared to pulmonary valves. This agrees with the histological and fluorescence study performed by Christov *et al.* [55]. Pulmonary leaflets, consequently, are approximately 18% thinner than aortic valves [59].

Although VICs can be found scattered in a relatively inhomogeneous manner, not localized to any particular region of the leaflet [60, 61], the spongiosa contains the bulk of the cellular population, due to its higher thickness compared to fibrosa and ventricularis. Despite the fact that the spongiosa is mechanically weaker than the ventricularis and fibrosa, the spongiosa is critical to compression resistance and dissipation of internal energy between the two supporting layers [47, 48, 62].

It is important to consider that differences in the architecture of the valves arise mainly between the outflow and inflow valves. A high degree of likeness is found between the aortic and pulmonary valves, and similarly between the mitral and tricuspid valves. This brings to light the importance of the differing embryological origins of these valves.

1.3.2 Cell Population

The cell population of heart valve leaflets can be categorized into two main groups: VECs and VICs. VECs cover the surfaces of cardiac leaflets and are continuous with the endocardium of the rest of the heart [22]. VECs differ significantly from other types of endothelial cells in the body, even from the neighboring aortic endothelial cells [2, 20]. For example, VECs reorder and rotate perpendicular to hemodynamic shear flow, while vascular ECs on the other hand rotate parallel to the flow [41, 63]. It clear that there are distinct functional, and likely phenotypic, differences between VECs and cells of the vascular system.

VICs however, are the most prevalent cell (compared to VECs) in cardiac leaflet tissues [20, 64-68]. Moreover, they are a dynamic population of cells, thought to be fundamental to the mechanical operation of the cardiac valves as well as tissue maintenance and structural integrity through synthesis and remodeling of the ECM [21, 22]. VIC cell-cell communication is particularly important to tissue remodeling [3]. Furthermore, their ability to sense and respond to alterations in physiological cardiac loading exhibits potential in the use of these cells for the seeding of bioprosthetic heart valves [42, 62].

There is some evidence for cell signaling and feedback pathways between VECs and VICs [2, 3, 20, 69] that may trigger structural and functional changes in the VIC population. This communication is important as VECs play an important role in the regulation of vascular tone, inflammation, thrombosis, and remodeling [2, 21].

VICs are vitally important to the last component of the heart valve leaflet: the extracellular matrix (ECM). VICs synthesize and secrete a variety of products including cytokines, chemokines, growth factors, proteases, as well as a number of ECM components (collagen, elastin, PGs, fibronectin, etc.) [20, 22, 51, 61, 66, 67, 70].

1.3.3 Extracellular Matrix

The hydrated network of ECM and its constituents, although not cellular, are a critical part of the heart valve tissue structure, development, and maintenance, with dynamic roles in valve morphogenesis, cell function (differentiation, migration, adhesion, sensing, survival, and growth), regulation of signaling pathways (growth factors,

hormones, and cytokines), diffusion control (macromolecules and microorganisms), and valve mechanical properties (hydration, lubrication between layers, strength, stiffness) [2, 21, 45, 51, 66, 70, 71]. The ECM is composed of insoluble macromolecules of collagen and elastin embedded in a lubricating fluid medium composed of water, ions, and soluble macromolecules - namely GAGs, PGs, and glycoproteins [22, 66, 72, 73]. The latter mentioned macromolecules play structural and communicatory roles in valve tissues.

PGs are a diverse group of macromolecules comprised of multiple polysaccharide chains called GAGs bonded to a single protein core through posttranslational modification [70]. Both GAGs and PGs are highly important to the viscoelastic properties of valve leaflets. These macromolecules are found mainly in the spongiosa where they aid in cushioning through resistance to compression, energy dissipation, hydration, cell migration and adhesion, and regulation of mechanical coupling between the outer layers of the leaflet [54, 74, 75].

Glycoproteins are adhesive proteins containing oligosaccharide chains and are involved in cell attachment, migration, and shape. They bind mainly to integrins on cells, forming a dynamic link to the ECM. One of the most common glycoproteins in valve tissue is fibronectin, which connects cells to collagen molecules of the ECM, playing a role in the regulation of signal transduction, cell adhesion proliferation, survival, gene induction, differentiation, and cell motility [22]. It may also add to the ability of VICs to generate contractile forces against the ECM [76].

1.4 Biological Soft Tissues

A biological tissue, on its most basic level, is an accumulation of specialized cells that carry out a specific function in a cellular organism. Tissues are classified either as hard or soft tissues, each with different characteristics and functions. In contrast with hard tissues, such as bone, soft tissues tend to undergo large deformations and exhibit nonlinear behaviors under physiological loading. Soft tissues consist of tendon, muscle, cartilage, and many parts of the vascular system for example, including arteries, myocardium, pericardium, and heart valves. Biological soft tissues are composite materials composed of populations of cells embedded in a matrix of elastin and collagen, and surrounded by an amorphous substance containing a variety of proteins,

polysaccharides, and fluids. As a result, the mechanical properties of entire tissues are dictated by the mechanical properties, proportions, geometry and orientation, and coupling of their individual constituents [77].

Under applied tensile loads *in vivo*, soft tissues elongate along the direction of loading, but the nature of this elongation is complex. Depending on the timescale of loading, contributions from elastic and viscoelastic deformations can blend with actual tissue growth and remodeling. In order to distinguish between effects of each in this two-part adaptive response, one must begin by forming an understanding of viscoelasticity and how it relates to these materials.

1.4.1 Elasticity and Viscoelasticity

Biological soft tissues are viscoelastic materials. To understand what this means, one must first recognize the differences between two types of ideal materials – viscous liquids and elastic solids.

First consider the simplest type of solid: a linear elastic solid. The term "elastic" is often incorrectly used to describe the characteristic of high stretch under relatively small load [78]. Rather than stretch, elastic materials exhibit extremely high resilience. A linear elastic solid is one that undergoes and maintains an instantaneous deformation under an applied load, with that deformation being directly proportional to the applied load, and then recovers instantaneously and absolutely after removal of the load. Elasticity describes the ability of the material to store and return energy via mechanical deformation, while the linearity specifies that the stress be directly proportional to the strain.

The term "elastic" points to Hooke's Law: "for relatively small deformations of an object, the displacement or size of the deformation is directly proportional to the deforming force or load." [79] This linear load-deformation relationship can be generalized to describe the relationship between stress and strain by introducing Young's modulus, or between shear stress and strain via the shear modulus [80]. Many materials are linearly elastic, and thus "Hookean", at small deformations, while very few maintain these characteristics at large deformations [81]. Most biological materials are mechanically much more complex [80].

A viscous material flows under an applied load, rather than stretching, and does not recover to its original dimensions after removal of the force. Unlike elastic materials, viscous materials cannot store energy. Instead, energy is dissipated during flow. Viscous deformations do not happen instantaneously, but rather occur under a time delay.

Viscoelasticity is a time-dependent material property marked by the presence of both viscous (liquid) and elastic (solid) characteristics. Viscoelastic materials can store and return some energy, but also dissipate some energy, and they exhibit unique strain-rate dependent behavioral characteristics including stress relaxation, creep, and hysteresis [80] (Fig. 1.3).

Stress relaxation is the time-dependent decrease in stress under an applied and sustained strain or extension. Conversely, creep is defined as the increase in strain (deformation) of a tissue under an applied and sustained or repeated stress. Hysteresis is the dissipation or loss of energy (generally through heat), under cyclic deformation: the difference between the energy stored during loading and that recovered during unloading. According to viscoelastic theory, creep and relaxation are both dissipative processes and are indicators of identical molecular mechanisms, simply manifested under different conditions.

The viscoelastic response of soft connective tissues is highly affected by both water and collagen content. Each of these factors plays an important role in the process of fiber recruitment, which is thought to be a fundamental component of the mechanism of the viscoelastic response [82, 83]. According to Thornton *et al.*, hypotonic (high water content) rabbit medial collateral ligaments undergo faster stress relaxation than their hypertonic (low water content) counterparts [83]. Conversely, increased resistance to creep is observed in ligaments with decreased water content. These findings are indicative of the essential need to conserve physiological water saturation levels of tissue when conducting biomechanical analysis of both static and dynamic properties.

Under applied load, all materials (elastic, viscous, viscoelastic) deform, or flow, resulting in an elongation or translation of the material parallel to the direction of the applied load and a decrease in thickness perpendicular to the loading direction. Viscoelasticity is of particular interest in the study of biological soft tissues in part due to the mechanical properties of the materials themselves, but also because of the physiological loads

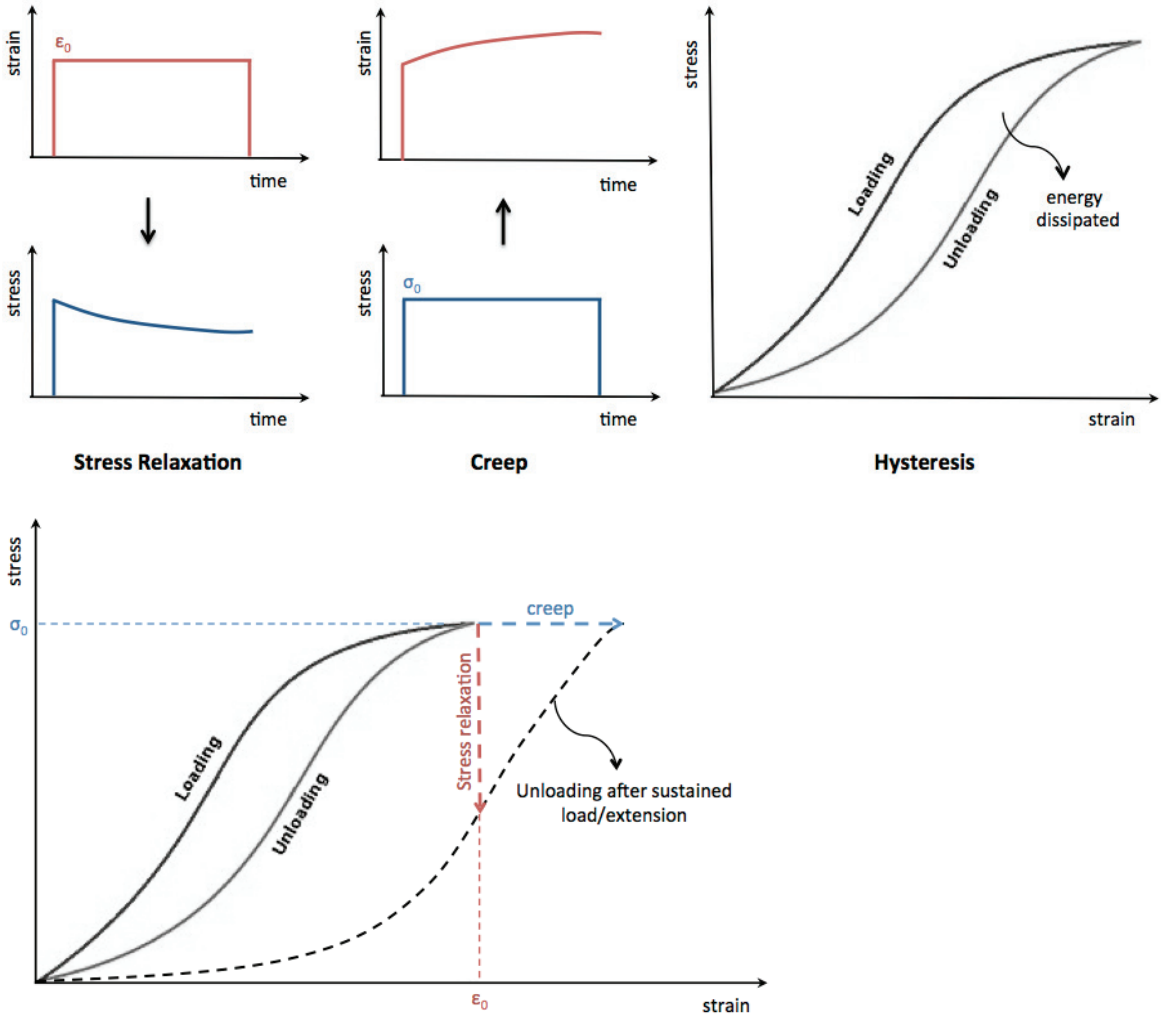

Figure 1.3 Viscoelastic behavior of soft tissues

Diagrams showing graphical representations of the mechanical properties of viscoelastic materials: stress relaxation, creep, and hysteresis.

experienced *in vivo*. Viscoelastic material behavior becomes evident under time-dependent loading of tissues.

In most physiological environments, particularly in the cardiovascular system, connective tissues are under cyclic or sustained loads rather than sustained deformations. For that reason, creep measurements are arguably more relevant to the study of these tissues [80, 84]. The mechanisms underlying creep behavior of soft tissues, however, are not fully understood. Hypotheses include reorientation of collagen fibers, molecular relaxations of the PG matrix around collagen fibers, relaxation within fibers themselves, uncrimping of collagen, and time-dependent effects at the fiber-matrix interface [85, 86].

1.4.2 Collagen and Elastin

Elastin is a rubber-like elastic protein characterized by high extensibility, low modulus of elasticity, high strain, and high resilience [78]. The material must be extremely durable since there appears not to be a turnover of elastin during the lifetime of animals [87, 88].

Collagen is one of the most abundant proteins in the animal kingdom and makes up approximately one third of all body proteins in humans [89]. Although collagen has a very low extensibility, and a high modulus of elasticity as compared to elastin, it is still considered an elastic protein. This is because the protein has high resilience and is capable of reversible deformation. In addition, collagen has a very high mechanical strength which has actually been shown to increase with age [89-91]. This may be attributed to the formation of intermolecular crosslinks with time [92].

In most human tissues, elastin and collagen lie in parallel to form intimate amorphous networks of connective tissue. The collagen acts as a supportive extracellular framework for cells which transmits forces, dissipates energy, regulates cell adhesion and migration, and prevents mechanical failure [93, 94]. As is characteristic of biological soft tissues, collagen is incompressible, viscoelastic, anisotropic, and behaves as a nonlinear material [95, 96]. The unloaded collagen network is composed of wavy (crimped) fibers, which align and straighten in the strain direction upon loading. As the collagen is aligned, the tissue becomes much stiffer. When the force is removed, the elastin acts to recoil the collagen fibers back to the wavy conformation. It is this reorientation of fibers that permits the characteristic high extensibility of these connective tissues [86].

1.4.3 Collagen Crosslinking

Although the molecular makeup of collagen is a significant contributor to the properties of collagenous materials, its crosslinking is essential to connective tissue stabilization and thus to overall performance. Connective tissue stability is associated then with the type and density of crosslinks within, which in turn is related to the rate of collagen turnover in that tissue. Crosslinking increases stability by decreasing the axial separation between molecules [97]. Without crosslinks, collagen fibers have no measureable mechanical strength [98, 99] but in contrast, excess quantities of crosslinks can over-stiffen the collagen fibers [100]. If the rate of collagen turnover is changed, the crosslinking will be altered. Consequently, there is great interest in the investigation of crosslinking in biological tissues as a method to investigate differences in tissue remodeling potential *in vivo*. The identification of a reliable experimental technique for this purpose, however, is challenging.

The collagen triple helix is stabilized by numerous hydrogen bonds, and inter- and intramolecular crosslinks. Intramolecular crosslinks reinforce within individual collagen molecules, while intermolecular crosslinks increase load transmission and mechanical strength between molecules in the collagen network [101, 102]. Intermolecular crosslinks prevent slippage of molecules past one another under applied tensile load [77, 99]. Interestingly, thermally stable intermolecular crosslinks may be more essential to the mechanical properties of biological tissues than their thermally labile intramolecular counterparts [103].

Intermolecular crosslinking of newly formed collagen fibrils occurs in two steps: (1) enzymic lysyl oxidase crosslinking, and (2) non-enzymic glycation crosslinking [98, 99, 104]. While the crosslinking profile (density and type) differs by collagen type, tissue type, and loading environment, the mechanisms of crosslink formation are identical [99]. The lysyl oxidase crosslinks, at least in their immature form, arise from telopeptides, which are the non-helical regions of the molecule, and join to helical regions on adjacent molecules [99, 105, 106]. In contrast, glycation crosslinks occur between helical regions. Glycation crosslinks have been implicated as the primary cause of age-related alterations in mechanical properties of tissue [99, 107], while their enzymic counterparts influence

the behaviors of collagenous tissues from development to adulthood. It is important to also note the existence of intra- and intermolecular disulphide bonds, which are found solely in native type III collagen, and are thought to play important roles in both thermal and mechanical stability of collagen [108, 109].

1.4.4 Denaturation and HIT

Although the scientific literature is prolific with studies of biochemical analysis of crosslinking in biological tissues, this technique is not appropriate for investigation of the precise relationship between crosslinking and mechanical properties of tissues: that is, types of crosslinks identified biochemically may not in fact be mechanically important [102]. Thermomechanical analysis, on the other hand, is inherently more reliable in the investigation of this relationship.

Various tests for determination of collagen stabilization exist, including thermal stability, solubilisation, and *in vivo* persistence [110]. The first two are more commonly used as they are inexpensive and effective techniques. Thermal stability is the measure of a material's ability to resist changes in dimension under changes in solution temperature. One common way to assess the thermal stability or, more accurately, the disruption of thermal stability of a material, is by determining the temperature at which it undergoes thermal denaturation.

Denaturation is the irreversible kinetic reorganization process by which proteins lose their native triple helical (low entropy) structure and transition into a less ordered, coiled (high entropy) denatured state by hydrolysis of intramolecular hydrogen bonding between chains [111] and chain solvation into water. This is often referred to as the helix-to-coil transition [112]. This process often occurs under the application of heat via increased molecular gyration, but can also result from applied mechanical or chemical stresses. The heating of collagen in a tissue does not always cause irreversible damage. If the tissue is heated moderately (i.e. below its denaturation temperature), it will undergo structural changes locally (small amounts of folding changes and hydrogen bond breakages), but overall the proteins will remain intact. In contrast, under severe heating, an irreversible change from native conformation to random structure takes place (i.e. denaturation).

Uncoupling occurs first in the thermally labile domains of the collagen fibril, which are more susceptible to thermal degradation because the hydrogen bonds in these regions are not stabilized by hydroxyproline residues [113, 114]. This results in the breakage of long sequences of hydrogen bonds and destabilization of the triple helical structure, after which the rest of the molecule falls apart in a cascade or unraveling action. Denaturation leads to the loss of both secondary and tertiary protein structure. The process does not however disrupt the covalent peptide bonds of the collagen backbone and hence the primary protein structure is retained. While partial denaturation can be reversible, total denaturation is an irreversible endothermic process [111, 115]. When no physical constraints are applied, denaturation causes a shortening of the molecule along its axis and a resultant increase in configurational entropy [115, 116].

The denaturation temperature (T_d), as its name implies, is the temperature at which hydrothermal denaturation occurs. The higher the T_d of a given material, the higher the thermal stability of that material. T_d can be raised through increases in both intramolecular and intermolecular crosslinking [115].

Denaturation, along with other thermal properties, is typically measured using one or several of the following thermoanalytical techniques [101, 102]:

1. Differential scanning calorimetry (DSC)
2. Shrinkage temperature tests
3. Hydrothermal isometric tension tests (HIT)

While DSC strictly assesses hydrothermal stability, shrinkage temperature and HIT tests are forms of thermomechanical analysis that study changes in dimension or mechanical properties associated with changes in temperature. These two tests are the most common methods used to study mechanically significant crosslinking in collagenous tissues.

HIT is an important and unique thermomechanical technique in that it directly evaluates the relationship between thermal and mechanical behaviors, both leading up to denaturation and post-denaturation. Under HIT protocol, a sample is mounted to an apparatus with two mechanical grips, one attached to a fixed rod and the other to an adjustable tension hook. The upper grip is attached to a load cell or strain gauge

cantilever for monitoring developed tension in a specimen. Specimens are then fully immersed in a bathing solution (generally distilled deionized water). The specimen is isometrically constrained (length fixed) in solution while gradually increasing the temperature of the solution at a rate of 1ºC/min from ~20ºC (room temperature) to a 90ºC (isotherm) [95, 110]. The temperature of the medium is then maintained at the 90ºC isotherm for 3-5 hours to assess the degree of crosslinking in the tissue based on the rate (halftime) of load decay, while the primary protein chains hydrolyze.

The HIT process captures three fundamental molecular transitions: (a) denaturation, (b) hydrolytic splitting of immature thermally labile crosslinks, and (c) hydrolysis of entire alpha chains [117]. Denaturation, in this protocol, is characterized by a sudden increase in sample tension at the denaturation temperature (T_d) [115, 118]. The tissue sample attempts to shrink along the primary fiber direction to take on a higher entropy, lower energy, and coiled configuration, but it is unable to shorten due to the isometric constraint. As a result, tension is developed in the sample, which can be recorded and paired with the corresponding transition temperature of denaturation. Above this temperature, the intermediate thermally labile crosslinks are broken, leaving only thermally stable crosslinks. While the temperature is maintained at the isotherm, a peptide chain hydrolysis-based relaxation is observed [119]. The rate of relaxation of a tissue has been shown to be independent of its non-collagenous constituents and can be closely correlated to the concentration of thermally stable crosslinks determining the mechanical integrity of the collagen network [120].

Intramolecular crosslinks prevent triple helix unwinding, thereby increasing T_d, while intermolecular crosslinks increase the half life of load decay in HIT relaxation, but may leave T_d relatively unaffected [117]. Together, denaturation temperature and halftime of load decay are representative of the quantity and quality of collagen crosslinking present in the tissue.

In addition to crosslinking, another factor that can influence the thermal stability (and hence T_d under HIT testing) is the non-collagen extracellular matrix composition of the tissue – namely proteoglycans. The proteoglycan population of the highly collagenous regions of the heart valve leaflet consists mainly of class I small leucine-rich

proteoglycans (SLRPs) decorin and biglycan [121, 122]. These PGs influence fibril formation and spacing between adjacent fibrils (reducing tissue thermal stability [123] via the polymer-in-a-box-theory [114]), but they also form physical bridges between fibrils that aide in force transmission and thus may influence mechanical properties of the tissues [121].

1.5 Cardiovascular Remodeling

1.5.1 Volume Overload Versus Pressure Overload

Sustained loading on the cardiovascular system results in passive deformation and compensatory remodeling of the tissue under the applied load. Hypertrophy is one of the most commonly observed remodeling mechanisms of the heart, particularly in the ventricles. Hypertrophy occurs when the rate of protein synthesis is higher than the rate of protein degradation – the same condition necessary for fibrosis in collagenous tissues. The two principal types of sustained pathological loading occur through pressure overload or volume overload. In comparing of a number of studies performed on contractile protein metabolism, Carabello *et al.* determined that the rate of contractile protein synthesis increases in pressure overload, while the rate of protein degradation decreases in volume overload [124].

Pressure overload is a condition characterized by an overall increase in systemic pressure due to a rise in systemic vascular resistance, thus increasing the afterload on the heart. Pressure overload results in concentric hypertrophy, where the original heart proportions are maintained. It generally leads to an increase in wall thickness to normalize the rise in wall stress and, as a result, an overall increase in the size of the heart and ventricle [124]. Pressure overload occurs naturally in conditions such as systemic hypertension and aortic stenosis [124].

Volume overload, in the context of the cardiovascular system, results due to an increase in blood volume that must be pumped by the heart, thereby increasing the preload on the heart. The result here is eccentric hypertrophy, in which the size and proportions of the heart are not maintained. While volume overload gives rise to a similar increase in heart or ventricle size as compared to pressure overload, volume overload hypertrophy is dictated by dilation of the ventricle (increase in chamber volume) to compensate for a

loss in stroke volume and to accommodate the increased output demand [124]. Accordingly, thickening of the ventricle wall occurs as a secondary adaptation to reduce the developed wall stress [125, 126]. However, in severely progressed chronic volume loading, this secondary wall thickening is interrupted resulting in extreme dilation of the ventricle and an inability of the thin wall to develop enough force to contract.

1.5.2 Physiological Versus Pathological Volume Overload

Volume overload and the cardiovascular changes that accompany it can occur either as physiological or pathological conditions. In the physiological context, adaptations result in compensatory changes in proportions and function of the heart [125]. These conditions generally involve moderate stresses applied gradually [127]. Small changes in cardiovascular loading are well tolerated by the compensatory mechanisms of the heart [128]. The most prevalent examples of physiological volume overload and tissue remodeling occur in exercise and pregnancy. Under pathological conditions, however, adaptations can occur as the result of an increased demand on the heart due to injury, defect, or failed feedback system that leads ultimately to maladaptation and eventual heart failure if not corrected. Pathological conditions more often involve the abrupt application of a severe stress, generally coupled with increased age or existing illness [127]. Several examples of pathological-induced volume overload are complete or partial heart block, the presence of a left-to-right shunt due to an atrial-septal-defect (ASD) [124, 129], or the more general consequential condition of heart failure. Although the etiology of each of these conditions, physiological and pathological, differs tremendously, the pathways of mechanical, molecular, and biochemical processes can be very much the same [130]. It is the degree of hypertrophy (adequate, inadequate, or overabundant) [124] that often leads to the development and progression of a pathology, regardless of whether the condition was pathological to begin with.

Cardiac remodeling occurs secondary to a change in the loading conditions of the physiological environment. In the case of volume overload, where the heart expands under sustained load, the complex and dynamic process of cell-driven remodeling occurs alongside the more fundamental mechanical process of elastic and/or viscoelastic deformation of the matrix. The timescale and distinct effect of each these two processes

differ, but the ultimate outcome is a summation of their influences. Deformation of tissues occurs quite simply as the result of applied force. Cardiac remodeling on the other hand is the manifestation of genomic, molecular, and cellular changes through alterations in dimensions, proportions, and function of the heart [130]. Distinguishing one dimensional change from another (deformation from remodeling) has proven to be a challenging task in the investigation of remodeling mechanisms of the heart.

1.5.3 Exercise

Exercise regimes can be broken down in to isometric and isotonic programs. The distinction between these two is instrumental in the understanding of pressure versus volume overload. Isometric (anaerobic) exercise involves a change in muscle contraction while muscle length is held constant. Isometric exercise is most often observed in resistance or strength training, and involves pressure overload to the heart due to compression of arteries without significant changes in cardiac size [131-133]. Isotonic (aerobic) exercise refers to a movement in which the tension in a muscle remains constant while the length of the muscle changes. Endurance training such as swimming and running are isotonic exercises and result in sustained volume loading of cardiovascular tissues.

Endurance exercise leads to increased blood volume, heart rate, cardiac output, and stroke volume to accommodate increased demands on the heart and muscles of the body [125, 134]. Under chronic volume loading of cardiovascular tissues due to excessive endurance exercise, hypertrophy, and particularly eccentric hypertrophy, occurs [131] along with an associated increase in left ventricular muscle mass [135]. All of these effects are similar to those experienced in the much more extensively studied conditions of pregnancy and cardiac failure [136].

1.5.4 Pregnancy

Pregnancy can be defined as a state of hypervolemia, meaning a volume-overload state. Maternal blood volume increases by 30-50% by 30-34 weeks gestation as compared to non-pregnancy [137-147]. This change takes place to establish and maintain uteroplacental perfusion and oxygenation for fetal demands. Beginning during the first trimester, whole blood volume reaches a 15% increase by 12 weeks and then continues to

rise more rapidly through the second trimester [148]. During the third trimester, the rate of increase slows and eventually levels out and is maintained for the last several weeks of gestation. Increases in blood volume are even higher with multi-fetal pregnancies [139].

Blood volume increases are due to rises mainly in plasma (blood fluid), but also erythrocyte numbers. Plasma volume expansion is one of the first hemodynamic changes to occur in pregnancy, visible by the 6th week, but reaching approximately 14% increase by 12 weeks [148]. Plasma levels rise 40-50% by term, while erythrocyte levels increase by a smaller but still remarkable 20-40% [138-141, 146]. Erythropoietin, a hormone that stimulates the production of erythrocytes, increases in pregnancy, and is responsible for the increased levels of circulating maternal erythrocytes. Concentrations of both plasma and erythropoietin peak (almost 50% above normal) during the third trimester [149, 150].

Because there is a disproportionate increase in plasma levels (more rapid) compared to red cell numbers, the maternal hematocrit decreases by approximately 12% as the whole blood becomes more diluted [140, 141, 146, 150, 151]. This is referred to as "anemia of pregnancy". The concentration of hemoglobin, the protein found in red blood cells that is necessary for the binding of oxygen, actually decreases slightly as the hematocrit drops, resulting in a decrease in viscosity of the circulating maternal blood [138, 152, 153]. The viscosity of whole blood is dependent both on hematocrit (at low shear rates) and also plasma viscosity (at higher shear rates) [152]. The drop in hematocrit, stopping between week 24 and 28, coincides with the increase in erythropoietin almost exactly [150].

As mentioned, blood plasma volume begins to increase at approximately 10-12 weeks gestation. This volume overload increases the preload on the heart. The maternal basal metabolic rate increases as well, as the fetus continues to develop, resulting in an increased blood flow rate and heart rate, as early as 4-5 weeks gestation [143, 146]. Studies on early pregnancy found a increase of approximately 10 beats per minute in the maternal heart rate during early pregnancy [145, 154, 155], while later investigation found increases of up to 15-20 beats per minute by the end of the third trimester [143, 147, 154, 156, 157]. These changes correspond to increases in heart rate of 12-30%.

Systemic vascular resistance decreases in pregnancy for two primary reasons: vasodilation, and shunting of blood flow through the low-resistance uteroplacental bed.

Changes in vascular resistance occur rapidly and dramatically: a 20-33% decrease by mid-pregnancy, largely due to hormonal stimulation [135, 139, 155, 157, 158]. Pulmonary vascular resistance decreases to a similar degree [139, 143, 158]. The afterload-reducing changes in vascular resistance and vasodilation are added to by the decrease in blood viscosity discussed previously.

Stroke volume is influenced by the heart rate, preload and afterload on the heart, and by ventricular contractility [143]. In response to increases in preload due to blood volume, and as a result of the decrease in vascular resistance and thus afterload, stroke volume increases and peaks at a 20-30% increase between 16-24 weeks gestation. It levels off thereafter [135, 136, 143, 146, 159].

Consider blood pressure as the product of a flow rate and resistance. The acting force in the cardiovascular system is cardiac output, or more specifically stoke volume and heart rate. The resistance is mainly due to systemic vascular resistance, associated with dilation or constriction of the blood vessels. Although the flow rates in pregnancy are dramatically increased, decreases in blood pressure parallel the decreases occurring in system vascular resistance. Mean arterial blood pressure actually decreases slightly in the first and second trimesters due to vasodilation, reaching the nadir of its drop around a similar 16-28 weeks [135, 136, 143, 155, 157]. Blood pressure gradually returns to pre-pregnant levels within the third trimester [139, 157].

Cardiac output ($\dot{Q}$) is used as a measure of the ability of the left ventricle to maintain both maternal and fetal perfusion. Cardiac output begins to increase in early pregnancy in order to accommodate the rapidly growing fetal oxygen and nutrients needs [136, 143, 156, 160]. It continues to rise through gestation but generally peaks at an approximately 30-50% increase before the third trimester (~24 weeks) [135, 136, 139, 146, 147, 155-159, 161, 162]. More than half of the rise in cardiac output occurs within the first 8 weeks of gestation [155].

Cardiac hypertrophy is defined as an enlargement of the heart due to increases in cell size (greater contractile apparatus) rather than cell number. This is an important adaptive response of the body to augmentations in workload and thus a need for increased or at least maintained contractility. The accuracy of standard measurement techniques, which

show increases in left ventricular contractility during pregnancy, are disputed [146]. Even so, left ventricular mass, volume, and wall thickness have been shown to increase in response to pregnancy-induced changes in hemodynamic load through eccentric cardiac hypertrophy [135, 143, 145, 156, 157, 161-166]. The right and left atria have been shown to gradually increase in diameter by 20 weeks and in area by 36 weeks gestation [167, 168]. Significant increases in valve annulus diameters have also been observed by 12 weeks in the maternal heart valves, peaking at 12-23% increases by full term [136, 157, 168]. Cardiac hypertrophy, and specifically ventricular hypertrophy, is likely due to hormonal triggers rather than simply changes in hemodynamic workload alone [164].

In addition to the changes occurring to heart structure in pregnancy, structural changes take place in the maternal vasculature as well. The aorta increases in area and compliance during normal human pregnancy [144, 146]. Increased aortic compliance in combination with decreased vascular resistance likely results in enhanced left ventricular performance, but can also increase the risk of vessel rupture [144]. Uterine arteries and veins also increase in diameter in pregnancy. Furthermore, uterine arteries show a reduction in elastin content in pregnancy and as a result have been observed to have increased distensibility [169].

In multiplet pregnancies (twins, triplets, etc.), hemodynamic alterations are even more pronounced than normal pregnancies. Maternal heart rate, stroke volume, and cardiac output are increased further above singleton pregnancy by 3.5%, 15%, and 20% respectively, and accompanied by further increases in chamber dimensions [136, 170, 171]. As well, uteroplacental blood flow, as measured by the placental clearance rate of maternal plasma hormone dehydroisandrosterone sulphate, increases by almost 40% in twin pregnancy as compared to singleton [172].

Parity refers to the number of times a female has given birth. In multiparous pregnancy, these cardiovascular changes are more pronounced. It is likely that adaptations that persist postpartum actually enhance changes that occur in subsequent pregnancies [170]. Aortic area and compliance are both significantly higher in multiparous women as compared to first time pregnancies [144]. However, in several studies by Dhawan *et al.* they found that multiparity induces long-term changes in vascular compliance and

reactivity, and thus alters the ability of the venous system to handle the volume overload state presented in subsequent pregnancies [173, 174].

In summary, pregnancy is a hyperdynamic (increased cardiac workload), hypermetabolic (increased metabolic rate and thus increased maternal oxygen consumption), hypervolemic (increased blood volume), and low resistance (venous dilation, decreased vascular resistance and systemic blood pressure) state [143, 159].

Structural changes take significantly longer to appear in pregnancy than functional changes [136]: Variations in heart rate, stroke volume, and cardiac output begin almost immediately and can be measured within several weeks of gestation, while structural changes in heart valve openings, ventricular size, and wall thickness (ventricular hypertrophy) appear much later as the end of the first trimester nears. Similarly, these structural adaptations appear to take longer to adapt back to baseline postpartum – if they are completely reversible at all [136, 145, 155]. Campos *et al.* found that the expansion of valve openings in the mitral, pulmonary and tricuspid valves did decrease but still remained 10-12% above baseline postpartum [168]. Hematological alterations are easily and rapidly reversed after pregnancy. Furthermore, most hemodynamic changes mediated by reproductive hormones are easily reversible [143]. However, increased blood volume contributes a variety of morphological and functional cardiovascular adaptations that do not all revert so quickly and completely.

1.5.5 Heart Failure

The volume overload experienced in pregnancy results in hemodynamic changes in heart rate and size that mimic cardiac failure [145, 175, 176]. Amazingly however, cardiac function, and particularly left ventricular function is maintained in pregnancy. Heart failure, by definition, is the inability of the heart to provide adequate blood and nutrient supply to the body. This pathological state is not in itself a unique condition but rather is the convergence of a number of pathological myocardial processes [177]. For example, heart disease is caused by maladaptation that has developed in an attempt to correct or compensate for altered hemodynamic loading due to defect (e.g. atrioseptal defect), injury (e.g. myocardial infarction), or insufficiency (e.g. aortic stenosis, or valve regurgitation). The resultant pathology, may be caused by the

superimposing of several of these conditions. For example, a small lesion in the wall of the atrial septum may be well tolerated for many years, but under the severe cardiac burden of myocardial infarction, the condition may become exacerbated and lead inadequate coaptation [178], resulting in mitral valve regurgitation and eventually cardiac failure. It is evident therefore, that the etiology of heart disease is varied. The primary focus here will be on volume overload pathways to heart failure.

Although heart failure patients exhibit similar volume overload states to non-pathological conditions like pregnancy and exercise, there are marked differences in the remodeling responses. The challenge in the study of pathophysiology of heart failure is understanding the transition from compensating adaptation under sustained loading, to decompensating conditions such as end-stage heart failure [179, 180]. At what point do the pathways of adaptation observed in physiological conditions such as exercise and pregnancy diverge from the pathological course leading to the failing heart? Quite simply, the tipping point occurs when the maladaptive forces overwhelm the adaptive forces [127, 179].

The compensated stage of pathological volume overload is described by the preservation of stroke volume and overall cardiovascular performance by adaptive remodeling of the myocardium, through hypertrophy and chamber dilation [177]. Although the demands on the heart are increased, adaptive mechanisms allow broadly maintained function. In the decompensated state of failure, these mechanisms are no longer sufficient to maintain adequate perfusion to the body [177]. The result is a progressive diminished contractile capacity, and, eventually, complete cardiac failure.

Mitral valve regurgitation, which is rarely found in pregnancy [181, 182], is characterized by a drastically different biochemical makeup in patients with congestive heart failure (CHF) [178, 183]: Grande-Allen *et al.* measured 15% increased collagen content, 59% increased glycosaminoglycan content, 78% increased DNA content, and 7% decreased hydration [183]. This agrees with Quick *et al.* who found that mitral valve collagen synthesis was increased 1.8 times under regurgitant conditions in sheep [184]. Further, CHF is associated with dysfunctional left ventricular myocardium [127, 185, 186].

One major distinction that may account for differences between pregnancy and heart failure is the fact that systemic vascular resistance declines throughout pregnancy [135,

139, 155, 157, 158, 181]. This resistance drop reduces the pressure overload (afterload) on the heart and likely allows the regurgitation to be much more tolerated [175, 181]. Pathological volume overload on the other hand is often accompanied by secondary pressure overload without a mechanism to reduce vascular resistance. As a result, severe compensatory ventricular dilation and heart failure can occur. It is likely that differences in hormone expression between pregnancy and heart failure account for the contrasting adaptive responses.

Relaxin, an important hormone in pregnancy, has been linked to connective tissue remodeling, and specifically collagen remodeling with stimulation of matrix metalloproteinases (MMPs; involved in collagen degradation), and inhibition of tissue inhibitors of metalloproteinases (TIMPs) [187-192]. Collagen remodeling has been documented in the uterus and cervix of pregnant rats [193, 194], but it is likely that remodeling of blood vessels, including the aorta, is also triggered by relaxin. The cardiovascular effects of relaxin are, to a large extent, not investigated. Although receptors have been identified in cardiac tissues, the location and density of relaxin receptors on other cardiovascular tissue are not clear, nor is how they change through gestation. The presence of altered hormone levels in pregnancy, and generally the presence of gender-specific hormones in men and women, likely plays a role in the physiology and pathophysiology of conditions accompanied by altered cardiovascular loading [195, 196]. For this reason, the use of relaxin as a pharmacological agent is of particular interest in early onset heart failure [196].

End-stage heart failure is associated with mitral valve stiffening that can contribute to valve regurgitation [178, 197]. Grande-Allen *et al.* found circumferential valve strips, radial valve strips, and chordae tendineae of failure hearts to be 60%, 23%, and 16% stiffer respectively compared to controls [197]. As a result, mitral valve leaflets exhibited 35% less extensibility, which may lead to an inability to stretch to form complete coaptation during valve closure. Further, mitral valve leaflets and chordae from congestive heart failure patients were significantly thinner than the control group. Wall thinning with ventricular chamber dilation leads to decreased myocyte contractility [198]. Kunzelman *et al.* also found increased myocardial stiffness accompanied by altered wall, leaflet, and chordae stress under the presence of mitral valve regurgitation [186].

It is clear that pathological cardiovascular remodeling, such as we see in heart disease, is distinctly different from physiological remodeling observed pregnancy. While both conditions are accompanied by a significant overload of blood to the heart, pregnancy is well tolerated in the maternal cardiovascular system, with overall heart function remaining relatively the same. In contrast, heart function is generally severely and irreversibly hindered in most forms of heart disease. The specific mechanisms of remodeling however, are not well understood, and require further investigation.

1.6 Valvular Remodeling

1.6.1 Cell Phenotype

Increasing experimental evidence over the last decade has brought to light the importance of VICs, a dynamic and heterogeneous population of cells, across a diverse set of roles in physiological development, maintenance, and pathology. The structural and functional properties of these cells appear to be highly dependent both on their embryonic origins, as well as the mechanical loading environment experienced *in vivo*.

VICs exhibit phenotypes of smooth muscle cells (SMCs), fibroblasts, and myofibroblasts [56] (cells that display features of both fibroblasts and SMCs [2, 3, 51]). In healthy adults, fibroblast-like cells are the predominant cell type, with the presence of little to no myofibroblasts [3, 57]. In valve disease states, however, the cell population is altered with a drastically increased population of activated myofibroblasts. It is not entirely clear whether these changes in cellular population occur via proliferation of the resident cells, or through migration of new cells to the region [22]. Recent studies show strong evidence to suggest that under altered physiological conditions, such as those observed in development, disease (e.g. myxomatous degeneration), or injury [21, 61, 67, 199], vast numbers of VICs experience a phenotypic change from quiescent fibroblast to activated myofibroblast. Further, these cells may have the ability to revert back to the quiescent phenotype upon return to normal loading [38, 42, 200]. This phenotypic plasticity is one feature of VICs that sets them apart from many other cell types in mammals [66]. Another unique feature of VICs is their pattern of force generation: increased contractile force as cell density decreases, and rapid, non-linear force generation, likely due to an intimately interconnected ECM network [201].

Based on these observations, VICs have come to be accepted as a heterogeneous population of cells, with as many as five phenotypes identified thus far in the literature (Figure 4) [20, 22, 42, 51, 57, 61, 64-67, 201]:

1. Embryonic progenitor endothelial/mesenchymal cells
2. Progenitor valvular interstitial cells (pVICs)
3. Quiescent valvular interstitial cells (qVICs)
4. Activated valvular interstitial cells (aVICs)
5. Osteoblastic valvular interstitial cells (obVICs)

Embryonic progenitor cells, as discussed previously, are those that undergo *endothelial mesenchymal transformation* (EMT) during fetal development at the onset of cardiac valve development [20-22]. These progenitor cells continue to differentiate into more specialized phenotypes, both for remodeling necessary for mature valve formation and later maintenance in normal adult heart valves. The process of EMT is crucial in the proper formation of heart valves in embryonic development. It has been hypothesized that the re-emergence of this process, or one very similar, may be responsible for the ability of mature valves to adapt to changes in mechanical loading later in life [20]. A number of regulatory proteins have exhibited significant effect on EMT in development, in particular the transforming growth factor (TGF-β) family [18, 20]. Interestingly, these same factors strongly influence VIC phenotype in mature valves [202, 203].

Progenitor VICs are the equivalent of valvular stem cells, but they do not have clearly defined origins or functions. They likely migrate to valve tissue from the bone marrow and systemic circulation in the presence of degeneration and disease [20]. Activation is also not clearly understood – it may be through direct differentiation to the aVIC phenotype, or indirectly from qVIC to aVIC [20].

Quiescent VICs dominate the cellular population of mature heart valves [20, 200]. In culture, qVICs are typically elongated, spindle-shaped cells with characteristics very similar to that of fibroblasts. These fibroblast-like cells, however, are structurally and functionally different from those of the pericardium and skin [204]. qVICs are important to the maintenance of healthy valve tissue mainly through the synthesis and secretion of

collagen and other ECM components: they are strongly associated with the synthetic phenotype [22]. In developing valves, fibroblast-like cells (likely qVICs) are also responsible for the synthesis of elastin, but this function is terminated by puberty [21].

The relationship between qVICs and aVICs is the most studied of all the 5 phenotypes. aVIC expression occurs when quiescent cells are activated under cellular signaling imposed by a change in the physiological loading environment. The change in conditions, most often observed in disease, triggers the differentiation of qVICs into aVICs. These activated cells take on characteristics more similar to SMCs than fibroblasts, but do not, in fact, differentiate fully to SMCs, such as those found in vascular tissues [20, 62, 66]. Their ability to continue to synthesize and secrete collagen and other ECM components while taking on SMC contractile behaviors substantiates a phenotypic uniqueness [66, 68]. These cells are referred to as myofibroblasts and are characterized by prominent stress fibers, and increased contraction and associated contractile proteins [22, 68]. Hence these cells have been associated with the contractile phenotype.

aVICs can be distinguished from their quiescent counterparts by the high expression of alpha-smooth muscle actin (α-SMA), fibroblast surface antigens, vimentin, and other contractile protein markers, which are not normally found in the interstitial cells of healthy valves [20, 22, 51, 61, 62, 66, 68]. Only 2-5% of cells exhibit expression of α-SMA in normal adult valves [57]. Increased aVIC expression (indicated by increased α-SMA) is accompanied by increased: ECM turnover (secretion / degradation), expression of MMPs and TIMPs (both major contributors to ECM turnover), cytokines (particularly TGF-β), proliferation, and migration [20, 22, 45]. In addition to α-SMA, expression of heat shock protein-47 (Hsp47) is used as an indicator of collagen synthesis [3].

ECM turnover, particularly that of collagen, is based on a delicate balance between synthesis and degradation [47, 89]. Normal collagen and elastin turnover in tissue is very slow, on the scale on months to years [100]. Leaflet matrix homeostasis and metabolism are critically important in maintenance of functional architecture of the tissue. In their quiescent state, VICs are predominantly synthesizing collagen, elastin and PGs, but as indicated previously, these cells are very responsive to a changing stress environment. When stimulated by a change in mechanical stress, VICs increase their expression of

proteolytic enzymes and exhibit elevated proliferation – this is particularly observed in development [34]. It is possible then, that changes in valve size during remodeling in adults may be due not only to ECM synthesis, but also cell hyperplasia.

There is a great deal of evidence for correlation between VIC cell stiffness and the stresses imposed on their leaflet tissues. VICs from the left-side (aortic valve – higher pressure side) of the ovine heart contain more α-SMA and Hsp47, exhibit higher contractility, and are two-times stiffer than those of the right-side (pulmonary valve – lower pressure) [3, 42]. Although the precise role of α-SMA is not well understood, it is definitely important in the alteration of cell stiffness in VICs. It is also believed to be important in the maturation of focal adhesions: mechanical linkages used to transduce mechanical forces into biochemical signals [205]. The α-SMA positive cells are more adherent, flattened, and slow growing relative to qVICs showing lower expression of α-SMA [61]. This adhesive characteristic can thus also be used to distinguish phenotypic cell populations in culture.

Interestingly, Desmoulière *et al.* studied the presence of myofibroblasts in wound healing in rats and observed that as healing progressed and the wound contracted, there was a significant increase in myofibroblast apoptosis [206, 207]. Furthermore, Rabkin-Aikawa *et al.* found that both in valve remodeling and disease in sheep and humans, expression of aVICs (cells containing α-SMA) was significantly increased as compared to healthy subjects [200]. Together, all this information suggests that the drastic increase in aVICs during injury and disease is likely due to a combination of cellular differentiation, proliferation, and migration, while the subsequent decrease in numbers may be due both to a transformation back to qVICs and an increase in apoptosis of these cells.

Osteoblastic VICs are another type of activated VICs that are responsible for calcification of cardiac valve tissue. Evidence points to the differentiation of obVICs from the same population of native qVICs and potentially from progenitor VICs as well. The promotion of this phenotypic pathway is regulated by the complex balance of a variety of factors including phosphates, phosphatases, proteases (e.g. MMPs) and growth factors (e.g. TGF-β) [20, 66, 68].

The important idea here is that VIC phenotype at any particular point in time is directly related to the remodeling requirements of the valve. These cells have a plastic, reversible phenotype that aides significantly in cell-cell communication, injury response, and tissue remodeling through protein synthesis and enzymatic degradation [2, 42, 56, 93].

1.7 Thesis Rationale

Cardiovascular disease is the single leading cause of death worldwide, accounting for almost 30% of all deaths worldwide [208] and a substantial 22% of deaths in Canada [209]. With an aging demographic, particularly in North America, the study of this disease is becoming increasingly important. Pathologists have shown that degraded valves (as in heart disease) are floppy and leaky, preventing them from opening and closing properly [210]. This condition causes an overload of blood to the heart, leading to heart failure, and even death. There is currently no medical approach to inducing repair of damaged valve leaflets. Valve failure is only treatable via surgical intervention or prosthetic replacement, generally involving open-heart surgery.

Interestingly, overload occurs in the heart in pregnancy as the maternal body adapts to accommodate the demands of the growing fetus. Further, pregnant women experience many changes to their bodies throughout pregnancy, and many of these changes can have severe cardiac implications. One such condition is heart valve regurgitation: backward flow of blood across a closed valve. In the absence of any valve remodeling in pregnancy, where large increases in blood volume occur, regurgitation would result due to incomplete coaptation of valve leaflets caused by orifice dilation. Indeed, 95% of normal pregnant women experience regurgitation on the right side (pulmonary and tricuspid) valves by full term [168]. Remarkably, although the left side valves experience higher TVPs, only 27% of pregnant women experience regurgitant flow in the mitral and none in the aortic valve [168], even though all valve orifices have expanded. So while the load on the left side of the heart is increasing, the ability of these valves to function remains almost the same.

Although many cardiovascular tissues have been shown to remodel when exposed to chronic changes in hemodynamic stresses, pregnancy presents a non-pathological volume-overload model characterized by rapid and dramatic hemodynamic changes. This

is emphasized by an increase in blood volume and cardiac output of up to 50% in humans [137]. This volume overload tremendously increases the mechanical loading in cardiovascular tissues, resulting in significant cardiac enlargement [136, 157, 166, 170].

Valve orifice areas of the mitral valve in humans have been shown to increase by 12-23% in pregnancy [136, 157, 168]. This annular dilation causes a substantial increase in the radius of curvature of the closed leaflet, and by the law of Laplace, the tension across the closed valve is significantly increased. Furthermore, this rise in tension is much greater than the rise in orifice area. FEA models predict that an 18% increase in orifice area would result in a more than 60% increase in tensile stress [211].

While the same overload that occurs in heart valve disease also occurs in the heart in pregnancy, remarkably, for some reason, these valves do not fail, and no one has studied why or how. It is possible that the answers to treatment for heart valve failures could lie in pregnancy research.

Furthermore, until recently, little attention has focused on the relation between pregnancy and subsequent maternal health. Data are now increasingly linking maternal vascular complications of pregnancy with an increased risk of vascular disease later in life. There is an increase in vascular risk factor with pregnancy, both in healthy populations as well as in complicated pregnancies [212]. Moreover, there is an increasing risk for maternal cardiovascular disease with every subsequent pregnancy [212-215]. This relationship is not well understood nor has it been the focus of much research.

The ability of the heart to adapt to pregnancy, a non-disease state, without failure is remarkable. This thesis aims to capture physiological remodeling of tissues that up until this point were thought incapable of remodeling. Understanding the valvular adaptations to pregnancy may be fundamental both to developing interventions and treatments for valve disease and heart failure, as well as improving maternal prognosis later in life, and appreciating how the implications of pregnancies can affect long-term vascular risk.

1.8 Objectives

The overall objectives of this study were to determine (i) how the mechanical function of load-bearing heart valve tissues adapts to pregnancy, and (ii) how the

structure and composition of these tissues remodel to accomplish this. Leaflets from all four heart valves (aortic, mitral, pulmonary, and tricuspid), from pregnant and non-pregnant animals, have been examined in an effort to understand the unique remodeling mechanism(s) that appear to be at play in pregnancy. The specific objectives of this study are laid out with a series of questions:

Q1. Are the valves remodeling during pregnancy?

Q2. How are the valves remodeling? Are these changes valve dependent?

Q3. What are the specific remodeling mechanisms?

The following hypotheses have guided the direction of this research:

H1. Gross structural changes occur in all the valves throughout pregnancy, with increases in valve length, thickness, and collagen content. The presence of such changes in tissue properties will provide evidence of valvular remodeling.

H2. Inflow valves (mitral and tricuspid) will change in dimension in a manner that parallels changes observed in the outflow valves (aortic and pulmonary).

H3. The remodeling mechanisms of the valves in pregnancy are through changes in (a) fiber architecture, (b) collagen content and turnover, (c) collagen crosslinking, (d) ECM composition, and (e) cell proliferation and phenotype. Pregnancy will result in the follow changes:

a) Fiber network architecture:

- Increased fiber splay (broader distribution of fiber angle)
- Increased orientation in the radial direction.

b) Collagen content:

- Accumulation of leaflet collagen

c) Collagen crosslinking:

- Decreased total crosslink content
- Increased immature crosslink content
- Decreased leaflet creep resistance

d) ECM composition:

- Altered collagen, elastin, GAG, and water content

e) VIC proliferation and phenotype:

- Increased cell number and/or density
- VIC phenotypic shift from quiescent to activated phenotype

To accomplish its objectives, this thesis is comprised of four publications broken down by chapters:

Chapter 2: *Physiological remodeling of the mitral valve during pregnancy* (2nd author paper, published AJP-Heart Circ Physiol, 2012) – cardiac and leaflet morphometric analysis, biaxial mechanical extensibility testing, crosslink content via hydrothermal isometric tension testing, and qualitative histological analysis of structural features of the mitral valve leaflet.

Chapter 3: *Pregnancy-induced remodeling of collagen architecture and content in the mitral valve* (1st author paper, in press, Annals of Biomedical Engineering (ABME)) – small angle light scattering of fiber architecture, quantitative histological analysis of collagen structure, and biochemical analysis of collagen content of mitral valve leaflet.

Chapter 4: *Biaxial creep resistance and structural remodeling of the aortic and mitral valves in pregnancy* (1st author paper, submitted, Annals of Biomedical Engineering (ABME)) – aortic and mitral valve viscoelastic creep properties, leaflet morphometric analysis, histological analysis, collagen and crosslink content, and extensibility testing expanded from previous work to include the aortic valve.

Chapter 5: *Pregnancy-induced remodeling of heart valves* (1st author paper, under revision by authors, AJP-Heart Circ Physiol) – comprehensive study of leaflet mechanical, morphometric, histological, biochemical, and hydrothermal isometric tension testing of all four valves to provide evidence of both structural and functional changes in pregnancy.

CHAPTER 2

Physiological Remodeling of the Mitral Valve During Pregnancy

Sarah M. Wells[1,2], Caitlin M. Pierlot[1], and Andrew D. Moeller[1]

[1]School of Biomedical Engineering, Dalhousie University, Halifax, Nova Scotia, Canada;

[2]Department of Physics and Atmospheric Science, Dalhousie University, Halifax, Canada

2.1 Introduction

Heart valves have an important physiological function in maintaining unidirectional blood flow and preventing regurgitation. The mitral valve in particular is closed during ventricular systole, preventing backflow of blood into the left atrium as the left ventricle (LV) ejects the stroke volume into the aortic outflow tract. Heart valves function under harsh mechanical demands, opening and closing ~35 million times in one year and supporting high transvalvular pressures across the closed leaflets. These functions translate into a complex combination of compressive, shear, and tensile stresses within the valve leaflet tissues. Finite-element models have shown that tensile stresses caused by transvalvular pressure are the most dominant on the valve leaflets [186], with peak transvalvular pressure corresponding to maximal engagement and loading of its collagen fibers [216].

There is growing evidence that heart valves are not passive static structures but can instead adaptively remodel to alterations in their loading conditions. Evidence for heart valve remodeling has largely been associated with disease states such as LV dysfunction or heart failure. Much attention has been paid to the mitral valve, given the significance of mitral regurgitation in LV dysfunctions such as dilated cardiomyopathy and heart failure [178, 185, 217, 218]. In these pathologies, altered cardiac structure and function, including annular dilation, are thought to elevate mechanical stresses on the mitral valve leaflets, which, in turn, induce “dysfunctional” remodeling of the tissue [197]. In vivo sheep models of LV dysfunction reveal alterations in the gross structure and composition of the leaflets: leaflet area, thickness [185], and collagen synthesis [219] are increased, with decreases in collagen concentration, presumably due to greater increases in other extracellular matrix components [186]. Similarly, explanted mitral valves from chronic heart failure patients are thicker and longer than those in control patients, with increased contents of collagen and cells and decreased water content [183]. Correspondingly, these valves are stiffer, less extensible, and less viscous than normal valvular tissue [197]. Together, human explant and in vivo sheep studies have demonstrated structural and mechanical alterations to the mitral valve that likely represent a compensatory response to pathological elevations in mechanical stress.

Less clear, however, is the remodeling capacity of mature heart valve tissues under non-pathological conditions. The purpose of the present study was to examine the remodeling capacity of mature heart valve leaflets in a non-pathological state, using the maternal circulation in pregnancy as a model. There are striking physiological cardiovascular changes in the maternal cardiovascular system of humans and other species as it accommodates the developing placenta and provides appropriate oxygen and nutrient delivery for the mother and fetus. In humans, blood volume is increased by ~40% during gestation, resulting in a volume overload state. The heart rate increases gradually over gestation by ~20 –25%, whereas stroke volume rapidly increases by 30% over the first half of gestation and then plateaus [157]. Cardiac output increases by ~50% by the third trimester, with more than half of that increase occurring in the first 8 weeks of pregnancy [157].

Not surprisingly, the heart undergoes dramatic remodeling in early pregnancy (EP) as it adapts to an increased volume load. These changes resemble those associated with training and exercise, including LV hypertrophy [136, 157], with a 52% increase in LV mass [166] and increased dimensions of the atrial and ventricular chambers [157, 166, 170]. The increase in cardiac dimensions includes annular dilatation of heart valves, with the orifice area increasing up to 14% in (human) aortic, pulmonary, and mitral valves [136, 157, 220]. Dilation of the heart valve annuli during pregnancy would be expected to trigger remodeling of the valve leaflets due to the associated increases in tensile stresses. Indeed, finite-element models of the aortic and mitral valves have showed that orifice dilation decreases leaflet coaptation and increases their radius of curvature and tensile stress, via the law of Laplace [211, 221]. An 18% annular dilatation, similar to that during human pregnancy, results in a more than twofold increase in stress in both the anterior and posterior leaflets [211].

It is interesting that, despite the large increase in valve orifice area, mitral regurgitation is relatively uncommon in pregnancy [168, 222]. One possible explanation for this is that the mitral valve has a large “functional reserve,” with a total leaflet area that is at least 1.5 times larger than that of the annulus [223]. This surplus area, located in the coaptation surface, allows the valve to experience orifice expansion under various hemodynamic conditions, such as volume loading, without developing mitral regurgitation [224].

Another possibility is that the mitral leaflets undergo adaptive remodeling during pregnancy, increasing leaflet area to maintain coaptation.

The objectives of the present study were to determine changes in the structure and mechanical properties of the bovine mitral valve anterior leaflet during pregnancy. Bovine tissues are commonly used in studies on cardiovascular tissue mechanics, especially those on native and chemically modified heart valve and pericardial tissues. This model, however, is advantageous for several other reasons. First, the bovine cardiovascular system makes adaptations to pregnancy similar to those in humans and other mammalian species, including blood volume expansion [225] and hypertrophic remodeling of the heart [226]. Second, bovine tissues obtained at slaughter are a consistent and reliable source of tissue from pregnant animals, especially where the age and reproductive history of the animal are obtainable. Third, the duration of bovine pregnancy may be estimated from the well-established relationship between the crown-to-rump length of the fetal calf and its gestational age [227]. Finally, the bovine model provides heart valve leaflet samples large enough for biaxial mechanical testing.

We hypothesized that, during pregnancy, the maternal bovine mitral valve undergoes adaptive remodeling similar to that observed in heart failure and other LV dysfunctions where chamber and orifice expansion take place. In particular, we hypothesized that the anterior leaflet enlarges during pregnancy with decreases in biaxial extensibility and that these changes will be associated with thermomechanical alterations to collagen that indicate structural remodeling and adaptation to elevated stress. Thus, we hypothesized that the mitral anterior leaflet collagen thermal stability will decrease, indicative of collagen turnover and remodeling, and collagen crosslinking will increase with the elevated leaflet stress during pregnancy. Here, we report the changes in *1*) leaflet morphometry and quasistatic biaxial mechanical properties, *2*) collagen thermal stability, and *3*) collagen crosslinking of the mitral valve anterior leaflet in pregnant cows and non-pregnant (NP) heifers. Changes in these parameters were also assessed as a function of pregnancy duration.

2.2 Methods

2.2.1 Tissue Harvest and Sample Preparation

All tissue harvest procedures were approved by the Animal Care Committee of Dalhousie University and were conducted in accordance with guidelines approved by the Canadian Council of Animal Care.

Bovine heart valve leaflets and valvular roots were harvested fresh from slaughter for food a local abattoir (Armstrong Food Services, Kingston, NS, Canada). Hearts were collected from heifers (cows that have reached sexual maturity and have never been pregnant, between the ages of 1 and 2 yr old) and from pregnant cows. Heart mass, volume, transverse circumference, and apical circumference were measured. From pregnant cows, fetal crown-to-rump lengths were measured, from which pregnancy duration was estimated for each cow [227]. A full-term bovine fetus is ~100 cm in length. Cows were divided into three groups: NP, EP, and late pregnancy (LP) according to their reproductive status and pregnancy duration (using fetal crown-to-rump length).

The mitral valve anterior leaflet was chosen since it has been shown to experience larger stresses than the posterior leaflet [228]. The leaflets were excised as close as possible to the valve root, washed in Hanks' physiological solution, and placed in Falcon tubes for transport. Tissues were transported back to the laboratory in Hanks' physiological solution including 6 mg/l trypsin inhibitor (lyophilosate) and an antibiotic-antimycotic agent containing 10,000 U/ml penicillin G, 10 mg/ml streptomycin sulfate, and 25 μg/ml amphotericin B (all chemicals from Sigma-Aldrich Canada, Oakville, ON, Canada).

2.2.2 Leaflet Morphometric Analysis

Each excised anterior leaflet was laid flat on a corkboard with the ventricular side facing up (Fig. 2.1A). Stick pins were placed at the leaflet insertion site of each chordae tendineae to mark *1*) the primary "strut" chordae; *2*) the secondary chordae, with diameters between 1 and 3 mm; and *3*) the tertiary chordae, with diameters of <1 mm (Fig. 2.1B). The very smallest chordae (i.e., small side branches or tissue that was translucent) were not counted. Digital images of the leaflets, pins, and accompanying scale bar were captured with a Nikon SMZ 800 dissection microscope and a Nikon

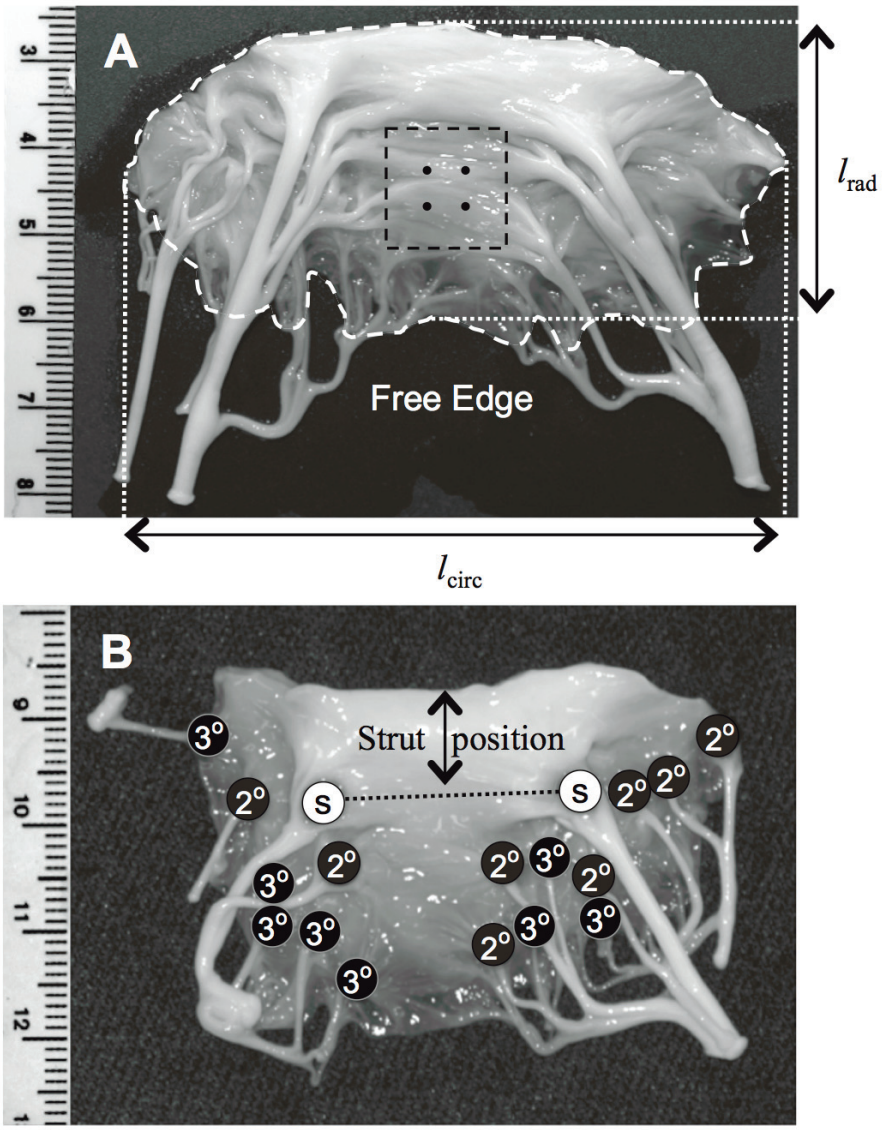

Figure 2.1 Methodology for measurement of leaflet morphology

A: image of an isolated mitral anterior leaflet showing the location of stick pins marking the insertion sites of strut chordae (S), secondary (2°) chordae (diameters > 1 mm), and tertiary (3°) chordae (diameters < 1 mm). The strut position was measured as the vertical distance between the midline connecting the two primary strut chordae and the attachment edge. *B*: image of an isolated mitral anterior leaflet showing dimensional measurements taken using ImageJ. The measurements taken were leaflet area (dashed outline), circumferential length (l_{circ}), and radial length (l_{rad}). Also shown is the region excised for biaxial mechanical testing and marker placement. Note the large collagen fiber bundles in the circumferential direction of the leaflet. Scale bars = 1 cm.

Coolpix 995 camera (Nikon, Tokyo, Japan). Digital images were then imported into image-analysis software (ImageJ, National Institutes of Health), and midline radial and circumferential lengths were measured. The freehand draw tool was used to trace the perimeter of the leaflet to obtain total leaflet area (Fig. 2.1A). The distance between the two primary strut chordae ("strut distance") and the position of this midline from the leaflet attachment site ("strut position") were also measured (Fig. 2.1B).

2.2.3 Biaxial Mechanical Testing

Leaflets were stored at 4°C in Hanks' physiological solution with protease and bacterial inhibitors as described above for no longer than 72 h until they were used for biaxial testing. A square sample of tissue was excised from the center belly region of the anterior leaflet between the attachment sites of the two prominent strut chordae tendineae (Fig. 2.1A), in an attempt to ensure a sample of similar mechanical characteristics. To prepare the samples, ~3 mm was trimmed from the base and the free edge of the leaflet.

Biaxial testing was carried out on a custom-built, servo-hydraulic biaxial testing apparatus (MTS, Eden Prairie, MN), as previously described [229] except with the use of suture-style grips [74, 229]. The device consists of two opposing pairs of servo-hydraulic actuators aligned orthogonally. Tests were carried out in biaxial configuration, using all four actuators. The two actuator pairs provided two axes, allowing independent deformation of the test samples in two perpendicular directions. Actuator waveforms were generated using T/RAC waveform generation (MTS). An actuator in each pair had an attached GSO series 1,000-g cantilever load cell (Transducer Techniques, Temecula, CA). The time, actuator position, and load data were acquired using a custom-written program under LabView software and a 12-bit analog-to-digital (A/D), digital-to-analog (D/A) PCI-6035E card (National Instruments, Austin, TX) on a Macintosh computer (Power Mac G4, Apple Computer, Cupertino, CA).

Video images of the sample surface were recorded with a charge-coupled device camera (Cohu 4190, San Diego, CA) to subsequently track surface deformation markers using ImageJ on a separate Macintosh computer (Power Mac G4, Apple Computer). Video capture was achieved at 15 Hz, and video and analog data were synchronized by a 5-V digital pulse originating from LabView via the D/A board.

A 000 silk suture with a 3-mm cutting needle was tied to one of five nylon pulleys of one grip. The suture was then inserted into four equidistant points along the edge of the tissue square, with the suture being around a nylon pulley on the grip between each insertion point. Nylon pulleys were used to allow low-friction motion of the silk sutures, maintaining near-uniform tension along the edge of the sample. The other three edges of the tissue sample were sutured in similar fashion. After the suturing of the tissue sample was completed, four small graphite markers were cyanoacrylate glued on the center of the sample in the shape of a ~5 × ~5-mm square, as previously described [74] (Fig. 2.1A). During the suturing and placement of the graphite markers, the tissue was continuously soaked in Hanks' physiological solution to prevent dehydration.

As in previous studies [74, 230], membrane tension was used to describe the loading of the tissue. Membrane tension was defined as the axial force per unit length of tissue over which it was applied (expressed in N/m). Once samples had been mounted, a small membrane tension (preload) of 0.5 N/m was placed on the samples. Samples were extended in both directions to approximately half of the extension required to produce a 60-N/m tension on both axes of the tissue. Once extended in this position, the gains on each of the MTS actuators were adjusted to produce the desired 60-N/m tensions in both directions. The actuators were returned to their original (preload) positions, and quasistatic, equibiaxial preconditioning was initiated. The tissue was preconditioned at a frequency of 0.05 Hz (20 s/cycle) for 10 cycles to a peak equibiaxial tension of ~60 N/m. Data acquisition occurred on the final (11th) cycle.

2.2.4 Analysis of Mechanical Testing Data

The graphite marker positions on the surface of the tissue were analyzed using a custom-written program under ImageJ. The pixel coordinates of the particle centers were used to determine the stretch ratios (previously defined in [74]) using a custom-written MathCAD program (Parametric Technology, Needham, MA) written by Dr. Michael Sacks (University of Pittsburgh). The biaxial extensibility was characterized by the axial stretch ratios (λ_C^{peak} (circumferential) and λ_R^{peak} (radial)) under peak equibiaxial membrane stress (60 N/m). The net extensibility of the tissue membrane was represented by the areal stretch under 60-N/m equibiaxial tension, which was calculated as follows:

$$\text{Areal stretch} = [\lambda_C^{peak} \times \lambda_R^{peak}] \times 100\%$$

The 60-N/m equibiaxial tension was chosen as it closely represents the deformation under peak diastolic load and it facilitates comparisons with a related study [74]. To assess the quasistatic elastic properties of the valve tissue over the entire loading range examined, tension versus areal stretch graphs were plotted using areal stretch values calculated at equibiaxial tensions of 1.0, 2.5, 5.0, 10.0, 20.0, 30.0, 40.0, 50.0, and 60.0 N/m.

2.2.5 Denaturation Temperature and Hydrothermal Isometric Tension Testing

Tissue preparation and sodium borohydride reduction. Denaturation temperature (T_d) tests (DTT) and hydrothermal isometric tension (HIT) experiments were conducted on the custom-built apparatus described by Lee et al. [110] following the modified protocol of Wells et al. [117] to determine T_d and proportions of immature to mature crosslinks. After biaxial mechanical testing, the square tissue sample was bisected circumferentially, producing two pieces of tissue with equal dimensions. One piece served as a control sample, and the other was treated with sodium borohydride ($NaBH_4$) to reduce and stabilize immature, thermally labile crosslinks [101, 117, 231]. Comparison of thermomechanical behavior with and without $NaBH_4$ stabilization provided an assessment of the relative contribution of immature crosslinks. The $NaBH_4$ stabilization procedure consisted of four 15-min treatments in a 0.1 mg/ml $NaBH_4$-borate buffer solution (pH 9.0) at 4°C with constant agitation. Untreated samples were subjected to the same conditions (pH, buffer, temperature, and agitation) except in the absence of $NaBH_4$. Untreated and stabilized samples were then rinsed in Hank's solution for 15 min at 4°C with constant agitation before thermomechanical testing. Finally, samples were washed for 10 min in Hanks' physiological solution.

DTT/HIT testing. The DTT/HIT testing allowed for the simultaneous testing of up to six samples, as previously described [101, 117]. Briefly, tissues strips were gripped between two spring clamps, where one clamp was attached to a rigid fixture and the other clamp was attached to an adjustable fixture attached to a strain gauged, cantilever load cell. Samples were extended to an initial load of 50 g and then held under isometric constraint for the duration of the test. Mounted samples were immersed in a 4-liter beaker of

distilled water, and the bath temperature was monitored with a centrally located thermistor probe positioned at the level of the samples. The water was heated with a Cimarec 2 plate heater (Barnstead-Thermolyne, Dubuque, IA) from room temperature at a rate of ~1°C/min to a 90°C isotherm. The temperature was held at this isotherm, 90 ± 0.5°C, for 3 h by an on/off heater control. Time, temperature, and load data were acquired, and heater control was achieved, using a custom-written LabView program on a Dimension 4800 computer (Dell Computing, Round Rock, TX) with a 12-bit A/D, D/A DAQ board (model NB-MIO-16L, National Instruments). Data points were collected at intervals of 1°C during the temperature ramp and at 30-s intervals during the isotherm portion of the test.

Analysis of DTT/HIT data. T_d of each sample was determined as the temperature at the first data point marking the beginning of a consistent rise in load as temperature was increased from room temperature to 90°C [117].

Data recorded at 30-s intervals during the 3-h 90°C isotherm was used to calculate the half-time of the exponential load decay ($t_{1/2}$). Le Lous et al. [232] previously described this as a Maxwell-type relationship using the following equation:

$$L(t) = L_{max}e^{-kt}$$

where $L(t)$ is the load at time t, L_{max} is the maximum load attained at the isotherm onset, and k is a constant denoting the slope of the curve. The following equation was used to calculate $t_{1/2}$:

$$t_{1/2} = -\frac{ln\left(\frac{1}{2}\right)}{k} = \frac{ln(2)}{k}$$

The logarithm of $L(t)/L_{max}$ was plotted against time (during the 90°C isotherm), and k was obtained over an 8,000-s time interval between the 2,000- and 10,000-s mark in the isotherm. This data interval was chosen because it represented an extremely linear portion of the logarithmic load decay curve, avoiding any thermoelastic contraction, which sometimes occurred at the beginning of the isotherm. The $t_{1/2}$ parameter was calculated from k using previously described methods [117].

2.2.6 Histological Analysis

Another set of mitral valve leaflets was collected from pregnant cows and NP heifers as described above. The anterior leaflets were divided in half along the radial direction, fixed from fresh in 10% neutral buffered formalin for a minimum of 48 h, embedded in paraffin, sectioned into 5-μm sections, and mounted on slides. One half of each leaflet was sectioned circumferentially for picrosirius red staining to examine collagen alignment and crimp, whereas the other half was sectioned radially for Verhoeff-van Gieson (VVG) staining to identify leaflet layering and elastin fibers (VVG Elastin Staining Kit, Polysciences, Washington, PA). Sections were deparaffinized, rehydrated, stained in Verhoeff's solution for 1 h, and differentiated in 2% ferric chloride for 1 min followed by several water washes, a counterstain, and dehydration for slide mounting. For picrosirius red staining, sections were deparaffinized, rehydrated, and then stained for 1 h with 0.1% picrosirius red solution. After staining, slides were rinsed with several water washes and then dehydrated for mounting.

Images were taken using a Nikon Eclipse E600 light microscope equipped with a polarized light filter and a Nikon Coolpix 995 digital camera (Nikon).

2.2.7 Statistics

Results are expressed as means ± SE, and *n* values used in the calculations are the numbers of animals providing samples for each group. Data collected from heifers (never-pregnant female cattle) were classified as NP. Data collected from pregnant cows were subdivided into two groups: EP and LP according to the fetal crown-to-rump length. Cows carrying fetuses with crown-to-rump lengths of 0–50 cm were classified as EP, and those carrying fetuses over 50 cm were classified as LP. By gestational age, these groups correspond to ~0–159 days of gestation for EP and 160–270 days of gestation for LP. To determine the differences between pregnancy groups, one-way ANOVA was performed followed by Tukey honestly significant difference comparisons among the three groups (the NP group and the two pregnancy groups). In the case of HIT data, this was preceded by two-way ANOVA that demonstrated no interactions between the factors of treatment (control vs. $NaBH_4$) and pregnancy state (NP, EP, and LP).

To assess the changes in any parameter as a function of pregnancy duration, data for each parameter were plotted as a function of gestational age and fitted with a least-squares linear regression. The regression was considered significant when $P < 0.05$. Statistical analyses were performed using JMP Statistical Software (version 5.0.1.2, SAS Institute, Cary, NC).

2.3 Results

2.3.1 Cardiac Dimensions

Bovine hearts underwent significant increases in mass, volume, and dimensions by LP. Heart mass in NP heifers was 2.13 ± 0.16 kg and remained unchanged during EP. In LP animals, however, heart mass was 44% greater than that of NP animals (Table 2.1). Similarly, heart volume was unchanged from NP animals (2.24 ± 0.17 liter) in EP but was increased 107% in LP animals (3.31 ± 0.26 liters) from NP values. Enlargement of the heart in LP occurred in both the circumferential and base-to-apex directions. For NP animals, mean heart circumference was 45.9 ± 1.3 cm in the transverse direction and 53.0 ± 1.2 cm in the apical direction. These values were increased 15% in LP animals from those of NP animals (Table 2.1).

2.3.2 Leaflet Morphology

The anterior leaflet of the bovine mitral valve underwent rapid and striking morphological changes during pregnancy, with increases in leaflet area and number of attachments by chordae tendineae. Figure 2.2 shows representative images of anterior mitral leaflets from a NP heifer (*A*), a pregnant cow at 94 days of gestation (Fig. 2.2B), and a near-term (261 days of gestation) cow (*C*). Mean anterior leaflet area increased 33% from NP animals (11.1 ± 0.6 mm^2) to EP animals (14.8 ± 1.0 mm^2) and then remained unchanged in LP animals (Fig. 2.3A). Increases in leaflet area were caused by rapid leaflet expansion during EP, in both the radial and circumferential directions. Radial leaflet length increased 20% from NP animals (2.5 ± 0.1 mm) to EP animals (3.0 ± 0.2 mm; Fig. 2.3B), and circumferential length increased 14% from NP animals (5.1 ± 0.1 mm) to EP animals (5.8 ± 0.3 mm; Fig. 2.3C).

While increases in anterior leaflet area during pregnancy were prominent, changes in the

Table 2.1 Changes in heart dimensions with pregnancy

	NP Group	EP Group	LP Group
Mass, kg	2.13 ± 0.16[a]	2.84 ± 0.15[a]	3.08 ± 0.23[b]
Volume, L	2.24 ± 0.17[a]	2.85 ± 0.17[a]	3.31 ± 0.26[b]
Heart circumference			
Transverse Circumference, cm	45.9 ± 1.3[a]	50.6 ± 1.3[a]	52.8 ± 1.9[b]
Apical Circumference, cm	53.9 ± 1.2[a]	58.2 ± 1.3[a]	61.0 ± 2.0[b]

Values are mean values ± SE of cardiac mass, volume, and dimension parameters for animals in the non-pregnant (NP; $n = 11$), early pregnant (EP; $n = 9$), and late pregnant (LP; $n = 4$) groups. Statistical comparisons were made among NP, EP, and LP groups using ANOVA followed by Tukey's honestly significant difference (HSD) multiple-comparison method. [a,b]Within each parameter, values labeled with the same letter were not significantly different.

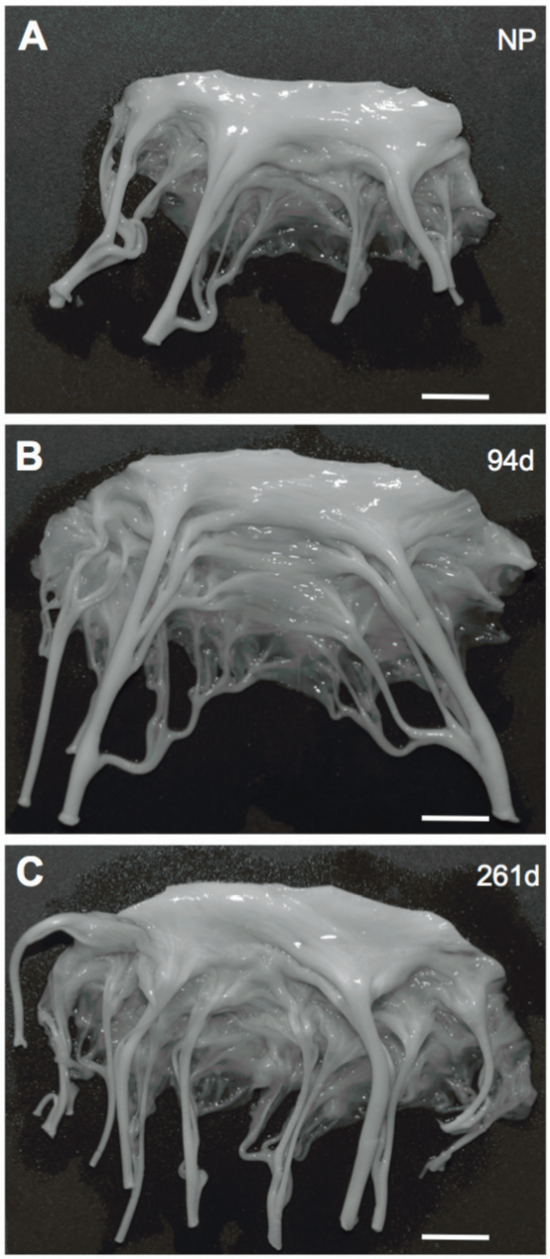

Figure 2.2 Morphological changes in mitral valve leaflet (images)

Representative images of the anterior mitral valve leaflet showing morphological changes with pregnancy and its duration. *A*: leaflet from the non-pregnant (NP) group (never-pregnant heifer). *B*: leaflet from a cow in the early pregnant (EP) group (94 days of gestation, ~1/3 through gestation). *C*: leaflet from a cow in the late pregnant (LP) group (261 days of gestation, close to full term). Scale bars = 1 cm.

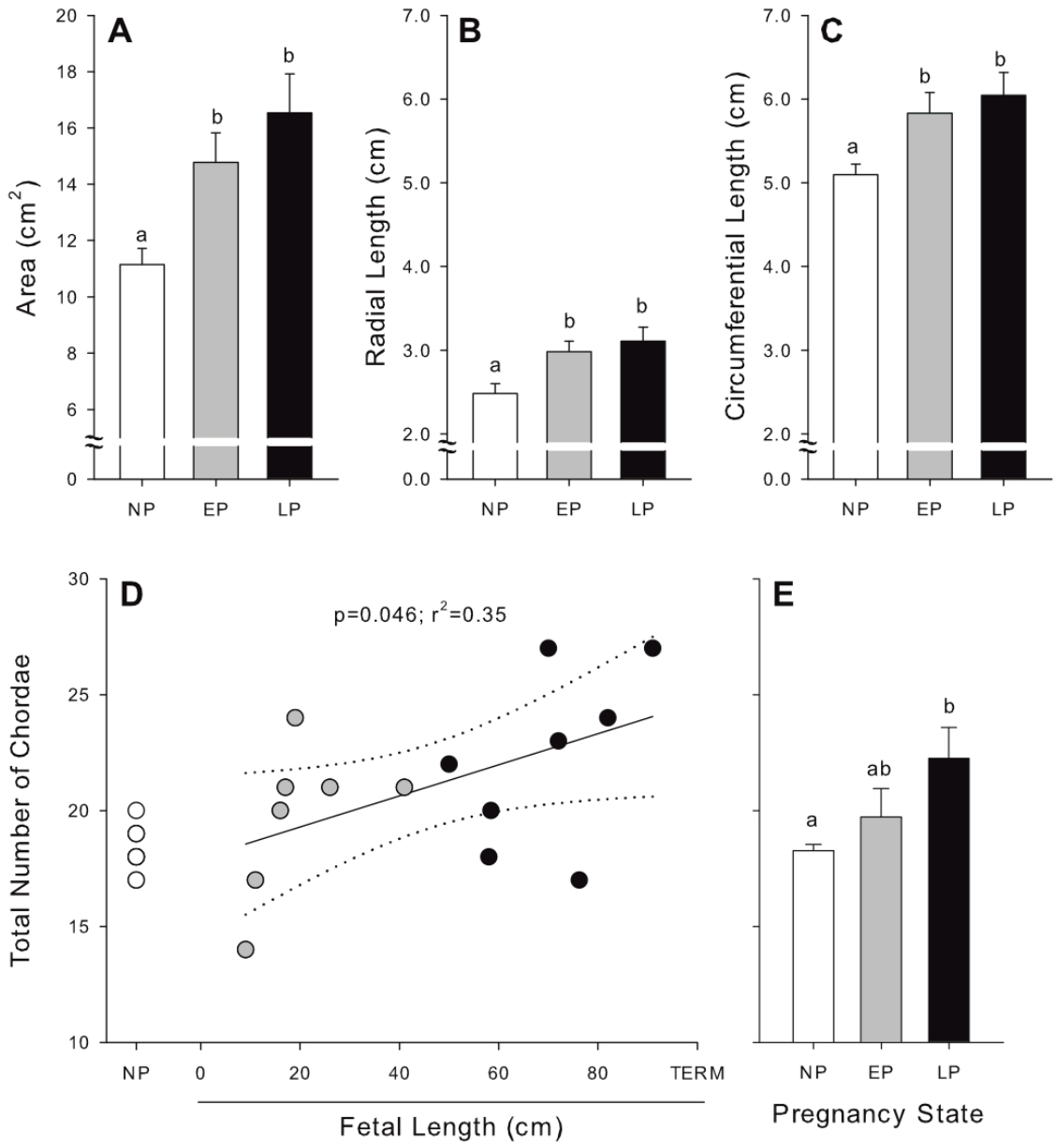

Figure 2.3 Morphological changes in mitral valve leaflet (plots)

Dimensions and chordae tendineae attachments of the anterior mitral leaflet from NP heifers and pregnant cows [EP (0–159 days of gestation) and LP (160–270 days of gestation)]. *A*: leaflet area (in cm^2). *B*: radial midline length (in cm). *C*: circumferential length (in cm). Values in *A–C* are means ± SE. *D*: total numbers of chordae tendineae attachments plotted for NP heifers (NP; open circles) and with fetal length (in cm) for EP (shaded circles) and LP (solid circles) animals. Note that only four distinct data points are visible in the NP group due to multiple samples having the same number of chordae. *E*: mean values of chordae attachments ± SE for the three pregnancy groups. Sample sizes (n) = 11, 8, and 7 for the NP, EP, and LP groups, respectively. [a,b]Values labeled with the same letter were not significantly different.

position and separation of the primary strut chordae were less so, likely a result of the large, inherent variability in their anatomy. ANOVA comparisons between NP, EP, and LP animals yielded *P* values of 0.19 for strut position and 0.06 for strut distance. However, increases in both parameters were revealed when comparisons were made between NP and (pooled) pregnant animals. The strut position in NP animals was 11.0 ± 0.6 mm (n = 9) and was increased to 12.7 ± 0.6 mm (n = 12) in pregnant animals (P = 0.037). Similarly, there was a trend (P = 0.06) toward increased strut distance in pregnant animals (27.8 ± 5.7 mm, n = 12) compared with NP animals (22.8 ± 5.7 mm, n = 9) However, when the strut position and distances were normalized to leaflet radial and circumferential lengths, respectively, they were unchanged with pregnancy, suggesting a uniform enlargement of the leaflet, at least between the primary struts and the attachment edge.

Accompanying the increase in leaflet area was a corresponding increase in the number of chordae tendineae to the ventricular surface. The total number of chordae attached increased linearly with pregnancy duration (fetal length; Fig. 2.3D), with mean values increasing by 22% from the NP state (18.3 ± 0.3) to the LP state (22.3 ± 1.3; Fig. 2.3E). This was a result of increases in the number of both secondary and tertiary chordae during pregnancy. The number of secondary chordae was significantly increased from NP animals (6.9 ± 0.4) to EP animals (8.0 ± 0.5), whereas the number of tertiary chordae was significantly increased from NP animals (8.9 ± 1.4) to LP animals (11.8 ± 2.9).

While both leaflet area and chordal attachments increased during pregnancy, the number of chordal attachments did not keep in step with the increase in leaflet area. There was a progressive decrease in the density of chordal attachments (number of attachments/cm^2) during pregnancy, with mean values decreasing 27% from the NP group (1.5 ± 0.1 attachments/cm^2) to the LP group (1.1 ± 0.1 attachments/cm^2, P = 0.049).

2.3.3 Leaflet Mechanical Properties

In all mitral valves from NP and pregnant animals, anterior leaflets were more extensible along the radial axis than the circumferential axis (Fig. 2.4), as previously reported in other species (sheep and pigs; Table 2.2). The net extensibility (represented

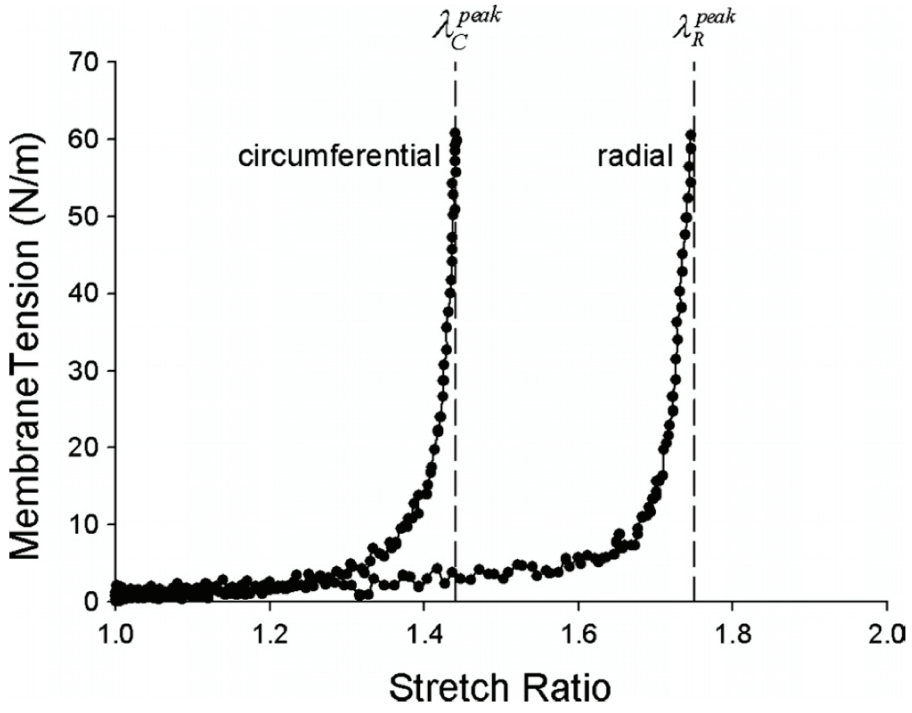

Figure 2.4 Representative equibiaxial tension-stretch ratio curve

Representative equibiaxial tension versus stretch ratio curves for bovine mitral anterior leaflet tissue. Leaflet tissue is loaded to 60-N/m peak equibiaxial tension in the circumferential and radial direction, and the resulting peak stretch ratios [peak circumferential stretch ratio (λ_C^{peak}) and peak radial stretch ratio (λ_R^{peak})] were obtained.

Table 2.2 Summary of leaflet mechanical properties from the present and previous studies

	Porcine Leaflets			Ovine Leaflets	Bovine Leaflets		
	Biaxial	Flow loop	In situ	In vivo	NP Group	EP Group	LP Group
Reference(s)	222*	205, 223	224	225*	Present study	Present study	Present study
λ_C^{peak}	1.12*†	1.08-1.1	1.02-1.04	1.22*	1.37 ± 0.05^{a}	1.23 ± 0.04^{b}	$1.29 \pm 0.03^{a,b}$
λ_C^{peak}	1.26*	1.30-1.32	1.14	1.65*	$1.67 \pm 0.06^{a,b}$	1.53 ± 0.07^{a}	1.75 ± 0.07^{b}
$\lambda_R^{peak}/\lambda_C^{peak}$	0.87*	0.83	0.90	0.74*	0.82	0.80	0.74
Areal Stretch	N/A*	1.42-1.47	N/A	N/A*	2.30 ± 0.11^{a}	1.91 ± 0.14^{b}	2.36 ± 0.10^{a}

Shown are mitral anterior leaflet mechanical properties from the present study and values obtained from previous studies for comparison. Peak circumferential stretch ratio (λ_C^{peak}), peak radial stretch ratio (λ_R^{peak}), the ratio of these values ($\lambda_R^{peak}/\lambda_C^{peak}$), and peak areal stretch are shown. Data from previous studies are shown for porcine leaflets tested *1*) under similar equibiaxial conditions [233], *3*) in a physiological left ventricular simulating flow loop [216, 234], and *3*) in an isolated porcine heart preparation (in situ) [235]. Data are also shown for ovine anterior leaflets assessed in vivo using the excised, stress-free leaflet as the reference state [236]. Data from the present study are mean values ± SE for bovine NP, EP, and LP groups. For each parameter, statistical comparisons were made between pregnancy groups from the present study using ANOVA followed by Tukey HSD multiple-comparison method. ^{a,b}Values labeled with the same letter were not significantly different. **t*-Test comparisons were made between mechanical data from our NP animals with those from Liao et al. [233] and Amini et al. [236]. †Significant difference from our mean NP value ($P < 0.05$). N/A, not applicable.

by peak areal stretch under 60-N/m equibiaxial tension) of anterior mitral valve leaflets significantly decreased during EP and returned to pre-pregnant values by term (Fig. 2.5, A and B; mean values and statistical comparisons are also shown in Table 2.2). There was a rapid decrease in peak areal stretch in early pregnancy, with mean values decreasing 30% from the NP group (2.30 ± 0.11) to the EP group (1.91 ± 0.14; Table 2.2 and Fig. 2.5B). Areal stretch then increased linearly with fetal development ($P = 0.018$; Fig. 2.5A), with mean values returning to pre-pregnancy values by LP (2.36 ± 0.10; Table 2.2 and Fig. 2.5B).

The reversible decrease in leaflet extensibility in EP was produced by changes in leaflet extensibility in both the circumferential and radial directions (Table 2.2 and Fig. 2.5, C–F). λ_C^{peak} under 60 N/m equibaxial tension decreased significantly from NP values (1.37 ± 0.05) by EP (1.23 ± 0.05; Table 2.2 and Fig. 2.5D). λ_R^{peak}, while not significantly altered from NP values (1.67 ± 0.06) by EP, rapidly and significantly increased over pregnancy duration (as assessed by fetal length, $P = 0.036$; Fig. 2.5E), with mean values increasing 14% by LP (1.75 ± 0.07; Table 2.2 and Fig. 2.5F).

In addition to observations at peak equibiaxial tension, the reversible decrease in anterior leaflet areal stretch in EP was also observed over almost the entire range of equibiaxial tension used in our experiments. Figure 2.6 shows mean areal stretch at each equibiaxial tension level for the NP, EP, and LP groups. At each equibiaxial tension level, above 5 N/m, mean areal stretch was decreased in EP animals from those of NP or LP animals (Fig. 2.6). The result was a significant shift to the left of the tension versus areal stretch curve during EP, revealing a striking, reversible decrease in leaflet extensibility.

2.3.4 Collagen Crosslinking (HIT Results)

T_d – Effects of Pregnancy. Collagen thermal stability decreased rapidly in EP. (Control) T_d was significantly decreased from the NP group (68.6 ± 0.5°C) to the EP group (66.4 ± 0.6°C) and remained unchanged into the LP group (66.2 ± 0.4°C, $P = 0.001$).

T_d – Effects of $NaBH_4$ Treatment. $NaBH_4$ treatment did not alter collagen thermal stability in any of the pregnancy groups. Results from two-way ANOVA revealed no

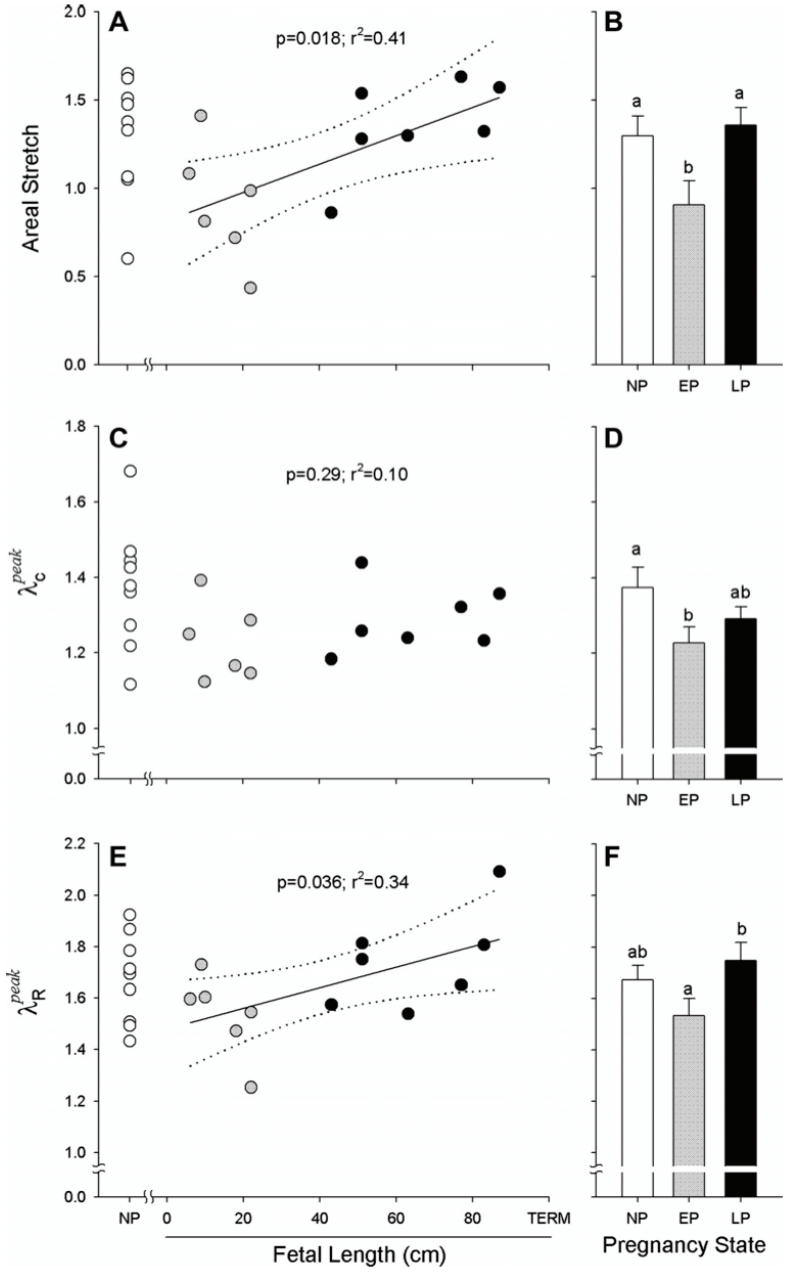

Figure 2.5 Biaxial mechanical properties (mitral)

Biaxial mechanical properties of the anterior mitral valve leaflet: peak values at 60-N/m equibiaxial tension. *A*, *C*, and *E*: peak areal stretch, λ_C^{peak}, and λ_R^{peak} as a function of fetal crown-to-rump length (100 cm ~ term) along with measurements from NP heifers. Regression lines with 95% confidence intervals are shown for the fetal data. *B*, *D*, and *F*: comparison of mean (± SE) values between pregnancy states (NP, EP, and LP). n = 9, 6, and 7 for NP, EP, and LP groups, respectively. [a,b]Values labeled with the same letter were not significantly different.

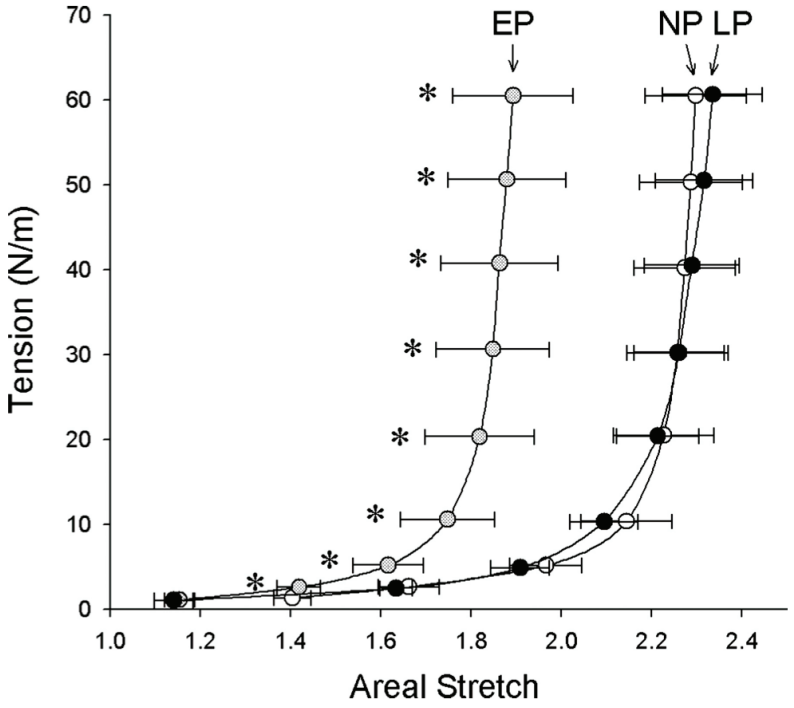

Figure 2.6 Tension versus areal stretch curves by pregnancy group (mitral)

Mean tension versus areal stretch curves for the anterior mitral leaflet at each pregnancy state (NP, EP, and LP). The areal stretch is shown as means ± SE at tension increments of 1.0, 2.5, 5.0, 10.0, 20.0, 30.0, 40.0, 50.0, and 60.0 N/m. n = 10, 6, and 9 for the NP, EP, and LP groups, respectively. *At each tension level, areal stretch values in the EP group were significantly lower than those of the NP or LP groups.

effect of $NaBH_4$ treatment on T_d of the tissue in any of the pregnancy groups (data not shown).

$t_{1/2}$ – Effects of Pregnancy. Load relaxation (in control tissues) during the 90°C isotherm became progressively slower from the NP state to the LP state, implying an increase in the content of mature collagen crosslinks over this interval. There was a trend toward a significant linear increase in HIT $t_{1/2}$ control with pregnancy duration (Fig. 2.7A), resulting in a progressive 70% increase in mean HIT $t_{1/2}$ control values from the NP group (8.6 ± 1.1 h) to the LP group (15.0 ± 1.9 h, $P = 0.02$; Fig. 2.7B).

$t_{1/2}$ – Effects of $NaBH_4$ Treatment. $NaBH_4$ treatment significantly increased HIT $t_{1/2}$ in all of the pregnancy groups ($P = 0.01$), as indicated by the solid lines connecting the control and $NaBH_4$ values within each pregnancy group in the interaction plot shown in Fig. 2.8. The increase in $t_{1/2}$ after $NaBH_4$ treatment reflects the presence of immature collagen crosslinks in the mitral anterior leaflet at all pregnancy states. As in previous studies, the relative increase in $t_{1/2}$ after $NaBH_4$ treatment (i.e., the ratio of $t_{1/2}$ in $NaBH_4$/$t_{1/2}$ in control) was used as an indicator of the ratio of immature to mature collagen crosslinking. This ratio was relatively low and, surprisingly, unchanged across pregnancy groups (mean values of $t_{1/2}$ in $NaBH_4$/$t_{1/2}$ in control: 1.4 ± 0.2 in the NP group, 1.7 ± 0.3 in the EP group, and 1.6 ± 0.3 in the LP group, $P = 0.63$), suggesting that the level of immature collagen crosslinking remained at a relatively low and constant level during pregnancy.

$t_{1/2}$ – Effects of $NaBH_4$ × Pregnancy. While the mitral valve tissue showed an increase in HIT $t_{1/2}$ in control by LP, there was no change in $t_{1/2}$ in $NaBH_4$-treated tissue between pregnancy states, suggesting that while mature crosslinks increased during pregnancy, total crosslinking remained unchanged. Paradoxically, this implies that the amount of immature crosslinking changed very little (or if anything was decreased) from the NP state to the LP state. Results from two-way ANOVA showed that there was no interaction between the factors of $NaBH_4$ and pregnancy state ($P = 0.46$; Fig. 2.8). The similar but modest increase in $t_{1/2}$ across pregnancy states suggests that the content of immature crosslinking was relatively low and, surprisingly, unchanged during pregnancy.

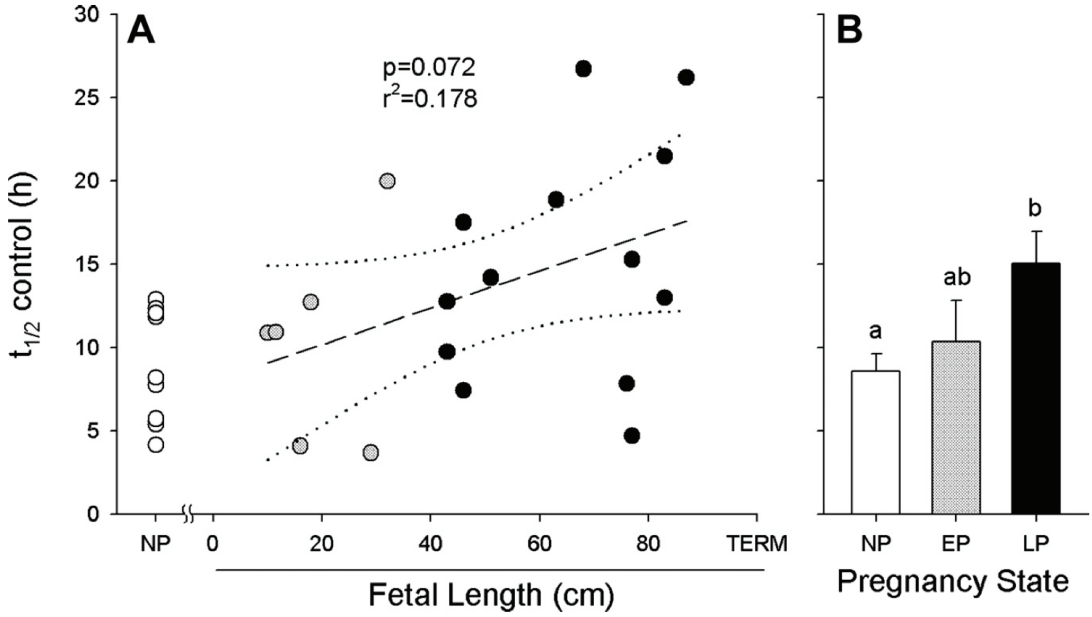

Figure 2.7 HIT load decay half-time for control tissues in pregnancy (mitral)

Isothermal load decay half-time ($t_{1/2}$; in h) for "control" tissues (those that did not undergo $NaBH_4$ treatment) obtained from hydrothermal isometric tension (HIT) experiments. Values are shown for all animals and show temporal changes with pregnancy duration (*A*) and as means ± SE for each pregnancy state (*B*). n = 10, 6, and 13 for the NP, EP, and LP groups, respectively. [a,b]Values labeled with the same letter were not significantly different.

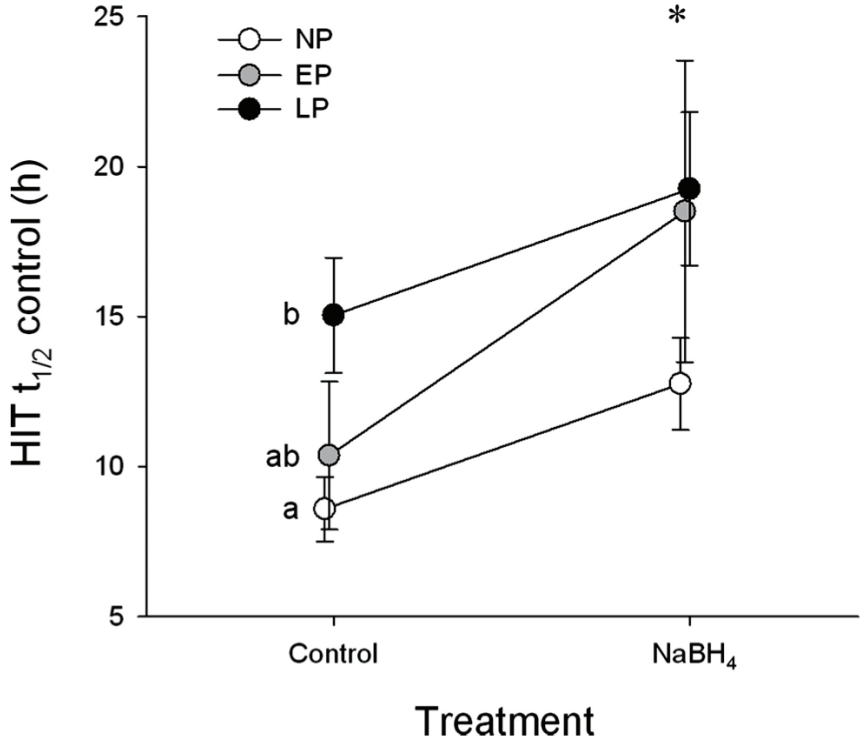

Figure 2.8 HIT load decay interaction plot (mitral)

Interaction plot showing HIT $t_{1/2}$ for control and $NaBH_4$-treated tissues for each pregnancy state (NP, EP, and LP). n = 10, 7, and 15 for the NP, EP, and LP groups, respectively. Control values are the same as those shown in Fig. 7. Results of two-way ANOVA are shown, where pregnancy state and $NaBH_4$ treatment had significant effects on $t_{1/2}$. Control $t_{1/2}$ values were compared between groups using subsequent one-way ANOVA. [a,b]Values labeled with the same letter were not significantly different. There was no interaction between $NaBH_4$ and pregnancy state, that is, $NaBH_4$ significantly elevated $t_{1/2}$ (although only slightly) in each pregnancy group (*). This observation suggests that the content of immature cross-linking is relatively low and, surprisingly, unchanged during pregnancy.

2.3.5 Leaflet Histological Properties

Histological analyses showed significant changes in the tri-layered structure and overall thickness of the anterior mitral leaflet during pregnancy. Figure 2.9 shows representative VVG-stained radial sections taken from the belly region of the leaflet. Full leaflet thickness is shown for a NP heifer in Fig. 2.9*A*, with higher-magnification images of the atrialis, spongiosa, and ventricularis shown in Fig. 2.9, B–D. The atrialis (Fig. 2.9B) was characterized by a large number of densely stained elastic fibers (stained black) and associated dense collagen. The spongiosa (Fig. 2.9C) was composed of a network of fine elastic and collagen fibers with large pores, which contain mainly hydrated glycosaminoglycans and proteoglycans (not stained by VVG). The ventricularis (Fig. 2.9D) was composed mainly of collagen (stained pink-purple), with valvular interstitial cells (nuclei stained black) with a thin outer layer of elastic fibers that was highly variable in thickness and density.

In EP (113 days of gestation; Fig. 2.9, E–H), the leaflet was much thicker, largely through thickening of the dominant, densely collagenous ventricularis. The atrialis was less dense, with sparse staining of elastic fibers (Fig. 2.9F), whereas the extracellular matrix of spongiosa showed some densification, with increased elastin and collagen staining and an elongation of its pores in the radial direction (Fig. 2.9G). In contrast, in LP (184 days of gestation; Fig. 2.9, I–L), the leaflet was reduced in thickness from that in EP, with further densification and elongation of the spongiosa (Fig. 2.9K) and a slightly more dense atrialis. In the near-term animal (Fig. 2.9; M–P), elongation of the spongiosa (Fig. 2.9O) and densification of the atrialis (Fig. 2.9N) were even more prominent.

Observations from picrosirius red-stained sections also suggested striking changes during pregnancy in collagen fiber crimp in the circumferential direction. Tissue from NP animals revealed a uniform, crimped structure with a period of ~15 μm (Fig. 2.10, A and B). This structure was much less spatially uniform in EP, with little or no change in the crimp period (Fig. 2.10, C and D). At the beginning of the LP period, there was a dramatic loss of collagen crimp, as shown in the tissue from a near-term animal (184 days of gestation; Fig. 2.10, E and F). Collagen crimp was regained near term (Fig. 2.10, G and H), but at a period almost double that in the NP animal.

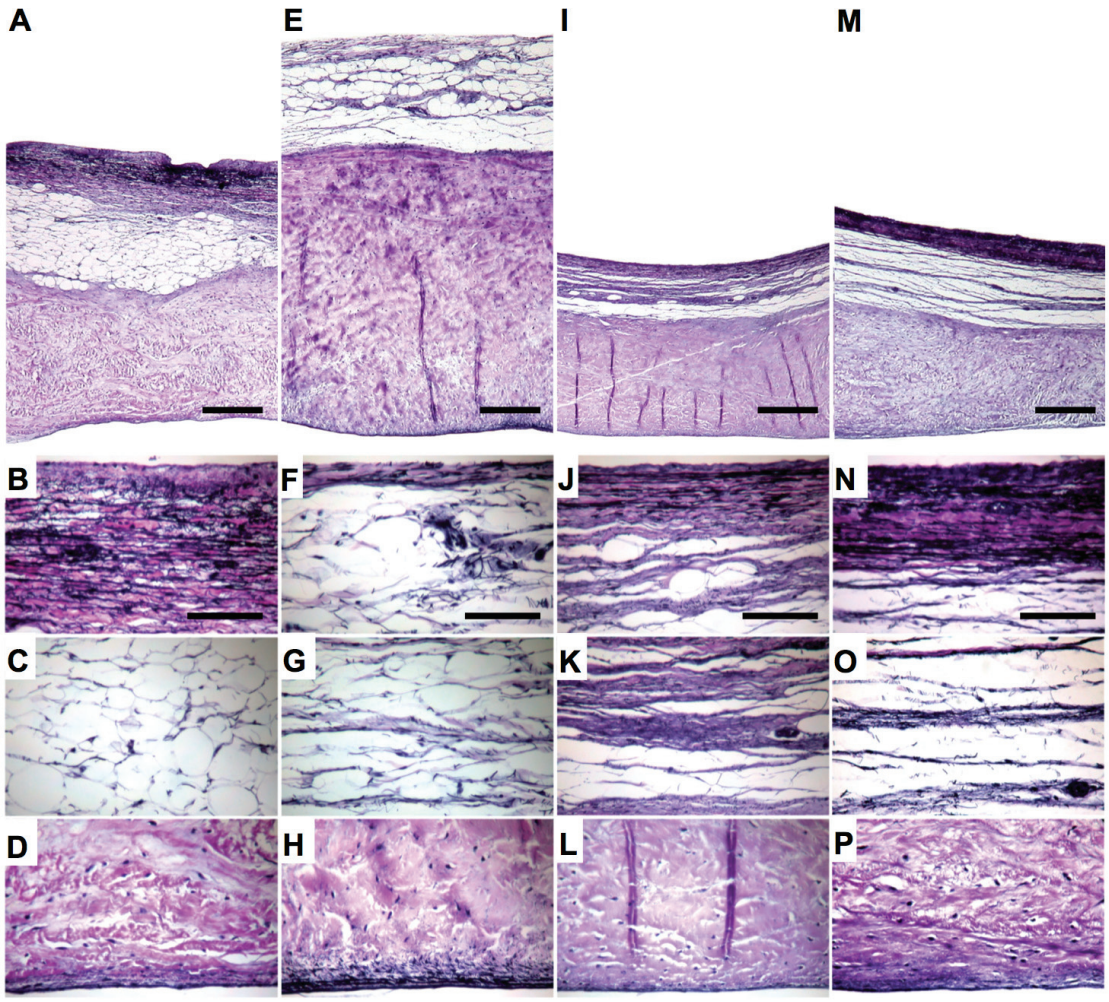

Figure 2.9 Leaflet layers with Verhoeff-van Gieson staining (mitral)

Representative Verhoeff-van Gieson (VVG)-stained radial cross-sections of the anterior mitral valve leaflet showing histological changes with pregnancy and its duration. In VVG-stained tissue, black denotes elastic fibers and cell nuclei and purple-pink denotes collagen fibers. (Proteoglycans/glycosaminoglycans are not stained.) Full-thickness cross-sections are shown in *A*, *E*, *I*, and *M*, with the atrialis at the top of the image and the ventricularis at the bottom. *B–D*, *F–H*, *J–L*, and *N–P* show higher- magnification images of the atrialis, spongiosa, and ventricularis for each sample in *A*, *E*, *I*, and *M*. *A*: full-thickness image from a NP heifer; *B–D*: atrialis (*B*), spongiosa (*C*), and ventricularis (*D*), respectively, from the same tissue. *E*: full-thickness image from a cow in the EP group (113 days of gestation); *F–H*: atrialis (*F*), spongiosa (*G*), and ventricularis (*H*), respectively, from the same tissue. *I*: full-thickness image from a cow in the LP group (184 days of gestation); *J–L*: atrialis (*J*), spongiosa (*K*), and ventricularis (*L*), respectively, from the same tissue. *M*: full-thickness image from cow in the LP group (240 days of gestation, close to term); *N–P*: atrialis (*N*), spongiosa (*O*), and ventricularis (*P*), respectively, from the same tissue. Scale bars = 200 μm in *A*, *E*, *I*, and *M*; scale bars = 100 μm in *B*, *F*, *J*, and *N* and are representative for the remaining images.

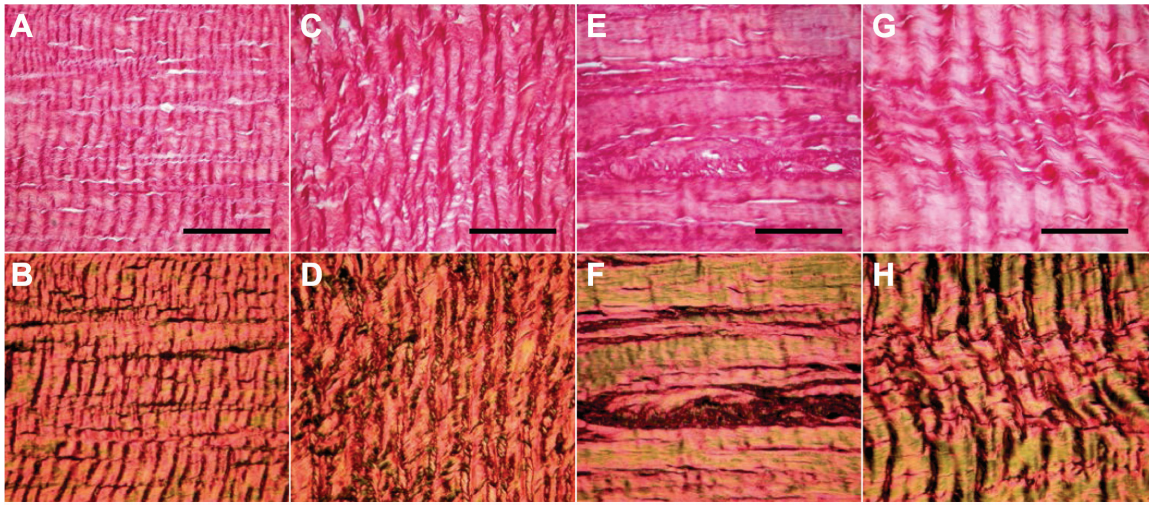

Figure 2.10 Collagen crimp with picrosirius red staining (mitral)

Representative images of picrosirius red-stained collagen in circumferential sections from the belly region of the leaflet taken without (*A*, *C*, *E*, and *G*) and with polarized light (*B*, *D*, *F*, and *H*) of tissue from a heifer in the NP group (*A* and *B*), a cow in the EP group (113 days of gestation; *C* and *D*), a cow in the LP group (184 days of gestation; *E* and *F*), and a near-term cow in the LP group (240 days of gestation; *G* and *H*). Scale bars = 100 μm.

2.4 Discussion

This study reported, for the first time, dramatic, adaptive remodeling in mature heart valve leaflets under non-pathological conditions. The anterior leaflet of the bovine mitral valve undergoes rapid increases in leaflet size and chordal attachments that may accommodate not just the increased orifice area but the inevitable increases in leaflet and chordal stresses that would accompany this expansion. Accompanying this increase in size was a surprising, biphasic change in leaflet extensibility: decreasing in EP and then reversing back to pre-pregnant values by LP. The results from this study suggest that the volume loading and valve orifice expansion during pregnancy trigger remodeling and tissue growth that increases the size and alters the material properties of the leaflet.

We observed a rapid 33% increase in leaflet area within the first 2 months of bovine pregnancy. This is similar to the 35% increase in systolic leaflet area reported in an echocardiographic assessment of patients with LV dysfunction [185]. Elevated leaflet stress (in pregnancy or LV dysfunction) is likely the trigger for physiological or pathological remodeling of the mature mitral valve. Indeed, elevation of leaflet stresses alone, imposed by papillary muscle tethering in adult sheep, triggered a 17% increase in leaflet area after 2 months [219]. In LV dysfunctions that involve orifice expansion, stresses on the valve leaflets are increased with their radius of curvature (by the law of Laplace) as more of the functional reserve of the leaflet is used and the coaptation area is decreased. As a result, leaflet length and area increase in parallel with annular diameter [183, 185]. Together, the results of the present and previous studies support our hypothesis that leaflet enlargement occurs along with the cardiac and orifice expansion during pregnancy, in a manner similar to leaflet enlargement in LV dysfunctions, at least those where chamber and orifice expansion take place. Such leaflet enlargement with mitral valve orifice expansion during pregnancy may serve to maintain coaptation and may explain the clinical absence of increased mitral regurgitation in the maternal circulation.

The increase in size of the bovine anterior mitral valve leaflet appears to be largely uniform across its area. We observed similar increases in both the radial and

circumferential directions, with radial length increasing 20% and circumferential length increasing 14% from NP animals (Fig. 2.3, B and C).

In addition, the relative position and separation of the primary strut chordae were increased in step with the leaflet radial and circumferential lengths, suggesting a uniform enlargement of the leaflet, at least between the primary struts and the attachment edge. It is unclear how this leaflet enlargement compares with that in LV dysfunction. Chaput and coworkers [185] suggested that the valve enlarges primarily through expansion in the circumferential direction, whereas Timek and co-workers [237] attribute it to a radial lengthening of the mitral leaflet, mainly near the free edge.

We compared the mechanical and thermomechanical properties of anterior mitral valve leaflets from NP animals with those reported in previous studies, and, where possible, statistical comparisons were performed. Our biaxial mechanical data are shown in Table 2.2, along with data from other studies on porcine and ovine anterior mitral valve leaflets. Included are previous data obtained using *1*) biaxial testing similar to that of the present study [233], *2*) intact valves in a physiological flow loop [216, 234], *3*) valves tested in situ [235], and *4*) valves assessed in vivo [236]. The latter study examined the effects of referential configuration on calculated mechanical parameters. Table 2.2 shows Amini et al.'s data [236], where the reference state was obtained from the excised, stress-free leaflet.

In general, relatively larger deformations (stretch ratios and extensibility) were observed using in vitro biaxial testing versus measurements from the studies on intact valves in physiological flow loops, either in situ or in vivo (Table 2.2). These differences arise largely from the choice of reference state in the strain or stretch ratio calculation. In the present study and that of Liao et al., a nearly stress-free configuration was used as the reference state, where the square biaxial specimen was loaded only enough to hold the sample flat. The other studies [216, 234, 235], on porcine valves, used intact but unloaded leaflets (whether mounted in a flow loop or in situ) as a reference state, which reflects the in situ geometry and residual stresses in the leaflet.

Data from NP animals in the present study were somewhat comparable with those from porcine anterior leaflets under biaxial testing. Our mean λ_C^{peak} (1.37 ± 0.05) was 23%

larger ($P = 0.003$) than that obtained for the porcine anterior leaflet (1.12 ± 0.05, $n = 5$) [233], whereas there was no significant difference between our λ_R^{peak} (1.67 ± 0.06) and that obtained for porcine valves (1.26 ± 0.04, $n = 5$; Table 2.2). The slightly higher circumferential extensibility in the present study is likely due to species-related differences.

There was, however, excellent agreement between our data from NP animals and those from Animi et al.'s ovine in vivo model [236], which used the excised, stress-free configuration as the reference state (Table 2.2). There was no significant difference between our λ_C^{peak} (for NP animals) and that of Amini et al. (1.22 ± 0.07, $n = 4$), and, similarly, no significant difference between our λ_R^{peak} and that of Amini et al. (1.65 ± 0.08, $n = 4$).

The greater stretch ratios in both directions in the present study translate into a larger areal stretch, as observed from porcine leaflets assessed in a physiological flow loop (the only previous studies where areal strain is reported). Mean areal stretch from the present study (from NP animals) was 2.3, indicating an average area increase of 130% from the unloaded state to peak equibiaxial loading conditions. This is ~60% larger than values reported for porcine anterior leaflets (1.42–1.47; Table 2.2). These differences are likely a result of the differences in both species and referential conditions between the two studies.

Interestingly, the relative stretches in the two principle directions were remarkably similar across species and study conditions (Table 2.2). The ratio of peak circumferential to radial stretch ratios from NP animals in our study (0.82) was very similar to the same ratio observed in porcine valves under biaxial testing (0.86 [230]) and physiological flow loop (0.83), as well as from ovine valves assessed in vivo (0.89 [238]), suggesting that the loading conditions were quite consist across testing protocols and species and are similar to conditions observed in vivo.

As for our thermomechanical data, values for NP animals from the present study (T_d = 68.6 ± 0.5°C, $t_{1/2}$ in control = 8.6 ± 1.1 h) were slightly higher than values reported for adult steers (T_d = 67.1 ± 0.50°C, $t_{1/2}$ in control = 3.2 ± 0.5 h [101]). These differences

may be sex related, since the cattle studied in the present and previous study were from similar ages (12–24 mo in the present study and 24–30 mo in the previous study).

Finally, our changes in the bovine heart mass and dimensions are comparable with those from previous studies on LV remodeling during pregnancy in humans. The 45% increase in heart mass during bovine pregnancy was comparable with the 52% increase in LV mass in humans [157]. Similarly, the 15% increase in heart circumference was comparable with the 12% increase in LV end-diastolic diameter in humans [166]. These comparisons support the validity of our bovine model to study cardiovascular adaptations to pregnancy.

One of the most striking observations from the present study was that the leaflet dimensions and mechanical properties did not change along the same timeline (or direction) during pregnancy. This may suggest that different remodeling mechanisms are at play in EP versus LP. New leaflet dimensions are attained in EP, with leaflet area increasing by 33%. Accompanying this enlargement is a 30% decrease in leaflet extensibility, largely in the circumferential direction. EP may therefore represent a period when valve leaflets attain the new anatomic/dimensional "set point" associated with the enlarged valve orifices necessary in pregnancy. We do note, however, that all measurements of cardiac mass and dimensions in the present study were not significantly increased until LP. While we do not have direct measurements of valve orifice areas, a previous study [157] has suggested that their enlargement with pregnancy is progressive. Regardless of the trigger, the mechanism underlying the EP enlargement of the leaflet may be achieved by one or more factors, including *1*) growth of new tissue, *2*) plastic deformation (permanent stretch) of existing tissue, or *3*) changes in collagen architecture. The simultaneous thickening of the leaflet in EP strongly suggests that tissue growth is occurring. Indeed, the transient increase in leaflet thickness in EP may underlie the shift to the left of the tension versus stretch curve. This may be followed by the mechanism proposed in heart failure, with plastic deformation of the tissue [197], as suggested by the subsequent thinning of the leaflet with apparent "elongation" of the fibrosa in the radial direction.

As for changes in collagen architecture, loss of collagen crimp could contribute to leaflet expansion in the circumferential direction; however, this appears to occur in LP, after the expansion has occurred.

In LP, whereas the enlarged leaflet dimensions are maintained, extensibility then increases (largely in the radial direction) back to pre-pregnant values by term. The trigger for this remodeling may be the increased stress in the leaflet that must accompany its enlargement. LP may then represent the phase where the valve leaflet becomes "entrenched" at these increased dimensions and, as it remodels toward normalizing leaflet stress, re-attains its pre-pregnancy mechanical properties. It is interesting to note that this response of the mitral leaflet parallels that seen in the artery wall in response to chronic increases in blood flow [239, 240]. Initially, the vessel diameter expands passively (in this case, with shear-induced vasodilation), achieving a larger-diameter lumen. The increased tensile stress (via the law of Laplace) triggers remodeling of the vessel wall, with hypertrophy of smooth muscle cells and increased extracellular matrix production. This stress-induced remodeling of the vessel wall has the dual effect of *1*) entrenching the vessel at this new, larger diameter and *2*) re-attaining the native mechanical properties of the vessel [239]. Such a mechanism may be at play here.

An understanding of the complex interplay between leaflet dimension and mechanical properties during mitral valve remodeling will require more detailed histological and biochemical analyses. Expansion of the leaflet with a biphasic change in extensibility could involve changes in leaflet thickness, collagen architecture, or even the intrinsic properties of the leaflet collagen itself (e.g., via crosslinking). Evidence suggests that all three of these factors are affected by pregnancy. Further studies will elucidate the contribution of these structural and material factors to the pregnancy-induced remodeling of the mitral leaflet. In particular, quantitative histological data on the biphasic changes in collagen crimp and leaflet thickness during pregnancy will allow us to examine their potential contributions to the biphasic changes in leaflet extensibility. In addition, biochemical and small-angle light scattering analyses are underway that will map pregnancy-related changes in composition and collagen fiber orientation over the entire leaflet area.

This study has also demonstrated, for the first time, an increase in the number of attachments of chordae tendineae on the mitral anterior leaflet as part of an adaptive remodeling response. This emphasizes that chordae, like leaflets, are dynamic, remodeling structures. This observation is in agreement with a previous study [241] that suggested that mitral valve chordae have fibroblasts capable of remodeling an extracellular matrix that appears, as in tendon, to be matched to physiological loading conditions. Increases in leaflet stresses during pregnancy would inevitably translate into elevated tensile stresses in the supporting chordae, triggering this interesting adaptive response of increased chordae attachments. Our observations raise questions regarding the mechanism underlying the increase in the number of chordal attachments during pregnancy-induced remodeling of the anterior leaflet. One possibility is that existing chordae split, beginning at their ventricular attachment site, as the leaflet surface expands. Further studies in our laboratory are investigating structural and mechanical alterations to the mitral valve chordae during pregnancy.

The increase in the number of chordal attachments during pregnancy did not quite keep in step with the increase in leaflet area. Thus, there is an overall decrease in chordae density during pregnancy that may result in further elevations of chordae stresses beyond those created by elevated leaflet stresses. This suggests that the process of increased chordae attachments (by chordal splitting or otherwise) may be unable to keep pace with the maternal cardiac adaptations to pregnancy (i.e., expansion of valve orifices and leaflet areas).

The remodeling of the mitral valve in pregnancy parallels some of the changes observed with pathological LV dysfunction. This is not surprising since many of the normal effects of pregnancy can resemble mild cardiac failure [181]. Indeed, the cardiovascular changes associated with pregnancy may unmask preexisting heart conditions or precipitate new onset heart failure [242]. It has been proposed that the altered cardiac structure and function in heart failure, which (as in pregnancy) leads to increased stresses on the mitral valve leaflets, induces “dysfunctional” remodeling of the tissue [197]. In patients with functional mitral regurgitation due to LV dysfunction, mitral valve leaflets enlarge, lengthening along their midline [237], increasing leaflet area by up to 35% [185]. In addition to these geometrical changes, leaflet composition [183, 184, 186] and

mechanical properties are altered in heart failure, with leaflets becoming stiffer, less extensible, and less viscous [197]. Grande-Allen and coworkers [197] proposed that in adaptation to LV dysfunction, mitral leaflets become permanently distended, thereby reducing extensibility and leading to decreased coaptation and mitral regurgitation. Thus, in these pathologies, the valve initially adapts to the increased size of the cardiac chambers and valve orifices, but with stiffened leaflets, this compensatory mechanism becomes insufficient, leading to mitral regurgitation [185, 243].

One important difference between human pregnancy and heart failure, however, is that mitral regurgitation becomes significant in heart failure [217] but not in pregnancy [168, 222]. The results of the present study raise the intriguing possibility that the reversal of extensibility (i.e., an increase back to NP properties) of the enlarged leaflets in LP contributes to the maintenance of coaptation. This may be the mechanism under which mitral regurgitation is largely uncommon in pregnancy, despite the large increase in valve orifice area [168, 222]. That is, with volume loading and valve orifice expansion, the mitral leaflet may not maintain coaptation simply due to its functional reserve but by adaptive remodeling and tissue growth that increases the size and alters the material properties of the leaflet. It is important to note, however, that we have no evidence of preserved mitral function in our bovine model, and we can only speculate that the same remodeling mechanism is at play in other species, including humans.

Further evidence for remodeling of the mitral leaflet during pregnancy was provided by our observation of a rapid decrease in the thermal stability of the tissue. In the present study, T_d of the anterior mitral leaflet decreased by over 2°C in EP. While the magnitude of this decrease may seem small, it is on the order of changes (increases) in T_d that are seen in cardiovascular tissues (in the pericardium [102] or heart valve leaflets [244]) during development, presumably as the collagen network matures and turnover decreases.

T_d is a measure of the hydrothermal stability of the collagen triple helix and is influenced by number of factors, including the degree of intrahelical hydrogen bonding, intrahelical crosslinking, and molecular packing. The latter factor, as described by the polymer in a box model [114], influences the molecular stability of collagen through the packing and proximity of surrounding molecules and is suspected to underlie the changes in T_d

observed with hydration [97]. Decreases in the thermal stability of collagen with mechanical loading conditions are also explained by this mechanism, where decreases in molecular packing (associated with increased collagen synthesis and turnover) are reflected by lower thermal stability of the tissue. In our previous study on perinatal heart valve development [244], we observed such changes in T_d after birth, when mechanical loading changes differentially between the aortic and pulmonary valves. The relationship between thermal stability and mechanical loading conditions is also seen in the adult heart, where leaflet T_d varies inversely with the maximum transvalvular pressure for that valve [101]. While these studies can only infer about the state of the collagen network from its thermal stability, studies from Merryman and coworkers [42, 245] directly demonstrated the relationship between transvalvular pressure and the tissue remodeling state: collagen synthesis is higher and valvular interstitial cells have a "more pronounced ability to remodel valvular tissues" under higher transvalvular pressures. Thus, extending the polymer in a box model to our data suggests that the thermal stability of the mitral leaflet decreases as a result of the increased collagen remodeling and/or turnover that would be expected to accompany the increased mechanical loading conditions on this tissue during pregnancy.

In keeping with previous work, this study examined the ratio of immature-to-mature crosslinking as a proxy for the proportion of more recently synthesized collagen and, hence, the "remodeling state" of the tissue. Thus, a higher proportion of immature crosslinks indicates a more rapid turnover rate of collagen [98, 244]. Treatment of our tissues with $NaBH_4$ significantly increased HIT $t_{1/2}$ for tissues from all pregnancy groups, indicating the presence of thermally labile, immature crosslinks. However, the magnitude of this increase was, surprisingly, unchanged across pregnancy groups, suggesting that the proportion of immature collagen crosslinks remains similar with pregnancy. In addition, the relative increase in isothermal $t_{1/2}$ after $NaBH_4$ stabilization was small (increased by less than a factor of 2) compared with other studies (e.g., a 25-fold increase in the ovine pericardium during development [102]), suggesting that the content of immature crosslinks remains relatively low throughout pregnancy. This was an extremely surprising observation. The present study has clearly shown that the anterior mitral valve leaflet undergoes rapid and complex alterations in its structure and mechanical properties

during pregnancy. While this elevated remodeling state results in a lower thermal stability, as expected, it apparently does so with no change in the proportion of immature crosslinking.

One potential explanation for this observation is that we may have underestimated the relative proportion of immature collagen crosslinking using HIT with the $NaBH_4$ stabilization technique. This method uses the ratio of thermally labile to borohydride-stabilized collagen crosslinks as an indicator of the ratio of immature to mature crosslinks. As we have previously pointed out [244], these two ratios are not synonymous. While hydrothermally stable crosslinks include mature crosslinks HHL and PYD, they also include the intermediate immature crosslink DHLNL, leaving only the intermediate crosslink HLNL as the truly hydrothermally labile crosslink. The thermal stability of the immature crosslink DHLNL would result in an underestimation of the immature-to-mature crosslink index assessed by HIT. It has recently been reported that valvular tissues contain relatively more ketoimine-derived crosslinks (including the thermally stable intermediate DHLNL as well as PYD) than aldimine-derived crosslinks (HHL and HLNL). Therefore, immature crosslinks may indeed be present in large amounts in the mitral anterior leaflet, and may be increasing during pregnancy, but the majority of them may be of the DHLNL form and thus undetectable using our technique. Further studies on mitral leaflet collagen crosslinking during pregnancy must be carried out using direct HPLC techniques.

While this study clearly demonstrated rapid and significant remodeling of the mitral anterior leaflet during pregnancy, we were not able to separate the roles of hemodynamic stresses and hormonal changes as potential triggers of this remodeling. The relationship between pregnancy hormones and tissue remodeling is complex and difficult to define, given the potential influence of plasma hormone levels and the presence of hormone receptors in the tissue of interest and receptor sensitivity. Nonetheless, hormonal changes during pregnancy have demonstrable effects on the remodeling of both reproductive and non-reproductive tissues. Growth hormone [246], estrogen [247], and relaxin [194] can trigger tissue remodeling, modulating the deposition and/or degradation of the extracellular matrix. These pregnancy hormones, which target collagen (the predominant structural load-bearing component of heart valve leaflets), would be of particular interest.

In summary, we demonstrated physiological, adaptive remodeling of the anterior mitral valve leaflet during the volume loading and cardiac expansion of bovine pregnancy. There was a rapid increase in leaflet area with a concomitant decrease in extensibility in EP, changes that parallel those in heart failure. There was also a surprising increase in the number chordal attachments that might accommodate the inevitable increases in chordal stresses. In LP, leaflet extensibility then increased, largely in the radial direction, back to its pre-pregnant value. This remodeling may serve to compensate for the increased physiological loading conditions associated with pregnancy by normalizing leaflet stress and maintaining coaptation. Understanding the mechanisms of mitral valve physiological remodeling in pregnancy could contribute to the development of alternative treatments of mitral valve pathological remodeling associated with LV dysfunction, where valve coaptation is not maintained. An understanding of these mechanisms will also be fundamental to the field of tissue engineering as it strives to direct the proper growth and function of heart valves and other load-bearing tissues.

2.5 Acknowledgements

The authors thank Dr. J. Michael Lee (School of Biomedical Engineering, Dalhousie University) and Dr. Michael S. Sacks (Department of Bioengineering, University of Pittsburgh) for the valuable input on the study as well as O.H. Armstrong Food Services for the supply of bovine tissues.

2.6 Author Contributions

Author contributions: SMW, CMP, and ADM conception and design of research; CMP and ADM performed experiments; SMW, CMP, and ADM analyzed data; SMW, CMP, and ADM interpreted results of experiments; More specifically, experimentation, analysis of data, and interpretation of results were performed largely performed by ADM in his MASc research (mitral valve biaxial mechanical and hydrothermal testing), and supplemented by data from CMP (cardiac size, leaflet morphology, and histology properties); SMW and ADM prepared figures; SMW and ADM drafted manuscript; SMW and CMP edited and revised manuscript; SMW, CMP, and ADM approved final version of manuscript

CHAPTER 3

Pregnancy-Induced Remodeling of Collagen Architecture and Content in the Mitral Valve

Caitlin M. Pierlot[1], J. Michael Lee[1,2], Rouzbeh Amini[3], Michael S. Sacks[4], and Sarah M. Wells[1],

[1]School of Biomedical Engineering, Dalhousie University, Halifax, Nova Scotia, Canada;

[2]Department of Applied Oral Sciences, Dalhousie University, Halifax, NS, Canada;

[3]Department of Bioengineering, University of Pittsburgh, Pittsburgh, PA, USA;

[4]Department of Biomedical Engineering and the Institute for Computational Science and Engineering, University of Texas at Austin

3.1 Introduction

Dramatic increases in blood volume and cardiac dimensions occur during pregnancy [136, 157, 248] as the maternal circulation accommodates the developing placental circulation. In humans, blood volume increases by approximately 40% during gestation, triggering left-ventricular hypertrophy and enlargement of the atrial and ventricular chambers [136, 157, 166, 170, 248]. Heart valve annular dilatation also occurs during pregnancy, with the orifice area of the mitral valve in humans increasing by up to 12% [157]. Annular geometry strongly affects the strains and stresses experienced by the collagen and elastin network of valve leaflets *in vivo*, particularly in the central region of the leaflet [236, 249]. Thus, annular dilation causes a substantial increase in the radius of curvature of the closed leaflet and, by the law of Laplace, the tension across the closed valve is significantly increased. Furthermore, this rise in tension is much greater than the rise in orifice area. Finite element models predict that an 18% increase in orifice area (similar to that observed in pregnancy) would result in a 40-50% increase in tensile stress in the anterior mitral valve leaflet, and a more than 60% increase in tensile stress in the belly of the leaflet [211]. Interestingly, mitral valve regurgitation, generally due to mitral valve prolapse with incomplete leaflet coaptation, is relatively uncommon in pregnancy [168, 222]. This might be explained by the mitral valve's large functional reserve: a surplus of the coaptation surface area that allows annular expansion without development of regurgitation [157, 224]. Another possible explanation, however, is that the mitral valve leaflets undergo adaptive remodeling during pregnancy.

To investigate this possibility, we previously examined the changes in bovine mitral valve dimensions and mechanical properties during pregnancy [236, 248, 249]. A bovine model was used due to important similarities to humans in singleton birth deliveries, hemodynamic changes and hormone levels [139, 211, 225, 250, 251], and gestational period [252, 253]. As well, the stage of bovine pregnancy can be estimated using the crown-to-rump length of the fetus [227]. That study showed, for the first time, significant adaptive remodeling of the bovine mitral valve during pregnancy, with striking increases in leaflet size and chordal attachments, as well as a biphasic change in leaflet extensibility [248]. Leaflets enlarged uniformly in both the radial and circumferential directions, resulting in a 33% increase in leaflet area, with a surprising 25% increase in

the number of chordae tendineae attachments into the ventricular surface. It is interesting that leaflet mechanical properties did not change in time-step or direction with leaflet geometry. Instead, leaflet extensibility rapidly decreased by 30% (leftward shift in the tension-stretch curve) in early pregnancy, then, remarkably, increased linearly over the remainder of gestation, returning to pre-pregnant mechanics by late pregnancy.

The results of our previous study led to the hypothesis that remodeling of the mitral valve anterior leaflet during pregnancy involves two phases. In early pregnancy, the leaflet enlarges, attaining its new anatomical/dimensional set-point corresponding to the increased orifice area. In late pregnancy, the enlarged leaflet dimensions are maintained while extensibility then increases (largely in the radial direction), back to pre-pregnant values by term. The trigger for this remodeling may be the increased stress in the leaflet that must accompany its enlargement. Late pregnancy may then represent the phase where the valve leaflet becomes "entrenched" at increased dimensions and, as it remodels toward normalizing leaflet stress, re-attains its pre-pregnancy mechanical properties. The reversal of extensibility (i.e., an increase back to pre-pregnant values) in late pregnancy could contribute to the maintenance of coaptation, and may be the mechanism via which mitral regurgitation is prevented in pregnancy, despite the large increase in valve orifice area [168, 222].

The purpose of the present study then, was to relate changes in leaflet size and mechanical properties (assessed in our previous study) to changes in the structural components of the leaflet, with a particular focus on collagen. Given the complex interplay between leaflet dimension and mechanical properties during mitral valve remodeling, detailed histological and biochemical analyses were called for. Expansion of the leaflet with a biphasic change in extensibility could involve changes in the thickness of the leaflet or it's individual layers, collagen fiber architecture, and/or collagen content. Thus, we sought to (i) determine changes in collagen fiber orientation (alignment and preferred direction), collagen crimp, thickness of the leaflet and its individual layers, and collagen content (total and acid/pepsin-soluble) during pregnancy, and to (ii) relate these changes to the previously observed pregnancy-induced changes in leaflet size and mechanical properties [248].

3.2 Methods

3.2.1 Tissue Harvest and Sample Preparation

All protocols for the harvesting of bovine tissues were approved by the University Committee on Laboratory Animals (UCLA) at Dalhousie University. The hearts of young female cattle were purchased as food from a local abattoir (Armstrong Food Services Limited, Kingston, Nova Scotia, Canada) immediately following slaughter. Hearts were collected from heifers (female cattle of sexual maturity which had never been pregnant), and from pregnant cows. To assess gestational age in pregnant cattle, fetal crown-rump length was measured, with a full term (278-290 days gestation) bovine fetus measuring approximately 100 cm [227]. Pregnant animals ranged in gestational age from 61 days (9 cm fetal length) to full term (98 cm fetal length).

All cattle were under 30 months of age, and due to imposed federal food regulations at Canadian Abattoirs, animals were inspected by a federally licensed meat inspector such that any animals exhibiting signs of illness were excluded from collection (Canadian Food Inspection Agency, CFIA). Cattle were divided into two groups: non-pregnant (NP), and pregnant (P) based on their reproductive status at slaughter.

Since the mitral valve displays differing structural properties between leaflets, with higher stresses experienced in vivo by the anterior leaflet [186, 228], all experiments used this leaflet. It was excised as close to the valve root as possible. Leaflets were washed with Hanks' physiological solution (pH 7.4) including 6 mg/l trypsin inhibitor (lyophilisate), and an antibiotic-antimycotic agent containing 10,000 units/ml of Penicillin G, 10 mg/ml streptomycin sulphate, and 25 μg/ml amphotericin B (Sigma-Aldrich Canada, Oakville, ON, Canada).

3.2.2 Small-Angle Light Scattering

Mitral valve leaflets from 4 non-pregnant heifers and 5 pregnant cows were fixed from fresh by immersion in 10% neutral buffered formalin for a minimum of 72 h, then prepared for small-angle light scattering (SALS) analysis of tissue fibrous structure. To increase translucency of tissues for optical SALS measurements, specimens were dehydrated and cleared in a graded glycerol/water solution (formalin → ethanol → water

→ glycerol), then stored in a final solution of 100% glycerol for transport to University of Pittsburgh for SALS measurement. The entire leaflet was mapped and separated into three regions using data from five different areas (Fig. 3.1): (i) Free-edge (regions 1 & 2), (ii) Belly (region 3), and (iii) Fixed-edge (regions 4 & 5).

The SALS protocol has been detailed previously [254-256]. Briefly, a non-polarized 4 mW HeNe laser (λ = 632.8 nm) is passed through the valve leaflet tissue. Scattering of photons from internal fiber structure produces a light intensity distribution ($I(\phi)$), which captures the distribution of fiber angles within the tissue. The degree of fiber orientation is proportional to the width of the intensity distribution and is expressed via the orientation index (OI): the angle range (from 0° to 180°) that contains one half of the total area under the $I(\phi)$ distribution and thereby represents 50% of the total fibers (Fig. 3.2). To clarify the physical interpretation for this index, a normalized orientation index (NOI) was calculated and exclusively used in the present study:

$$\mathrm{NOI} = \frac{90° - \mathrm{OI}}{90°} \times 100\ \%$$

NOI ranges from 0 % (completely random) to 100 % (completely aligned) fiber network, providing an indicator of the degree of fiber alignment [233, 257-259]. High NOI values are characteristic of highly oriented fiber networks (narrow distribution peak), and low NOI values indicate less oriented, more random networks (broad distribution peak). The centroid of the fiber distribution obtained from the SALS data (ϕ_c) is indicative of the preferred fiber direction (ϕ_p) of the internal fiber network, although rotated by 90° from that direction. Comparison of the scattered light intensity distribution (NOI), and preferred fiber direction (ϕ_p), between non-pregnant and pregnant animals was used to determine whether collagen fiber reorientation is occurring in pregnancy.

3.2.3 Histological Analysis

For histological analysis, valves were collected from another set of animals. Leaflets from 22 animals (9 non-pregnant heifers and 13 pregnant cows) were divided to produce two symmetric halves of the leaflet (Fig. 3.3), both fixed from fresh in 10% neutral buffered formalin for a minimum of 72 h, dehydrated in 70% ethanol, embedded in paraffin, sectioned into 5μm serial sections, mounted on slides, and dried at 57°C for a

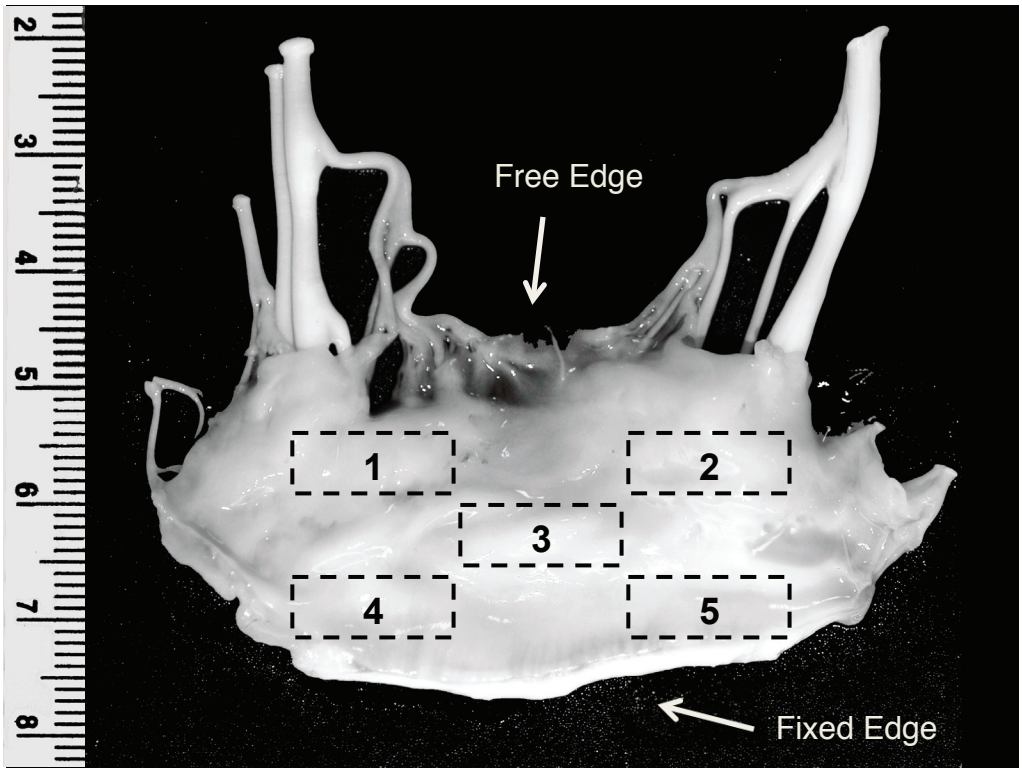

Figure 3.1 Leaflet regions used for SALS analysis

Image of an isolated heifer mitral valve leaflet: Orientation index for SALS analysis was examined in five regions of the anterior mitral valve leaflet: two nearer the free-edge (regions 1 & 2), two nearer the fixed edge (regions 4 & 5), and one centered in the belly region (region 3) of the leaflet. Ruler scale is in cm.

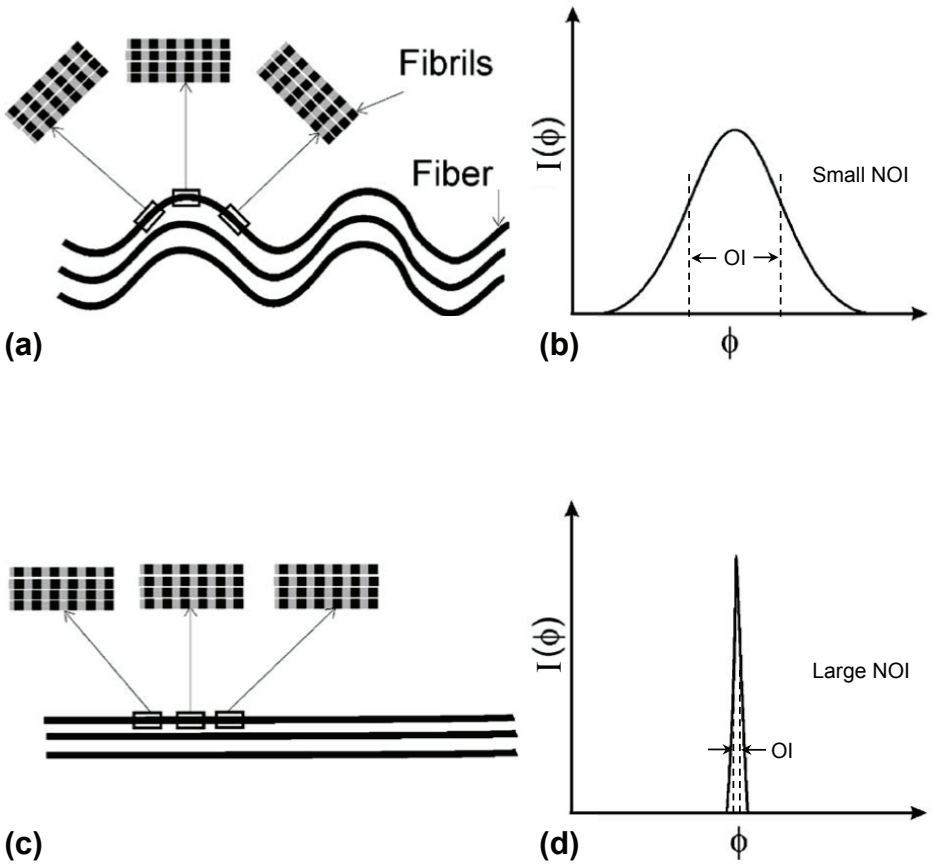

Figure 3.2 Schematic showing the contribution of crimp to SALS OI

Schematic exhibiting contributions of collagen crimp to scattered light distribution (I(φ) and orientation index (OI) as measured by SALS: (a) small-scale, local changes in fiber orientation due to crimp, (b) corresponding broad intensity peak with a large OI (small NOI), (c) straightened or stretched fiber, and (d) corresponding narrow intensity peak with small OI (large NOI). Alternating light and dark bands depicted in (a) and (d) represent the periodic arrangement of collagen fibers (D-bands). This figure was modified with permission from Liao et al., Figure 9, page 85 [233].

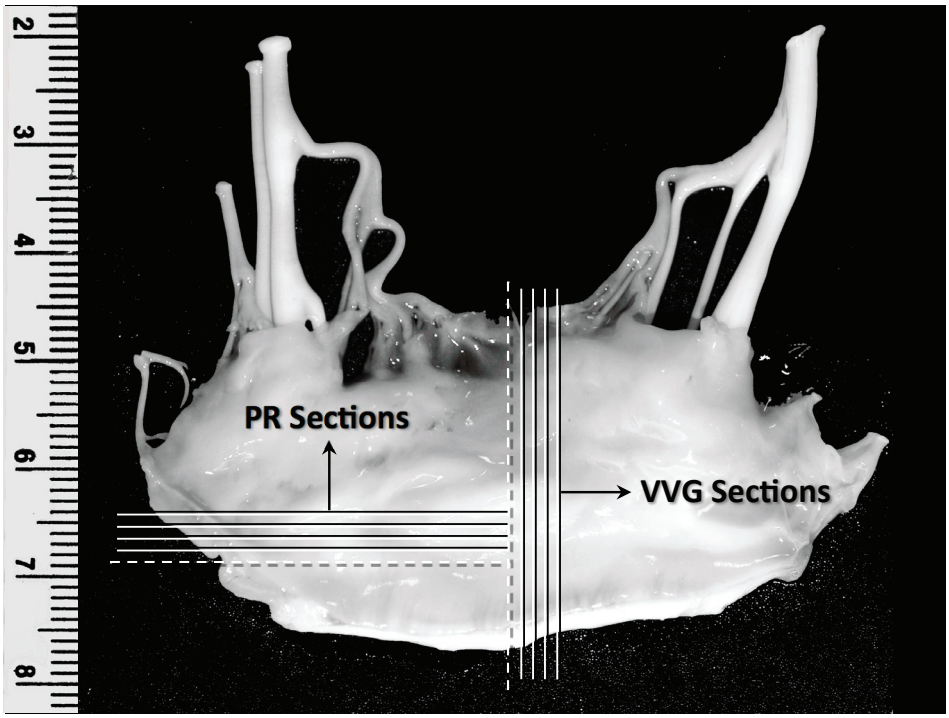

Figure 3.3 Histological sectioning of leaflet tissues

Histological sectioning: Each leaflet was dissected along the dotted lines to divide the leaflet in half and expose the belly region for sectioning. 5 μm serial sections were cut starting at the dotted lines to obtain circumferential sections for picrosirius red (PR) staining to examine collagen alignment and crimp, and radial sections for Verhoeff-Van Gieson (VVG) staining to identify leaflet layering and layer thicknesses. Ruler scale is in cm.

minimum of 24 hours. Embedding and sectioning was performed by the Histology Research Services Laboratory (Faculty of Medicine, Dalhousie University). Circumferential cross-sections were cut from one half of the leaflet for picrosirius red (PR) staining to examine collagen alignment and crimp. Radial cross-sections were cut in the other half of the leaflet for Verhoeff-Van Gieson (VVG) staining to identify leaflet layering (Verhoeff-Van Gieson Elastin Staining Kit, Polysciences, Inc., Washington, PA) (Fig. 3.3). Each radial section contained the complete leaflet cross-section from the free edge to the fixed edge. For both staining protocols, sections were deparaffinized in xylene and rehydrated in graded ethanol/water solutions. For picrosirius red staining protocol, circumferential sections were stained for 1 h with 0.1% Picrosirius Red solution, followed by several water washes. For Verhoeff-Van Gieson staining, radial sections were stained for 1 hour with Verhoeff's solution, differentiated in 2% ferric chloride for 1 minute, followed by several water washes. All stained slides were then dehydrated in ethanol and cleared in xylene for mounting.

3.2.4 Collagen Crimp Analysis

Images were taken using a Nikon Eclipse E600 light microscope equipped with a polarizer and a 10MP AmScope digital camera. Collagen crimp was characterized by two measures: (i) crimp length, peak-to-peak measurement of crimp period, and (ii) the percentage of leaflet area which was crimped. For both measures, 6 adjacent images were taken at 40x objective magnification along the circumferential direction, spanning 2 mm of the belly region of the leaflet, and analyzed using ImageJ software (National Institutes of Health). For crimp length measurements, a line was drawn across the centerline of each image (through the center of the image, aligned to the principal crimp direction) and every distinguishable crimp length along that line was recorded (Fig. 3.4). For crimped area measurements, a grid (300 μm^2/square) was placed on each image. The number of grid points in contact with crimped tissue, as well as the total number of grid points in contact with tissue (crimped or uncrimped) was recorded. The ratio of crimped-to-total grid points was then used to calculate the area percentage of the leaflet occupied by crimped. Both crimp length and crimped area were averaged across all 6 images. Blinded measurements were made by three observers, with excellent agreement between observer counts.

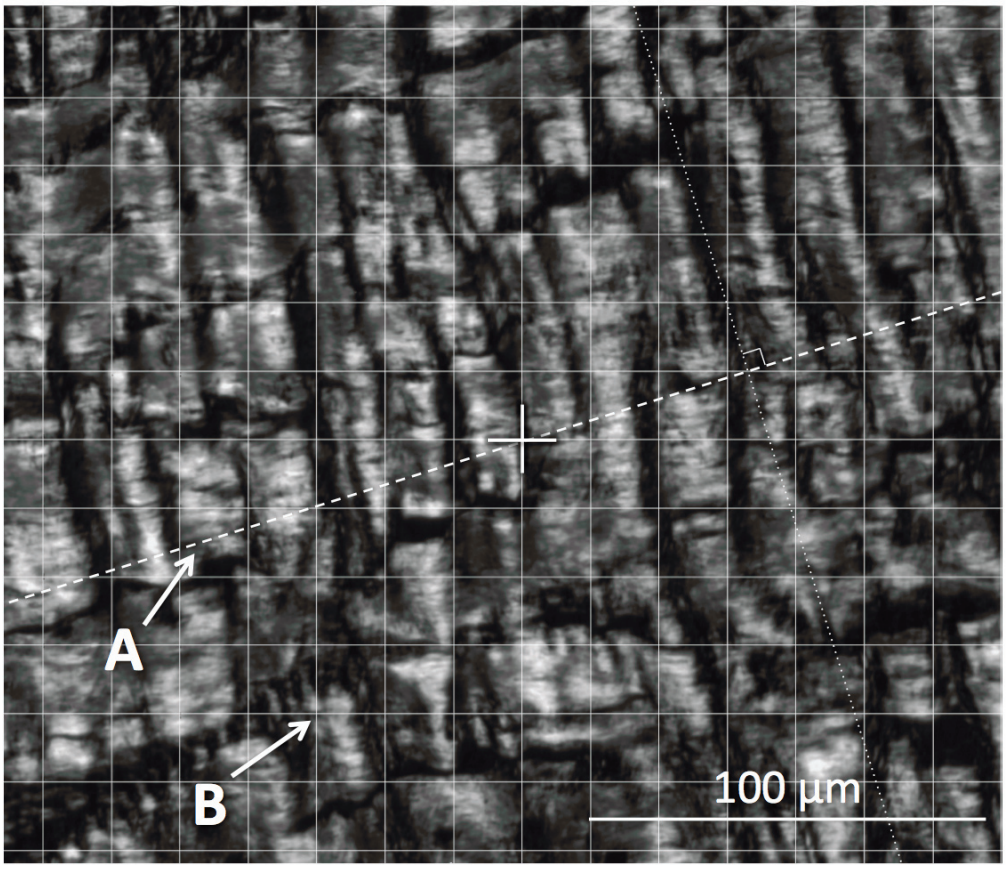

Figure 3.4 Methodology for collagen crimp measurement

Collagen crimp measurement: Crimp length measurements in each image were taken along a line passing through the center of the image and normal to the crimp direction (A), and averaged across all 6 adjacent images. Crimped area measurements were taken at each intersection of gridlines (B), as the ratio of crimped-to-total grid points (grid = 300 μm^2/square) across consecutive images, to calculate the area percentage of the leaflet occupied by crimp.

3.2.5 Leaflet and Layer Thicknesses

VVG stained sections were photographed at low magnification (using a 5x or 10x objective) along the entire length of the valve leaflet, using a Zeiss Axioplan 2 Imaging Microscope (Cellular & Molecular Digital Imaging Facility, Faculty of Medicine, Dalhousie University) and analyzed using AxioVision software (Release 4.8.1). ImageJ imaging software plugins MosaicJ [260] and TurboReg [261] were used to stitch together one large mosaic image for each sample. An array of lines was placed on each mosaic such that 25 vertical lines transected the full thickness of the tissue along the length of the leaflet (Fig. 3.5). Thickness measurements, of the full leaflet as well as of each layer, were taken at each gridline. From these measurements the following parameters were extracted: total thickness, fibrosa thickness, spongiosa thickness, and atrialis thickness. Thickness measurements were then averaged across the length of the leaflet for each valve sample, producing these same four parameters for each individual valve leaflet.

3.2.6 Collagen Content

For each biochemical assay, valves were collected from yet another set of animals: 25 hearts (10 non-pregnant heifers and 15 pregnant cows) for hydroxyproline collagen assay, and 24 hearts (9 non-pregnant heifers, and 15 pregnant cows) for Sircol collagen assay. Heart valve leaflets for both collagen assays were excised, wrapped in cheesecloth soaked in Hanks' physiological solution, placed immediately in the -86°C freezer, and stored until they could be tested. The first set of frozen leaflets were freeze-dried for a minimum of 52 h. Dry samples of approximately 10 mg dry weight, from the belly region of the leaflet, were weighed and recorded. Total collagen content was estimated using the hydroxyproline assay described by Woessner [262]. Assay product was read using a microplate reader (Synergy HT, Bio-Tek Instruments Inc., Winooski, Vermont) to measure dye absorbance at a wavelength of 561 nm. Comparison of sample absorbance to a generated standard absorbance curve was used to quantify the hydroxyproline present in each leaflet sample. The quantity of collagen in each sample,

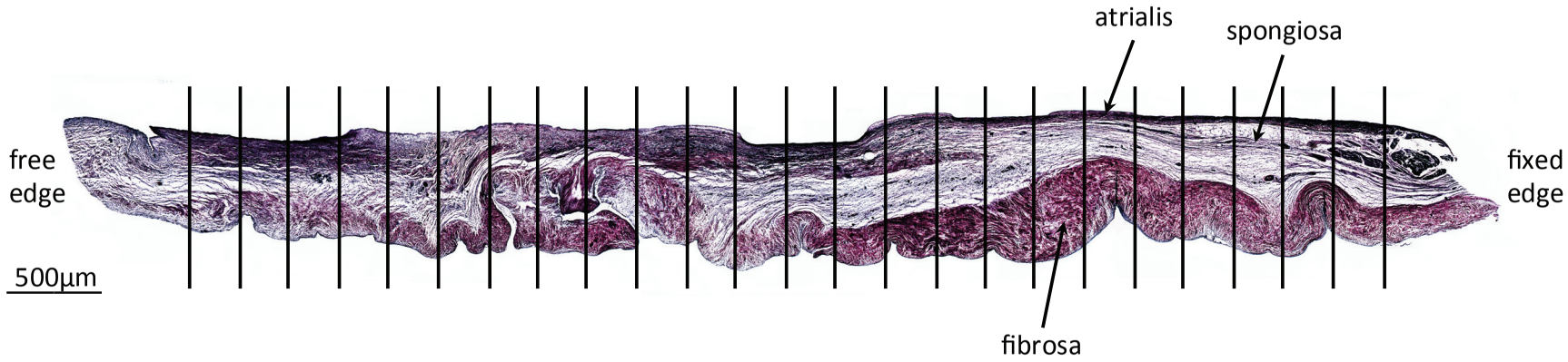

Figure 3.5 Methodology for leaflet and layer thickness measurements

Leaflet and layer thickness measurements (mitral valve anterior leaflet): An array of 25 vertical lines, normal to the leaflet surface, was placed on each mosaic of the complete leaflet section, with lines transecting the full thickness of the tissue along the length of the leaflet, from the fixed edge to the free edge. Thickness measurements, of the full leaflet as well as each layer, were taken at each line and then averaged across the length of the leaflet for each valve sample.

normalized to dry weight, was determined by dividing the quantity of hydroxyproline by 0.1277, based on a study by Keeley et al. [263].

The Sircol Collagen Assay Kit (Biocolor Ltd., Carrickfergus, UK: Accurate Chemical & Scientific Corporation, Westbury, NY, USA) was used to assess the content of acid and pepsin-soluble collagen. This extractable form of collagen is often interpreted to be newly laid down collagen that is not sufficiently crosslinked into the network to resist solubilization. For this study, the second set of frozen leaflets were thawed and dissected to take samples from the belly of the leaflet, and weighed prior to testing. All samples were assayed in duplicate for extractable collagen, and compared to a set of blanks and standards. Following the assay, a microplate reader (Synergy HT, Bio-Tek Instruments Inc., Winooski, Vermont) was used to measure the dye absorbance of each prepared plate at 555 nm. Dry weight measures of extractable collagen were calculated using the wet/dry weights from each valve.

3.2.7 Statistics

All results are expressed as the mean ± standard error of the mean (SEM), with the n value representing the number of animals per group. All data is divided into two groups: NP (non-pregnant), and P (pregnant). Statistical comparisons were made using t-Test comparisons between the two groups. The pregnant group was also further divided into EP (early pregnant) and LP (late pregnant) groups according to fetal crown-to-rump length: Cows carrying fetuses of crown-to-rump length < 45 cm (0–169 days) were classified as EP, and those carrying fetuses > 55cm (193–270 days) were classified as LP – the mid-pregnancy group of 45–55 cm (169–193 days) was omitted in this comparison to obtain a more accurate separation of early and late groups. A one-way ANOVA was performed, followed by Tukey honestly significant difference comparisons among the three groups (NP, EP, and LP). To evaluate changes in any parameter as a function of pregnancy duration, data were plotted as a function of gestational age and fitted with a least-squares linear regression. None of our measurements from the current study showed significant correlations with pregnancy duration (fetal length or early versus late pregnancy), as in our earlier study [248]; however, significant differences were detected between the grouped pregnant animals and non-pregnant animals. For this reason, data

from this study and from our previous study are presented here as mean values for pregnant (P) and non-pregnant (NP) animals. For analysis of the SALS data, statistical comparisons were made in each of the three regions of the valve leaflet. All statistics presented are two-tailed t-test comparisons between the non-pregnant and pregnant groups. For each of SALS, histology, hydroxyproline, and Sircol assays, tissue was collected from a separate set of animals, therefore statistics are unpaired.

Results were considered significant for $p < 0.05$. Outliers were defined as data points falling outside of the following range: [25^{th} quantile – 1.5 × (interquantile range)] to [75^{th} quantile + 1.5 × (interquantile range)], where interquantile range = 75^{th} quantile – 25^{th} quantile. These data points were excluded from further analysis. Two outliers were removed from P % crimp, one removed from P leaflet thickness, one removed from NP atrialis thickness, and one NP removed from total collagen content. All statistical analyses were performed using JMP Statistical Software (Version 10.0, SAS Institute, Inc., Cary, NC).

3.3 Results

3.3.1 Small-Angle Light Scattering

The light-level collagen fiber architecture of the bovine heart valve leaflet was mapped across the entire valve via measurements of the orientation index and preferred fiber direction (Fig. 3.6). Fiber alignment of the leaflets decreased during pregnancy in the belly region of the leaflet only, as indicated by a significant 20% decrease ($p = 0.0174$) in the normalized orientation index (NOI) from non-pregnant (NOI = 45.8 ± 0.5 %) to pregnant (NOI = 36.5 ± 1.9 %) (Fig. 3.7). The orientation indices in the free edge and fixed edge regions were unchanged in pregnancy (Table 3.1). The preferred fiber direction (ϕ_p) was referenced to the circumferential axis of the leaflet from the SALS distribution centroid (ϕ_c) as $\phi_c - 90°$. This is the direction plotted as the small arrows in Figure 3.6. To describe the rotation of preferred fiber direction away from the circumferential direction, the absolute value of the preferred fiber direction was calculated as:

$$\phi_p = |\phi_c - 90°|$$

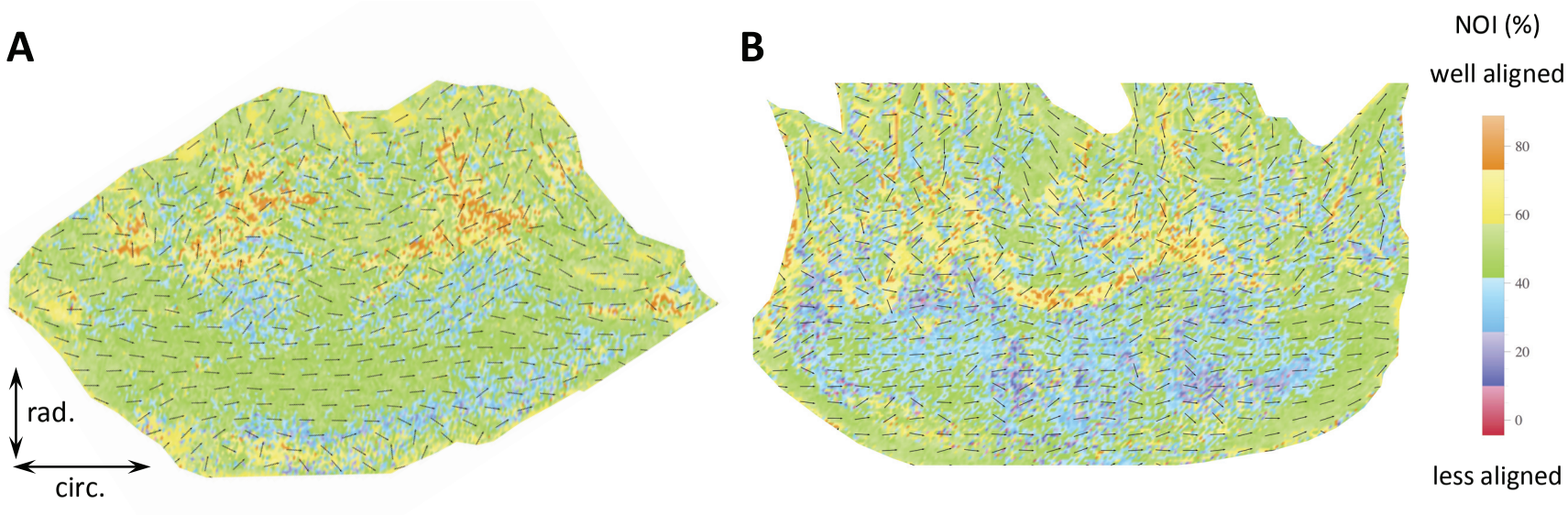

Figure 3.6 SALS color maps of fiber alignment and preferred fiber direction

Color maps of fiber alignment (normalized orientation index, NOI) and preferred fiber direction (ϕ_p; indicated by arrow direction) from the excised anterior mitral valve leaflet for (A) non- pregnant (NP) and (B) pregnant (P) animals. In the belly region of non-pregnant animals, the collagen fiber network was moderately well aligned (green) with a very uniformly, circumferentially aligned preferred fiber direction (horizontal vectors). In the belly region of pregnant animals, fiber alignment is reduced (purple-blue) and there is a loss of the very uniform fiber direction (rotated vectors).

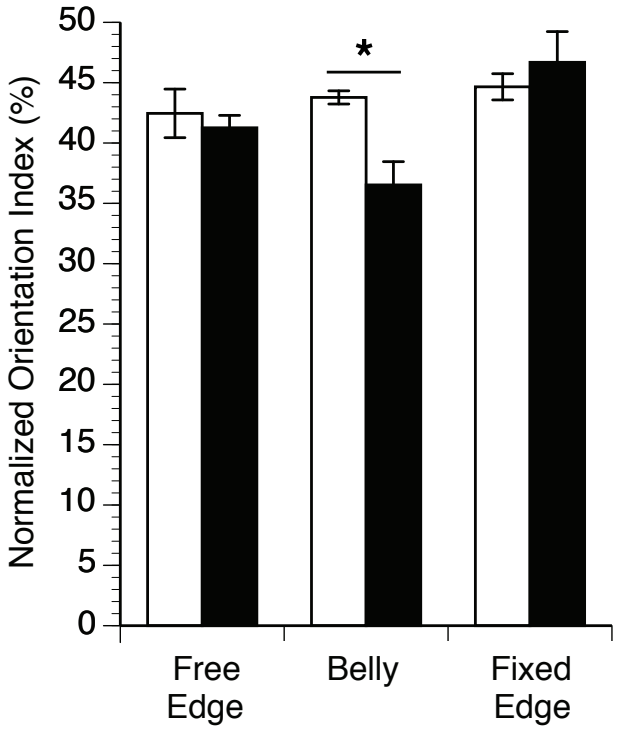

Figure 3.7 Regional normalized orientation index plot (mitral)

Regional normalized orientation index (in percent) of the anterior mitral valve leaflet from non-pregnant (open bars; n = 4) and pregnant (filled bars; n = 5) animals. Bars indicate means ± SE. Statistical comparisons were made in each region (free edge, belly, and fixed edge), between non-pregnant and pregnant groups using two-tailed t-Test comparisons of groups. Columns labeled with an asterisk showed a statistically significant change with pregnancy.

Table 3.1 Changes in small-angle light scattering (SALS) measurements by leaflet region with pregnancy

	Region	Non-pregnant (4)	Pregnant (5)	ΔNOI	p-value
NOI (%)	Free Edge	42.5 ± 2.0	41.3 ± 1.0	–	0.6221
	Belly	43.8 ± 0.5	36.5 ± 1.9	↓	0.0174
	Fixed Edge	44.6 ± 1.1	46.7 ± 2.5	–	0.4944
ϕ_p (°)	Free Edge	15.5 ± 2.6	17.3 ± 3.0	–	0.3294
	Belly	1.8 ± 1.1	13.3 ± 2.9	↑	0.0072
	Fixed Edge	15.8 ± 4.3	13.1 ± 1.9	–	0.7034

Values are means ± SE of regional normalized orientation index (NOI) and preferred fiber direction (ϕ_p) relative to the circumferential direction, for animals in the non-pregnant (NP; n = 4), and pregnant (P; n = 5) groups. Statistical comparisons in each region of the leaflet were made between NP and P groups for each parameter using two-tailed t-Test comparisons and are presented with the corresponding p value.

The collagen fiber bundles of the non-pregnant group were initially closely aligned along the circumferential direction of the leaflet (ϕ_p = 1.8 ± 1.1 °), but rotated somewhat toward the radial axis of the leaflet in pregnancy (ϕ_p = 13.3 ± 2.9 °) (p = 0.0072, Fig. 3.8), in the belly region only.

Together, this radial rotation of fibers and the decrease in fiber alignment, correspond to a larger angular deviation of collagen fibers from the preferred fiber direction (i.e. increased fiber splay). In the free edge and fixed edge regions of the leaflets from the non-pregnant group, collagen fiber bundles were aligned away from the circumferential direction at 15.5 ± 2.6 ° (free edge) and 15.8 ± 4.3 ° (fixed edge) respectively. This structure was unchanged in pregnancy (Table 3.1).

3.3.2 Collagen Crimp

Although the entire valve leaflet was examined for structural changes in the collagen network using the SALS technique, alterations were found only in the belly region of the leaflet. Analysis of picrosirius red-stained samples was therefore conducted in the belly region to determine how changes in collagen crimp were contributing to the apparent increased fiber alignment in that region (Fig. 3.9). A summary of all structural, mechanical, and thermal data obtained for the belly region of the bovine anterior mitral valve leaflet from our present and previous studies [248] are shown in Table 3.2. Collagen crimp results showed a remarkable 186% increase in crimp length (p=0.0079) from non-pregnant (22.9 ± 1.2 μm) to pregnant (65 ± 15 μm) (Table 3.2, Fig. 3.10A). This increase in crimp length was accompanied by a 45% decrease in the percentage of leaflet area occupied by crimped tissue (p=0.0116) from non-pregnant (40.2 ± 6.0 %) to pregnant (22.8 ± 3.0 %) (Table 3.2, Fig. 3.10B).

3.3.3 Leaflet and Layer Thickness

The mitral anterior leaflet thickness was unchanged during pregnancy. However, considering the layers separately, the atrialis became 46% thinner (p = 0.0447), while the fibrosa was 53% thicker (p = 0.0372) (Table 3.2). The spongiosa thickness was not significantly changed in pregnancy.

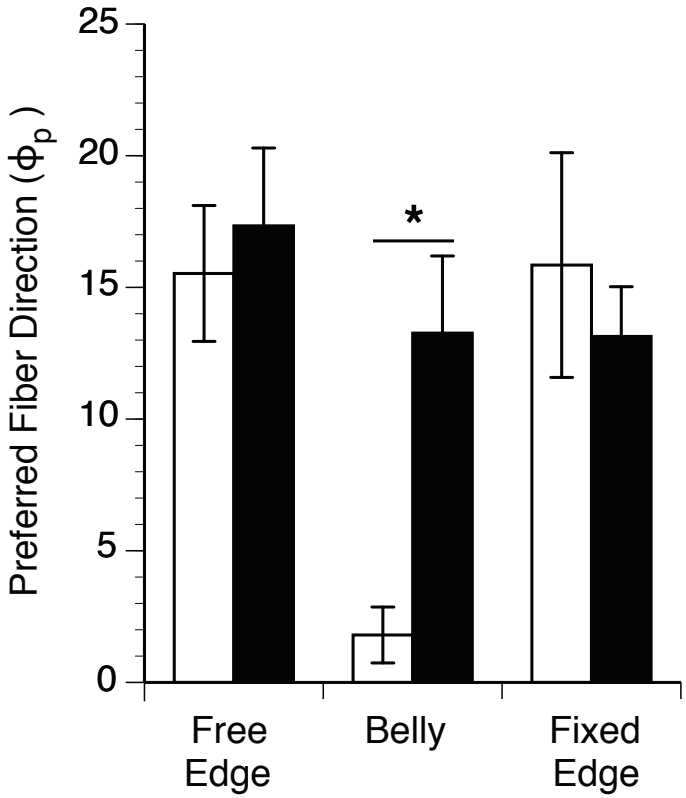

Figure 3.8 Regional preferred fiber direction plot (mitral)

Regional preferred fiber direction (absolute angle in degrees) of the anterior mitral valve leaflet from non-pregnant (open bars; n = 4) and pregnant (filled bars; n = 5) animals. Bars indicate means ± SE. The direction of ϕ_p here is referenced to the circumferential axis. Statistical comparisons were made in each of the five regions, between non-pregnant and pregnant groups using two-tailed t-Test comparisons of groups. Columns labeled with an asterisk showed a statistically significant change with pregnancy.

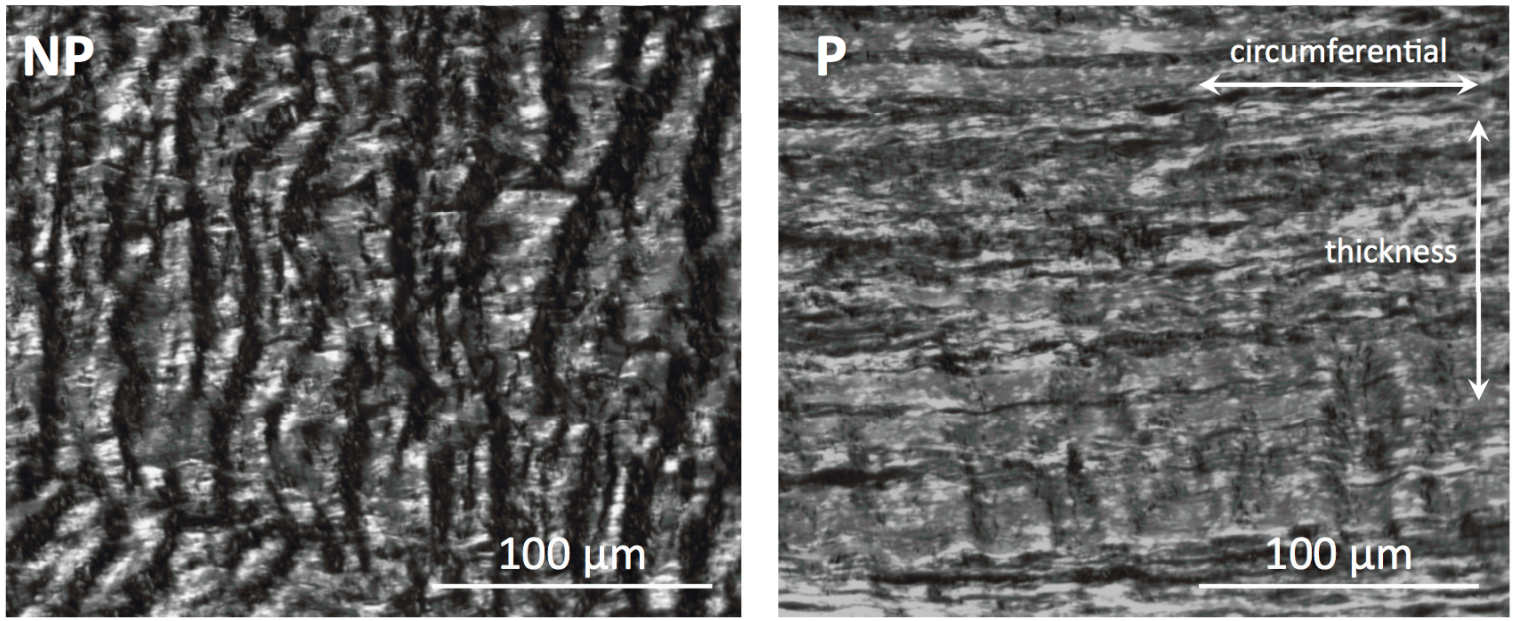

Figure 3.9 Visual comparison of collagen crimp between NP and P animals

Histological sections taken along the circumferential direction under polarized light microscopy in the belly region of the anterior mitral valve leaflet for non-pregnant (NP) and pregnant (P) animals. In non-pregnant animals, the collagen fiber network was highly undulated, covered almost entirely with crimped fibers. In pregnant animals, crimp length was greatly increased and the undulations had virtually disappeared. Leaflet circumferential and thickness axes are indicated by arrows.

Table 3.2 Summary of all changes in mitral anterior leaflet with pregnancy

	Non-pregnant	Pregnant	Δ	p-value
SALS measurements (belly)				
NOI, %	43.8 ± 0.5(4)	36.5 ± 1.9(5)	↓	0.0174
ϕ_p, degrees	1.8 ± 1.1(4)	13.3 ± 2.9(5)	↑	0.0072
Crimp measurements				
Crimp length, μm	22.9 ± 1.2(9)	65 ± 15(13)	↑	0.0079
Crimped area, %	40.2 ± 6.0(9)	22.8 ± 3.0(11)	↓	0.0116
Leaflet dimensions				
Thickness, μm	1170 ± 75(9)	1194 ± 59(11)	-	0.4011
Radial length†, cm	2.5 ± 0.1(11)	3.0 ± 0.1(15)	↑	0.0016
Circumferential length†, cm	5.1 ± 0.1(11)	5.9 ± 0.2(15)	↑	0.0008
Area†, cm^2	11.1 ± 0.6(11)	15.6 ± 0.9(15)	↑	0.0003
Layer thickness, μm				
Fibrosa	540 ± 130(9)	833 ± 76(11)	↑	0.0372
Spongiosa	431 ± 85(9)	346 ± 76(11)	-	0.4694
Atrialis	221 ± 40(8)	135 ± 22(10)	↓	0.0447
Collagen content, % dry wt.				
Total collagen	56.7 ± 3.0(9)	66.0 ± 3.3(13)	↑	0.0256
Extractable collagen	0.6 ± 0.1(5)	0.6 ± 0.1(9)	-	0.6638
Water, % wet wt.	81.4 ± 0.7(10)	80.6 ± 0.6(12)	-	0.4228
Leaflet stretch				
Areal stretch†	2.37 ± 0.09(7)	2.11 ± 0.11(12)	biphasic	0.0439
λ_R^{peak} †	1.67 ± 0.06(9)	1.67 ± 0.06(13)	-	0.9721
λ_C^{peak} †	1.37 ± 0.03(7)	1.26 ± 0.03(14)	biphasic	0.0153
HIT measurements				
T_d†, ºC	68.6 ± 0.2(10)	66.3 ± 0.2(22)	↓	<0.0001
$t_{1/2}$ control†, hours	8.6 ± 1.8(10)	13.6 ± 1.6(19)	↑	0.0144
$t_{1/2}$ treated†, hours	11.5 ± 2.5(7)	17.1 ± 1.7(19)	↑	0.0039
Immature crosslinking index†	1.6 ± 0.2(7)	1.3 ± 0.1(17)	-	0.4385

Values are means ± SE of normalized orientation index (NOI), preferred fiber direction (ϕ_p), crimp length, leaflet crimped area, total leaflet thickness, radial leaflet length, circumferential leaflet length, leaflet area, fibrosa, spongiosa, and atrialis thickness, total collagen content (hydroxyproline assay), extractable (acid/pepsin-soluble) collagen (Sircol assay), water content, areal stretch, peak radial stretch ratio, peak circumferential stretch ratio, denaturation temperature (T_d), and halftime of load decay ($t_{1/2}$), for animals in the non-pregnant (NP), and pregnant (P) groups. Statistical comparisons were made between NP and P groups for each parameter using t-Test comparisons and are presented with the corresponding p value. n values for the pregnancy groups are presented in brackets for each measurement. †Data from Wells et al. [248] for (i) NP animals and (ii) all pregnant animals.

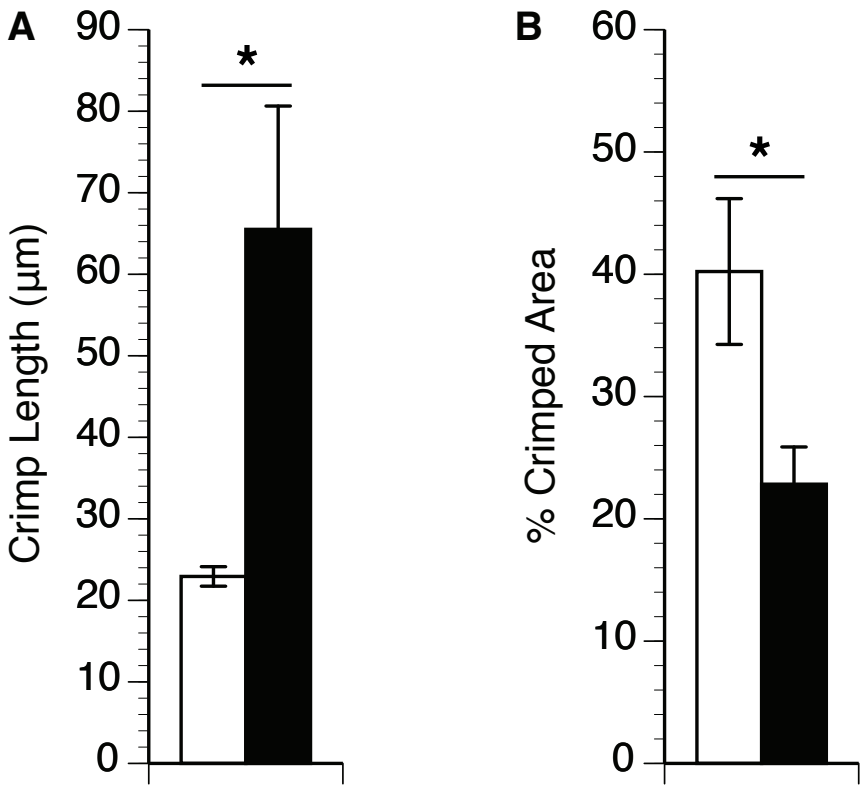

Figure 3.10 Collagen crimp length and percentage of crimp plots (mitral)

Collagen crimp length and percentage of leaflet area occupied by crimped (% Area Crimped) of the anterior mitral valve leaflet from non-pregnant (open bars; n = 9) and pregnant (filled bars; n = 13) animals. A: collagen crimp length (in µm). B: leaflet crimped area (in %). Bars indicate means ± SE. Statistical comparisons were made between non-pregnant and pregnant groups using two- tailed t-Test comparisons of groups. Columns labeled with an asterisk showed a statistically significant change with pregnancy.

3.3.4 Collagen Content

Alongside the increase in fibrosal thickness, mitral valve total collagen content (concentration by hydroxyproline assay) increased by 16% ($p = 0.0256$), from non-pregnant (56.7 ± 3.0 % dry wt.) to pregnant (66.0 ± 3.3 % dry wt.) (Table 3.2). This suggests that collagen was preferentially laid down in the fibrosa. The concentration of acid/pepsin soluble (perhaps newly-synthesized) collagen was very low in non-pregnant animals (0.6 ± 0.1 % dry wt.), and was surprisingly unchanged with pregnancy (Table 3.2). Water content was unchanged in pregnancy.

3.4 Discussion

Pregnancy is a physiological condition characterized by rapid and dramatic increases in blood volume and cardiac dimensions, thereby resulting in significant increases in valve leaflet tension. In our previous study [248], we showed, for the first time, significant pregnancy-induced adaptive remodeling of the anterior leaflet of the bovine mitral valve, with large increases in leaflet size and a biphasic change in leaflet extensibility. Leaflets enlarged uniformly in both the circumferential and radial directions, resulting in a 40% increase in leaflet area. Collagen denaturation temperature decreased 2.4°C, indicative of significant collagen remodeling, while significant increases in HIT load decay for control ($t_{1/2}$-control) and treated ($t_{1/2}$-treated) samples signified increases in both mature and total crosslinking respectively. These findings raised the question of how structural and material factors, such as changes in leaflet thickness and collagen architecture, might be contributing to the mechanisms of pregnancy-induced remodeling of the mitral valve. The present study sought to answer that question.

Despite the large and rapid increases in leaflet area during pregnancy, the gross collagen fiber architecture was largely maintained across the leaflet. However, significant changes in collagen fiber orientation and alignment were observed in the belly region, where there was a decrease in fiber alignment (NOI decreased 17%), with an 11.5° rotation of the preferred fiber direction away from the circumferential axis (toward the radial axis). These structural changes were accompanied by a remarkable loss in collagen fiber crimp, with the percentage area occupied by crimp nearly halved, and the crimp length nearly

doubling. Accompanying these changes was a 46% thinning of the atrialis, and a 53% thickening of the fibrosa, with a 16% increase in total collagen content. We have previously shown that the collagen denaturation temperature, a measure of thermal stability, decreases in pregnancy. This, combined with the leaflet area expansion, fibrosa thickening, and increased collagen content, together signify that new collagen is being synthesized. Curiously, our results indicate that very little newly-synthesized, immature collagen was present in native conditions and during pregnancy. Acid/pepsin-soluble collagen remained low and only a small proportion of immature crosslinking was evident.

As a whole, these results demonstrate that pregnancy provokes rapid remodeling of collagen in the belly of the mitral valve anterior leaflet. It is surprising that none of our structural components paralleled the biphasic changes which we observed in leaflet biaxial extensibility [248]. Instead, the observed structural changes suggest that leaflet extensibility should have been unidirectionally reduced from non-pregnant to pregnant animals. There must be, therefore, some other mechanism occurring in pregnancy, which modulates leaflet biomechanics.

For our studies, we have used a bovine model, which closely parallels many essential features of human pregnancy. Indeed, this is the first study to characterize the collagen fiber network in the bovine mitral valve. We saw close agreement between the results obtained for our non-pregnant animals compared to other animal models: NOI was only slightly higher in the current study (43.8 ± 0.5 %) than has been previously reported for porcine mitral [264], aortic [49, 257, 265], and pulmonary [257] valve leaflets. Preferred fiber direction (1.8 ± 1.1º) runs along the circumferential axis of the valve leaflet, which is in agreement with previous studies in porcine [49, 254, 255, 257, 264, 265], canine [266], and murine models [267]. Crimp length (22.9 ± 1.2 μm) was only slightly higher than that reported for the belly region of native and zero pressure-fixed porcine aortic and pulmonary valve leaflets [257, 268-270], and more recently for porcine mitral valve leaflets [46]. Similar reports of collagen fiber crimp have also been noted in other cardiovascular tissues such as porcine mitral valve chordae [271]), and bovine pericardium [85, 272-275]) which is often used to construct heart valve bioprostheses. Leaflet crimped area (40.2 ± 6.0 %) also closely matches previous studies in porcine

pulmonary and aortic valves under zero pressure-fixation of leaflet tissues [257]. The structure and composition of the bovine anterior mitral valve leaflet is also similar to that in other species. Bovine mitral valve leaflet thickness (1.17 ± 0.08 mm) very closely compares to thickness measurements reported in human [183, 276], ovine [186, 219], and porcine [44, 211, 258, 277] mitral valves. Further, Kunzelman and colleagues [277] reported similar measurements and proportions of leaflet layer thickness in porcine anterior mitral valve leaflets. Collagen content in the present study (56.7 % dry weight) was similar to that in sheep [186] and humans [210, 278, 279], as was water content in humans [210, 279]. These findings support the validity of the bovine model for mitral valve studies, and thereby as a means to examine structural and biochemical changes in the mitral valve anterior leaflet in pregnancy.

Changes in collagen fiber alignment and orientation were observed in the central belly region of the valve leaflet in pregnancy, however no significant changes were found in the fixed edge and free edge regions. First of all, the fixed edge regions of the valve leaflet are reported to be loaded almost uniaxially, radial to the valve annulus [264, 280, 281]. As the valve orifice expands in pregnancy, the loading direction would be relatively unchanged. Thus significant reorientation of fibers is not unexpected here. When addressing the free edge of the leaflet though, one must consider architecture and leaflet function. While the fibrosa is the primary load-bearing layer due to its dense network of circumferentially aligned collagen fibers, it extends from the annulus through only two-thirds of the leaflet. It is completely absent along the free edge [282]. The mitral valve, in particular, has a great deal of redundant tissue in the closed valve position (0.5–1.0 cm in humans), between the coaptation line and free edge of the leaflet (zone of apposition) [218]. Therefore the free edge region of the leaflet would not be subjected to the same pregnancy-induced increase in tensile stresses experienced by the leaflet between the coaptation line and the fixed edge (or the annulus). The absence of altered collagen alignment in the free edge in pregnancy is therefore not surprising, but for a different reason from that in the fixed edge.

While the SALS orientation index reflects changes in the large-scale splay of the collagen bundles, it is also affected by the small-scale, local changes in fiber orientation due to waviness or crimp. The latter effect is shown in Figure 3.2A, where local fiber orientation

varies along the length of a crimped fiber, resulting in a broad intensity peak (Fig. 3.2B) with a small NOI, indicating a low degree of fiber alignment. By contrast, straight fibers (Fig. 3.2C) will generate a single, narrow intensity peak (Fig. 3.2D) with a large NOI, indicating a high degree of fiber alignment. Thus, while the SALS technique provides a simple, accurate measure of the collagen fiber angular distribution in the tissue, it is unable to distinguish the contributions of large-scale splay and small-scale crimp. For this reason, previous studies on heart valve leaflets have performed paired measurements of crimp length along with SALS orientation index. Those studies captured increases in fiber orientation (increased NOI) that were dominated by decreases in crimp with both (i) cyclic loading [254, 268] and (ii) stress-state during fixation [49, 257]. In particular, pooled data from those studies demonstrated that an increase in crimp length is associated with narrowing of the SALS scattered light plot, as evidenced by an overall trend toward increasing NOI (Fig. 3.11).

In keeping with this approach, we also examined changes in collagen crimp length using polarized light microscopy. Collagen fiber crimp was assessed only in the belly region of the leaflet for two reasons: (i) it was only in this region where the SALS OI data was altered during pregnancy, and (ii) we wished to relate changes in crimp to changes in the equibiaxial extensibility that we observed in this region during pregnancy [248]. The mitral leaflet underwent a significant loss of collagen crimp during pregnancy (Fig. 3.10), where crimp length more than doubled while the percent area occupied by crimp was nearly halved. This change is concurrent with leaflet expansion in the circumferential direction (Fig. 3.12). Despite the significant loss in crimp, the overall collagen fiber orientation (NOI) decreased during pregnancy, indicating that increased collagen fiber splay away from the circumferential axis overwhelmed the decrease in crimp.

Altered composition of the extracellular matrix, particularly the increase in collagen content (expressed as percent dry weight), demonstrates that pregnancy is associated with the growth of new matrix. While total leaflet thickness was unchanged, the fibrosa became 53% thicker—likely due to the accumulation of collagen—and the atrialis thinned by 46%. Interestingly, these changes do not parallel those seen in mitral valve remodeling in heart failure, despite the fact that both conditions produce elevated stresses in the mitral leaflet [184, 186, 197, 248, 283]. While leaflet length and collagen content

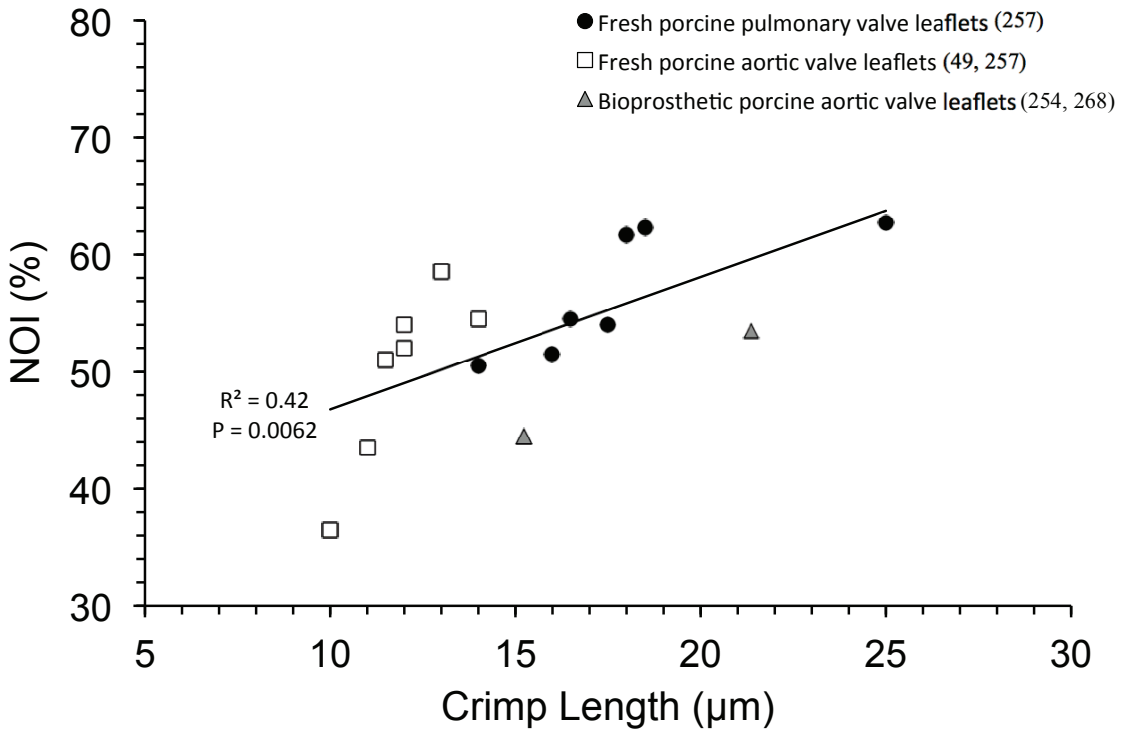

Figure 3.11 Relationship between crimp length and NOI from previous studies

Increases in crimp length (overall loss of crimp) are associated with an increase in alignment (NOI), as evidenced by previous studies of bioprosthetic heart valves using paired measurements of crimp length and SALS NOI [49, 254, 257, 268]. Data points are mean values from each study.

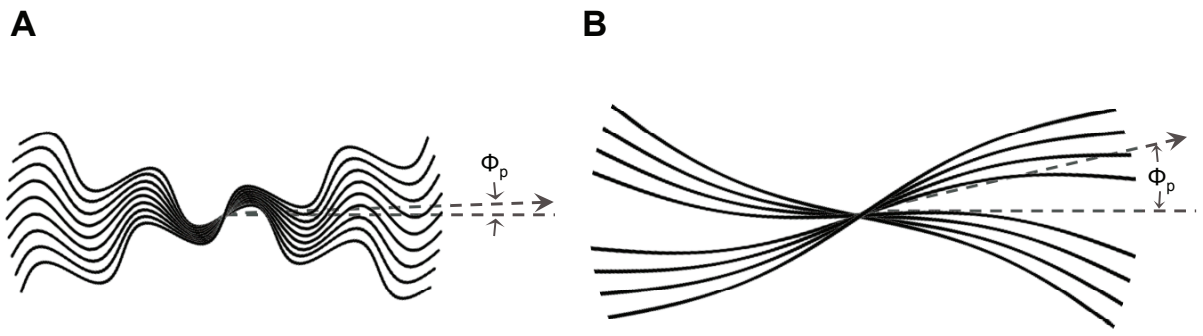

Figure 3.12 Schematic of collagen fiber architecture changes in pregnancy

Schematic representing the changes in collagen fiber architecture of the bovine mitral valve anterior leaflet during pregnancy. There is an increase in the crimp length, a decrease in the overall presence of crimp, and rotation of the fibers towards the radial direction, increasing fiber splay and resulting in circumferential lengthening.

increase in heart failure, they also thicken with a decrease in water content, suggesting that mitral valve remodeling during pregnancy is not the same as the "pathological" remodeling associated with heart failure.

Results from the current and previous study [248] together demonstrate that new collagen is synthesized in the leaflet during pregnancy. It is curious, therefore, that the Sircol assay used in the present study showed that little acid/pepsin-soluble collagen was present in the native bovine mitral anterior leaflet, and that this amount remained unchanged during pregnancy. This suggests limited presence of uncrosslinked "new" collagen. This result is in agreement with HIT crosslinking profiles observed in pregnancy [248]. In such analyses, the ratio of $t_{1/2}$-treated / $t_{1/2}$-control is used as an indicator of the ratio of total (mature plus immature) to mature crosslinking, and is thus referred to as the immature crosslinking index [101, 248]. This index provides a measure of the degree of collagen turnover in a tissue [98, 101, 244, 284, 285]. Interestingly, the immature crosslinking index in the mitral valve has not been shown to change during pregnancy, and is significantly lower than the values reported for the ovine pericardium [102] and ovine aorta [117] during development. This result again suggests that mature, crosslinked collagen dominates and this characteristic is unchanged in pregnancy. It is possible that, in pregnancy, valve collagen is crosslinked more quickly after synthesis and assembly: a hypothesis worthy of further investigation.

This study and its antecedent [248] have demonstrated both structural and mechanical alterations to mitral valve tissues in pregnancy, providing insight into the mechanisms of valve remodeling. Functionally, these results indicate that as the valve leaflet enlarges in pregnancy, there is a drastic loss of crimp, which is associated with reduced extensibility, namely through a loss of circumferential stretch. Collagen crimp and fiber orientation have been shown to contribute to tissue extensibility in heart valve and pericardial tissues [254, 268, 274, 286]. Under in vitro cyclic loading there is (i) an increase in crimp length as collagen fibers un-crimp (straighten) in the direction of loading, and (ii) rotation of the fibers towards the preferred direction (direction of loading), together causing an increase in SALS NOI (fiber alignment). However, in pregnancy, we have reported a decrease in fiber alignment. We attribute the decrease in SALS NOI to the rotation of fibers toward the radial direction, increasing the angular splay (i.e. wider distribution of angles) of the

collagen bundles. This fiber rotation and loss of crimp may be associated with the concurrent radial leaflet lengthening that also occurs in pregnancy. In fact, stretch-induced fiber reorientation toward of the direction of the applied tensile force has been well documented throughout the literature [286-291]. Finite element (FE) models of the biaxially loaded aortic valve leaflet indicate circumferential fiber rotation, and an increase in fiber alignment [290] as in cyclic loading – completely the opposite of our model. These differences may be attributed to Driessen's assumption that valve leaflet dimensions do not change. Quite the contrary, we have reported tremendous increases in leaflet dimensions in pregnancy, indicating not only the turnover of tissue, but also tissue growth to accommodate the expanding valve orifice. Future FE models of fiber re-orientation may therefore need to include the possibility of leaflet enlargement.

Interestingly, the changes in collagen fiber architecture and content did not occur in synchrony with the leaflet expansion and extensibility shift reported previously [248]. Alterations in normalized orientation index, preferred fiber direction, crimp length, layer thickness, and collagen content were only detected between non-pregnant and pregnant animals, whereas leaflet expansion and loss of extensibility occurred largely in early pregnancy. This suggests that in early pregnancy, the valve leaflet has enlarged through what is likely a passive expansion and, as a consequence, has lost any reserve of physiological extensibility. Nevertheless, the expansion of the valve leaflet allows the valve to maintain complete coaptation, even under the annular expansion of early pregnancy. The return of biaxial extensibility in late pregnancy must indicate adaptive tissue remodeling. Surprisingly, however, there is no detectable recovery of collagen crimp in late pregnancy. Further studies to evaluate structural alterations through pregnancy, particularly on the biphasic timeline of early and late pregnancy, would greatly improve our understanding of the contributions to the structural and mechanical leaflet properties under the triggers of volume loading and orifice expansion.

While this study has taken the first step to begin to examine structural changes in the collagen fiber network, research is still needed both in the investigation of hormonal triggers as well as changes in biochemical composition (such as elastin, proteoglycans, and glycosaminoglycans) and crosslinking profiles. Particularly, the evaluation of differences in the degree and maturity of crosslinking in pregnant and non-pregnant

animals could be assessed through thermomechanical (HIT, DSC, etc.) and biochemical methods in parallel with biomechanical measurements of time-dependent viscoelastic materials properties, which are highly dependent on the degree of crosslinking in a tissue. Future work must also involve performing non-equibiaxial mechanical testing to (i) assess axial cross-coupling: a factor that would be expected to decrease given the increased splay of the fiber architecture, and (ii) to inform a constitutive model of the leaflet and its remodeling process. Furthermore, the inclusion of other heart valve types (aortic, pulmonary, and tricuspid) could provide insight into valve-specific mechanisms of adaptive remodeling.

3.5 Acknowledgements

The authors thank Lucas Tedesco (Department of Bioengineering, University of Pittsburgh) for performing SALS data acquisition, Patricia Colp (Department of Pathology, Dalhousie University) for sharing expertise in histological staining techniques, Maxine Langman (Department of Applied Oral Sciences, Dalhousie University) for providing biochemical technical expertise, as well as O.H. Armstrong for the supply of bovine tissues.

3.6 Author Contributions

Author contributions: CMP, MSS, SMW, and JML conception and design of research; CMP analyzed data; CMP, and RA, performed experiments; CMP, SMW, and JML interpreted results of experiments; CMP prepared figures and drafted manuscript; CMP, SMW, JML, RA, and MSS edited, revised and approved final version of manuscript.

CHAPTER 4

Biaxial Creep Resistance and Structural Remodeling of the Aortic and Mitral Valves in Pregnancy

Caitlin M. Pierlot[1], Andrew D. Moeller[1], J. Michael Lee[1,2], and Sarah M. Wells[1],

[1]School of Biomedical Engineering, Dalhousie University, Halifax, Nova Scotia, Canada;

[2]Department of Applied Oral Sciences, Dalhousie University, Halifax, NS, Canada

4.1 Introduction

Although many cardiovascular tissues have been shown to remodel when exposed to chronic changes in hemodynamic stresses, few studies have examined the capacity of heart valves to remodel in a non-pathological state. Interestingly, volume overload similar to that experienced under the pathophysiology of heart failure [292], occurs in the heart in pregnancy as well, as the maternal circulation accommodates the developing feto-placental unit. Blood volume and cardiac output are increased by ~50%, accompanied by cardiac enlargement [136, 157, 248] with expansion of valve orifices. Valve orifice areas of the aortic, mitral, pulmonary, and tricuspid valves in humans have been shown to increase by 13-23% by full term pregnancy [157, 168]. Such expansion leads to a rise in the leaflet radius of curvature and, by the law of Laplace, the tensile stress across the closed leaflet is increased. Finite-element models of the anterior mitral valve leaflet predict that an 18% increase in orifice area would result in a 40-50% increase in tensile stress [211].

Although stemming from different embryological origins, both the aortic and mitral valves experience increased loading during pregnancy. Our previous studies examining changes in the bovine anterior mitral valve leaflet structure, dimensions, and mechanical properties, showed that mitral valve remodeling occurs in response to pregnancy [248, 293]. No studies have investigated the remodeling response of the aortic valve to this same physiological condition. For our mitral studies, we used a bovine model due to important similarities with humans in singleton birth deliveries, hemodynamic changes and hormone levels [139, 211, 225, 250, 251], and gestational period [252, 253]. Further, the duration of bovine pregnancy can be estimated via a linear relationship with the crown-to-rump length of the fetus [227]. We showed, for the first time, significant adaptive remodeling of the mitral valve during pregnancy, with dramatic increases in leaflet size and chordal attachments, accompanied by alterations in fiber architecture and composition of the leaflet. These changes contributed to an overall loss in collagen thermal stability and a biphasic change (decrease, then increase) in leaflet extensibility [248, 293].

Those results suggest that pregnancy-induced remodeling of the mitral valve anterior leaflet involves a two-phase process. In early pregnancy, the leaflet enlarges through what is likely a passive expansion, attaining a new dimensional set-point at the enlarged orifice diameter but with reduced extensibility. In late pregnancy, these enlarged dimensions are maintained, but leaflet extensibility is increased back to pre-pregnant values, suggesting an active remodeling process that maintains coaptation. The mechanism(s) underlying this biphasic remodeling of the mitral valve during pregnancy remains unclear. Our follow-up study [293] showed that changes in collagen fiber architecture and content did not occur in synchrony with the leaflet expansion and shift in extensibility. There must be, therefore, some other structural mechanism(s) occurring in pregnancy, modulating leaflet biomechanics.

The purpose of this paper was to build on previous studies of adaptive heart valve remodeling in pregnancy by: (i) relating changes in leaflet size and mechanical properties to changes in structural elements of the collagen network, including collagen crosslinking, while (ii) expanding studies to include both the aortic and mitral valves. This study also focuses on the behavior of the valve leaflet material examined through changes in dynamic creep resistance. Such biomechanical behavior is key to leaflet redundancy and regurgitation, and is sensitive to changes in tissue structure, particularly collagen crosslinking. The specific objectives of the current study were to investigate changes in mechanical properties (resistance to creep and extensibility) and macroscopic dimensions of valve leaflets, and to relate these changes to structural alterations in the collagen network, including collagen content and crimp, leaflet and individual layer thickness, collagen denaturation temperature, and crosslinking profile. We expected to uncover similar evidence of extracellular matrix (particularly collagen) remodeling in both valves via a loss of crimp and an increase in collagen deposition. Further, we predicted that increased collagen turnover in pregnancy would result in a decrease in the thermal stability of the leaflet tissues associated with a drop in crosslinking (or an increase in the proportion of immature crosslinks), thus decreasing tissue creep resistance. However, we found that while both the aortic and mitral valves appear to remodel mainly in the same manner, and as predicted, with respect to structural and biochemical changes in the collagen network, the two valves exhibit opposing

mechanical creep behaviors (increasing in the aortic valve and decreasing in the mitral valve) in pregnancy.

4.2 Methods

4.2.1 Tissue Harvest and Sample Preparation

All protocols for the harvesting of bovine tissues were approved by the University Committee on Laboratory Animals (UCLA) at Dalhousie University. The hearts of young female cattle were purchased as food from a local abattoir (Armstrong Food Services Limited, Kingston, Nova Scotia, Canada) immediately following slaughter. Hearts were collected from heifers (female cattle of sexual maturity which had never been pregnant), and from pregnant cows. To assess gestational age in pregnant cattle, fetal crown-rump length was measured, with a full term (278-290 days gestation) bovine fetus measuring approximately 100 cm [227]. Pregnant animals ranged in gestational age from 61 days (9 cm fetal length) to 256 days (87 cm fetal length).

All cattle were under 30 months of age. Due to imposed federal food regulations at Canadian Abattoirs, all animals were inspected by a federally licensed meat inspector such that animals exhibiting signs of illness were excluded from collection (Canadian Food Inspection Agency, CFIA). Cattle were divided into two groups: non-pregnant (NP), and pregnant (P) based on their reproductive status at slaughter. Where sufficient data were available, the pregnant group was divided again into EP (early pregnant) and LP (late pregnant) groups based on pregnancy duration (assessed by fetal crown-to-rump length).

Due to structural consistency between aortic valve leaflets, all three leaflets of the aortic valves were excised. However, since the mitral valve displays differing structural features between leaflets, with higher stresses experienced in vivo by the anterior leaflet [186, 228], all experiments used this leaflet. Leaflets were washed with Hanks' physiological solution (pH 7.4) including 6 mg/l trypsin inhibitor (lyophilosate), and an antibiotic-antimycotic agent and containing 10,000 units/ml of Penicillin G, 10 mg/ml streptomycin sulphate, and 25 μg/ml amphotericin B (Sigma-Aldrich Canada, Oakville, ON, Canada).

4.2.2 Mechanical Testing

The aortic and mitral valve leaflets for mechanical testing were excised on location, immersed immediately in Hanks' physiological solution, and transported back to the lab on ice. A 1cm-square specimen was cut from the center belly region of each leaflet (Fig. 4.1A). Tissue samples were stored in 4ºC overnight and tested within 72 hours of excision.

As described in our previous study [248], all mechanical testing was conducted on a custom-built, servo-hydraulic biaxial testing apparatus (MTS, 458 Series, Eden Prairie, MN), equipped with four servo-hydraulic linear actuators (two opposing pairs) in a planar biaxial configuration, allowing for independent deformation of the tissue samples in two perpendicular directions, connected on each axis to a GSO series 1,000-g cantilevered load cell (Transducer Techniques, Temecula, CA). Specimens were sutured (3-0 coated, braided silk, 75cm continuous suture) between four suture-style tissue grips, using one suture per sample edge, and mounted into the biaxial testing apparatus – one grip at the end of each actuator. The biaxial testing "grip" consists of an actuator bolt attachment and a removable bar with 5 mounted nylon pulleys. For mounting, the grips were held in a mounting template designed by Dr. Stephen Waldman (Dalhousie University), and soaked continuously with Hanks' physiological solution to avoid dehydration. The suture for each sample side was tied to the first nylon grip and then passed through the tissue at 4 equidistant points along the edge. At each pass, the suture was fed through the next nylon pulley. The pulleys ensure uniform tension along the edge of the specimen by allowing frictionless relative motion of the suture. All four edges were sutured into place in the same manner.

Immediately prior to testing, a 2 by 2 grid of four small graphite markers for optical strain measurement was affixed to the sample using cyanoacrylate glue (Fig. 4.1B). The entire experiment was recorded by video so that actual deformation of the sample (displacement of markers) could be measured in both the radial and circumferential directions. The deformation of the tissue cannot be accurately determined from the displacement of the actuators because, as the material is loaded, a variety of factors can play into the recorded strain, for example: (a) suture self-adjustment on their pulleys, (b)

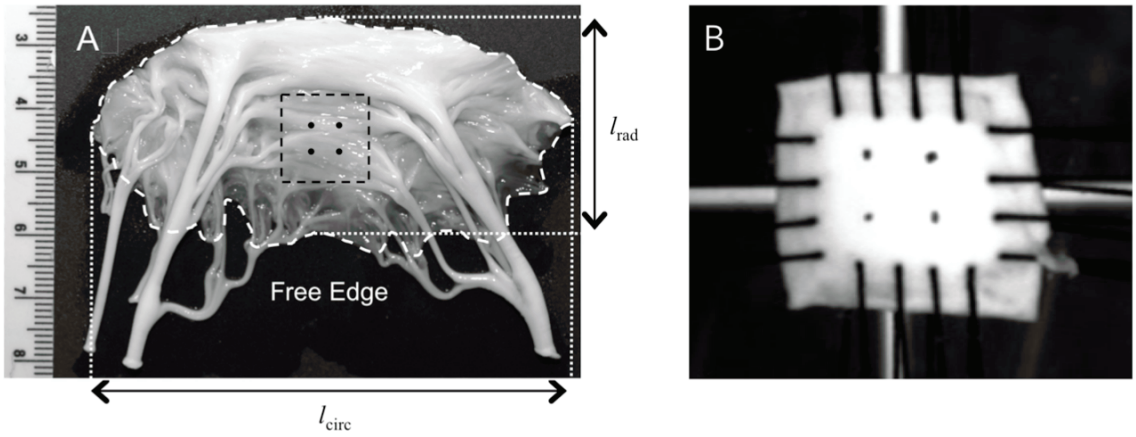

Figure 4.1 Methodology for dimensional and mechanical experiments

A. Image of an isolated heifer mitral leaflet showing dimensional measurements taken using imageJ: leaflet area (dashed outline), circumferential length (l_{circ}), and radial length (l_{rad}). The region excised for biaxial mechanical extensibility and creep testing is outlined and imaging marker placement in a 2 by 2 grid is shown. Scale bar = 1 cm. B. Image of excised square specimen of the anterior mitral leaflet mounted and sutured between grips in the biaxial mechanical testing system.

suture stretch, (c) deformation of suture holes, etc. Tracking of a grid of four small marker positions throughout the experiment allowed the determination of the true radial and circumferential time-dependent deformations. Throughout the duration of the mechanical experiments, the specimens were maintained in a Hanks' physiological solution bath at 37 ºC. Biaxial mechanical loads were applied as membrane tension (expressed in N/m) – the axial force per unit length of tissue over which the force is applied.

4.2.3 Extensibility Testing

For extensibility testing, 22 bovine hearts were collected in total: 9 from heifers, and 13 from pregnant cows. Actuator waveforms were generated using T/RAC waveform generation (MTS). The time, actuator positions, and load data were acquired using a custom-written LabVIEW program (Version 6.1, National Instruments, Austin, TX) and a 12-bit analog-to digital PCI 6035E card (National Instruments, Austin, TX) on one of two Macintosh computers (Power Mac G4, Apple Computer, Cupertino, CA). Video images of the specimen surface and marker displacement were recorded at 15 Hz with a charge-coupled device camera (Cohu 4190, San Diego, CA) and the second Macintosh computer. In preparation for data recording, a small preload membrane tension of 0.5-N/m was applied equibiaxially. Specimens were then extended in both the circumferential and radial directions, to roughly 30-N/m (producing half of the desired peak 60-N/m tension) along both axes. MTS actuator control amplifier gains were then increased to produce the peak 60-N/m tension, again in both directions. The actuators were then returned to their preload reference state, ready for initiation of quasistatic, equibiaxial testing across a range of tensions up to a peak tension of 60-N/m. The peak equibiaxial tension of 60-N/m was selected for consistency and comparison with previous related studies [74, 248]. Tissue specimens were preconditioned for 10 cycles to the peak tension, at 0.05 Hz, and data acquisition was performed immediately afterwards under the final (11th) cycle.

Extensibility Data Analysis. Analysis of mechanical data was detailed previously [248], and is briefly outlined here. The displacement of the 4 graphite markers on the specimen surface was analyzed using a custom-written program in ImageJ (National Institutes of

Health). Marker positional data were used to calculate the axial stretch ratios along the circumferential and radial axes using a custom-written MathCAD program (Parametric Technology, Needham, MA) written by Dr. Michael Sacks (University of Pittsburgh). Peak biaxial extensibility was defined by the axial stretch ratios (λ_C^{peak} (circumferential extensibility) and λ_R^{peak} (radial extensibility)) under peak equibiaxial membrane tension (60-N/m). The net tissue extensibility was represented by the areal stretch under peak tension and was calculated using the following equation:

$$\text{Areal Stretch}^{peak} = (\lambda_C^{peak} \times \lambda_R^{peak})$$

Finally, tension versus areal stretch graphs were plotted using areal stretch values calculated under equibiaxial tensions of 1.0, 2.5, 5.0, 10.0, 20.0, 30.0, 40.0, 50.0, and 60.0-N/m, to assess leaflet tissue properties over the entire loading range examined under biaxial loading.

4.2.4 Dynamic Creep

For the creep study, 24 bovine hearts were collected in total: 14 from heifers, and 10 from pregnant cows. Using LabVIEW (Version 2010, National Instruments, Austin, TX), a creep-loading protocol was programmed for use on our servo-hydraulic biaxial testing system. Specimens were extended manually to a 2-N/m membrane tension preload in both the radial and circumferential directions, then loaded equibiaxially to the maximum physiological membrane tension experienced in vivo on the closed valve (Table 4.1). Creep behavior of collagen likely depends strongly on its stress-state, thus creep tests were designed to assess material properties at the physiological stress-state of the collagen, specific to each valve type. Figure 4.2 depicts the loading protocol used: First the sample was subjected to 5 preconditioning cycles of loading to the specified peak load. This was followed by 10 cyclic loading cycles, where samples were loaded to the peak tension, held at that load for 90 seconds during which tissue creep (marker displacement) was recorded, and then unloaded to zero load state. Lastly, a 30-minute static loading cycle was performed. Tissue deformation via marker location was recorded throughout the experiment by a CCD camera (Cohu 4190, San Diego, CA), and stored on DVD. An LED light was mounted within the view frame of the camera and programmed

Table 4.1 Transvalvular pressure (TVP) versus leaflet tension

	TVP (mmHg)	Maximum Tension (N/m)
Aortic Valve	92	62
Mitral Valve	144	96

Maximum bovine transvalvular pressure experienced *in vivo* across the closed valve [101] and the corresponding maximum tension across the valve, calculated using the law of Laplace (T=pr/2), assuming a leaflet radius of curvature r = 0.01 m^2.

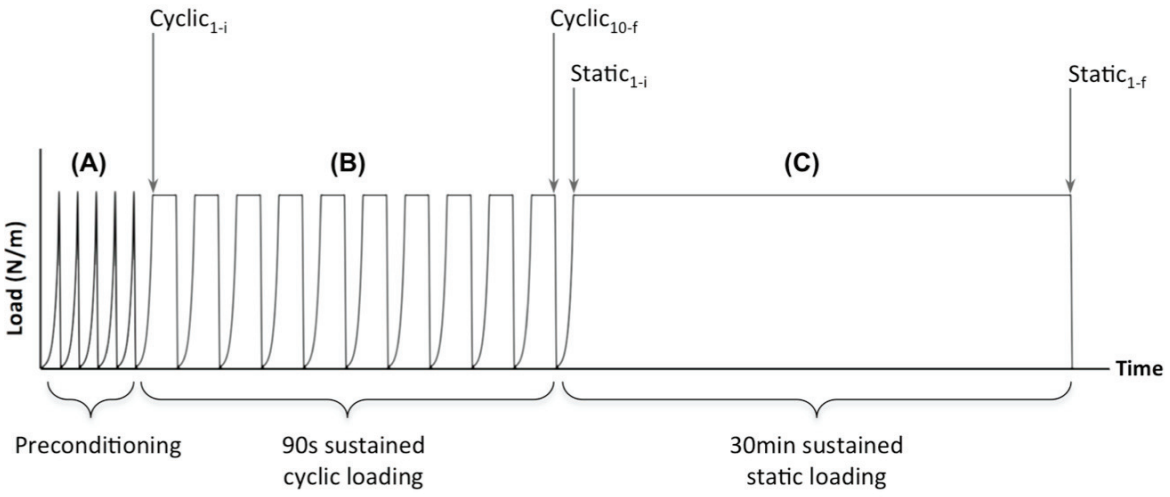

Figure 4.2 Biaxial mechanical creep loading protocol

First the sample was subjected to 5 cycles of preconditioning to the target peak load (A). This was followed by 10 loading cycles, where samples were loaded to the peak tension, held at that load for 90 seconds during which tissue creep was recorded, and then unloaded to zero load state (B). Lastly, a 30-minute static loading cycle was performed (C). For cyclic creep, maximum tissue deformation in the final cycle 10 ($cyclic_{10\text{-}f}$) was referenced to the initial tissue dimensions prior to creep loading in cycle 1 ($cyclic_{1\text{-}i}$). For static creep, the final maximum tissue deformation in static loading ($static_{1\text{-}f}$) was referenced to initial tissue dimensions prior to static creep loading ($static_{1\text{-}i}$). For overall creep, maximum tissue deformation in static loading ($static_{1\text{-}f}$) was referenced to the initial tissue dimensions in cycle 1 ($cyclic_{1\text{-}i}$). Statistical comparisons between non-pregnant and pregnant animals were made for each measure of leaflet creep (cyclic, static, and overall).

to blink at the start and end of each loading segment to visually separate the cyclic and static loading segments during image analysis.

Creep Data Analysis. Post-experimental image analysis was performed using the protocol explained here in brief. DVD video files (.vob) were converted to AVI format using the open source video transcoder HandBrake (The Handbrake Team, Version 0.9.3). VirtualDub, a video capture and processing utility was used to convert the AVI video files to JPEG image stacks (Aspect ratio 480x352; Frame rate 1 fps), separating cyclic and static loading segments using the LED light indictor in the video. Image stacks were then imported into image analysis software (ImageJ, National Institutes of Health). The belly region of the leaflet was selected, and the area outside was cleared in the entire stack of images to eliminate interference of sutures and the surrounding area in the analysis. The image stack was then inverted such that the markers would show as white on a black background. The displacement of the markers was then tracked using the ImageJ plugin ParticleTracker (Guy Levy and Janick Cardinale, MOSAIC group, ETH, Zurich), and output into MS Excel as x and y coordinates of each marker, throughout the experiment. These coordinates were then used to calculate the area enclosed by the 4 markers (forming a convex quadrilateral) at each timepoint.

For each leaflet tissue sample, marker area was reported during the creep loading (sustained load) portion of the experiment, at the loading points noted in Fig. 4.2. Under cyclic loading, peak marker area during each cycle was referenced back to cycle 1. For the purpose of this study, *cyclic creep* was defined as the increase in marker area from the beginning of cycle 1 to the end (or peak) of cycle 10, providing a measure of cumulative creep over the entire cyclic loading segment. *Static creep* was calculated as the percent increase in marker area between the peak of the static segment as compared to the initial marker area at the start of static creep loading. Finally, a measure of *overall creep* was determined by calculating the increase in marker area between the peak of the static segment (final experimental creep data point), and the initial marker area of cycle 1 (first experimental creep data point).

Statistical comparisons between non-pregnant and pregnant animals were performed using percent areal creep (fractional increase in area enclosed by the tissue markers

during creep loading). This measure is used as an indicator of the creep occurring along both axes of the valve leaflet. The data set in the current study was limited to non-pregnant and early pregnant groups only due to limited availability of animals in later stage pregnancy.

4.2.5 Leaflet Dimensions

Fresh, excised aortic and mitral valve leaflets from 10 non-pregnant heifers and 15 pregnant cows, were laid out flat, ventricular aspect up, on a flat surface. Digital images were captured of the excised leaflets and a reference scale bar using a (Nikon D50) camera (Nikon, Tokyo, Japan). Images were imported into image-analysis software (ImageJ, National Institutes of Health), where radial midline length and circumferential midline length were measured, and the freehand selection tool was used to outline the perimeter of the leaflet to calculate the total area of the leaflet (Fig. 4.1A).

4.2.6 Biochemical Analysis

Immediately following the capturing of digital images for valve dimension analysis, the same aortic and mitral leaflets were frozen (-86°C) and subsequently freeze-dried for a minimum of 52 h. Dry samples of approximately 10 mg dry weight, from the belly region of the leaflet, were weighed and recorded. Total collagen content was estimated using an hydroxyproline assay, following the protocol of Woessner [262]. Assay product was read using a microplate reader (Synergy HT, Bio-Tek Instruments Inc., Winooski, Vermont) to measure dye absorbance at a wavelength of 561 nm. Comparison of sample absorbance to a generated standard absorbance curve was used to quantify the hydroxyproline present in each leaflet sample. The quantity of collagen in each sample, normalized to dry weight, was determined by dividing the quantity of hydroxyproline by 0.1277, based on a study by Keeley *et al.* [263].

4.2.7 Histological Analysis

For histological analysis, aortic and mitral valves were collected from another set of animals. Leaflets from 22 animals (9 non-pregnant heifers and 13 pregnant cows) were divided to produce two symmetric halves of the leaflet (Fig. 3.3). Both halves were fixed from fresh in 10% neutral buffered formalin for a minimum of 72h, dehydrated in

70% ethanol, embedded in paraffin, sectioned into 5μm serial sections, mounted on slides, and dried at 57°C for a minimum of 24 hours. Embedding and sectioning was performed by the Histology Research Services Laboratory (Faculty of Medicine, Dalhousie University). Circumferential cross-sections were cut from one half of the leaflet for picrosirius red staining to examine collagen alignment and crimp. Radial cross-sections were cut in the other half of the leaflet for Verhoeff-Van Gieson staining of collagen, elastin, and cell nuclei, to identify leaflet layering (Verhoeff-Van Gieson Elastin Staining Kit, Polysciences, Inc., Washington, PA) (Fig. 3.3). Each radial section contained the complete leaflet cross-section from the free edge to the fixed edge. For both staining protocols, sections were deparaffinized in xylene and rehydrated in graded ethanol/water solutions. For picrosirius red staining protocol, circumferential sections were stained for 1 h with 0.1% Picrosirius Red solution, followed by several water washes. For Verhoeff-Van Gieson staining, radial sections were stained for 1 hour with Verhoeff's solution, differentiated in 2% ferric chloride for 1 minute, followed by several water washes. All stained slides were then dehydrated in ethanol and cleared in xylene for mounting.

4.2.8 Collagen Crimp Analysis

Images were taken of picrosirius-strained sections using a Nikon Eclipse E600 light microscope equipped with a polarizer and a 10MP AmScope digital camera. Collagen crimp was characterized by two measures: (i) crimp length, the peak-to-peak measurement of one crimp period, and (ii) percentage of the leaflet area which was crimped. For both measures, six contiguous images were taken at 40x objective magnification along the circumferential direction, spanning 2 mm into the belly region of the leaflet, and analyzed using ImageJ software (National Institutes of Health). For crimp length measurements, a line was drawn across the centerline of each image (through the center of the image, aligned to the principal crimp direction) and every distinguishable crimp length along that line was recorded (Fig. 3.4). For crimped area measurements, a grid (300 μm^2/square) was placed on each image. The number of grid points in contact with crimped tissue, as well as the total number of grid points in contact with tissue (crimped or uncrimped) was recorded. The ratio of crimped-to-total grid points was then used to calculate the area percentage of the leaflet occupied by crimped collagen. Both

crimp length and crimped area were averaged across all 6 images. Blinded measurements were made by three observers, with excellent agreement between observer counts, and these measurements were averaged.

4.2.9 Leaflet and Layer Thicknesses

Verhoeff-Van Gieson stained sections were photographed at low magnification (using a 5x or 10x objective) along the entire length of the valve leaflet, using a Zeiss Axioplan 2 Imaging Microscope (Cellular & Molecular Digital Imaging Facility, Faculty of Medicine, Dalhousie University) and analyzed using AxioVision software (Release 4.8.1). ImageJ imaging software plugins MosaicJ [260] and TurboReg [261] were used to stitch together one large mosaic image for each sample. An array of lines was placed on each mosaic such that 25 vertical lines transected the full thickness of the tissue along the length of the leaflet (Fig. 3.5). Thickness measurements, of the full leaflet as well as of each layer, were taken at each gridline. From these measurements the following parameters were extracted: total thickness, fibrosa thickness, spongiosa thickness, ventricularis thickness (aortic valve only), and atrialis thickness (mitral valve only). Thickness measurements were then averaged across the length of the leaflet for each valve sample, producing these same four parameters for each individual valve leaflet.

4.2.10 Denaturation Temperature and Hydrothermal Isometric Tension Testing

Leaflets from the aortic and mitral valves of another 10 non-pregnant heifers and 23 pregnant cows were used for thermomechanical testing.

Tissue Preparation and Sodium Borohydride Reduction. Collagen denaturation temperature (T_d) tests (DTT) and hydrothermal isometric tension (HIT) experiments were conducted using a custom-built experimental apparatus described previously by Lee *et al.* [110] and using the revised protocol of Wells *et al.* [117] to look for changes in T_d with pregnancy and to provide a measure of the proportions of immature to mature crosslinks. A square tissue sample from the belly of the leaflet was bisected circumferentially, to provide two equidimensional strips of tissue. One strip was left untreated and used as a control sample, while the other was treated with sodium borohydride ($NaBH_4$). $NaBH_4$ treatment chemically reduces thermally labile (immature) collagen crosslinks to produce

thermally stable (mature) crosslink products [97, 101, 113, 117, 231, 248] which remain intact during hydrolysis of the collagen backbone throughout HIT experiments. The $NaBH_4$ reduction therefore results in an increase in the quantity of thermally stable crosslinks in the tissue and hence an increase in the halftime of load decay ($t_{1/2}$) of the sample. When analysis of samples treated with borohydride is used in combination with untreated samples, a comparison of the rates of load decay can provide an indicator of the ratio of total crosslinks (labile and stable) to thermally stable crosslinks in a tissue. $NaBH_4$ treated samples were subjected to four repeated tissue treatments in a 0.1 mg/ml $NaBH_4$–borate buffer solution (0.05M KCl and 0.05M H_3BO_3, pH 9.0) at 4°C under constant agitation. Control samples were subjected to identical buffer conditions with the exclusion of $NaBH_4$. All samples were then washed for ten minutes in Hanks' physiological solution.

DTT/HIT Testing. The testing apparatus allowed for the testing of up to six samples simultaneously. Control and treated tissue strips were mounted between two mechanical grips, one attached to a rigid fixed rod and the other to an adjustable tension hook. The upper grip was attached to an adjustable strain gauged (Vishay Micro-Measurements Inc., Shelton, Connecticut) cantilever for monitoring of the developed tension in the specimen. Specimens were preloaded to a load of 50 g, fully immersed in room temperature distilled deionized water, and isometrically constrained for the duration of the experiment. The temperature of the water bath was raised at a rate of ~1°C/min using a Cimarex 2 plate heater (Barnstead-Thermolyne, Dubuque, IA), from ~20ºC (room temperature) to 90°C using a thermistor probe at sample depth to monitor the bath temperature. Following the heating segment, a 90°C isotherm was maintained for three hours by on/off computer heater control to assess the degree of crosslinking in the tissue based on the rate (halftime) of load decay. Thermal stability was evaluated by the denaturation temperature and by the load decay at high temperature, which is indicative of collagen structure and the degree of crosslinking in the material. Time, temperature, and load data were acquired using a custom-written LabVIEW program (National Instruments TM, Austin, TX) on a Dimension 4800 computer (Dell Computing, Round Rock, TX) via a 12-bit A/D, D/A DAQ board (Model NB-MIO-16L, National Instruments, Austin, TX). Data points were

collected at intervals of 1°C during the heating segment, and at 30s intervals during the isotherm.

Analysis of DTT/HIT Data. Without $NaBH_4$ treatment, HIT process captures three fundamental molecular transitions in leaflet collagen: (a) denaturation, (b) hydrolytic splitting of immature thermally labile crosslinks, and (c) hydrolysis of entire alpha chains [117]. Denaturation, in this protocol, is characterized by a sudden increase in sample tension at the denaturation temperature [115, 118]. The tissue sample attempts to shrink along the primary fiber direction to take on a higher entropy coiled configuration; however, it is unable to shorten due to the isometric constraint. As a result, tension is developed in the sample, which can be recorded. Above this temperature, any intermediate, thermally labile crosslinks are broken, leaving only thermally stable crosslinks. While the temperature is maintained at the isotherm, peptide chain hydrolysis occurs and load relaxation is observed [119]. The rate of relaxation of a tissue has been shown to be independent of its non-collagenous constituents and is closely correlated to the concentration of thermally stable crosslinks in a collagen sample [120].

Intramolecular crosslinks prevent triple helix unwinding, thereby increasing T_d, while intermolecular crosslinks increase the half life of load decay in HIT relaxation, but leave T_d relatively unaffected [117]. Together, denaturation temperature and halftime of load decay are representative of the quantity and quality of collagen crosslinking present in the tissue.

According to Le Lous [232, 294], load decay under the isotherm is described by a Maxwell-type exponential decay:

$$L(t) = L_{max}e^{-kt}$$

where $L(t)$ is load at time t, L_{max} is the maximum load achieved after the start of the isotherm, and k is the relaxation constant. The halftime of load decay $t_{1/2}$ can be calculated as:

$$t_{1/2} = -\frac{ln\left(\frac{1}{2}\right)}{k} = \frac{ln(2)}{k}$$

The term $-k$ is the slope of the $ln(L(t)/L_{max})$ versus time plot which was obtained over an 8,000 s time interval between 2,000 s and 10,000 s (linear region) of the HIT experiment local decay results.

4.2.11 Statistical Analysis

All results are expressed as the mean ± standard error of the mean (SEM), with the n value representing the number of animals per group. All data are divided into two groups: NP (non-pregnant), and P (pregnant). Statistical comparisons were made using two-tailed t-test comparisons between the two groups. The pregnant group was also further divided into EP (early pregnant) and LP (late pregnant) groups according to fetal crown-to-rump length: Cows carrying fetuses of crown-to-rump length < 45 cm (0–169 days) were classified as EP, and those carrying fetuses > 55cm (193–270 days) were classified as LP. The mid-pregnancy group of 45–55 cm (169–193 days) was omitted in this comparison to obtain a more complete separation of early and late groups. The biaxial mechanical (extensibility) and thermomechanical data used in this study for the mitral valve come from the dataset published by Wells *et al.* [248], but reanalyzed under different pregnancy divisions by duration. That previous study defined early pregnancy as ~0-159 days of gestation, and late pregnancy from 160-270 days. By contrast, the current study divides gestation in half using fetal crown-to-rump length, as defined above. A one-way ANOVA was performed, followed by Tukey honestly significant difference for comparisons among the three groups (NP, EP, and LP). To evaluate changes in any parameter as a function of pregnancy duration, data were plotted as a function of gestational age and fitted with a least-squares linear regression. Lastly, cumulative cyclic areal creep was plotted by valve as a function of each creep cycle (1-10) and fitted with a power law least squares regression for each pregnancy group (NP and EP). An ANCOVA was performed to compare regressions between pregnancy groups.

Results and regressions were considered significant for $p < 0.05$. Outliers were defined as data points falling outside of the following quantile-based range: [25^{th} quantile – 1.5*(interquantile range)] to [75^{th} quantile + 1.5*(interquantile range)], where interquantile range = 75^{th} quantile – 25^{th} quantile. These data points were excluded from further analysis. For the aortic valve, one outlier was removed from NP radial length, one

from NP circumferential length, one from NP area, one from P ventricularis thickness, one from P crimp length, one from NP % static creep, one from NP % overall creep, one from NP T_d, one from NP $t_{1/2}$-treated, two from P immature index and one from NP immature index. For the mitral valve, three outliers were removed from P radial length, one from P leaflet thickness, one from NP atrialis thickness, two from P % crimp, one from NP collagen content, one from NP % cyclic creep, one from P % static creep, one from P % overall creep, one from NP $t_{1/2}$-treated, one from P $t_{1/2}$-treated, three from P immature index and one from NP immature index. All statistical analyses were performed using JMP Statistical Software (Version 10.0, SAS Institute, Inc., Cary, NC).

4.3 Results

4.3.1 Leaflet Extensibility

In all valves from non-pregnant and pregnant animals, leaflets were more extensible in the radial direction than the circumferential direction, as previously reported in humans [39], sheep [236], and pigs [216, 233-235, 295, 296]. Net extensibility of the aortic and mitral valve leaflets underwent a biphasic shift during pregnancy, decreasing in early pregnancy, and increasing back in late pregnancy (Table 4.2). Specifically, peak areal stretch at 60-N/m equibiaxial tension decreased 11% and 20% in the aortic and mitral valves respectively, from non-pregnant to early pregnant groups (Fig. 4.3D & J), then increased linearly with fetal growth (Fig. 4.3A & G), returning to pre-pregnant values by late pregnancy.

The biphasic changes in net extensibility (areal stretch) described above were produced by changes in leaflet extensibility in both the circumferential and radial directions (Table 4.2, Figure 4.3). Peak circumferential extensibility (λ_C^{peak}) decreased in early pregnancy, paralleling the changes observed in net extensibility, but was unchanged into late pregnancy. λ_C^{peak} decreased in early pregnancy, by 8% in the aortic valve (significant at $p<0.10$ only), and 10% in mitral valves (Fig. 4.3E & K), and showed no correlation with fetal length in both valves (Fig. 4.3B & H). Peak radial extensibility (λ_R^{peak}) however, was largely unchanged in pregnancy (Fig. 4.3C, F & L), with one exception: λ_R^{peak} in the mitral valve increased linearly with fetal growth (Fig. 4.3I).

Table 4.2 Summary of leaflet mechanical changes in the belly region of mitral and aortic valve leaflets with pregnancy

		Non-pregnant	Early pregnant	Late pregnant	p-value	All pregnant	Δ pregnancy	p-value
Aortic	Areal stretch	2.45 ± 0.07(9)[a]	2.18 ± 0.07(7)[b]	2.46 ± 0.09(4)[ab]	0.0196	2.30 ± 0.06(12)	biphasic	0.0630
Valve	λ_R^{peak}	1.79 ± 0.04(9)	1.75 ± 0.06(7)	1.84 ± 0.07(4)	0.6108	1.80 ± 0.04(13)	-	0.8674
(60 N/m)	λ_C^{peak}	1.36 ± 0.04(10)	1.25 ± 0.03(8)	1.34 ± 0.05(4)	0.0578	1.28 ± 0.02(13)	↓	0.0325
Mitral	Areal stretch‡	2.37 ± 0.09(7)[a]	1.89 ± 0.13(6)[b]	2.29 ± 0.15(4)[ab]	0.0375	2.11 ± 0.11(12)	biphasic	0.0439
Valve	λ_R^{peak} ‡	1.67 ± 0.06(9)	1.58 ± 0.07(7)	1.77 ± 0.10(4)	0.2872	1.67 ± 0.06(13)	-	0.9721
(60 N/m)	λ_C^{peak} ‡	1.37 ± 0.03(7)[a]	1.23 ± 0.03(8)[b]	1.29 ± 0.04(4)[ab]	0.0250	1.26 ± 0.03(14)	biphasic	0.0153

Values are means ± SE of leaflet areal stretch, peak radial stretch ratio (λ_R^{peak}), and peak circumferential stretch ratio (λ_C^{peak}), for animals in the non-pregnant (NP), early pregnant (EP), late pregnant (LP), and all pregnant (P) groups. Aortic and mitral valves were tested under 60 N/m equibixial tension. Statistical comparisons were made between NP and P groups using t-Test comparisons of groups and are presented with the corresponding p value ($p<0.05$ considered significant). Statistical comparisons among NP, EP, and LP groups were made using one-way ANOVA followed by Tukey honestly significant difference (HSD) multiple-comparison method. n values for the pregnancy groups are presented in brackets for each measurement. ‡Results for mitral valves were previously presented by Wells *et al.* [248] but data from pregnant animals were re-analyzed using the different pregnancy-split used in this study.

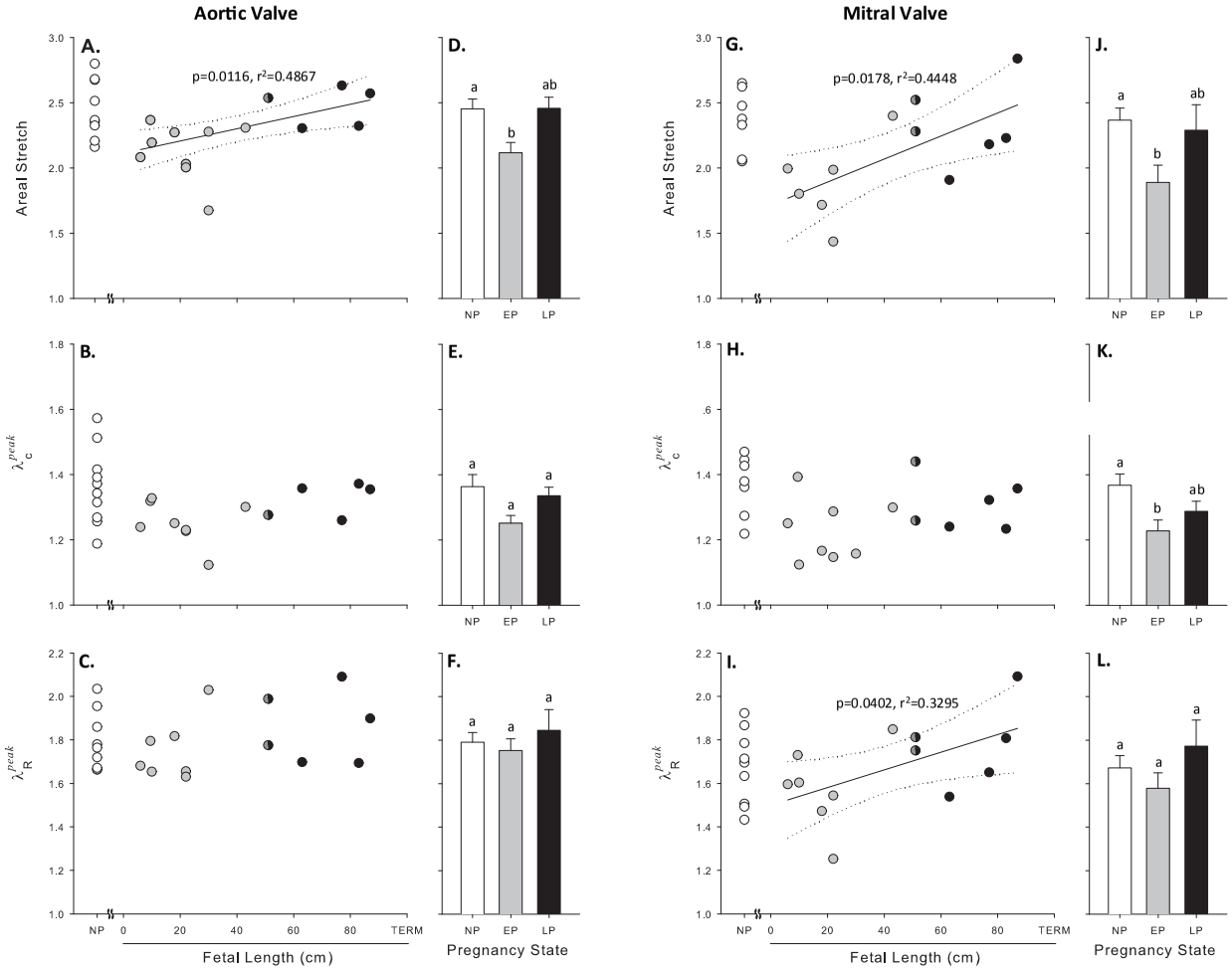

Figure 4.3 Biaxial mechanical properties (aortic & mitral)

Biaxial mechanical properties of the aortic (A-F) and mitral (G-L) valve leaflets: peak values at 60-N/m equibiaxial tension. A & G: peak areal stretch; B & H: λ_C^{peak}; and C & I: λ_R^{peak}, as a function of fetal crown-to-rump length (100 cm ~ term) along with measurements from non-pregnant heifers. Regression lines with 95% confidence intervals are shown for the fetal data. D-F, and J-L: comparison of mean (± SE) values between pregnancy states (non-pregnant, early pregnant, and late pregnant), using one-way ANOVA followed by Tukey honestly significant difference (HSD) multiple-comparison method. [a,b]Values labeled with the same letter were not significantly different ($p>0.05$).

Areal stretch was also calculated over the whole range of equibiaxial tensions used in our mechanical loading experiment (Fig. 4.4). In the aortic and mitral valves, at each tension above 5-N/m, mean areal stretch decreased from non-pregnant to early pregnant animals (leftward shift of the tension stretch curve), then increased in late pregnancy, indicating a reversible decrease in leaflet extensibility (Fig. 4.4A & B).

4.3.2 Leaflet Creep

Extensions during cyclic and static areal creep of the mitral and aortic valves were small but significantly non-zero ($p<0.0001$). Significant pregnancy-induced differences in leaflet creep were found in both the aortic and mitral valves, but the direction of these changes was valve-specific. In the aortic valve, under a peak load of 62-N/m, cyclic creep more than doubled in early pregnancy (Table 4.3). Static and overall creep of the aortic valve, however, were unchanged in pregnancy. Conversely, in the mitral valve, under a peak load of 96-N/m, leaflet tissues demonstrated a 38%, 57%, and 50% decrease in cyclic, static, and overall creep respectively between non-pregnant and early pregnant groups. No correlations between areal creep and fetal length were found in either valve.

Strong power law relationships were found between peak areal creep and cycle number for non-pregnant and early pregnant groups, in both the aortic and mitral valves (Fig 4.5). Comparison of these power regressions between non-pregnant and pregnant animals also demonstrate an increase in creep in early pregnancy in the aortic valve ($p<0.0001$) and a decrease in areal creep in early pregnancy in the mitral valve ($p<0.0001$), across all cycles.

4.3.3 Leaflet Dimensions

Heart valve leaflets experienced remarkable changes in dimensions (Table 4.4): increases in radial length, circumferential length, and overall leaflet area, largely occurring early in pregnancy. Aortic valve leaflet area increased by 54% from non-pregnant to early pregnant animals, with no change into late pregnancy. Mitral valve leaflet area increased by 42% from non-pregnant to early pregnant animals, and again was maintained into late pregnancy. These early pregnancy changes were dominated by

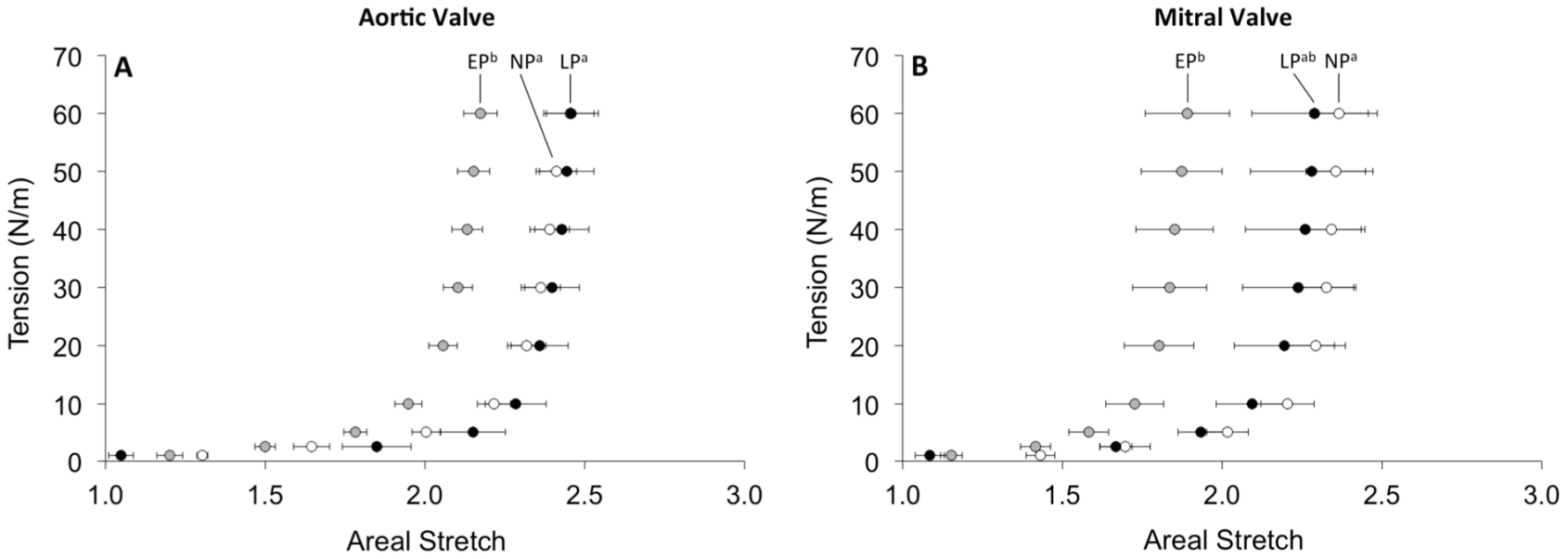

Figure 4.4 Tension versus areal stretch curves by pregnancy group (aortic & mitral)

Mean tension versus areal stretch curves for the aortic (A) and mitral (B) valve leaflets, for each pregnancy state (non-pregnant, early pregnant, and late pregnant). Areal stretch is plotted as means ± SE at tension increments of 1.0, 2.5, 5.0, 10.0, 20.0, 30.0, 40.0, 50.0, and 60.0-N/m. At each tension level above 5-N/m, areal stretch in EP animals was significantly less than those for the NP and LP groups. [a,b]Values labeled with the same letter were not significantly different ($p>0.05$).

Table 4.3 Leaflet areal creep under equibiaxial tension with pregnancy

	Creep Type	Areal Creep, %			
		Non-pregnant	Early pregnant	Δ pregnancy	p-value
Aortic Valve (62 N/m)	Cyclic	1.0 ± 0.3(6)	2.1 ± 0.1(4)	↑	0.0054
	Static	1.0 ± 0.1(8)	0.8 ± 0.1(6)	–	0.2527
	Overall	1.7 ± 0.2(8)	1.9 ± 0.5(6)	–	0.7372
Mitral Valve (96 N/m)	Cyclic	1.6 ± 0.3(8)	1.0 ± 0.1(6)	↓	0.0492
	Static	0.7 ± 0.1(9)	0.3 ± 0.1(6)	↓	0.0157
	Overall	2.2 ± 0.4(9)	1.1 ± 0.1(6)	↓	0.0164

Values are mean ± SE of percentage leaflet areal creep (cyclic, static, and overall) for animals in the non-pregnant (NP), and pregnant (P) groups. Valve leaflets were tested under equibixial tension of 62 N/m for the aortic valve and 96 N/m for the mitral valve. Statistical comparisons in each valve type were made between NP and P groups using t-test comparisons and are presented with the corresponding p value ($p<0.05$ considered significant). n values for each parameter in the NP and P groups are presented in brackets.

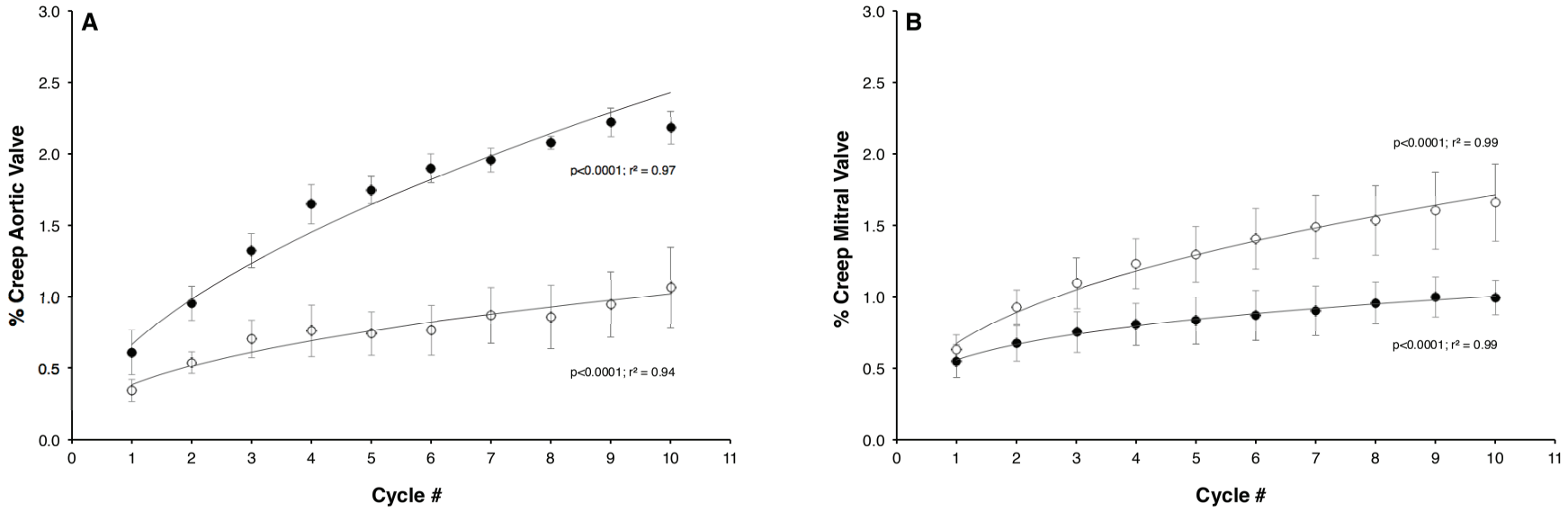

Figure 4.5 Cumulative cyclic creep by pregnancy group (aortic & mitral)

Cumulative cyclic creep (in percentages), normalized to cycle 1, for the aortic (A), and mitral (B) valves, showing power curve fits to non-pregnant (open circles) and pregnant (solid circles) data for all cycles. p value and r^2 for the non-linear least squares fit are indicated for each curve.

Table 4.4 Summary of leaflet dimensional changes in the belly region of aortic and mitral valve leaflets with pregnancy

		Non-pregnant	Early pregnant	Late pregnant	p-value	All Pregnant	Δ pregnancy	p-value
Aortic Valve	Radial length, cm	2.02 ± 0.04(9)[a]	2.47 ± 0.14(7)[ab]	2.74 ± 0.15(6)[b]	0.0035	2.63 ± 0.11(15)	↑	<0.0001
	Circ. length, cm	3.25 ± 0.07(9)[a]	4.18 ± 0.22(7)[b]	4.86 ± 0.23(6)[b]	0.0001	4.58 ± 0.20(15)	↑	<0.0001
	Area, cm^2	5.21 ± 0.15(9)[a]	8.02 ± 0.81(7)[b]	10.77 ± 0.87(6)[b]	0.0004	9.57 ± 0.75(15)	↑	<0.0001
	Thickness, μm	730 ± 67(9)	-	-	-	848 ± 53(15)	-	0.0921
	Fibrosa	267 ± 30(9)	-	-	-	338 ± 25(15)	↑	0.0423
	Spongiosa	249 ± 33(9)[a]	408 ± 45(6)[b]	226 ± 55(4)[ab]	0.0259	290 ± 38(15)	biphasic	0.2135
	Ventricularis	200 ± 41(9)	-	-	-	195 ± 14(14)	↓	0.4503
Mitral Valve	Radial length, cm	2.64 ± 0.13(10)	2.90 ± 0.12(7)	2.93 ± 0.13(6)	0.1334	2.93 ± 0.04(12)	↑	0.0235
	Circ. length, cm	4.44 ± 0.12(10)[a]	5.43 ± 0.24(7)[b]	6.29 ± 0.26(6)[b]	<0.0001	5.86 ± 0.21(15)	↑	<0.0001
	Area, cm^2	10.54 ± 0.62(10)[a]	15.0 ± 1.1(7)[b]	17.6 ± 1.2(6)[b]	0.0004	16.45 ± 0.92(15)	↑	<0.0001
	Thickness[‡], μm	1170 ± 75(9)	-	-	-	1194 ± 59(11)	-	0.4011
	Fibrosa[‡]	540 ± 130(9)	-	-	-	833 ± 76(11)	↑	0.0372
	Spongiosa[‡]	431 ± 85(9)	-	-	-	346 ± 76(11)	-	0.4694
	Atrialis[‡]	221 ± 40(8)	-	-	-	135 ± 22(10)	↓	0.0447

Values are means ± SE. Early pregnant and late pregnant groups were included where data was significant or meaningful. Statistical comparisons were made between non-pregnant and pregnant groups using t-test comparisons of groups and are presented with the corresponding p value ($p<0.05$ considered significant). Statistical comparisons among non-pregnant, early pregnant, and late pregnant groups were made using one-way ANOVA followed by Tukey honestly significant difference (HSD) multiple-comparison method. n values for the pregnancy groups are presented in brackets for each measurement. [‡]Results for mitral valve leaflet and layer thicknesses were previously presented by Wells *et al.* [248].

large, rapid, increases in circumferential length in both valves, and added to by more gradual increases in radial length.

4.3.4 Leaflet and Layer Thickness

Total leaflet thickness was not substantially changed in pregnancy in either the aortic or mitral valve; however, the fibrosa thickness increased substantially in both valves, with less dramatic valve-specific changes occurring in the other anatomical layers of the leaflet. In the aortic valve, a 16% increase (significant at $p<0.1$ level only) in leaflet thickness was found, accompanied by a 27% unidirectional increase in fibrosa thickness, a linear increase in ventricularis thickness with increasing fetal growth (Fig. 4.6A), and a biphasic change in spongiosa thickness – increasing by 64% in early pregnancy and decreasing linearly with fetal growth back toward pre-pregnant values by late pregnancy (Fig. 4.6B). In the mitral valve, total leaflet and spongiosa thicknesses were unchanged in pregnancy, while fibrosa thickness increased 54% and atrialis thickness decreased 39% between non-pregnant and pregnant animals.

4.3.5 Collagen Crimp

Collagen crimp analysis showed drastic alterations during pregnancy, with dramatically increased crimp length resulting in an almost complete loss of crimp in both the aortic and mitral valve leaflets (Fig. 3.9, Table 4.5). Crimp length increased 216% in the aortic valve and 186% in the mitral valve, between non-pregnant and pregnant animals (Fig. 4.7A). In both valves, this increase in crimp length was accompanied by a 24% (aortic) and 43% (mitral) decrease in the percentage of leaflet area occupied by crimp. In the aortic valve, leaflets from the non-pregnant group were very tightly, and nearly completely, crimped, while the collagen network of leaflet from pregnant animals became less, but still moderately, crimped. In the mitral valve, leaflets were much less crimped, even in the non-pregnant group, while in pregnant animals the presence of crimping was almost non-existent. No significant trends in collagen crimp were found with pregnancy duration; however, when broken down by early and late pregnancy groups, the percentage of crimped leaflet area in the aortic valve decreased 39% ($p=0.0097$) in early pregnancy, but then returned to pre-pregnant values by late pregnancy (Fig. 4.7B).

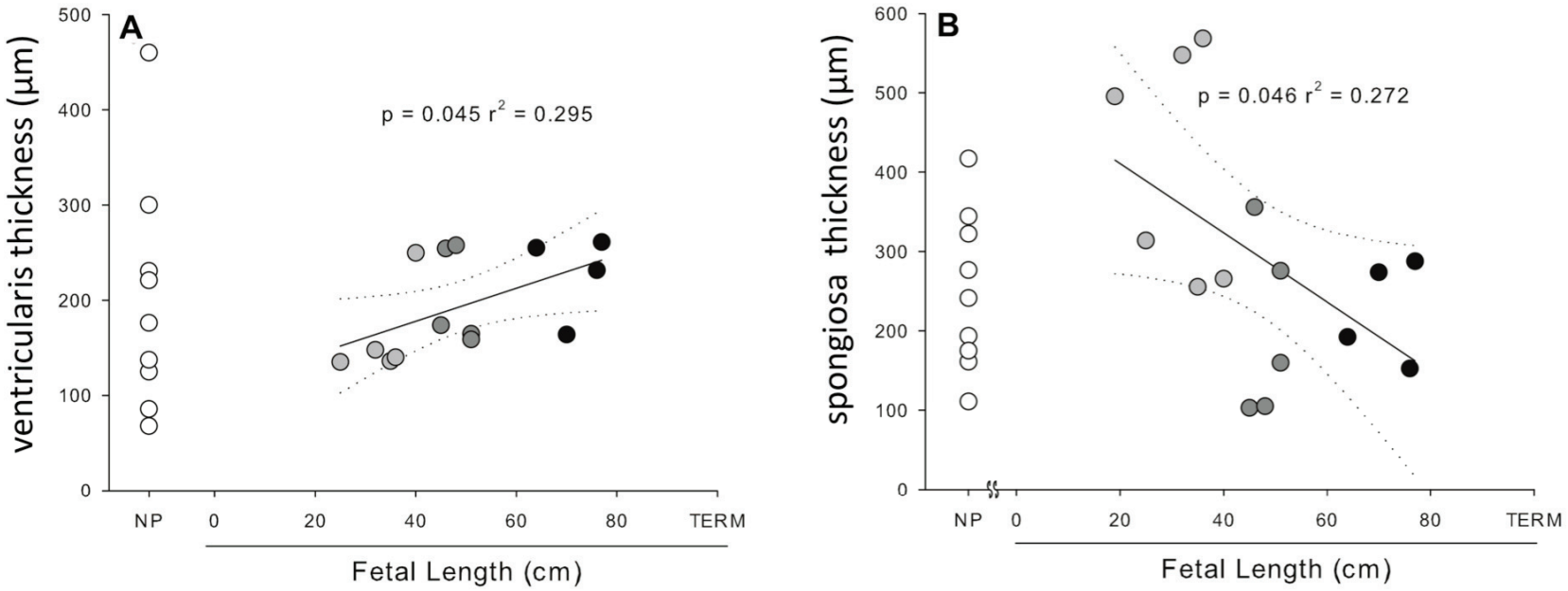

Figure 4.6 Aortic valve layer thickness versus fetal length plots

A: ventricularis thickness (in µm) and B: spongiosa thickness (in µm), of the aortic valve leaflet for non-pregnant heifers (open circles) and with fetal length (in cm) for early-pregnant (shaded circles) and late pregnant (solid circles) animals. Mid-pregnant animals (45-55cm fetal length; 169-193 days of gestation) are indicated by the 4 circles shaded slightly darker than early pregnant animals. Regression lines with 95% confidence intervals are shown for the fetal data. p value and r^2 for the least-squares regressions are indicated for each curve.

Table 4.5 Collagen content and crimp changes in the belly region of the leaflet with pregnancy

		Non-pregnant	All pregnant	Δ pregnancy	p-value
Aortic Valve	Crimp length, μm	3.7 ± 0.5(9)	11.7 ± 2.9(15)	↑	0.0089
	Crimped area, %	94.2 ± 1.0(9)	71.7 ± 7.6(15)	↓	0.0052
	Collagen, %	59.8 ± 2.1(10)	64.4 ± 1.7(15)	↑	0.0493
Mitral Valve	Crimp length‡, μm	22.9 ± 1.2(9)	65 ± 15(13)	↑	0.0079
	Crimped area‡, %	40.2 ± 6.0(9)	22.8 ± 3.0(11)	↓	0.0116
	Collagen‡, %	56.7 ± 3.0(9)	66.0 ± 3.3(13)	↑	0.0256

Values are means ± SE. Early pregnant and late pregnant groups are not included here as no significant changes were found with gestational timeline for any of the recorded parameters. Statistical comparisons were made between non-pregnant and pregnant groups using t-test comparisons and are presented with the corresponding p value ($p<0.05$ considered significant). n values for groups are presented in brackets for each measurement. ‡Results for mitral valves were previously presented by Wells *et al.* [248].

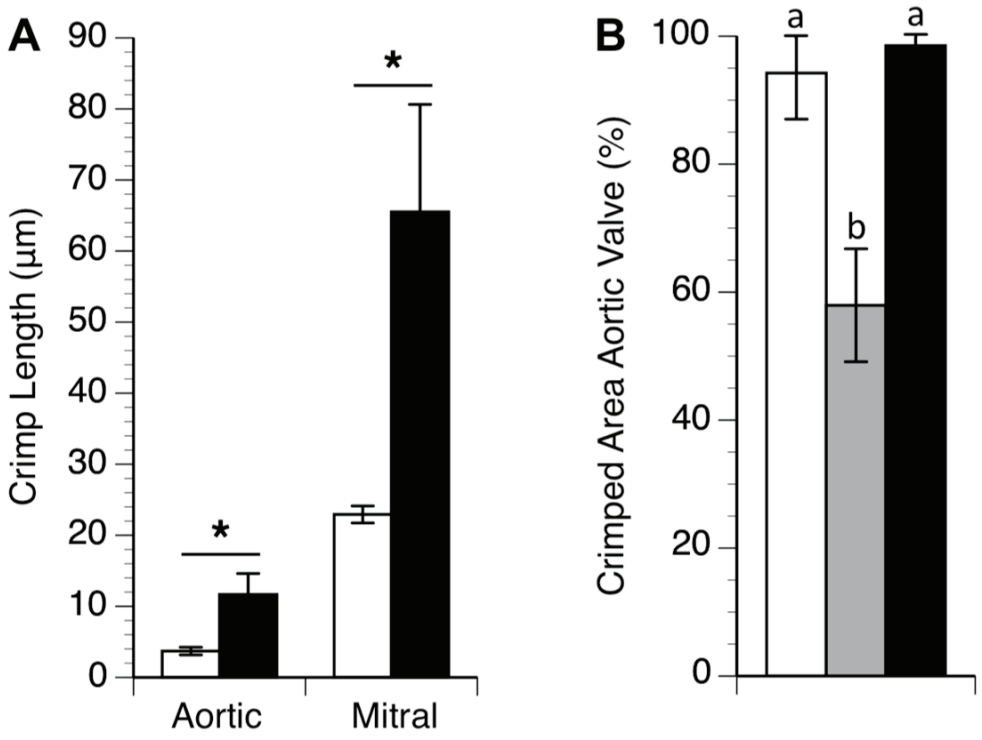

Figure 4.7 Collagen crimp plots (aortic & mitral)

A: Collagen crimp length (in µm) from aortic and mitral valve leaflets of non-pregnant (open bar) and pregnant (filled bar) animals. Values are mean ± SE. Statistical comparisons were made between NP and P groups using t-Test comparisons of groups. Columns labeled with an asterisk denote a statistically significant change ($p<0.05$). B: leaflet crimped area (in %) of the aortic valve leaflet from non-pregnant heifers (open bar), early pregnant (shaded bar) and late pregnant (filled bar). Values are mean ± SE. Statistical comparisons were made among pregnancy groups using one-way ANOVA followed by Tukey honestly significant difference (HSD) multiple-comparison method. [a,b]Values labeled with the same letter were not significantly different ($p>0.05$).

4.3.6 Leaflet Biochemical Composition

Biochemical analysis of heart valve leaflet tissues demonstrated significant increases in collagen content during pregnancy (Table 4.5). Total collagen content, determined by hydroxyproline assay, increased between non-pregnant and pregnant animals, by 8% in the aortic valve and 16% in the mitral valve.

4.3.7 DTT/HIT Experiments

T_d – Effect of Pregnancy. The collagen denaturation temperature for both the aortic and mitral valves decreased in early pregnancy and was then maintained into late pregnancy (Table 4.6). Specifically, the aortic and mitral valve T_d each fell 1.9°C from non-pregnant to early pregnant animals. No significant correlation was found between denaturation temperature and gestational age in either valve.

T_d – Effect of Treatment. A two-way ANOVA demonstrated that collagen thermal stability, as indicated by T_d, was not significantly altered by $NaBH_4$ treatment in any pregnancy groups (data not shown).

$t_{1/2}$ – Effect of Pregnancy. Pregnancy resulted in increased total and mature crosslink content in both the aortic and mitral valves. Under HIT testing, halftime of load decay of control (non-$NaBH_4$-treated) specimens increased 140% in the aortic valve by early pregnancy, and 95% in the mitral valve by late pregnancy (Table 4.6) compared to the non-pregnant group, implying an increase in mature crosslink content. In $NaBH_4$-treated samples, pregnancy resulted in significant increases in halftime of load decay in both the aortic and mitral valves (Table 4.6), indicating an increase in total crosslink content. Furthermore, aortic $t_{1/2}$-treated increased 79% in early pregnancy and was unchanged into late pregnancy. However no differences were found in $t_{1/2}$-treated between non-pregnant, early, and late pregnancy groups in the mitral valve.

$t_{1/2}$ – Effect of Treatment. A two-way ANOVA demonstrated that (i) $t_{1/2}$ was significantly altered by $NaBH_4$ treatment of leaflet tissues in the pregnant group ($p=0.0002$), and (ii) interactions between treatment group and pregnancy group were significant ($p=0.0012$), requiring sample treatment to be considered in each pregnancy group separately. Load relaxation was found to be dependent on treatment group in the mitral valve only. In the

Table 4.6 Summary of leaflet HIT measurements in the belly region of the leaflet with pregnancy

		Non-pregnant	Early pregnant	Late pregnant	p-value	All pregnant	Δ pregnancy	p-value
Aortic Valve	T_d, ºC	68.7 ± 0.4(9)[a]	66.8 ± 0.4(10)[b]	67.3 ± 0.5(9)[ab]	0.0209	66.8 ± 0.3(23)	biphasic	0.0005
	$t_{1/2}$ control, hrs	8.0 ± 2.5(10)[a]	19.2 ± 3.0(7)[b]	18.5 ± 2.8(8)[b]	0.0107	18.5 ± 2.0(19)	↑	<0.0001
	$t_{1/2}$ treated, hrs	11.3 ± 2.1(7)[a]	20.2 ± 2.1(7)[b]	18.7 ± 2.0(8)[b]	0.0153	20.9 ± 1.6(19)	↑	0.0003
	Crosslink index	1.3 ± 0.2(6)	1.0 ± 0.2(6)	1.1 ± 0.1(8)	0.7033	1.2 ± 0.1(18)	-	0.8849
Mitral Valve	T_d‡, ºC	68.6 ± 0.2(10)[a]	66.7 ± 0.4(9)[b]	66.3 ± 0.3(9)[b]	0.0003	66.3 ± 0.2(22)	↓	<0.0001
	$t_{1/2}$ control‡, hrs	8.6 ± 1.8(10)[a]	10.6 ± 2.0(8)[ab]	16.8 ± 2.0(8)[b]	0.0182	13.6 ± 1.6(19)	↑	0.0144
	$t_{1/2}$ treated‡, hrs	11.5 ± 2.5(7)	16.7 ± 2.2(9)	19.2 ± 2.5(7)	0.1071	17.1 ± 1.7(19)	↑	0.0039
	Crosslink index‡	1.6 ± 0.2(7)	1.6 ± 0.2(8)	1.1 ± 0.2(6)	0.2563	1.3 ± 0.1(17)	-	0.4385

Values are means ± SE. Statistical comparisons were made between non-pregnant and pregnant groups using t-tests and are presented with the corresponding p value. Statistical comparisons among non-pregnant, early pregnant, and late pregnant groups were performed using one-way ANOVA followed by Tukey honestly significant difference (HSD) multiple-comparison method. n values for the pregnancy groups are presented in brackets for each measurement. ‡Results for mitral valves were previously presented by Wells *et al.* [248] but data from pregnant animals were re-analyzed using the different pregnancy-split used in this study.

non-pregnant group, $NaBH_4$ treatment of the mitral valve resulted in a 34% increase in $t_{1/2}$, compared to control, while in the pregnant group, $NaBH_4$ treatment increased $t_{1/2}$ by 26% (Table 4.6). These results indicate that mitral leaflet tissues from both control and pregnant groups contained immature crosslinks. The lack of difference between control and treated tissues in the aortic valve indicates that there is an absence of immature collagen crosslinks in both the non-pregnant and pregnant groups.

Immature Crosslink Index. The native valve population of immature collagen crosslinks was low and surprisingly remained so in pregnancy. The ratio of $t_{1/2}$-treated to $t_{1/2}$-control (immature crosslinking index) was small (<1.6:1) and not significantly altered in any pregnancy groups, in either aortic or mitral valves (Table 4.6).

4.3.8 Summary of Results

Our results show that bovine pregnancy is accompanied by mechanical and structural alterations: biphasic changes in leaflet stretch, valve-specific changes in creep resistance, increases in leaflet size and thickness, straightening out of collagen fibers resulting in an overall loss of collagen crimp, increased collagen content, decreased thermal stability, and alterations in collagen crosslinking.

4.4 Discussion

This study demonstrates remarkable physiological remodeling of mature heart valve leaflets in the maternal cardiovascular system, in both the aortic and mitral valves, and with the two valves remodeling in largely the same way despite their very different embryological origins. We have shown identical changes during pregnancy in leaflet extensibility (biphasic changes in leaflet stretch), leaflet dimensions (unidirectional leaflet area expansion and fibrosa thickening with virtually no changes in overall leaflet thickness), collagen crosslinking (increased mature crosslinking) and thermal stability (drop in denaturation temperature). Crimp structure and concentration of collagen also changed similarly across valves during pregnancy. Crimp length and content increased in both valves, but the increases were larger in the mitral valve. The area of the leaflet occupied by crimped collagen decreased in both valves in pregnancy, however the change was unidirectional in the mitral valve and biphasic in the aortic valve, indicating some degree of recovery in late pregnancy.

By contrast, some features like equibiaxial creep demonstrated contrary, valve-dependent changes—suggesting valve-specific remodeling. In the aortic valve, cyclic creep doubled in early pregnancy, while in the mitral valve creep measured in all segments of the loading protocol (cyclic, static, and overall) decreased by approximately half. Several further dissimilarities were found between the valves with respect to when during pregnancy changes appeared, particularly in leaflet extensibility and crosslinking. Together, these differences provide the first evidence of valve-specific remodeling during pregnancy, indicating that the structural mechanisms responsible may be different and/or occurring at different rates.

Until recently, it has been widely held that heart valves cannot remodel in a non-pathological setting. This study and our previous studies [248, 293] have shown that physiological remodeling does in fact occur. Pregnancy results in significant changes to the geometry of the valve leaflets, through leaflet expansion of the aortic and mitral valves (shown in the present study) as well as via the formation/splitting of chordae attachments in the mitral valve [248]. It is important to recognize, though, that tissue expansion can occur in two ways: (i) by passive stretching of the tissue, or (b) by the growth of new material. Distinguishing one from the other is vital to understanding the mechanisms of remodeling, and may be strongly demonstrated by changes in the internal structure and composition of the leaflet.

Geometrically, leaflet expansion in pregnancy occurred by lengthening in both the circumferential and radial directions. The dominant contributor to the rapid expansion of the leaflet was circumferential lengthening, occurring in sync with the leaflet areal expansion. By contrast, radial expansion occurred more gradually through pregnancy. It is interesting that during this areal expansion the overall thickness of the leaflets was largely unchanged in pregnancy. Thinning alone would have been suggestive of passive stretch; however, retained thickness under areal expansion must indicate addition of new leaflet material. We hypothesize that, during pregnancy, heart valve leaflets undergo a two-phase remodeling process. In early pregnancy, the leaflets stretch passively as the valve orifices expand. This is followed by remodeling of the enlarged leaflet tissues back toward a normal structure-function relationship. The most notable piece of evidence for this unique remodeling process is the biphasic shift in leaflet areal stretch revealed by in

vitro extensibility testing. In both the aortic and mitral valves, areal stretch decreased in early pregnancy, resulting in the leftward shift of the tension-stretch curve. This is strongly suggestive of an overstretched leaflet material. After this, with increasing gestational age of the fetus, leaflet stretch under testing returned to pre-pregnant values. Here again, peak circumferential extensibility mirrored this biphasic behavior. Thus, leaflet extensibility is rapidly lost in early pregnancy—largely in the circumferential direction—then is gradually regained over the remainder of pregnancy, suggesting a recovery of the leaflets' pre-pregnant mechanical properties.

Mechanisms for this 2-phase remodeling process are more difficult to define. Leaflet enlargement in early pregnancy must include growth of new tissue, as the leaflet area increases without thinning of the tissue. While circumferential lengthening of the leaflet could result from the preferential addition of new tissue in that direction, it may also result from changes in the collagen fiber architecture since fibers of the collagen network in heart valve leaflets are mainly circumferentially aligned [49, 254, 255, 257, 264, 266, 267, 293]. Our data suggests that loss of circumferential extensibility in early pregnancy was due, at least in part, to the straightening (or uncrimping) of the collagen network. The result would have been lengthening, but also stiffening, in the circumferential direction. It is less clear how the leaflets recover their pre-pregnant extensibility. The mechanical data would suggest a recovery of collagen crimp in late pregnancy; however, this was only the case in the aortic valve where the percentage of leaflet area occupied by crimp decreased in early pregnancy and recovered in late pregnancy (Fig. 4.7). Loss of collagen crimp in late pregnancy has been reported in other tissues and is thought to be a relaxin-mediated process. Pinheiro *et al.*, reporting on the mouse pubic symphysis in late pregnancy, noted that in the last 3 days alone of pregnancy, crimp angle was decreased and crimp length increased more than 37%, as the interpubic ligament became increasingly compliant [193]. It is not known if heart valve leaflets contain relaxin receptors, however, the accumulation of collagen in both the aortic and mitral valve leaflets suggests that other factors override the action of relaxin, which is normally collagen-degrading [297].

In this paper, aortic and mitral leaflet biomechanics were assessed by examining changes in dynamic resistance to biaxial creep. Collagen fiber mobility and resistance to rearrangement could thus be assessed as biomechanical sequelae to pregnancy-induced

changes in leaflet architecture. We note that these experiments were *not* intended as an assessment of the leaflets' physiological behavior under sustained physiological loading. Rather, they sought biomechanical evidence of remodeling, expressed under biaxial, physiologically relevant loading. The leaflet tissues examined here are soft, viscoelastic materials which both store and dissipate strain energy under various loading conditions [298]. Two features of viscoelastic biomechanics bear special attention here (Fig. 4.8). Stress relaxation is the time-dependent decrease in stress under an applied and sustained strain or extension. Conversely, creep is defined as the increase in strain (deformation) of a tissue under an applied and sustained (or repeated) stress. In most physiological environments, particularly in the cardiovascular system, connective tissues are under cyclic or sustained loads rather than sustained deformations. For that reason, creep measurements are perhaps more relevant to the study of these tissues [84, 298]. The mechanisms underlying creep behavior, however, are not fully understood, but likely include reorientation of collagen fibers, relaxation of the proteoglycan matrix around collagen fibers, relaxation within fibers themselves, uncrimping of collagen, and time-dependent effects at the interface between the fiber and the matrix [85, 86].

While the magnitude of in vitro creep observed in the present study was small, these tissues nonetheless did creep. This result differs from the conclusions drawn by Grashow *et al.* and Stella *et al.* who argued that valve tissues exhibit no measureable creep, while they do exhibit stress relaxation [295, 299, 300]: that is, that the mechanisms responsible for viscoelastic creep and stress relaxation are "functionally independent". In particular they suggested that the lack of creep can be attributed to the presence of a protective load-locking mechanism involving the gradual recruitment of collagen fibers [233, 301]. Nonetheless, as is indicated in Figure 4.8, stress relaxation and creep are two sides of the same coin, both resulting in a shift of the stress-strain curve. Unlike the previous studies cited above, our results agree with established viscoelastic theory. The aortic and mitral valve leaflet tissues did have the ability to undergo biaxial creep—at least after isolation in vitro. The observed pregnancy-induced changes in creep behavior were strongly valve-specific: increasing in the aortic valve as expected, but decreasing in the mitral valve, contrary to expectations.

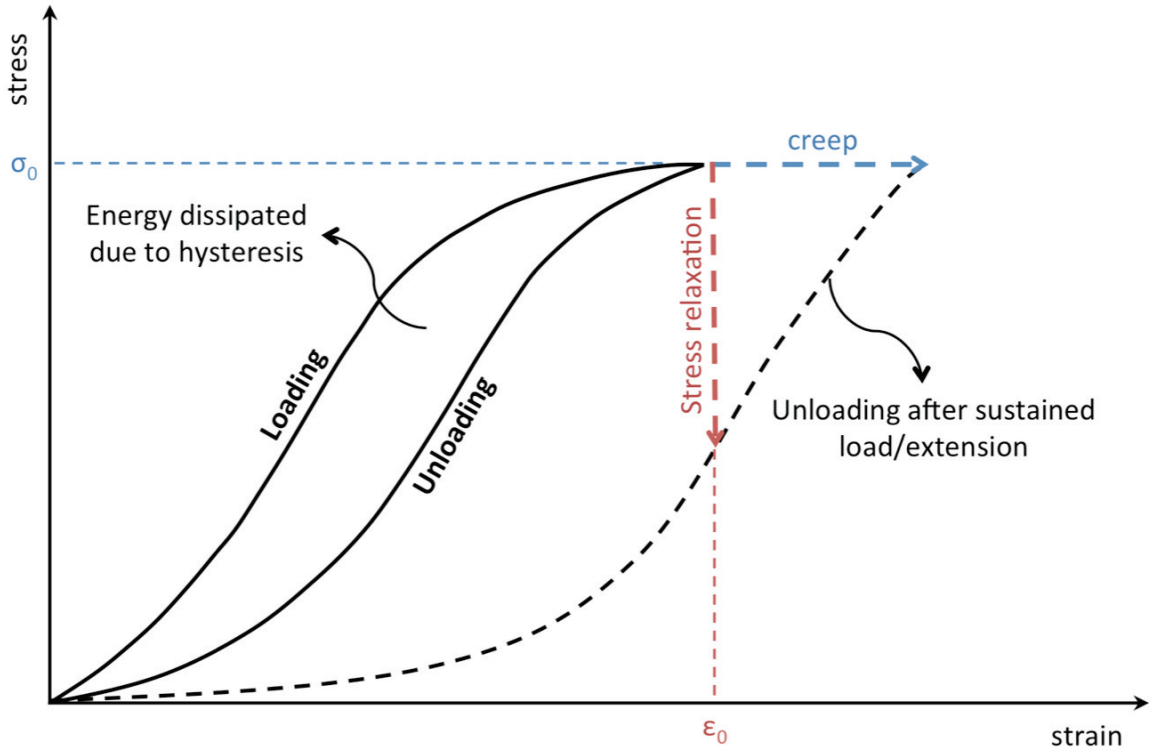

Figure 4.8 Relationship between viscoelastic creep and stress relaxation

Diagram showing graphical representations of the viscoelastic mechanical properties of stress relaxation, creep, and hysteresis. Stress relaxation and creep are indicators of identical molecular mechanisms, as indicated by the projection of each on to the same unloading curve shown as a dotted line.

One of the principal determinants of leaflet biomechanics must be the crosslinking state of the constituent collagen network. HIT provides information on both the thermal stability of collagen fibers (denaturation temperature testing) and the overall integrity of the collagen network which they form (isothermal relaxation half-times). It is significant that, in contrast to biochemical counting of various crosslink types, HIT assesses *biomechanically functional* crosslinking and, via $NaBH_4$ reduction it can semi-quantitatively characterize the hydrothermal maturity of the crosslink population. In the present study, we expected that the collagen denaturation temperature would decrease due to increased collagen turnover and remodeling in pregnancy [101, 248]. This hypothesis was confirmed, with a loss of leaflet collagen thermal stability early in pregnancy. Since the immature crosslinking index in isothermal relaxation provides an indication of the degree of collagen turnover in a tissue [98, 101, 244, 284, 285], we expected to see a noticeable increase with pregnancy. Surprisingly, while we found the total crosslink content and the mature crosslink content both increased in the valve leaflets during pregnancy, there was little (mitral valve) to no (aortic valve) evidence of newly formed immature crosslinks. This is a completely remarkable result for strongly remodeling tissues. Mature-crosslinked collagen appears to dominate in aortic and mitral valve tissues: a feature unchanged in pregnancy. As we have suggested previously [293] it is possible that valve collagen is crosslinked more quickly after synthesis and assembly in valve leaflets. If this is the case, it is a potentially unique feature of pregnancy worthy of further study.

Enzymatic crosslinks are present initially in immature forms that are thermally labile and susceptible to hydrolysis under changes in pH and temperature. As the collagen matrix "matures" over time, these crosslinks can mature to more stable, hydrolysis-resistant mature crosslinks [101]. Mature crosslinks give additional stability to the collagen fibers and are most commonly found in mature tissues, that is, in tissues which are not actively growing or remodeling. As an example, high levels of immature crosslinks have been found in collagenous tissues of the human uterus, a tissue which experiences high turnover of collagen [302, 303], while increased levels of mature crosslinks have been observed in older tissues [92, 107, 304, 305]. The terminology typically used to describe tissue crosslinking can be misleading. It is important to consider the difference between

the terms *immature* and *mature* and the respective terms *hydrolytically (thermally) labile* and *hydrolytically (thermally) stable*. Labile versus stable refers to thermal and chemical properties of the crosslinks and their ability to resist cleavage. Immature crosslinks (also referred to as intermediate crosslinks) are difunctional links, and can be divided into aldimines and keto-amines, when initially laid down in the collagen [105]. While mature crosslinks are all thermally stable, and immature aldimine crosslinks are thermally labile, the immature keto-amine crosslink HLKNL is hydrothermally and acid stable even after initial formation [99, 306]. As a result, when investigating the crosslink profile of collagenous tissues under HIT, crosslink maturity is not synonymous with thermal stability. A tissue which is resistant to crosslink hydrolysis shows a long half-time of decay but could have a large population of freshly formed keto-amine crosslinks [101, 285]. That caveat being noted, there is evidence to suggest that aldimine crosslinks may be more mechanically relevant than their keto-amine counterparts due to striking similarity between biochemical HPLC crosslink analysis and HIT load decay results in bovine valve leaflets [101].

An overall increase in total crosslinking in pregnancy, paralleled by an increase in mature crosslinks, should have increased resistance to creep (via the reduction in sliding between collagen fibers). The highly crosslinked collagen network in the mitral valve did show very little creep. However, the increase in creep in the aortic valve in pregnancy, despite the fully crosslinked collagen network, is a remarkable finding of valve-specific remodeling. This result could develop with an increase in collagen turnover and a significant increase in the proportion of immature crosslinks, but our HIT data does not indicate a change in immature crosslinking. This result may nonetheless be attributed to the immature crosslink population, if the thermally stable immature crosslink HLKNL were preferentially formed. Biochemical methods have shown this crosslink to be present in both aortic and mitral valve tissues in mature heart valves [101]. This possibility requires further investigation of the specific crosslinking profile using a biochemical technique such as HPLC.

In isolation, our crosslinking data (increasing, mature crosslinking only) would suggest that the left side valves were maturing rather than remodeling [284, 302, 307]. Nonetheless, this study demonstrates that new collagen is being synthesized in the leaflet

during pregnancy as reflected by (i) the growth of new tissue accompanying leaflet expansion and fibrosa thickening, (ii) the decrease in denaturation temperature (thermal stability) of the leaflet tissue, and (iii) the increased concentration of collagen in that tissue. The concentration of collagen increased and the thickness of the leaflet layers were altered, all this despite the dramatic leaflet area expansion. The most striking change in leaflet layer dimensions in pregnancy was an increase in thickness of the fibrosa, the main load-bearing layer of the leaflet. Since the fibrosa is composed predominantly of collagen, thickening of the fibrosa in pregnant animals is likely associated with the accumulation of collagen revealed via biochemical analysis.

The ability of the heart and its valves to adapt to pregnancy, a non-disease state, without failure is remarkable. This study has captured physiological remodeling of bovine mitral and aortic valve leaflets, tissues that up until very recently were thought to be incapable of remodeling. The presence of such rapid and extensive remodeling may be the reason for the apparent regurgitation resistance in pregnancy [168, 222, 308-311]. While both the aortic and mitral valves experience annular dilatation and increased loading during pregnancy, only 27% of normal pregnant women experience mitral regurgitant flow by full term—and there is nearly zero occurrence of regurgitation in the aortic valve [168]. This clinical finding may be indicative of the sort of valve-specific remodeling described here. Nonetheless, in cardiac pathologies such as left ventricular dysfunction, valve regurgitation is significant, often leading to heart failure [178, 185]. That said, valvular remodeling in pregnancy, particularly early in gestation, is not likely initiated by mechanical triggers (like valve orifice expansion) alone. For example, ectopic pregnancy, which occurs outside of the uterus, is still accompanied by anatomical changes in the uterus similar to those observed in normal early pregnancy [151]; there, mechanical stimulation cannot be the dominant remodeling trigger. Hormonal cues occur in parallel with mechanical triggers, particularly via the actions of the pregnancy hormone relaxin, and may play an equally important role in the adaptive remodeling processes of the heart valves. Relaxin is an important peptide hormone in pregnancy, linked to connective tissue remodeling (particularly collagen catabolism) in the uterus and cervix of pregnant rats [312]. It has a potential role in remodeling the extracellular matrix of cardiovascular tissues as well; however, its precise actions remain to be fully elucidated. Such hormonal

cues are absent in pathological conditions such as heart failure. Understanding valvular remodeling in response to pregnancy as described here may be fundamental to improving the prognosis of the mother later in life by understanding how the implications of pregnancies can affect long-term vascular risk. It may also prove valuable in developing interventions and treatments for valve disease and heart failure as well.

4.5 Acknowledgements

The authors thank Patricia Colp (Department of Pathology, Dalhousie University) for sharing expertise in histological staining techniques, Maxine Langman (Department of Applied Oral Sciences, Dalhousie University) for providing biochemical technical expertise, Mariya Turchin, Chantell Cleversey, and Jessi Bak (Dalhousie Integrated Science Program; DISP) for their assistance with histological analysis, as well as O.H. Armstrong for the supply of bovine tissues.

4.6 Author Contributions

Author contributions: CMP, SMW, and JML conception and design of research; CMP analyzed data; CMP and ADM performed experiments – more specifically, biaxial mechanical and hydrothermal testing experiments were performed by ADM, while all other experiments were performed by CMP; CMP analyzed data; CMP, SMW, and JML interpreted results of experiments; CMP prepared figures and drafted manuscript; CMP, SMW, and JML edited and revised manuscript; CMP, SMW, JML and ADM approved final version of manuscript.

CHAPTER 5

Pregnancy-Induced Remodeling of Heart Valves

Caitlin M. Pierlot[1], Andrew D. Moeller[1], J. Michael Lee[1,2], and Sarah M. Wells[1],

[1]School of Biomedical Engineering, Dalhousie University, Halifax, Nova Scotia, Canada; and [2]Department of Applied Oral Sciences, Dalhousie University, Halifax, NS, Canada

5.1 Introduction

Heart valves are complex and dynamic biological structures that play an elaborate role in functional heart efficiency, ensuring unidirectional blood flow by opening and closing more than 3 billion times in a lifetime. In the past, research surrounding the adaptation of heart valve tissues has focused on pathological conditions such as left ventricular (LV) dysfunction [185], mitral valve regurgitation [237], myxomatous degeneration [54], and heart failure [197]. Recent studies from our laboratory however, have demonstrated the capacity of maternal heart valve leaflets to remodel under the altered hemodynamics of pregnancy – a non-pathological condition [248, 293, 313]. Pregnancy is accompanied by an increase in blood volume and cardiac output of ~50%, as the maternal circulation accommodates the developing feto-placental unit. This is accompanied by cardiac enlargement [136, 157, 248] with expansion of valve orifices (by 12-23% in humans) [136, 157, 168] that elevate stresses in the leaflets. [211]. Our studies so far have reported dramatic increases in leaflet size, accompanied by alterations in fiber architecture and composition of both the aortic and mitral valve leaflets, contributing to a decrease in thermal stability, a reversible shift in leaflet extensibility, and valve-specific alterations in dynamic resistance to creep [248, 293, 313]. Together, these results provide strong evidence of both collagen turnover during pregnancy as well as maturation of the native leaflet collagen, suggesting that the aortic and mitral heart valve leaflets undergo a complex restructuring of their collagen matrix under the altered cardiovascular loading of pregnancy.

While remodeling in pregnancy has been described in the aortic and mitral valves, it is important to examine all four valves due to differences in their (i) embryological origin or (ii) mechanical loading conditions which may affect their remodeling response. Specifically, the inflow valves (mitral and tricuspid) arise solely from tissues of the endocardial cushions in the developing heart tube, while outflow valves (aortic and pulmonary) are also derived from immigrating neural crest cells [18, 25, 314-316]. On the other hand, higher transvalvular pressures in the left side of the heart (~120 mmHg versus ~25 mmHg in the right side [3]) result in higher tensile stresses in the mitral and aortic valve leaflets. The remodeling response to pregnancy may be valve-specific as there is evidence to suggest that (i) the state of the collagen matrix (thermal stability and

turnover), and (ii) valvular interstitial cell (VIC) phenotype and activity are valve-specific, and may be influenced by the embryological origin and/or the loading conditions of the tissue. For instance, Aldous et al. found that increasing transvalvular pressure (TVP) could be correlated to decreasing denaturation temperature, suggesting that collagen thermal stability is related to the in vivo loading of the valve [101]. Further, based on HIT tissue relaxation times, inflow valves appear to contain significantly less mature and total crosslinks compared to outflow valves, indicating that the remodeling rate of inflow valves is faster than, or at least that the molecular maturity of the inflow valves is less than, that of the outflow valves [101]. Other studies from Merryman et al. describe a correlation between VIC phenotype and TVP, with VICs from the higher TVP left-sided valves that (i) were significantly stiffer [3], (ii) contained higher contents of heat shock protein 47 (Hsp47, a collagen synthetic protein) and (iii) alpha smooth muscle actin (α-SMA, a cytoskeletal protein marker of the "activated" VIC phenotype [20, 61]) [3], and (iv) showed increased contractility [42]. Together, these studies suggest that valves from the higher-pressure left side of the heart have VICs in the activated, synthetic state, with increased rates of collagen turnover that together increase the "remodeling potential" of the tissue.

Based on these studies, we hypothesized that the right-sided heart valves would exhibit a decreased remodeling response to pregnancy in comparison to the striking response of the mitral and aortic valves. This hypothesis is supported by the prevalence of regurgitation in pregnant women. It is intriguing that while 95% of pregnant women experience regurgitation on their right side (low pressure), pulmonary and tricuspid valves, only 27% experience regurgitant flow on the mitral and none in the aortic valve [168], suggesting these only the left-sided valve leaflets remodel during pregnancy to maintain coaptation.

The purpose of this paper was to investigate the mechanisms of pregnancy-induced remodeling in all 4 valves of the heart, expanding on our previous studies to include the right-side tricuspid and pulmonary valves. Furthermore, understanding the basis and timeline of the specific mechanisms behind the structural and mechanical valvular adaptation in pregnancy requires a better appreciation of how the cellular (density and phenotype) and other extracellular components (collagen, elastin, glycosaminoglycans

(GAGs), and water) of the leaflet are changing. This cross-section of valve tissues will allow us to investigate the presence of valve-specific, loading-specific (left-side versus right side valves), and origin-specific (inflow versus outflow valves) differences in remodeling mechanisms.

5.2 Methods

5.2.1 Tissue Harvest and Sample Preparation

Protocols for the harvesting of bovine tissues were approved by the University Committee on Laboratory Animals (UCLA) at Dalhousie University. Bovine hearts were purchased as food from a local abattoir (Armstrong Food Services Limited, Kingston, Nova Scotia, Canada) immediately following slaughter. Hearts were collected from heifers (sexually mature, never pregnant female cattle), and from pregnant cows. To assess gestational age in pregnant cattle, fetal crown-rump length was measured, with a full term (278-290 days gestation) bovine fetus measuring approximately 100 cm [227]. Pregnant Animals ranged in gestational age from 61 days (9 cm fetal length) to 256 days (87 cm fetal length). Due to imposed federal food regulations at Canadian Abattoirs, all cattle were under 30 months of age and did not exhibit signs of illness (Canadian Food Inspection Agency, CFIA).

Due to structural consistency between aortic and pulmonary valve leaflets, all three leaflets of these valves were excised. Since the mitral and tricuspid valves possess significant structural and anatomic differences between leaflets, all experiments used the larger anterior (mitral) and posterior (tricuspid) leaflets. The mitral valve anterior leaflet experiences higher in vivo stresses as compared to the posterior leaflet [186, 228]. There is, however, no evidence to suggest that the tricuspid valve leaflets differ in mechanical properties, therefore to ensure consistency with previous studies [101] the larger posterior leaflet was used. All leaflets were excised as close to the valve root as possible. Leaflets were washed with Hanks' physiological solution (pH 7.4) including 6 mg/l trypsin inhibitor (lyophilosate), and an antibiotic-antimycotic agent and containing 10,000 units/ml of Penicillin G, 10 mg/ml streptomycin sulphate, and 25 µg/ml amphotericin B (Sigma-Aldrich Canada, Oakville, ON, Canada).

5.2.2 Mechanical Extensibility Testing

Aortic, mitral, pulmonary, and tricuspid valve leaflets for mechanical testing were excised on location, immersed immediately in Hanks' physiological solution, and transported back to the lab on ice. A 1cm-square specimen was cut from the center belly region of each leaflet (Fig. 4.1A). Tissue samples were stored in 4ºC overnight and tested within 72 hours of excision.

As described in our previous study [248], mechanical testing was conducted on a custom-built, servo-hydraulic biaxial testing apparatus (MTS, 458 Series, Eden Prairie, MN). Briefly, specimens were mounted (3-0 coated, braided silk, 75cm continuous suture) between four suture-style grips and mounted into the testing device with the radial and circumferential directions aligned with the testing device axes. Deformation of the sample was measured by optical tracking of a 2 by 2 grid of four small graphite markers (Fig. 4.1B). Biaxial mechanical loads were applied as membrane tension (expressed in N/m) – the axial force per unit length of tissue over which the force is applied. Throughout the duration of the mechanical experiments, the specimens were maintained in a Hanks' physiological solution bath at 37 ºC.

Extensibility tests were performed on valves from 9 non-pregnant heifers, and 13 pregnant cows, as described previously [248, 313]. Specimens were then extended in both the circumferential and radial directions, from a pre-load of 0.5-N/m to a peak equibiaxial tension of 60-N/m as in previous studies. Specimens were preconditioned for 10 cycles to the peak tension, at 0.05 Hz, and data acquisition was performed on a final (11th) cycle.

Extensibility Data Analysis. Analysis of mechanical data was detailed previously [248], and is briefly outlined here. The displacement of the 4 graphite markers on the specimen surface was analyzed using ImageJ (National Institutes of Health), and their positional data were used to calculate the axial stretch ratios: λ_C^{peak} (circumferential extensibility) and λ_R^{peak} (radial extensibility) under peak equibiaxial membrane tension (60-N/m). The net tissue extensibility was represented by the areal stretch under peak tension and was calculated using the following equation:

$$\text{Areal Stretch}^{peak} = (\lambda_C^{peak} \times \lambda_R^{peak})$$

Finally, tension versus areal stretch graphs were plotted using areal stretch values calculated at equibiaxial tensions of 1.0, 2.5, 5.0, 10.0, 20.0, 30.0, 40.0, 50.0, and 60.0-N/m, to assess leaflet tissue properties over the entire loading range examined under biaxial loading.

5.2.3 Leaflet Dimensions

Dimensions of leaflets from the aortic and mitral valve were presented in our previous study [313] and are extended here to include the pulmonary and tricuspid valves. Fresh, excised aortic and mitral valve leaflets from 10 non-pregnant heifers and 15 pregnant cows, were laid flat and photographed (Nikon D50 camera, Nikon, Tokyo, Japan) with a reference scale bar. Images were imported into image-analysis software (ImageJ, National Institutes of Health), where radial midline length and circumferential midline length were measured, and the freehand selection tool was used to outline the perimeter of the leaflet to calculate the total area of the leaflet (Fig. 4.1A).

5.2.4 Biochemical Analysis

Following imaging for leaflet dimensions, the same group of valves (from 10 non-pregnant heifers and 15 pregnant cows) were prepared for biochemical assays for total and acid-soluble collagen, glycosaminoglycans and elastin. Heart valve leaflets for all assays were wrapped in cheesecloth soaked in Hanks' physiological solution, placed immediately in the -86°C freezer, and stored until they could be tested. The first set of frozen leaflets were freeze-dried for a minimum of 52 h. Dry samples of approximately 10 mg dry weight, from the belly region of the leaflet, were weighed and recorded. Total collagen content (normalized to dry weight) was estimated from the hydroxyproline content [263] following the protocol of Woessner [262].

Biocolor biochemical assay kits (Biocolor Ltd., Carrickfergus, UK : Accurate Chemical & Scientific Corporation, Westbury, NY, USA) were used to assess the content of sulphated glycosaminoglycans (sGAG; Blyscan Assay), elastin (Fastin Assay), and acid and pepsin-soluble collagen (Sircol Assay). This extractable form of collagen is often interpreted to be newly laid down collagen that is not sufficiently crosslinked into the

network to resist solubilisation. For these studies, the second set of frozen leaflets were thawed and dissected to take samples from the belly of the leaflet, and weighed prior to testing. All samples were assayed in duplicate, and compared to a set of blanks and standards. Following the assay, a microplate reader (Synergy HT, Bio-Tek Intruments Inc., Winooski, Vermont) was used to measure the dye absorbance of each prepared plate at a specified wavelength (656 nm : Blyscan, 513 nm : Fastin, and 555 nm : Sircol). Dry weight measures of glycosaminoglycans, elastin, and extractable collagen were calculated using the wet/dry weights from each valve.

5.2.5 Histological Analysis

Leaflet histology from aortic and mitral valves was presented in our previous study [313]. In the present study, we extend these analyses to include the pulmonary and tricuspid valves, with the addition of immunohistochemical assessment of VICs in all four valves.

Leaflets were collected from another set of animals (9 non-pregnant heifers and 13 pregnant cows) and prepared for histological analysis as described in our earlier study [313]. Each leaflet was divided to produce two symmetric halves of the leaflet (Fig. 3.3), that were fixed (10% neutral buffered formalin), embedded, and sectioned into 5μm serial sections. Circumferential cross-sections were cut from one half of the leaflet for picrosirius red staining to examine collagen alignment and crimp. Radial cross-sections were cut in the other half of the leaflet for Verhoeff-Van Gieson staining to identify leaflet layering (Verhoeff-Van Gieson Elastin Staining Kit, Polysciences, Inc., Washington, PA) as well as immunohistochemical (IHC) staining of activated phenotype marker alpha-smooth muscle actin (α-SMA) (Fig. 3.3). Each radial section contained the complete leaflet cross-section from the free edge to the fixed edge.

5.2.6 Collagen Crimp Analysis

Images were taken of picrosirius-strained sections using a Nikon Eclipse E600 light microscope equipped with a polarizer and a 10MP AmScope digital camera. Collagen crimp was characterized by: (i) crimp length, (peak-to-peak measurement of one crimp period) and (ii) percentage of the leaflet area which was crimped. For both measures, six contiguous images were taken at 40x objective magnification along the

circumferential direction, spanning 2 mm into the belly region of the leaflet, and analyzed using ImageJ software (National Institutes of Health). For crimp length measurements, a line was drawn across the centerline of each image and every distinguishable crimp length along that line was recorded (Fig. 3.4). For crimped area measurements, a grid (300 μm^2/square) was placed on each image and the number of grid points in contact with tissue (crimped or uncrimped) was recorded. The ratio of crimped-to-total grid points was then used to calculate the area percentage of the leaflet occupied by crimped. Both crimp length and crimped area were averaged across all 6 images for each valve. Blinded measurements were made by three observers, with excellent agreement between observer counts. Data for each valve represents the average of those from the three observers.

5.2.7 Leaflet and Layer Thicknesses

Verhoeff-Van Gieson stained sections were photographed at low magnification along the entire length of the valve leaflet (Zeiss Axioplan 2 Imaging Microscope with AxioVision software (Release 4.8.1) and images from each valve were assembled into a single mosaic using ImageJ with plugins MosaicJ [260] and TurboReg [261]. An array of lines was placed on each mosaic such that. Thickness measurements, of the full leaflet as well as of each layer (fibrosa, spongiosa, and ventricularis (outflow valves only) or atrialis (inflow valves only)), were taken at 25 equidistant vertical lines that transected the full thickness of the tissue along the length of the leaflet (Fig. 3.5) Thickness measurements were then averaged across the length of the leaflet for each valve sample.

5.2.8 Cell Density and Phenotype

Radial leaflet sections were also used for immunohistochemistry (IHC) staining of alpha-smooth muscle actin (α-SMA) to identify alterations to cell phenotype associated with pregnancy, using the standard IHC protocol detailed by Ramos-Vara et al., and explained here briefly [317]. Slides were deparaffinised, rehydrated, and pretreated with heat-induced epitope retrieval (HIER). This antigen retrieval process modifies the molecular conformation of proteins by removing protein crosslinking caused by aldehyde-based fixatives [317-319], improving subsequent IHC staining. Tris-ethylenediaminetetraacetic acid (EDTA) buffer (pH 9) was used in the HIER process. To

reduce non-specific background staining, endogenous peroxidases were blocked using hydrogen peroxide and endogenous biotin protein was blocked with avidin/biotin protein block. Incubation of the primary antibody (monoclonal mouse anti-human smooth muscle actin, M0851, Dako) was performed in humid chambers at 37 °C overnight. The secondary biotinylated antibody (Biotin, Dako) was applied, followed by the application of streptavidin-peroxidase conjugate (horseradish peroxidase – HRP) to bind to biotin for signal amplification. Diaminobenzidine-HRP (DAB) was then used to allow for visualization of streptavidin-HRP, and finally slides were counterstained with Mayer's hematoxylin solution and Scott's water, dehydrated, and mounted with glass cover slips. Antibody optimization for stain quantity and intensity was performed prior to the staining of all leaflet tissues and was determined to be at a dilution of 1:200 for both the primary α-SMA antibody as well as the IgG2a negative isotype control (Mouse IgG2a, X0943, Dako). All samples were stained along with a negative control (no primary antibody), an isotype control, and a positive control.

Digital images were taken across the thickness of the valve leaflet at 40x objective magnification (Zeiss Axioplan 2 Imaging Microscope and imaging software (AxioVision, Release 4.8.1). Cell counting was performed using ImageJ imaging software Count Cell plugin and two counter types: Type 1 counts all nuclei (total cell number); Type 2 counts α-SMA-positive nuclei (α-SMA+ cell number) (Fig. 5.1). The percentage of α-SMA-positive cells (% α-SMA+) was calculated from the ratio of positive stained cells to total cell count.

5.2.9 Denaturation Temperature and Hydrothermal Isometric Tension Testing

Collagen thermal stability and crosslinking were presented in our previous study for the aortic and mitral valve [313] using denaturation temperature testing (DTT) and hydrothermal isometric tension (HIT) tests. The present study extended these analyses to include the pulmonary and tricuspid valves.

Leaflets were collected from another set of animals (10 non-pregnant heifers and 23 pregnant cows) for DTT and HIT testing as described previously [110, 117, 313]. Briefly, circumferential strips cut from the belly of the leaflet were mounted under isometric

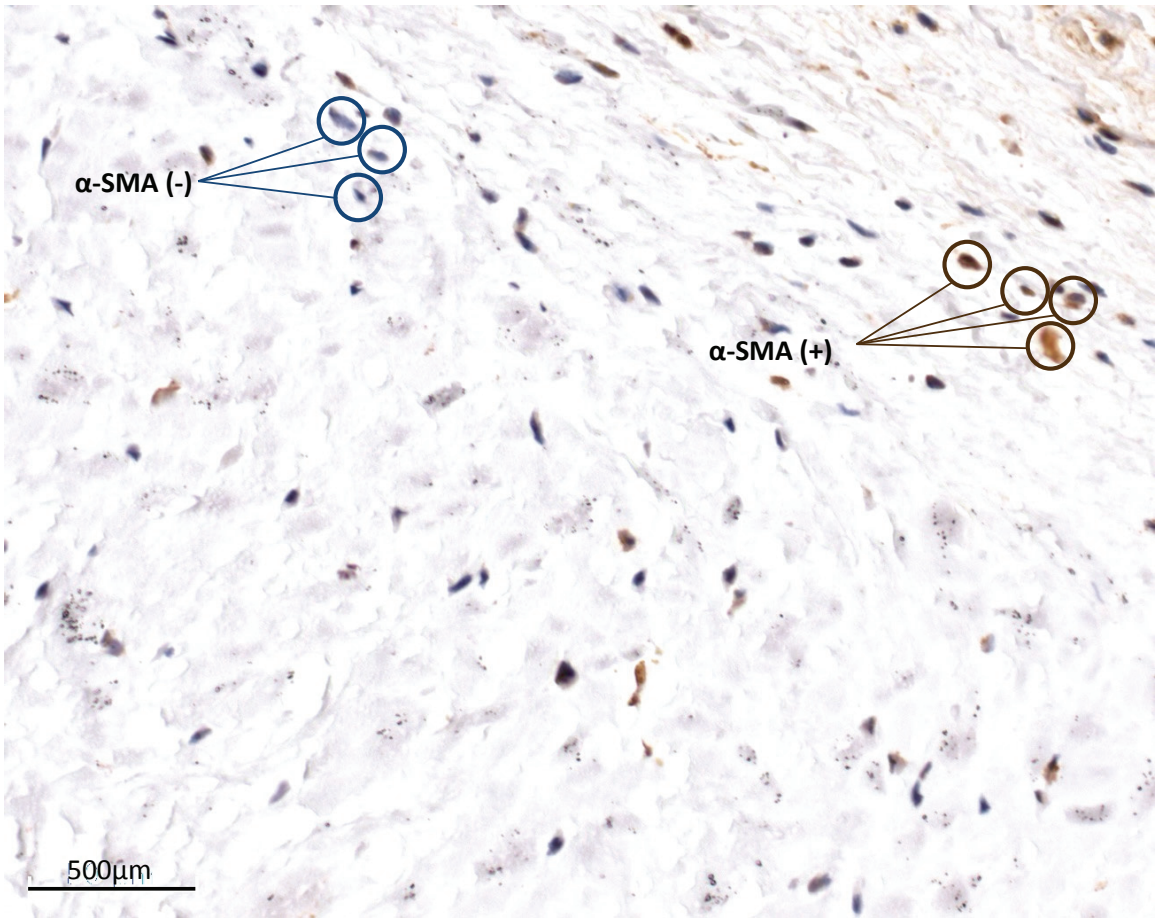

Figure 5.1 Methodology for measurement of cell density and phenotype

Cell density and phenotype measurements were performed using two counter types: Type 1 counts all nuclei (total cell number); Type 2 counts (α-SMA-positive nuclei (α-SMA+ cell number). Cells staining purple/blue are α–SMA-negative (no expression of α-SMA), while cells staining brown are α-SMA-positive (expression of α-SMA). Scale bar = 500µm.

tension in a bath of distilled water. The denaturation temperature, Td, is indicated by a sharp increase in tension [115, 118] as the bath temperature is increased from ~20ºC (room temperature) to 90°C. Following the heating segment, a 90°C isotherm was maintained for three hours. Under these conditions, the isometric tension is largely supported by the denatured collagen in the sample. The tension decays as peptide bonds of the collagen network hydrolyse allowing slippage of the chain fragments [119]. The rate of relaxation of a tissue has been shown to be independent of its non-collagenous constituents and is closely correlated to the concentration of thermally stable crosslinks in a collagen sample [120]: the more crosslinks present, the slower the relaxation rate. The tension relaxation half-time ($t_{1/2}$) thus provides an indicator of mature collagen crosslinking. An index of total collagen crosslinking was obtained from the HIT $t_{1/2}$ of paired tissue samples after immature crosslinks were reduced to a heat-stable form with $NaBH_4$ [117].

5.2.10 Statistical Analysis

All results are expressed as the mean ± standard error of the mean (SEM), with the n value representing the number of animals per group. All data is divided into two groups: NP (non-pregnant), and P (pregnant).

Effects of pregnancy within each valve: Statistical comparisons were made using two-tailed t-test comparisons between the pregnant and non-pregnant groups. The pregnant group was also further divided into EP (early pregnant) and LP (late pregnant) groups according to fetal crown-to-rump length, as in our previous study [313]. Cows carrying fetuses of crown-to-rump length < 45 cm (0–169 days) were classified as EP, and those carrying fetuses > 55cm (193–270 days) were classified as LP. The mid-pregnancy group of 45–55 cm (169–193 days) was omitted in this comparison to obtain a more complete separation of early and late groups. The biaxial mechanical (extensibility) and thermomechanical data used in this study for the mitral valve come from the dataset published by Wells et al. [248]**,** but reanalyzed under different pregnancy state divisions. That previous study defined early pregnancy as ~0-159 days of gestation, and late pregnancy from 160-270 days. By contrast, the current study divides gestation in half using fetal crown-to-rump length, as defined above. A one-way ANOVA was performed,

followed by Tukey honestly significant difference comparisons among the three groups (NP, EP, and LP). To evaluate changes in any parameter as a function of pregnancy duration, data were plotted as a function of gestational age and fitted with a least-squares linear regression.

Effects of valve on pregnancy response: Lastly, comparisons were made between valves of differing anatomical positions: (i) left-side (aortic and mitral) valves versus right-side (pulmonary and tricuspid) valves to reveal the effects of loading conditions on the remodeling response, (ii) inflow (mitral and tricuspid) valves versus outflow (aortic and pulmonary valves) to reveal the effects of embryological origin on the remodeling response, and (iii) individual valve types (aortic, mitral, pulmonary, and tricuspid independently), to uncover the presence of valve-specific remodeling. In these three cases, this was preceded by two-way ANOVA to test for an interaction between anatomical location and pregnancy state. Statistical comparisons of left-side versus right-side valves, and of inflow versus outflow valves, were made using t-Test comparisons of groups. To compare individual valve types, one-way ANOVA was performed, followed by Tukey honestly significant difference comparisons among the four valves.

Results and regressions were considered significant for $p < 0.05$. Outliers were defined as data points falling outside of the following quantile-based range: [25^{th} quantile – 1.5*(interquantile range)] to [75^{th} quantile + 1.5*(interquantile range)], where interquantile range = 75^{th} quantile – 25^{th} quantile. These data points were excluded from further analysis. All statistical analyses were performed using JMP Statistical Software (Version 10.0, SAS Institute, Inc., Cary, NC).

5.3 Results

5.3.1 Leaflet Mechanical Properties

Effect of Pregnancy: In all valves from non-pregnant and pregnant animals, leaflets were more extensible in the radial direction than the circumferential direction, as previously reported in humans [39], sheep [236], pigs [216, 233-235, 295, 296], and cows [248, 293, 313]. Peak areal stretch at 60-N/m equibiaxial tension (net extensibility) in the aortic, mitral, and pulmonary valves decreased 11%, 20%, and 14% respectively (Table 5.1), during early pregnancy, then increased linearly with fetal growth (Fig. 5.2A, D, G),

Table 5.1 Summary of leaflet mechanical changes in the belly region of the leaflet with pregnancy

		Mechanical Measurements						
		Non-pregnant	Early pregnant	Late pregnant	p-value	All pregnant	Δ pregnancy	p-value
Aortic	Areal stretch‡	2.45 ± 0.07(9)^{a}	2.18 ± 0.07(7)^{b}	2.46 ± 0.09(4)^{ab}	0.0196	2.30 ± 0.06†(12)	biphasic	0.0630
Valve	λ_R^{peak} ‡	1.79 ± 0.04(9)	1.75 ± 0.06(7)	1.84 ± 0.07(4)	0.6108	1.80 ± 0.04(13)	-	0.8674
	λ_C^{peak} ‡	1.36 ± 0.04(10)	1.25 ± 0.03(8)	1.34 ± 0.05(4)	0.0578	1.28 ± 0.02*(13)	↓	0.0325
Mitral	Areal stretch‡	2.37 ± 0.09(7)^{a}	1.89 ± 0.13(6)^{b}	2.29 ± 0.15(4)^{ab}	0.0375	2.11 ± 0.11*(12)	biphasic	0.0439
Valve	λ_R^{peak} ‡	1.67 ± 0.06(9)	1.58 ± 0.07(7)	1.77 ± 0.10(4)	0.2872	1.67 ± 0.06(13)	-	0.9721
	λ_C^{peak} ‡	1.37 ± 0.03(7)^{a}	1.23 ± 0.03(8)^{b}	1.29 ± 0.04(4)^{ab}	0.0250	1.26 ± 0.03*(14)	biphasic	0.0153
Pulmonary	Areal stretch	2.65 ± 0.13(7)^{a}	2.13 ± 0.10(7)^{b}	2.78 ± 0.15(4)^{a}	0.0019	2.35 ± 0.09*(15)	biphasic	0.0461
Valve	λ_R^{peak}	1.97 ± 0.08(8)^{a}	1.67 ± 0.06(9)^{b}	2.13 ± 0.10(4)^{a}	0.0016	1.82 ± 0.07(15)	biphasic	0.1395
	λ_C^{peak}	1.35 ± 0.02(7)	1.35 ± 0.03(9)	1.30 ± 0.04(4)	0.2415	1.29 ± 0.02*(15)	↓	0.0324
Tricuspid	Areal stretch	2.41 ± 0.09(7)	2.08 ± 0.09(8)	2.05 ± 0.18(2)	0.0530	2.15 ± 0.09*(12)	↓	0.0323
Valve	λ_R^{peak}	1.62 ± 0.06(7)	1.58 ± 0.07(8)	1.60 ± 0.09(4)	0.0016	1.63 ± 0.06(14)	-	0.9117
	λ_C^{peak}	1.49 ± 0.02(7)^{a}	1.32 ± 0.02(8)^{b}	1.40 ± 0.04(2)^{ab}	0.0006	1.34 ± 0.02***(12)	biphasic	<0.0001

Values are mean values ± SE of leaflet areal stretch, peak radial stretch ratio (λ_R^{peak}), and peak circumferential stretch ratio (λ_C^{peak}), for animals in the non-pregnant (NP), early pregnant (EP), late pregnant (LP), and all pregnant grouped together (P) groups. Statistical comparisons were made between NP and P groups using t-Test comparisons of groups and are presented with the corresponding p value. Statistical comparisons among NP, EP, and LP groups using one-way ANOVA followed by Tukey honestly significant difference (HSD) multiple-comparison method. [a,b]Within each parameter, values labeled with the same letter were not significantly different. n values for the pregnancy groups are presented in brackets for each measurement. p value ranges are indicated as follows: † = $p < 0.1$; * = $p < 0.05$; ** = $p < 0.01$; *** = $p < 0.001$. ‡Mechanical measures of extensibility and areal stretch for the mitral and aortic valve leaflets previously presented by Pierlot and colleagues [313].

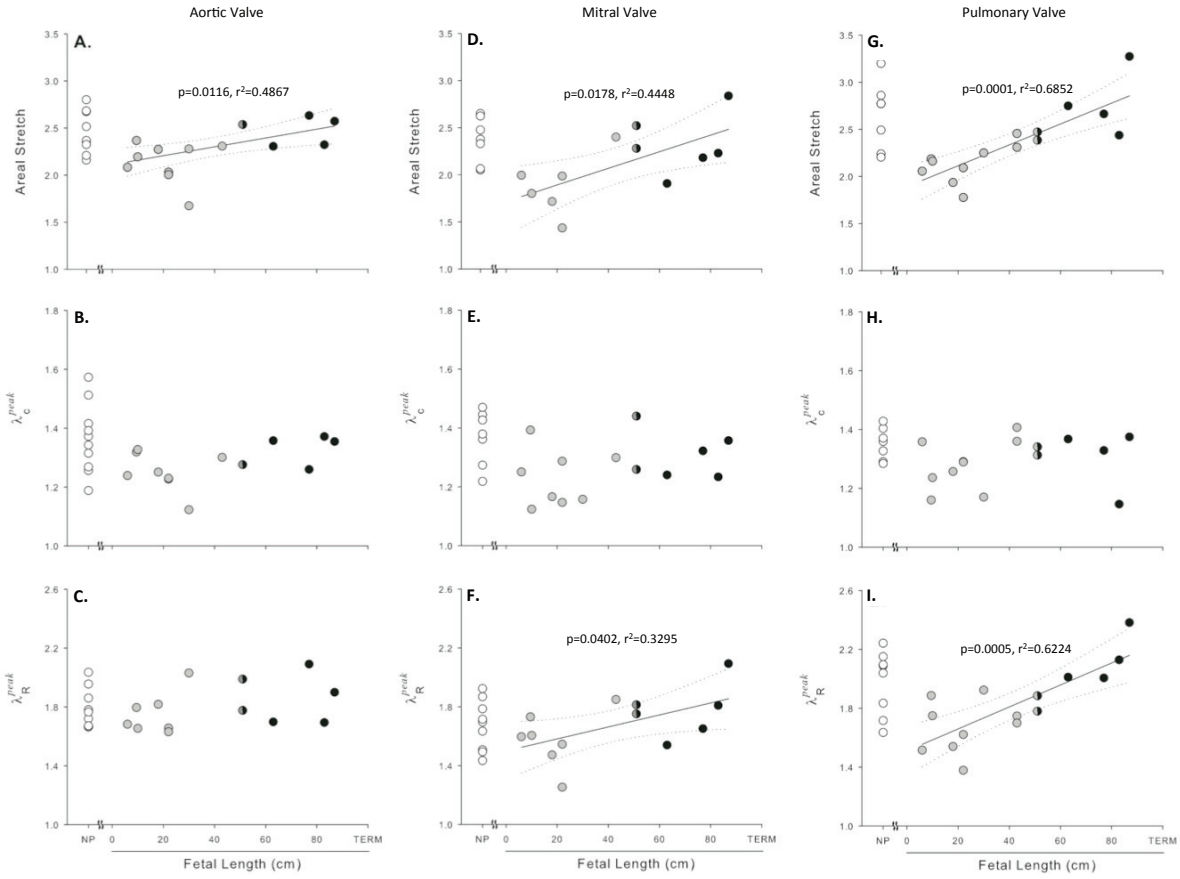

Figure 5.2 Biaxial mechanical properties (aortic, mitral, and pulmonary)

Biaxial mechanical properties of the aortic (A-C), mitral (D-F), and pulmonary (G-I) valve leaflets: peak values at 60-N/m equibiaxial tension. Peak areal stretch, λ_C^{peak}, and λ_R^{peak}, as a function of fetal crown-to-rump length (100 cm ~ term) along with measurements from NP heifers (open circles). Pregnant groups are shaded based on gestation: EP (0-169 days of gestation; shaded circles), MP (170-192 days; 1/2 shaded circles), and LP (193-270 days of gestation). Regression lines with 95% confidence intervals are shown for the fetal data where significant.

returning to or above pre-pregnant values by late pregnancy (Table 5.1). The tricuspid valve, however, showed unidirectional, 11% decrease in extensibility from non-pregnant to pregnant animals, with decreases largely in early pregnancy, signified by a 14% decrease (significant at $p<0.10$ only) in areal stretch in early pregnancy (Table 5.1).

The changes in leaflet extensibility during pregnancy were contributed to by changes in extensibility in both the circumferential and radial directions (Table 5.1). Peak circumferential extensibility (λ_C^{peak}) decreased overall in pregnancy (with all pregnant animals grouped together) in the aortic (6%) and pulmonary (4%) valves, while decreases in λ_C^{peak} were detected in early pregnancy in the mitral (10%) and tricuspid (11%) valves. While peak radial extensibility (λ_R^{peak}) was significantly decreased (15%) in early pregnancy only in the pulmonary valve (Table 5.1), it linearly increased with pregnancy duration in the mitral (Fig. 5.2F) and pulmonary valve (Fig 5.2I), thereby contributing to the recovery of the pre-pregnant extensibility in late pregnancy.

Areal stretch was also assessed over the whole range of equibiaxial tensions used in our mechanical loading experiment (Fig. 5.3). In the aortic, mitral, and pulmonary valves, at each tension above 5-N/m, mean areal stretch decreased from non-pregnant to early pregnant animals (leftward shift of the tension stretch curve), and then increased in late pregnant animals, indicating a reversible decreases in leaflet extensibility (Fig. 5.3A-C). In the tricuspid valve, mean areal stretch at each tension decreased from non-pregnant to early pregnant animals (leftward shift of tension stretch curve), and remained unchanged in late pregnancy, representing an irreversible decrease in leaflet extensibility (Fig. 5.3D).

Effect of Valve Type: Areal stretch of the inflow valves (mitral and tricuspid) was 7% lower than the outflow valves, mainly due to a lower radial extensibility in these valves – this relationship was present in non-pregnant animals and was also preserved in pregnancy.

5.3.2 Leaflet Dimensions

Effect of Pregnancy: Bovine heart valve leaflets underwent remarkable changes in macroscopic leaflet dimensions during pregnancy (Fig. 5.4). Increases in leaflet area (Fig. 5.5A) as well as both radial and circumferential dimensions were found in all four

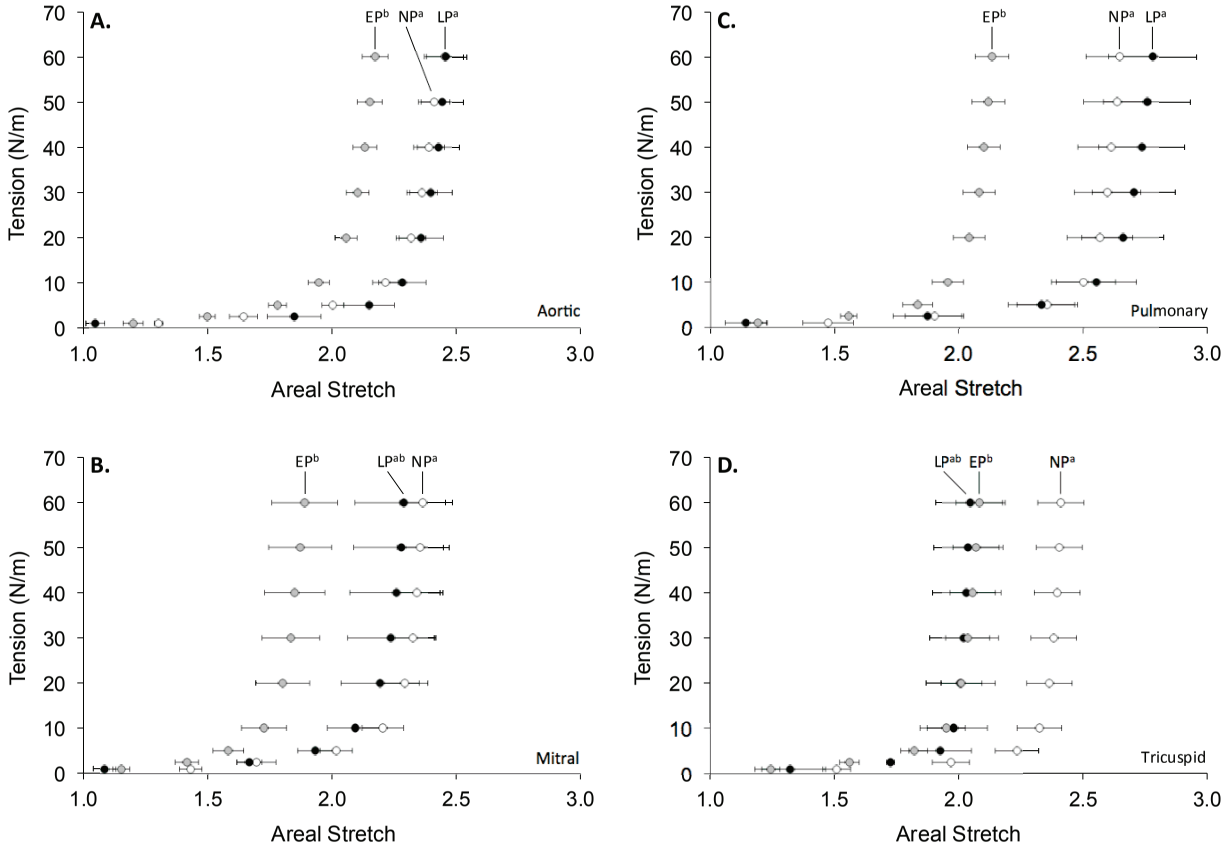

Figure 5.3 Tension versus areal stretch curves by pregnancy group (all valves)

Mean tension versus areal stretch curves for the aortic (A), mitral (B), pulmonary (C), and tricuspid (D) valve leaflets, at each pregnancy state (NP, EP, and LP). Areal stretch is plotted as means ± SE at tension increments of 1.0, 2.5, 5.0, 10.0, 20.0, 30.0, 40.0, 50.0, and 60.0 N/m. Statistics shown with each pregnancy group are valid for every tension level above 5 N/m. [a,b]Values labeled with the same letter were not significantly different.

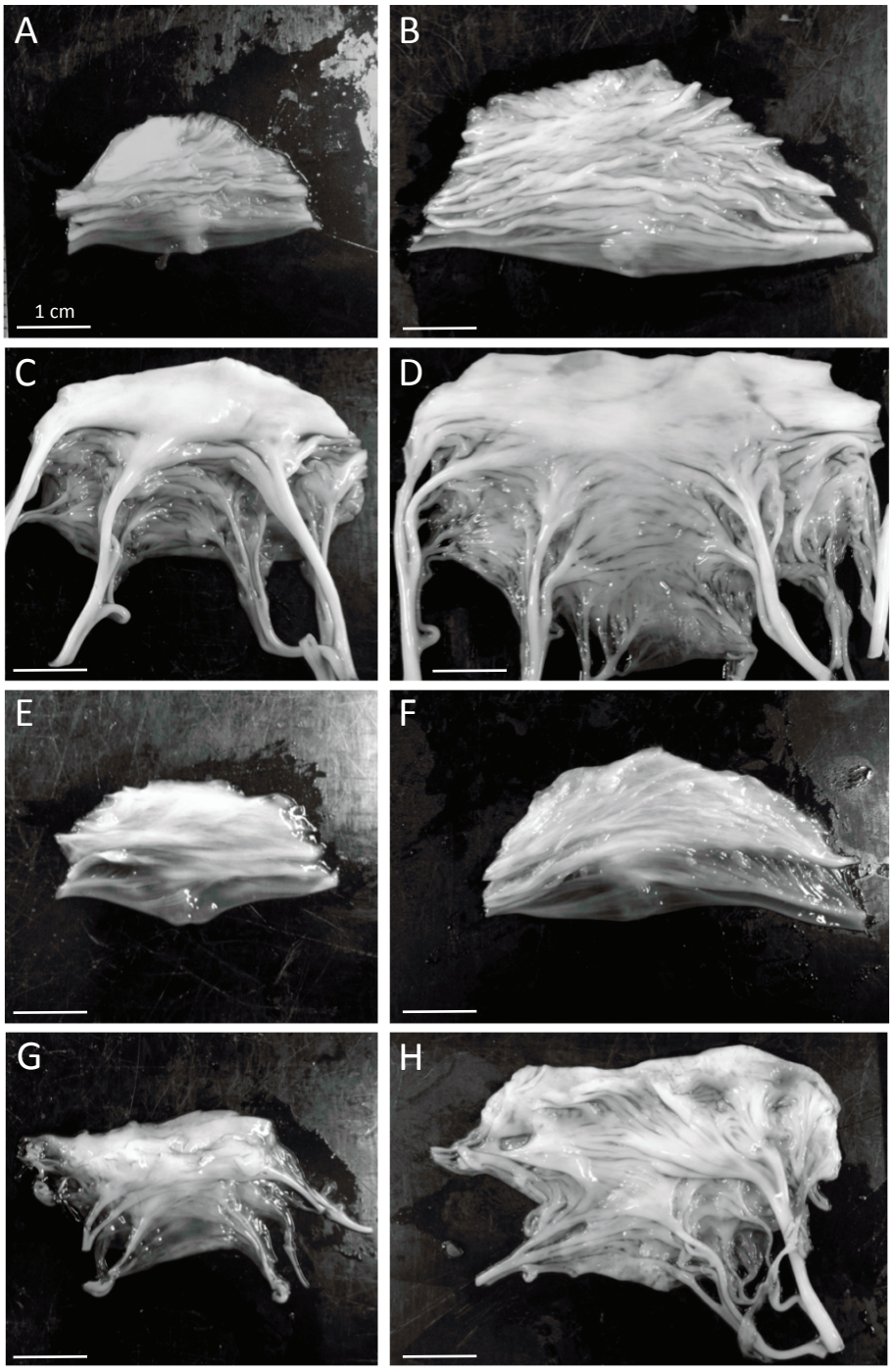

Figure 5.4 Images of morphological changes in pregnancy (all valves)

Representative images of leaflet, of each valve type, showing morphological changes with pregnancy. A, C, E, and G: leaflets from the non-pregnant (NP) group of the aortic, mitral, pulmonary, and tricuspid valves respectively. B, D, F, and H: leaflets from the pregnant (P) group of the aortic, mitral, pulmonary, and tricuspid valves respectively. Scale bar = 1 cm.

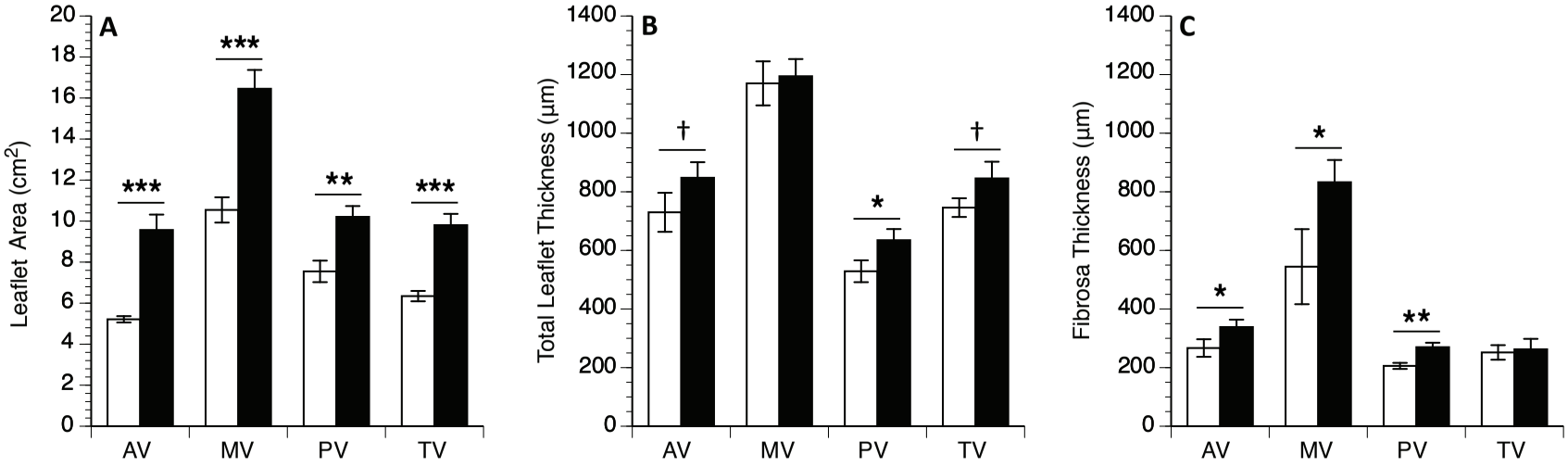

Figure 5.5 Valve leaflet and layer dimension plots (all valves)

Valve leaflet dimensions from NP heifers (open bars) and pregnant cows (filled bars) for aortic (AV), mitral (MV), pulmonary (PV), and tricuspid valves (TV). A: leaflet area (in cm^2). B: total leaflet thickness (in µm). C: fibrosa thickness (in µm). Values are means ± SE. Statistical comparisons were made between NP and P groups using t-Test comparisons of groups. Columns labeled with asterisks denote a statistically significant change: † = $p < 0.1$; * = $p < 0.05$; ** = $p < 0.01$; *** = $p < 0.001$.

valves during pregnancy (Table 5.2): Mean leaflet area increased 84%, 56%, 35%, and 55% between non-pregnant and pregnant groups in the aortic, mitral, pulmonary and tricuspid valves respectively, contributed to by 11-30% increases in radial length and 19-41% increases in circumferential length across the valves.

Effect of Valve Type: Valve leaflet area is the only parameter where two-way ANOVA showed significant differences with valve type (aortic, mitral, pulmonary, tricuspid) and pregnancy state (non-pregnant, pregnant), as well as a significant interaction between the groups ($p = 0.0124$). These results signify that differences in leaflet area should be considered in non-pregnant and pregnant groups separately, in each of the valves. One-way ANOVA showed a significant effect of valve type in both non-pregnant and pregnant animals, with the mitral valve, not surprisingly, significantly larger than all other valves in both groups. (Table 5.2 and Fig. 5.5A).

In addition, inflow valve leaflets were 33% larger in area than outflow valves, mainly due to a larger circumferential length in these leaflets – a characteristic that was conserved in pregnancy. Left side valve leaflets were 26% larger than right side valve leaflets, again due to their larger circumferential lengths. Interestingly, while the right-sided leaflets remained smaller in pregnancy, their circumferential lengths increased to become similar to those of the left-sided valves. , Thus, the larger circumferential length of the left-sided valve leaflets is not conserved in pregnancy.

5.3.3 Leaflet and Layer Thickness

Effect of Pregnancy: Leaflet and layer thicknesses were moderately altered with pregnancy (Table 5.3). Total leaflet thickness increased in all valves except, surprisingly, for the mitral. Leaflet thickness increased with weak significance in the aortic (16%) and tricuspid (13%) valves between non-pregnant and pregnant animals (Fig. 5.5B, Table 5.3). A stronger correlation was found in the pulmonary valve: thickness increased 20% in pregnancy (Fig. 5.5B, Table 5.3).

While the overall thickness of the leaflet increased in pregnancy, the thickness of each leaflet layer was also investigated. The most striking increases in leaflet thickness were attributed to alterations in the fibrosa, with significant increases between non-pregnant and pregnant groups in all valves except the tricuspid: aortic fibrosa thickened 27%, the

Table 5.2 Changes in leaflet dimensions with pregnancy

	Leaflet dimensions: Length, cm; Area, cm^2							
	Aortic Valve‡		Mitral Valve‡		Pulmonary Valve		Tricuspid Valve	
	Non-pregnant	Pregnant	Non-pregnant	Pregnant	Non-pregnant	Pregnant	Non-pregnant	Pregnant
Rad. Length	2.02 ± 0.04(9)	2.63 ± 0.11***(15)	2.64 ± 0.13(10)	2.93 ± 0.04*(12)	2.23 ± 0.13(10)	2.77 ± 0.08**(14)	2.10 ± 0.09(10)	2.49 ± 0.08**(15)
Circ. Length	3.25 ± 0.07(9)	4.58 ± 0.20***(15)	4.44 ± 0.12(10)	5.86 ± 0.21***(15)	3.85 ± 0.16(10)	4.58 ± 0.16**(14)	3.81 ± 0.14(10)	4.62 ± 0.15**(15)
Area	5.21 ± 0.15(9)	9.57 ± 0.75***(15)	10.54 ± 0.62(10)	16.45 ± 0.92***(15)	7.55 ± 0.52(10)	10.21 ± 0.53**(14)	6.34 ± 0.25(9)	9.80 ± 0.55***(15)

Values are mean values ± SE of leaflet dimensions for animals in the non-pregnant (NP), and pregnant (P) groups: radial (rad.) midline length (in cm), circumferential (circ.) midline length (in cm), and overall leaflet area (in cm^2). Statistical comparisons were made between NP and P groups using t-Test comparisons of groups and p value ranges are indicated as follows: † = $p < 0.1$; * = $p < 0.05$; ** = $p < 0.01$; *** = $p < 0.001$. n values for each parameter in the NP and P groups are presented in brackets for each valve.
‡Results for aortic and mitral valve leaflet dimensions previously presented by Pierlot and colleagues [313].

Table 5.3 Changes in leaflet thickness and individual layer thicknesses

	Thickness, μm							
	Aortic Valve‡		Mitral Valve‡		Pulmonary Valve		Tricuspid Valve	
	Non-pregnant	Pregnant	Non-pregnant	Pregnant	Non-pregnant	Pregnant	Non-pregnant	Pregnant
Total	730 ± 67(9)	848 ± 53†(15)	1170 ± 75(9)	1194 ± 59(11)	529 ± 37(9)	635 ± 38*(15)	746 ± 32(8)	846 ± 57†(14)
Fibrosa	267 ± 30(9)	338 ± 25*(15)	540 ± 130(9)	833 ± 76*(11)	206 ± 10(8)	270 ± 15**(15)	252 ± 25(8)	262 ± 36(13)
Spongiosa	249 ± 33(9)	290 ± 38(15)	431 ± 85(9)	346 ± 76(11)	170 ± 17(8)	236 ± 34(15)	260 ± 28(8)	324 ± 44(13)
Ventricularis/Atrialis	200 ± 41(9)	195 ± 14(14)	221 ± 40(8)	135 ± 22*(10)	105.0 ± 8.4(9)	125 ± 14(13)	270.8 ± 9.4(7)	228 ± 28(13)

Values are mean values ± SE of total leaflet thickness and individual leaflet layer thicknesses (in μm): fibrosa thickness, spongiosa thickness, and ventricularis (outflow valves) or atrialis (inflow valves) thickness, for animals in the non-pregnant (NP), and pregnant (P) groups. Statistical comparisons were made between NP and P groups using t-Test comparisons of groups and p value ranges are indicated as follows: † = $p < 0.1$; * = $p < 0.05$; ** = $p < 0.01$; *** = $p < 0.001$. n values for each parameter in the NP and P groups are presented in brackets for each valve. ‡Results for leaflet and layer thickness previously presented by Pierlot and colleagues, for the mitral [293] and aortic [313] valves.

mitral 54%, and the pulmonary 31% in pregnancy (Fig. 5.5C, Table 5.3). The concurrent thinning of the mitral atrialis (by 39%) resulted in its unchanged leaflet thickness with pregnancy (Fig. 5.5C, Table 5.3). Interestingly, we observed a weak linear trend toward decreasing spongiosa thickness (Fig. 5.6A) and increasing ventricularis thickness (Fig. 5.6B) with increasing gestational age in the aortic valve only.

Effect of Valve Type: Total leaflet thickness and fibrosa thickness in this study were 40% and 94% higher respectively in (higher-loaded) left side valve leaflets compared to right side leaflets (Table 5.3). Total leaflet—and individual layer thicknesses—were all larger in inflow valve leaflets compared to outflow valves (Table 5.3) Again, these differences were conserved in pregnancy.

5.3.4 Collagen Crimp

Effects of Pregnancy: Analysis of PR-stained samples was conducted in the belly region of the leaflet (Fig. 3.9). Remarkable changes were found in collagen fiber crimp with pregnancy (Table 5.4). Crimp length increased 216% in the aortic valve, 186% in the mitral valve, 42% in the pulmonary valve, and 61% in the tricuspid valve, between non-pregnant and pregnant groups (Fig. 5.7A). There was a corresponding decrease in the percentage of the leaflet which was crimped: crimped area decreased 24%, 43%, and 28%, in the aortic, mitral, and pulmonary valves respectively with pregnancy, but with no significant change in the tricuspid valve of pregnant animals (Fig. 5.7B).

Effects of Valve Type: Anatomical differences in crimp architecture were found only between inflow and outflow valves, and these differences were maintained in pregnancy. Crimp length was 97% higher in inflow valve leaflets compared to outflow valve leaflets, was correlated with the presence of 45% lower leaflet area occupied by crimp in these same inflow valves.

5.3.5 Leaflet Biochemical Composition

Effect of Pregnancy: Biochemical analysis of heart valve leaflet tissues demonstrated a significant alteration in leaflet composition in pregnancy, across all 4 valves (Table 5.5). Total collagen content, determined by hydroxyproline assay,

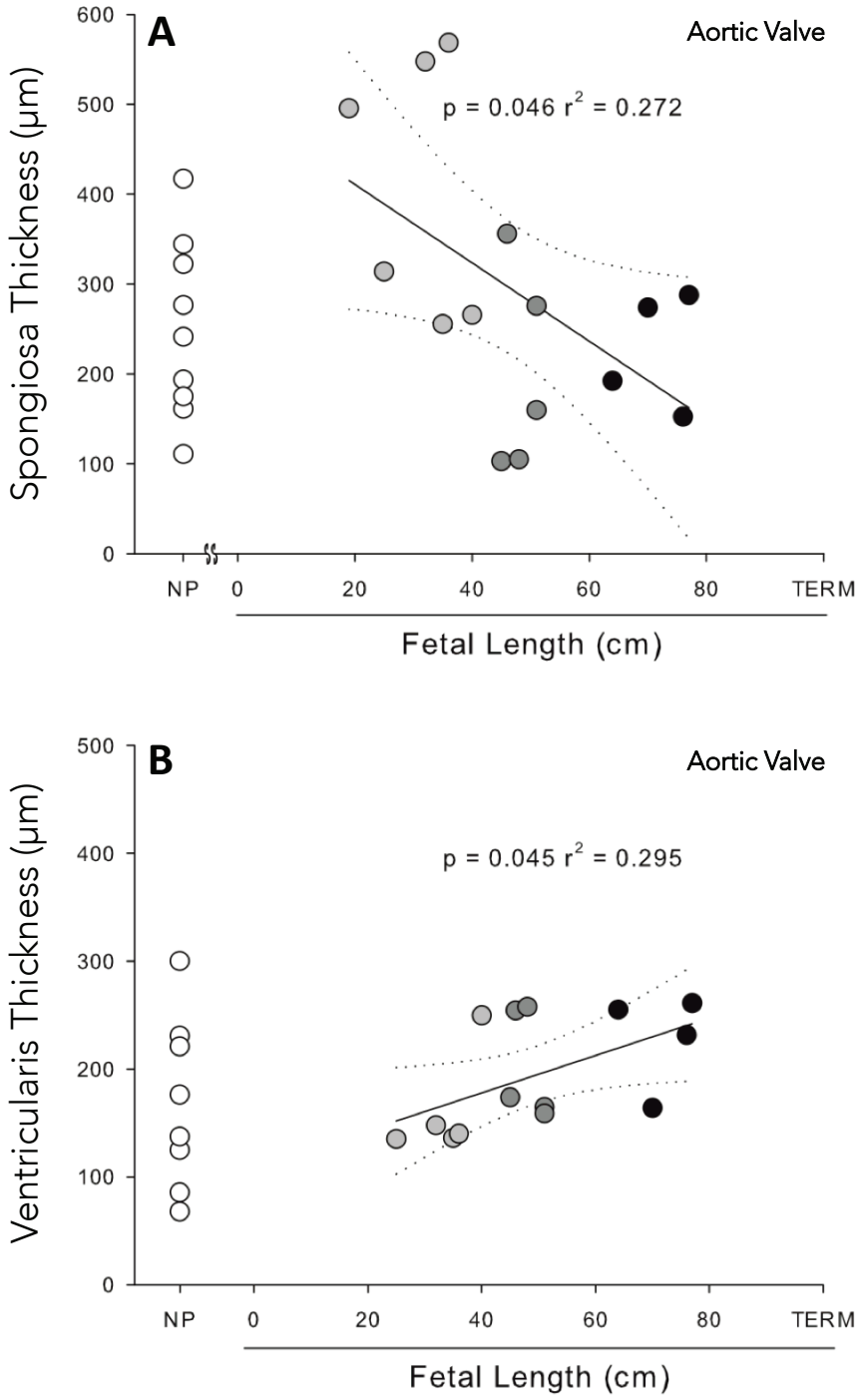

Figure 5.6 Aortic valve leaflet layer thicknesses versus fetal length

Aortic leaflet layer thickness plotted for NP heifers (NP; open circles) and with fetal length (in cm) for P (shaded circles) animals. A: Spongiosa thickness (in µm). B: Ventricularis thickness (in µm). p value and r^2 are indicated for each curve.

Table 5.4 Changes in collagen crimp with pregnancy

	Collagen crimp: Wavelength, μm; Crimped Area, %							
	Aortic Valve‡		Mitral Valve‡		Pulmonary Valve		Tricuspid Valve	
	Non-pregnant	Pregnant	Non-pregnant	Pregnant	Non-pregnant	Pregnant	Non-pregnant	Pregnant
Crimp Wavelength	3.7 ± 0.5(9)	11.7 ± 2.9**(15)	22.9 ± 1.2(9)	65 ± 15**(13)	15.4 ± 1.2(9)	21.8 ± 3.1*(15)	6.1 ± 0.6(9)	9.8 ± 0.9**(11)
% Crimped Area	94.2 ± 1.0(9)	71.7 ± 7.6**(15)	40.2 ± 6.0(9)	22.8 ± 3.0*(11)	85.5 ± 3.2(9)	61.3 ± 6.2**(15)	58.2 ± 9.9(9)	46.8 ± 9.4(11)

Values are mean values ± SE of crimp wavelength (in μm) and percentage of leaflet area which is crimped (% Crimped Area) for animals in the non-pregnant (NP), and pregnant (P) groups. Statistical comparisons were made between NP and P groups using t-Test comparisons of groups and p value ranges are indicated as follows: † = $p < 0.1$; * = $p < 0.05$; ** = $p < 0.01$; *** = $p < 0.001$. n values for each parameter in the NP and P groups are presented in brackets for each valve. ‡Results for collagen crimp of the aortic and mitral valve leaflets previously presented by Pierlot and colleagues, for the mitral [293] and aortic [313] valves.

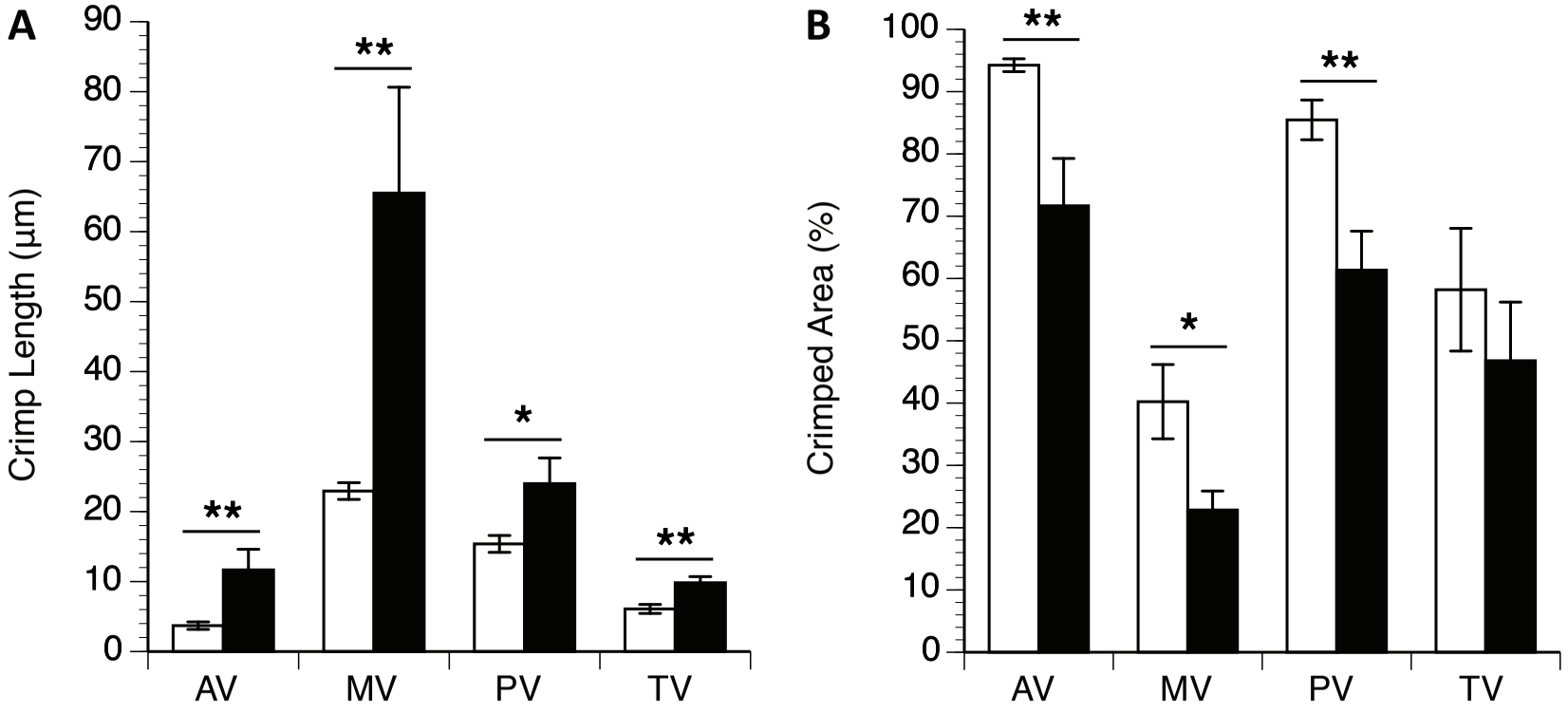

Figure 5.7 Collagen crimp plots (all valves)

Collagen crimp length and percentage of leaflet area which is crimped (% Area Crimped) from NP heifers (open bars) and pregnant cows (filled bars) for aortic (AV), mitral (MV), pulmonary (PV), and tricuspid valves (TV). A: collagen crimp length (in µm). B: leaflet crimped area (%). Values are means ± SE. Statistical comparisons were made between NP and P groups using t-Test comparisons of groups. Columns labeled with asterisks denote a statistically significant change: † = $p < 0.1$; * = $p < 0.05$; ** = $p < 0.01$; *** = $p < 0.001$.

Table 5.5 Biochemical measures by percentage

	Extracellular Matrix Content, % dry wt.							
	Aortic Valve		Mitral Valve		Pulmonary Valve		Tricuspid Valve	
	Non-pregnant	Pregnant	Non-pregnant	Pregnant	Non-pregnant	Pregnant	Non-pregnant	Pregnant
Total collagen	59.8 ± 2.1(10)‡	64.4 ± 1.7*(15)‡	56.7 ± 3.0(9)‡	66.0 ± 3.3*(13)‡	55.5 ± 1.9(9)	61.5 ± 1.9*(15)	43.0 ± 2.2(10)	54.2 ± 1.9**(14)
New collagen	1.1 ± 0.1(5)	1.0 ± 0.1(8)	0.6 ± 0.1(5)‡	0.6 ± 0.1(9)‡	2.6 ± 0.6(4)	1.4 ± 0.1(8)	1.9 ± 0.2(4)	2.0 ± 0.3(9)
Elastin	10.0 ± 0.7(5)	4.1 ± 0.5**(8)	6.2 ± 0.6(8)	2.8 ± 0.4**(8)	13.8 ± 0.7(5)	5.6 ± 0.6***(8)	11.5 ± 1.1(5)	5.0 ± 0.4**(6)
sGAG	3.3 ± 0.4(5)	2.0 ± 0.2*(9)	3.3 ± 0.5(4)	1.6 ± 0.2*(8)	2.3 ± 0.2(5)	0.8 ± 0.2**(9)	1.3 ± 0.2(4)	0.7 ± 0.2*(6)
Water	87.8 ± 0.3(10)	88.0 ± 0.4(12)	81.4 ± 0.7(10)‡	80.6 ± 0.6(12)‡	89.0 ± 0.2(10)	88.0 ± 0.5(12)	88.1 ± 0.6(10)	87.4 ± 0.5(12)

Values are mean values ± SE of biochemical extracellular matrix measures for animals in the non-pregnant (NP), and pregnant (P) groups: total collagen content (in %), newly synthesized / pepsin-soluble collagen content (in µg/mg tissue), sGAG content (in µg/mg tissue), and elastin content (in µg/mg tissue). Statistical comparisons were made between NP and P groups using t-Test comparisons of groups and p value ranges are indicated as follows: † = $p < 0.1$; * = $p < 0.05$; ** = $p < 0.01$; *** = $p < 0.001$. n values for each parameter in the NP and P groups are presented in brackets for each valve. ‡Results of biochemical analysis previously presented by Pierlot and colleagues: mitral valve leaflet collagen and water content [293] and aortic valve leaflet total collagen content [313].

increased with pregnancy across all valve types: percentage of total collagen content increased 8% in the aortic valve, 16% in the mitral valve, 11% in the pulmonary valve, and 26% in the tricuspid valve. The quantity of extractable collagen however, as investigated by the Sircol Bicolor Assay, was unchanged with pregnancy, as compared to non-pregnant animals.

Elastin content present in tissues decreased uniformly across all the valves in pregnancy: elastin content decreased 59% in the aortic valve, 55% in the mitral valve, 59% in the pulmonary valve, and 56% in the tricuspid valve.

Similarly, there was a loss of sulfated GAG content with pregnancy across all the valves as well: sGAG content decreased 39% in the aortic valve, 52% in the mitral valve, 65% in the pulmonary valve, and 46% in the tricuspid valve. Results of the analysis of water content between non-pregnant and pregnant animals in each of the valves is reported in Table 5.5: the percentage of water content is unchanged in pregnancy across all 4 valves.

Effect of Valve Type: Examination of biochemical measures by heart side found that total collagen content was 15% higher, sGAG content 98% higher, extractable collagen 57% lower, and elastin content 37% lower in left side heart valve leaflets compared to right side valve leaflets. On the other hand, total collagen content was 10% higher in outflow valve leaflets compared to inflow valves. All of these effects were conserved in pregnancy.

5.3.6 Cell Density and Phenotype

Effects of Pregnancy: Immunohistochemical studies showed a reduction in total cell (VIC) density in pregnancy (by approximately 24-29%) (Fig. 5.8, Table 5.6) while the percentage of activated cells (i.e. those cells staining positive for alpha-smooth muscle actin) was surprisingly unchanged (Table 5.6). While the percentage of activated VICs—on average—did not change with pregnancy in any valve, we observed an actual decrease in their content with gestation in the mitral valve: expressed as both density (Fig. 5.9A) and percentage of activated cells (Fig. 5.9B).

Effect of Valve Type: No significant differences in total cell density were found between the left- versus right-side valves, however, the density and proportion of activated cells

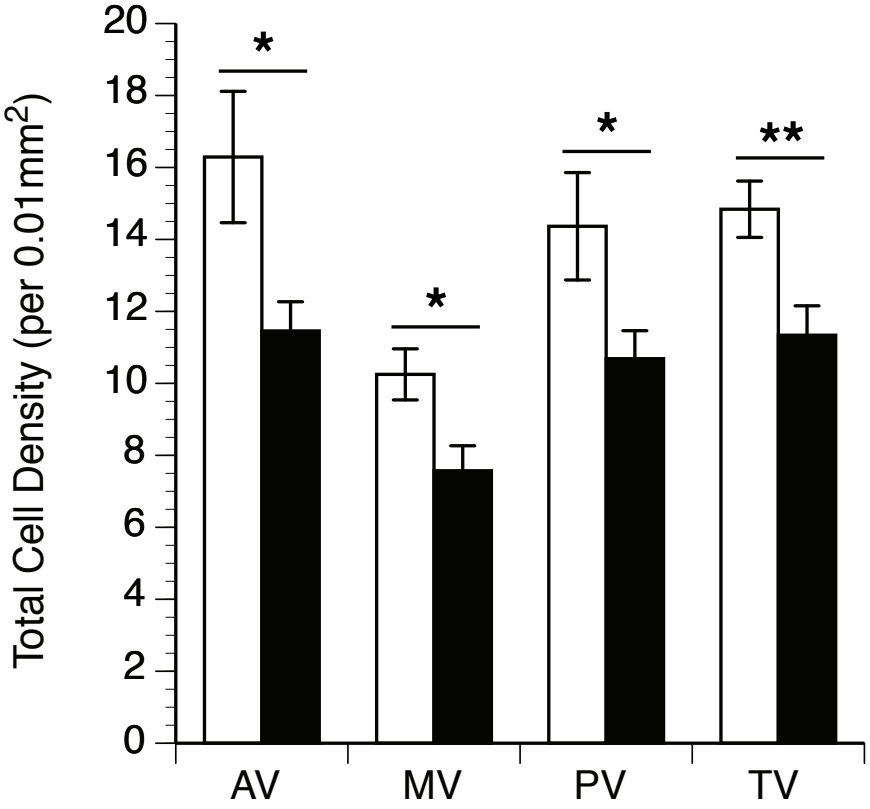

Figure 5.8 Total cell density plot (all valves)

Total cell density (in cells per 0.01 mm^2) of each valve leaflet from NP (open bar), and P (filled bar) animals, for aortic (AV), mitral (MV), pulmonary (PV), and tricuspid valves (TV). Values are means ± SE. Statistical comparisons were made between NP and P groups using t-Test comparisons of groups. Columns labeled with asterisks denote a statistically significant change: † = $p < 0.1$; * = $p < 0.05$; ** = $p < 0.01$; *** = $p < 0.001$.

Table 5.6 Cell density and phenotype

	Cell Density, # cells per 0.1 mm^2							
	Aortic Valve		Mitral Valve		Pulmonary Valve		Tricuspid Valve	
	Non-pregnant	Pregnant	Non-pregnant	Pregnant	Non-pregnant	Pregnant	Non-pregnant	Pregnant
Total Cell Density	16.3 ± 1.8(8)	11.5 ± 0.8*(15)	10.2 ± 0.7(9)	7.6 ± 0.7*(11)	14.4 ± 1.5(9)	10.7 ± 0.8*(15)	14.8 ± 0.8(8)	11.3 ± 0.8**(13)
α-SMA+ Cell	8.7 ± 1.7(8)	5.6 ± 0.8(15)	4.5 ± 0.6(9)	3.0 ± 0.4†(12)	4.8 ± 1.4(9)	3.1 ± 0.5(15)	4.2 ± 0.6(8)	3.2 ± 0.3(13)
% α-SMA+ Cells	52.6 ± 7.9(8)	46.4 ± 3.8(15)	43.5 ± 4.4(9)	41.4 ± 6.8(11)	29.4 ± 6.0(9)	28.5 ± 3.7(15)	27.5 ± 3.4(8)	27.8 ± 1.9(13)

Values are mean values ± SE of total cell number per 0.01 mm^2 (1×10^4 μm^2), α-SMA+ cell number per 0.01 mm^2 (1×10^4 μm^2), and percentage of α-SMA+ cells (% α-SMA+) for animals in the non-pregnant (NP), and pregnant (P) groups. Statistical comparisons were made between NP and P groups using t-Test comparisons of groups and p value ranges are indicated as follows: † = $p < 0.1$; * = $p < 0.05$; ** = $p < 0.01$; *** = $p < 0.001$. n values for each parameter in the NP and P groups are presented in brackets for each valve.

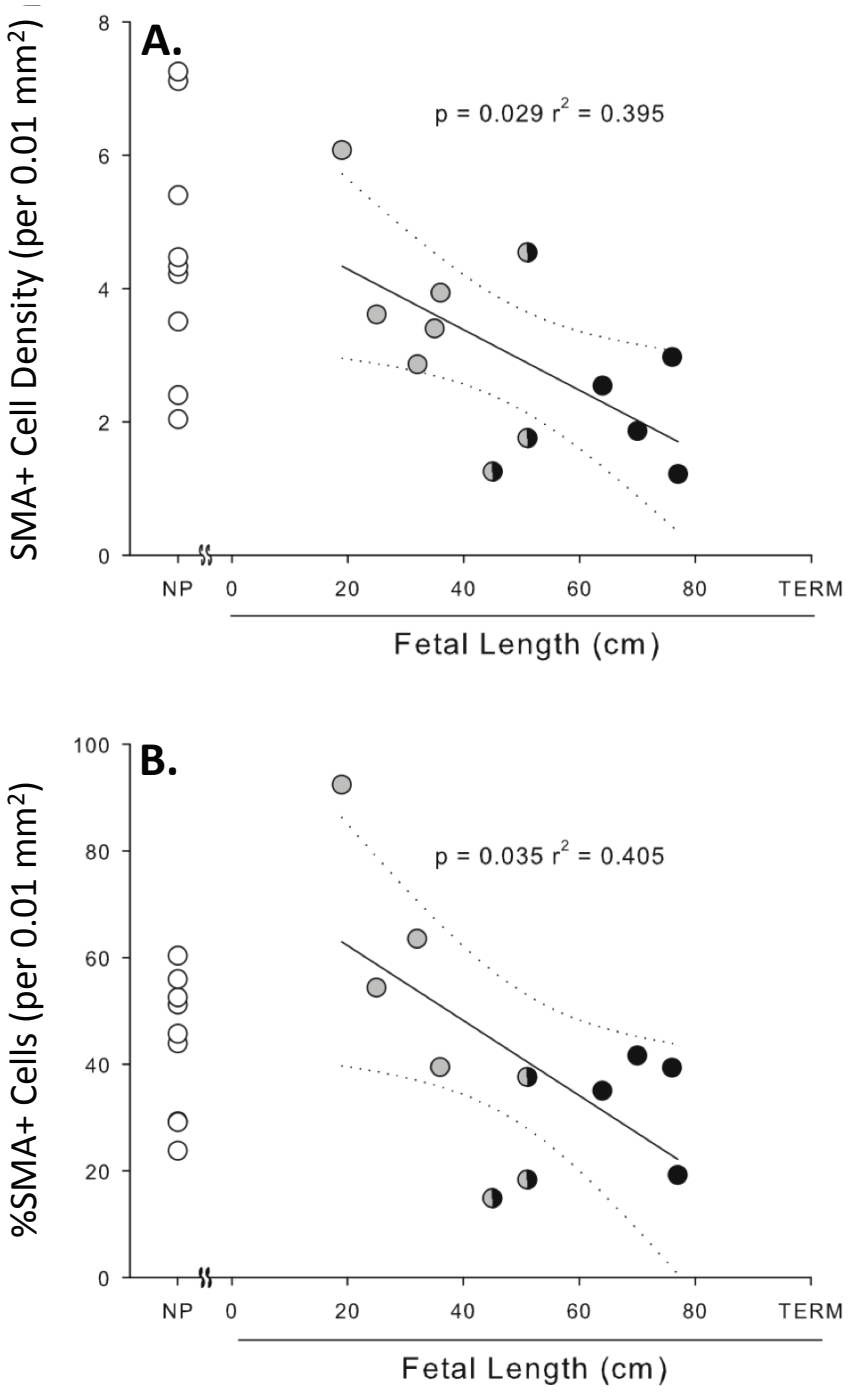

Figure 5.9 Mitral valve α-SMA expression versus fetal length

Mitral leaflet α-SMA measurements plotted for NP heifers (NP; open circles) and with fetal length (in cm) for P (shaded circles) animals. A: α-SMA+ cell density (in cells per 0.01 mm^2). B: % α-SMA+ cells (in %). p value and r^2 are indicated for each curve.

were 43% and 61% higher respectively in left side heart valves compared to right side heart valves, and this difference was maintained in pregnancy. Thus, as expected, the higher-loaded, left-side valves possess more "activated" VICs in both non-pregnant and pregnant animals.

On the other hand, outflow valves contained significantly higher cell densities, of both total (17% higher) and α-SMA+ cells (43% higher), compared to inflow valve leaflets, and these differences were conserved in pregnancy.

5.3.7 DTT/HIT Experiments

T_d – Effect of Pregnancy. Collagen thermal stability was decreased in all heart valve tissues during pregnancy (Table 5.7). Specifically, T_d decreased by 1.9°C, 2.3°C, 1.1°C, and 1.9°C, in the aortic, mitral, pulmonary, and tricuspid valves respectively, between NP and P animals.

T_d – Effect of Valve Type. As expected, and consistent with previous studies (Ref Ali's paper), collagen thermal stability (Td) was significantly lower in left side valve leaflets compared to right side valves. Interestingly, this difference was similar in magnitude to the changes observed during pregnancy (between 1 and 2°C). This difference was also maintained in pregnant animals.

T_d – Effect of Treatment. A two-way ANOVA demonstrated that collagen thermal stability, as indicated by T_d, was not significantly altered by $NaBH_4$ treatment in any pregnancy groups (data not shown).

$t_{1/2}$ – Effect of Pregnancy. Halftime of load decay (or load relaxation time) of HIT control specimens ($t_{1/2}$ control) increased 131% in the aortic valve, 58% in the mitral valve, 126% in the pulmonary valve, and 96% in the tricuspid valve in pregnant animals compared to the non-pregnant group (Table 5.7), indicating there was an increase in mature crosslink content with pregnancy in all valves.

$t_{1/2}$ – Effect of Treatment in Pregnancy. In the $NaBH_4$ treated samples, pregnancy also resulted in a significant increase in load relaxation time in all valves but the tricuspid. $t_{1/2}$ treated was higher in pregnancy in the aortic (85%), mitral (49%), and pulmonary (77%)

Table 5.7 HIT Collagen Stability and Crosslinking Profile

	HIT Measurements: T_d, ºC; $t_{1/2}$, hours							
	Aortic Valve‡		Mitral Valve‡		Pulmonary Valve		Tricuspid Valve	
	Non-pregnant	Pregnant	Non-pregnant	Pregnant	Non-pregnant	Pregnant	Non-pregnant	Pregnant
T_d	68.7 ± 0.4(9)	66.8 ± 0.3***(23)	68.6 ± 0.2(10)	66.3 ± 0.2***(22)	70.5 ± 0.2(10)	69.4 ± 0.4*(22)	69.8 ± 0.2(10)	67.9 ± 0.3***(19)
$t_{1/2}$ control	8.0 ± 2.5(10)	18.5 ± 2.0***(19)	8.6 ± 1.8(10)	13.6 ± 1.6*(19)	8.5 ± 2.4(9)	19.2 ± 2.2***(20)	5.6 ± 0.9(10)	11.0 ± 0.8***(20)
$t_{1/2}$ treated	11.3 ± 2.1(7)	20.9 ± 1.6***(19)	11.5 ± 2.5(7)	17.1 ± 1.7**(19)	19.6 ± 5.8(10)	34.6 ± 4.8*(20)	12.7 ± 1.6(9)	11.3 ± 1.2(18)
Crosslink index	1.3 ± 0.2(6)	1.2 ± 0.1(18)	1.6 ± 0.2(7)	1.3 ± 0.1(17)	2.6 ± 0.5(9)	2.0 ± 0.3(20)	2.3 ± 0.2(9)	1.1 ± 0.1***(18)

Values are mean values ± SE of denaturation temperature (T_d), halftime of load decay ($t_{1/2}$), and immature crosslinking index, for animals in the non-pregnant (NP), and pregnant (P) groups. Statistical comparisons were made between NP and P groups using t-Test comparisons of groups and p value ranges are indicated as follows: † = $p < 0.1$; * = $p < 0.05$; ** = $p < 0.01$; *** = $p < 0.001$. n values for each parameter in the NP and P groups are presented in brackets for each valve. ‡HIT results for the mitral and aortic valve leaflets previously presented by Pierlot and colleagues [313].

valves compared to the non-pregnant group (Table 5.7), indicating total collagen crosslinking (mature plus immature) was increased in pregnancy in these valves.

$t_{1/2}$ – Effects of Valve Type. Mature crosslinking (indicated by $t_{1/2}$-control) of tricuspid valve leaflet tissues was significantly lower than that of the aortic and pulmonary valves (but not significantly different from the mitral valve), while mature crosslinking of the aortic, mitral, and pulmonary valves was not significantly different. Total crosslinking (indicated by $t_{1/2}$-treated) was 21% lower in left-side valves compared to right-side valves (values shown in Table 5.7). Both of these results were present in the non-pregnant group and conserved in pregnancy.

$t_{1/2}$ – Effect of Treatment. A two-way ANOVA demonstrated that (i) $t_{1/2}$ was significantly altered by $NaBH_4$ treatment and pregnancy, and (ii) interactions between treatment group and pregnancy group were significant, requiring sample treatment to be considered in each pregnancy group separately.

In the non-pregnant group, $NaBH_4$ treatment resulted in an increase in $t_{1/2}$ in all valves but the aortic. In particular, $t_{1/2}$ treated was significantly higher than $t_{1/2}$ control in the mitral (34%), pulmonary (131%), and tricuspid (209%) valves (Table 5.7), reflecting the presence of immature crosslinks in those valves, with a lack of immature crosslinks in the aortic valve leaflets.

In the pregnant group however, $NaBH_4$ treatment increased $t_{1/2}$ only in the pulmonary valve (Table 5.7), suggesting that immature crosslinks are conserved only in this valve during pregnancy.

Lack of difference between control and treated tissues indicated an absence of immature collagen crosslinks in these tissues: aortic NP, aortic P, mitral P, tricuspid P. Significant differences on the other hand indicated the presence of immature crosslinks: mitral NP, pulmonary NP, pulmonary P, and tricuspid NP. Another indicator of the crosslinking profile of these tissues is the immature crosslink index. The ratio of $t_{1/2}$ treated (total crosslinking) to $t_{1/2}$ control (mature crosslinking) (or the immature crosslinking index) was found to be small (less than 2.6:1) and was not significantly altered in pregnancy in the aortic, mitral, and pulmonary valves (Table 5.7). This result signifies that the native

population of immature crosslinks was low in these valves and surprisingly remained so in pregnancy.

5.3.8 Summary of Results

Leaflet areal stretch in all valves declined in early pregnancy, however in all valves with the exception of the tricuspid valve, mechanical properties were regained by late pregnancy – biphasic shift in extensibility. We reported similar increases in leaflet dimensions across the valves, including increasing radial midline length and circumferential midline length, and a corresponding expansion of overall leaflet area. In addition to these increases in surface area, we observed altered thicknesses of the leaflet, mainly through a thickening of the fibrosa, the primary load-bearing layer, in the aortic, mitral, and pulmonary valves. Similarly, crimp length increased in all valves, associated with an overall loss in the presence of crimp. Our biochemical studies reported increases in total collagen content, and decreases in sGAG and elastin content across all four heart valves in pregnancy. Our cellular studies described a significant decrease in total cell density associated with pregnancy, accompanied by a remarkable lack of change in proportion of those cells expressing the activated cell phenotype (expressing α-SMA). Finally, all valves experienced a loss of thermal stability indicated by a decrease in denaturation temperature, and an increase in collagen crosslinking. Crosslinking profiles determined by HIT experiments differed in a valve-specific manner.

5.4 Discussion

Our previous studies have shown non-pathological remodeling in left-side aortic and mitral maternal heart valve leaflets in bovine pregnancy, with changes in leaflet size, composition, and structure [248, 293, 313]. The current study presents a comprehensive ex vivo investigation of pregnancy-induced remodeling across all four heart valves, including the right-side pulmonary and tricuspid valves. We observed similar remodeling in all of the maternal valves, with drastic changes in leaflet dimensions, structure, ECM composition, and cellular density. These results have shown, more specifically, that all the valves expanded in pregnancy, via, in part at least, an increase in the production of collagen, with associated changes in the biochemical

makeup of the ECM and the structure of the collagen network (i.e. loss of crimp, crosslink maturation, and reduction in thermal stability).

Heart-side differences were evident in many parameters assessed in this study, and speak to the differences in the mechanical loading environment in vivo (peak TVP). Differences between inflow and outflow valves, which most likely stem from differing embryological origins of the valves, have also surfaced throughout the present study. Surprisingly, however, virtually no differences in pregnancy remodeling response were found between left and right side valves, or between inflow and outflow valves. A two-way ANOVA demonstrated that while differences in leaflet area, thickness, extracellular matrix content, cellular phenotype, and thermal stability were found between left and right side valves (differing mechanical environments) in non-pregnant animals, these differences were conserved in pregnancy. Similarly, inflow and outflow valves of the non-pregnant group differed in size, collagen content, crimp structure, cell density, and mechanical properties, but again these differences were conserved in pregnancy. There was only one relationship that was altered in pregnancy: in the non-pregnant group, leaflet dimensions in the circumferential leaflet direction were not significantly different between left-side and right-side valves. However, in pregnancy, circumferential length was significantly higher (by 13%) in left-side valves compared to right-side valves, even though all valve leaflets enlarged. This result signifies that the valves of the higher pressure left-side of the heart enlarge via circumferential expansion to a larger degree than the right-side valves. It is possible that orifice expansion in left-side valves in pregnancy is higher than right-side valves, however previous reports of valve annular diameters range a great deal between studies so it is difficult to obtain a precise measurement for comparison between valves: valve orifice expansion has been shown to range from approximately 12-23 % in pregnancy, with no obvious differences between valves [157, 168].

Comparison of valve position differences in the current study with previous studies, does reveal large agreement in expected valve-specific remodeling potential. Merryman et al. found that VICs isolated from left-side valves contained significantly higher levels of α-SMA (cytoskeletal protein) and Hsp47 (collagen synthetic protein) [3] and were significantly stiffer [42] than right-side valves, suggesting that the cellular population of

left-side valves are primed for enhanced tissue remodeling in response to changes in tissue stress. Aldous et al. reported that denaturation temperature was inversely related to TVP [101, 244], indicating that valves exposed to higher pressures in vivo (i.e. left-side valves) are less thermally stable than those which experience lower pressures (i.e. right-side valves) – reduced thermal stability is an inherent property of remodeling tissues [248]. The present study confirmed the presence of a higher proportion of aVICs (expressing α-SMA) and lower denaturation temperature in left-side compared to right-side valves. Together all of these studies suggest that left-side valves posses a higher remodeling potential than right-side valves, and thus would be expected to display an enhanced remodeling response under altered hemodynamic loading. The present study, however, showed no evidence of such a response in pregnancy.

Several differences were, however, found between the remodeling behaviors of the valves, mainly with the tricuspid valve. The loss of mechanical extensibility in early pregnancy and subsequent recovery in late pregnancy, previously observed in the aortic and mitral valves [313], was found in the pulmonary valve as well. However, in the tricuspid valve, areal stretch decreased in early pregnancy but was not regained by full term. Furthermore, in the tricuspid valve, we did not observe the same thickening of the fibrosa, decrease in percentage of leaflet area occupied by crimp, or increase in total crosslinking, that were found in all other valve types. Clearly the tricuspid valve remodels in a unique manner in pregnancy.

Another difference in the remodeling behavior during pregnancy was seen in the aortic leaflet area. A two-way ANOVA of valve leaflet area in pregnancy, showed a significant effect of valve type. In non-pregnant animals, mean leaflet area of the aortic valve was significantly lower than that of the mitral, pulmonary, and tricuspid valves. In pregnancy however, although all valves expanded, aortic valve leaflet expansion was strikingly higher (84%) than any of the other valves (35-56%), such that aortic leaflet area in the pregnant animals was not significantly different from that of the pulmonary or tricuspid valves. That is, the remodeling response of the aortic valve, at least in terms of leaflet expansion, is much greater than that of any of the other valves. This result may provide insight into the valve-specific differences in regurgitation observed in pregnancy in the

clinical setting [168]. It is possible that the enhanced response of the aortic valve is responsible for the lack of regurgitation present in that valve, even with significant orifice dilation. A lesser response in the mitral valve may still result in minimal regurgitation across that valve due to a potentially large reserve of redundant tissue [248, 320], allowing the valve to maintain coaptation even as the orifice expands. Coaptation areas are only reported in the literature for the aortic and mitral valves. Sohmer et al. reported a total coaptation area in the human aortic valve of 161 mm^2, with an average coaptation area for each of the three leaflets (tri-leaflet valve) of 54 mm^2, as measured by 3D echocardiography [321]. In a similar study of the human mitral valve, Saito et al. showed a total coaptation area of 160 mm^2, almost identical to that of the aortic valve [322]. Averaging this total coaptation area over the two leaflets (bi-leaflet valve), assuming equal contributions to coaptation, would give a larger 80 mm^2 coaptation area, almost double that of the aortic valve leaflet. However, in their study, coaptation area was calculated by subtracting the closed leaflet area (mid-systole) from the total leaflet area (at the onset of valve closure), with no distinction between the contributions of the anterior leaflet from the posterior leaflet. In fact, the anterior mitral valve leaflet may on its own be sufficient to overlay the full valve orifice [323] and thus may contribute more to the coaptation area than the posterior leaflet – adding to the disparity between the functional tissue reserve of the mitral valve and each of the other valves. Without the presence of a significant tissue reserve in the pulmonary and tricuspid valves, a diminished remodeling response associated with insufficient leaflet expansion would likely result in significant regurgitation.

Heart valve expansion has been previously reported mainly in cases of disease intervention (pulmonary autograft after Ross Procedure [324-326]) and valve pathology, but little attention has focused on non-pathological alterations in leaflet size. The increases in leaflet area reported in the current study (as much as 84%) are much higher than the increases in mitral valve systolic leaflet area observed in patients with LV dysfunction (35%) [185] and mitral regurgitation (resulting in chronic valve tethering) (30%) [322], as well as the 17% increase in mitral leaflet area found in sheep with mitral valve regurgitation caused by experimental papillary muscle tethering (over 61 days) [219]. Furthermore, when gestational timeline is considered in the current study,

significant alterations in leaflet area are found to be occurring in early pregnancy (0-169d) in all valves except the pulmonary valve, where the area increase occurs by late pregnancy (data not shown). More specifically, data from the current study shows a 42% increase in mitral valve leaflet area in early pregnant animals (0–169 days gestation), which is similar to the 33% increase reported previously by Wells et al. for the mitral valve leaflet in the first 159 days of gestation. Thus, leaflet expansion is also rapid in pregnancy – another indication that something else, in addition to elevated stress, is driving this remodeling process. It is likely that hormones play a significant role in the modulation of growth and remodeling in pregnancy, particularly in early in gestation.

Surprisingly, overall leaflet thickness of the aortic, pulmonary, and tricuspid valve leaflets was only moderately increased in pregnancy, not keeping in step with the expansion in leaflet area to normalize leaflet stress (via the law of Laplace). However, a prominent thickening was observed in the fibrosa – the predominant load-bearing layer. Fibrosa thickness increased 27–54 % across the aortic, mitral, and pulmonary leaflets, undoubtedly due to increased ECM protein synthesis corresponding to the increased collagen concentration observed in all four leaflets. The overall thickness of the mitral valve was not significantly changed in pregnancy, however thickening of the fibrosa in this valve was also accompanied by a thinning of the atrialis. These opposing thickness changes (similar in magnitude) likely counteracted each other sufficiently to minimize any changes to the overall thickness of the mitral valve leaflet.

Structural alterations to the collagen network of the valve leaflet were investigated in order to understand the mechanisms responsible for the mechanical and dimensional changes observed across the heart valves. Collagen crimp characterization provides unique information about internal tissue structure of the leaflet, and changes in crimp contribute to changes in leaflet size and mechanical extensibility. The present study reports drastic increases in crimp length in all valve types, which was correlated to an overall loss in crimp structure in the collagen network. In the mitral valve in particular, with close to a 3-fold increase in crimp length in pregnancy, the crimp structure is almost non-existent (only 23% leaflet area remaining occupied by crimp) in the pregnant group.

In keeping with our previous studies, investigation of the leaflet biaxial mechanical properties was performed. Biaxial mechanical data revealed a biphasic change in leaflet areal stretch, resulting in a leftward shift of the tension-areal stretch curve in early pregnancy, and a return to pre-pregnant values by late pregnancy – this result occurred in the aortic, mitral, and pulmonary valves. In the tricuspid valve however, leaflet overall extensibility was not regained. These changes in areal stretch were mainly influenced by changes in circumferential extensibility, with lesser contributions of radial changes. Radial extensibility was largely unchanged between non-pregnant and pregnant animals (aortic, mitral, and tricuspid valves), however extensibility in this direction did increase with increasing gestational age of the fetus in the mitral and pulmonary valves. We speculate that the loss in circumferential extensibility in early pregnancy is due in part to the straightening (or uncrimping) of the collagen network, causing lengthening, but also stiffening, in the circumferential direction. Furthermore, areal stretch in both valves increased linearly with increasing gestational age of the fetus. This result indicates that the extensibility of the valve leaflet is gradually regained through gestation, by a mechanism likely related to the structural remodeling of the leaflet tissue.

Biochemical changes to the extracellular matrix of the valve leaflet in pregnancy occurred in total collagen content, elastin content, and sulfated GAG content, but surprisingly these were not accompanied by any changes in extractable collagen or water content. Specifically, total collagen concentration (% dry weight), assessed by hydroxyproline assay, increased 8–26 % across all valves between non-pregnant and pregnant animals. This finding indicates that while the valve leaflet expands in pregnancy, the quantity of collagen in the leaflet tissue not only keeps up with the extreme increase in leaflet size, but remarkably the leaflet actually increases in collagen content. It is not surprising then, that as collagen is synthesized in pregnancy, the fibrosa layer enlarges as a direct result of the expanding collagen network. The lack of fibrosa thickening in the tricuspid valve leaflet however, is puzzling, especially considering collagen content increases significantly in this valve. However, total tricuspid leaflet thickness mildly increased in pregnancy. It is possible that dissimilarities in network properties (i.e. collagen fiber density) or remodeling response (i.e. where new collagen is

being laid down) between the tricuspid valve and the other valves are responsible for differences in layer thicknesses.

Elastin and sGAG contents (% dry wt.) decreased 55–60% and 40–60% respectively in pregnancy, in similar magnitude to the expansion in leaflet area reported in pregnant animals compared to non-pregnant animals. It is probable that the actual quantity of these molecules did not change dramatically, but rather the leaflet expansion and accumulation of collagen altered the biochemical composition of the leaflet, causing the concentration of elastin and sGAGs to decrease. Normal elastin turnover in particular, has been shown to occur relatively slowly in vivo in adult animals [88, 327-329], but may be accelerated under certain physiologic and pathophysiologic conditions. For example, enhanced elastin degradation (and turnover) occurs under several non-pathological settings such as growth, wound healing, remodeling, and pregnancy [88, 330-333]. Determination of whether native elastin content is maintained (decreasing concentration simply with leaflet expansion) or decreased (increased degradation) in pregnancy can be estimated from this study by comparing the change in leaflet volume (area and thickness) to the change in concentration of the protein – elastin content actually decreased closer to 13–34% in pregnancy. A similar calculation indicates that sGAG content may actually have increased in pregnancy in the aortic valve, which experiences greater leaflet expansion than the other valves. Elastin synthesis does in fact occur in the aorta during pregnancy – the vessel expands, becoming wider but not thicker, and its elastin concentration actually increases [334] – the opposite of what we have observed in the valve leaflets. Investigation of elastinolytic enzymes (elastases) responsible for the degradation of elastic fibers would better substantiate the finding of the loss of elastin. Furthermore, the presence of proteinases responsible for degradation of other components of the extracellular matrix (i.e. MMPs), particularly collagen, would be equally as valuable. The MMP family of 24 different proteases (23 found in humans [335]) is traditionally subdivided into collagenases, gelatinases, stromelysins, matrilysins, metalloelastases, and membrane type MMPs [335, 336]. Collagenases (MMP–1, –8, –13, and –18) breakdown intact collagen while gelatinases (MMP–2, and –9) digest denatured collagen (or gelatins). These same gelatinases, as well as mouse and human macrophage metalloelastases (HME and MME: MMP–12) and matrilysin (MMP–7) degrade insoluble

elastin [335, 336]. The presence of specific MMPs in valve tissues is uncertain. In general, it is agreed that, MMP–1, –2, and –3 are expressed by the interstitial cells for normal, healthy valves [67, 337], although an absence of MMP-3 has been reported by other studies [338, 339]. MMP–9 expression has been identified in degenerative valve tissues [337] and pericardial-derived bioprosthetic heart valves [340]. The identification of the presence, up–, or down–regulation of any of these MMPs responsible for degradation of collagen and/or elastin, as well as their tissue inhibitory metalloproteinases (TIMPs) would be beneficial in determining how the rates of ECM turnover are altered in pregnancy.

Interconnections between collagen fiber bundles of the valve ECM are likely provided in large part by the presence of an elastin matrix [298, 341]. Elastin fibers are thought to play an important role in (i) valve recoil during closure, and (ii) preservation of the native corrugated collagen structure [48, 58, 341], thus aiding in the maintenance of a pre-stress in the fibrosa [2]. That is, the elastin is contributes to some degree to the sustaining of the crimp structure of the collagen network. As elastin content decreases and collagen content increases in pregnancy, a loss of pre-stress in the fibrosa may be providing a mechanism for crimp loss.

sGAG content, like elastin content, decreased 40–60% in pregnancy. GAGs are long-chain linear polysaccharides that are negatively charged due to the presence of sulphate and uronic acid groups [342]. This negative charge gives GAGs a high affinity for water binding. Loss of glycosaminoglycan content decreases the viscoelasticity of the tissue, but this effect is mainly due to decreased water binding [343]. In the current study however, water content was maintained in pregnancy, even though sGAG content decreased. It is possible that while sGAG content decreases in pregnancy, non-sulfated hyaluronan content is preferentially maintained, allowing water content to be maintained in pregnancy. However, this hypothesis requires further investigation. Our previous study, which investigated the effect of pregnancy on biaxial creep behavior of the excised aortic and mitral valve leaflet tissues, lacked insight into whether altered water content in pregnancy could have affected this viscoelastic material behavior [313]. Clearly the unchanged water content reported in the current study removes any contribution of altered water content to differences in valvular creep behavior in pregnancy.

Increasing experimental evidence over the last decade has brought to light the importance of valvular interstitial cells (VICs), across a diverse set of roles in physiological development, maintenance, remodeling, and pathology. VICs are a dynamic and heterogeneous population of cells exhibiting phenotypes of smooth muscle cells (SMCs), fibroblasts, and myofibroblasts [56]. Myofibroblasts are cells that display properties of fibroblasts and SMCs [2, 3, 51]. In healthy adults, fibroblast-like cells are the predominant cells type, with the presence of few or no myofibroblasts [3, 57]. Recent studies suggest that under altered physiological conditions, such as those observed in development [21, 200], disease (e.g. myxomatous degeneration [61, 200]), or injury [67], VICs experience can a phenotypic change from quiescent fibroblast to activated myofibroblast (or aVICs). aVICs can be distinguished from their quiescent counterparts by high expression of contractile protein markers not normally found in the interstitial cells of healthy valves – particularly α-SMA [20, 61]. Elevated aVIC expression (indicated by increased α-SMA) has been correlated to increased: ECM turnover (secretion and degradation) [45]; expression of matrix metalloproteinases (MMPs) and tissue inhibitors of metalloproteinases (TIMPs) [20, 45, 57], both as the major contributors to ECM turnover; cytokines, particularly TGF-β [20]; expression of other cytoskeletal proteins (Hsp47) [3]; and VIC proliferation and migration [20, 22]. Thus we expected a rise in the proportion of aVICs in pregnancy to provide a mechanism (and indicator) of leaflet remodeling.

Remarkably, through all the previous mentioned changes in pregnancy, leaflets from all valves became surprisingly less cellular during pregnancy: total cell density decreased by 24–29% across the valves. Yet, there was no observed increase in the proportion of aVICs (α-SMA-positive cells). These results were entirely unexpected. Similar to the reduction in elastin and sGAG content, the loss of cell density may be related directly to leaflet expansion. Absolute cell number may have been unchanged, or even increased slightly, but these changes may have been overwhelmed by the significant leaflet expansion, resulting in an apparent decrease in cell density. In addition, we had expected to, but did not, see a significant shift in cell phenotype of the valvular interstitial cells (VICs). Interestingly, Schoen et al. reported that only 2–5% of cells exhibit expression of α-SMA in normal human adult valves [21, 57, 200], while the current study estimated

that the proportion of cells expressing α-SMA in bovine animals was much higher at 52.6%, 43.5%, 29.4%, and 27.5% in the aortic, mitral, pulmonary, and tricuspid valves respectively. It is not clear whether this discrepancy is due to species- and gender-related differences or differences in methodology.

Thus, the surprising cellular and phenotypic results of the present study may reflect: (i) a decrease in cell density secondary to an increase in leaflet size, and/or (ii) the presence of subpopulations of cells [316], with specified functions, which are up-regulated or down-regulated under the altered cardiovascular loading in pregnancy. Further analysis of the validity of this assumption is necessary. In addition to α-SMA, expression of heat shock protein-47 (Hsp47) is indicator of collagen synthesis [3] and can be used as an alternative phenotypic indicator. Future studies would also benefit from reverse transcription polymerase chain reaction (RT-PCR) experiments for identification of phenotypic indicator genes expressed by VICs in pregnancy.

In addition to cellular phenotype, HIT thermomechanical techniques can provide valuable information about the thermal stability, and thus the remodeling state of a tissue, based on the temperature at which it denatures (T_d) as well as the profile of crosslinks present in the collagenous tissue. More specifically, T_d is used as an indicator of the hydrothermal stability of the collagen molecule and is affected by a variety of factors, from hydrogen bonding and crosslinking to the molecular packing of the collagen fiber lattice, as described by the polymer-in-a-box mechanism [114]. Collagen turnover would be associated with a loss of the closely packed molecular configuration, resulting in a decrease of T_d (decreased thermal stability). In addition to denaturation temperature, thermomechanical testing in combination with $NaBH_4$ treatment is valuable in providing three pieces of information about the tissue specimens: (i) mature crosslink content ($t_{1/2}$ of control samples), (ii) total crosslink content ($t_{1/2}$ of $NaBH_4$-treated samples), and (iii) the presence of immature crosslinks in each group of animals (immature crosslinking index – ratio of $t_{1/2}$-treated to $t_{1/2}$-control). The immature crosslinking index provides an indication of the degree of collagen turnover and/or maturation in a tissue [98, 101, 244, 284, 285].

In the present study, we report decreases in denaturation temperature by 1.1–2.3 ° between non-pregnant and pregnant animals. Interestingly, this is on the same order of magnitude of the change observed during significant structural remodeling that occurs during development in fetal pericardium [102] and heart valves [244], as well as maternal pericardium in pregnancy [344].

One of the most surprising findings in the present study is the lack of immature crosslinking in tissues from both non-pregnant *and* pregnant animals. In the aortic valve, non-pregnant and pregnant animals both showed no indication of immature crosslinking (no differences between control and treated $t_{1/2}$). In the mitral and tricuspid valves, the presence of immature crosslinks was indicated in non-pregnant animals but, paradoxically, not in pregnant animals. In the pulmonary valve, immature crosslinks were indicated to be present in both non-pregnant and pregnant animals.

For the aortic, mitral, and pulmonary valves, proxies for mature and total crosslinking ($t_{1/2}$-control and $t_{1/2}$-treated respectively) increased with no change in the immature crosslinking index. This result indicates that the valvular collagen network is dominated by mature collagen crosslinks in these three valves. In the tricuspid valve on the other hand, while mature crosslinking increased (as indicated by an increase in $t_{1/2}$-control), $t_{1/2}$-treated was unchanged and the immature crosslinking index decreased in pregnancy. This finding, which is unique to the tricuspid valve, indicates a reduced proportion of immature crosslinks present in pregnant animals, with immature crosslinking almost completely absent in the pregnant group. This shift in the balance of crosslink maturity in pregnancy (mature $\uparrow$ and immature $\downarrow$) resulted in no apparent change in total crosslinking. Therefore, in the tricuspid valve, HIT suggests that immature crosslinks present in non-pregnant animals simply matured through pregnancy, without the addition of any new crosslinks.

Both of these results are puzzling because we have shown in our present and previous studies, that new collagen is added to the leaflet during pregnancy. Nonetheless, the immature crosslinking index was unchanged in the aortic, mitral, and pulmonary valves, and even decreased in the tricuspid valve. Further, while collagen turnover resulted in increased levels of extractable collagen, our biochemical assay showed very little

extractable collagen in valve tissues in general, and no change in pregnancy. As hypothesized in our study of the mitral valve, it is conceivable that the native valve collagen is crosslinked at a faster rate than can be captured in our pregnancy study [293], but this stands to be proven. An additional possibility, discussed in depth previously [313], relates to immature keto-amine crosslink HLKNL, which is hydrothermally and acid stable and not classified properly by the HIT technique [99, 306]. If high levels of this specific crosslink are present in valve tissues, and/or are preferentially laid down under pregnancy-induced leaflet remodeling, this would result in a significant discrepancy between the hydrolytically stable and the mature crosslink populations. In fact, Aldous et al. reported that valvular tissues of bovine steers contain significantly more keto-amine-derived crosslinks than aldimine-derived crosslinks [101]. The use of a biochemical method of crosslink measurement, such as high-performance liquid chromatography (HPLC), to assess the specific crosslink population, in parallel with HIT experiments to provide information regarding the mechanical relevance of the crosslink population [101], before and during pregnancy, together would greatly clarify this issue. Evidence of the increased presence of immature crosslinking HLKNL in pregnancy would greatly substantiate the strong evidence of leaflet remodeling in the present study.

While the increased volume loading and resultant cardiac and orifice expansions experienced in pregnancy resemble the changes associated with heart failure and other LV dysfunctions, the pathways of remodeling (physiological versus pathophysiological) of the conditions are very different. The increases in leaflet area presented in the current study appear to be occurring uniformly along both axes of the leaflet: circumferential length is increased 19–41% while radial length is increased a similar 11–30% across the valves. Conversely, leaflet expansion in patients with LV dysfunction occurs mainly through circumferential expansion [185]. Elevated mechanical stresses on heart valve leaflets, produced in heart failure, are associated with increased concentrations of GAGs, cells, and DNA, decreased water content and viscosity, and increased and more disorganized collagen, causing the leaflets to become increasingly less extensible [183, 197, 278]. Pregnancy is associated with increased collagen content, decreased alignment of collagen fibers, and a loss in extensibility, however the mechanical extensibility of the leaflet is regained in late pregnancy, an adaptation that never occurs in heart failure.

Furthermore, pregnancy results in decreased concentrations of GAGs and cells, and maintained water content, completely the opposite of what is observed in patients with congestive heart failure. It is clear that pregnancy and pathological heart disease follow distinctly different pathways of remodeling, likely related to differences in hormone profiles and signaling pathways of these conditions.

In conclusion, we have demonstrated that all four heart valves of the maternal heart undergo significant adaptive remodeling during bovine pregnancy, resulting in increased leaflet size, a gestation-dependent biphasic shift in mechanical properties, an overall loss of collagen crimp, altered extracellular matrix composition and crosslinking profile, and decreased thermal stability, yet with no change in the proportion of cells expressing markers of the activated phenotype. These structural and mechanical changes clearly show that valvular remodeling during pregnancy is distinct from pathological remodeling (e.g. associated with heart failure). Differences in valve properties based on anatomical location emphasize the importance of both the mechanical loading environment and the embryological origins of each valve in determining the properties of the VICs and their surrounding matrix. Nevertheless, for the most part the remodeling response of all four valves was similar in pregnancy, regardless of heart side or inflow/outflow position. This is however, the first study to provide evidence of an enhanced remodeling response via leaflet expansion in the aortic valve, which may be responsible for preserved function of this valve observed in pregnancy the clinical setting, compared to the other valve types. This unique finding requires further investigation with an in-depth focus on valve-specific remodeling. Understanding the triggers and mechanisms of physiological remodeling during pregnancy would be fundamental to developing treatments for valve pathologies as well as understanding and improving maternal health during pregnancy and later in life.

5.5 Acknowledgements

The authors thank Patricia Colp (Department of Pathology, Dalhousie University) for sharing valuable expertise in histological staining techniques, Maxine Langman (Department of Applied Oral Sciences, Dalhousie University), Mariya Turchin, Jessi Bak, Leah Johnston, Jimena Prado, and Chantell Cleversey (Dalhousie Integrated

Science Program; DISP) for their assistance with histological analysis, and Ellen Brennan-Pierce (School of Biomedical Engineering, Dalhousie University, now at College of Engineering, Colorado State University) for providing biochemical technical expertise, as well as O.H. Armstrong for the supply of bovine tissues.

5.6 Author Contributions

Author contributions: CMP, SMW, and JML conception and design of research; CMP analyzed data; CMP and ADM performed experiments – more specifically, ADM performed biaxial mechanical and hydrothermal testing while CMP performed all other experiments; CMP analyzed data; CMP, SMW, and JML interpreted results of experiments; CMP prepared figures and drafted manuscript; CMP, SMW, and JML edited and revised manuscript; CMP, SMW, JML and ADM approved final version of manuscript.

CHAPTER 6

Conclusion

6.1 Summary

This research is the first to present such a comprehensive investigation of heart valve remodeling. Together these studies have indisputably demonstrated that pregnancy results in rapid and significant remodeling of bovine heart valve leaflets. We have shown uniform leaflet enlargement of the valve leaflet, both along the radial and circumferential axes of the leaflet, as well as increased chordal attachments (mitral valve). Tissue expansion, however, can occur in two ways: (i) by passive stretching of the tissue, or (ii) by growth of new material. Distinguishing one from the other is important, and most directly performed by determining whether the internal structure and/or composition of the leaflet are changing. Internal fiber architecture of heart valve leaflets was altered via radial rotation of fibers, decreased fiber alignment (deviation of fibers away from the preferred fiber direction), and a loss in collagen crimp – concurrent with leaflet expansion in the circumferential direction. Thus not only is the valve leaflet geometry changing in pregnancy, but there are confirmed changes in the internal fiber structure as well.

Mechanical studies were performed in the belly regions of the leaflet to determine the material effects of the alterations. These studies were not intended to investigate physiological mechanics, but rather the material properties of the tissues in vitro. Creep resistance for example, is sensitive to changes in tissue structure, particularly collagen crosslinking – that is crosslinks reduce fiber mobility thus increasing creep resistance. During turnover, collagen fibers are first synthesized and assembled, and then crosslinked in a later step. Therefore, the presence of smaller quantities of crosslinks indicates newer collagen. This, however, was not the case in bovine pregnancy. Creep studies demonstrated alterations in dynamic resistance to creep in a valve-specific manner (increased in mitral and decreased in aortic valve), while extensibility studies revealed a biphasic shift in leaflet stretch – decreased areal stretch in early pregnancy (consistent with the loss of fiber crimp) followed by a reversal in late pregnancy to (or close to) pre-pregnant values. Crosslink content (mature and total) in pregnancy, assessed via thermomechanical methods, increased, indicating that the valve leaflet is fully crosslinked in pregnancy, resulting in very little creep. However, these studies have conclusively shown that the heart valve is remodeling in pregnancy, so it is surprising that we would not observe a decrease in crosslinking secondary to an increase in collagen

turnover. Investigation of the leaflet biochemical composition was thus needed to clarify this question.

We observed large alterations in extracellular matrix composition, particularly by the increase in total collagen content, confirming that the dramatic leaflet expansion is not simply occurring due to passive stretching, but in fact there is a growth of new collagenous tissue. The substantial thickening of the leaflet fibrosa is explained by this increase in collagen content. Pepsin-/acid-soluble (extractable) collagen content however was low in valve leaflets of non-pregnant animals, and remained unchanged in pregnancy. This is collagen which is not sufficiently crosslinked into the network to resist solubilisation – generally thought to be newly synthesized collagen – thus this result is puzzling. New collagen *is* being synthesized, reflected by (i) growth of new tissue accompanying leaflet expansion, (ii) decreased denaturation temperature (thermal stability) of the leaflet tissue, and (iii) the increased concentration of collagen in that tissue. However, the new-collagen assay and HIT crosslinking profiles show little to no evidence of new collagen or new crosslinks in native or pregnancy animals heart valves. This unexpected result suggests again, that mature crosslinked collagen dominates valve tissues and this feature is unchanged in pregnancy. As mentioned previously, it is possible that, in pregnancy, valve collagen is crosslinked more quickly after synthesis and assembly – a potentially unique feature of pregnancy and a hypothesis worthy of further investigation. Importantly, biochemical studies confirm a change in composition of the valve leaflets in pregnancy. These leaflets are getting bigger in pregnancy, but on the structural and compositional level, they have become very different tissues.

Lastly, alterations in cellularity of the heart valve leaflets were investigated, and demonstrated a decrease in total cell density, while the percentage of the activated cells remained unchanged. Clearly, there is not a hyperplasic response in pregnancy, and if cells are mitosing, it is not occurring at a fast enough rate to keep in step with the leaflet expansion. However, most surprising is the lack of increase in activated VICs. These results may reflect: (i) a decrease in cell density secondary to an increase in leaflet size, and/or (ii) the presence of subpopulations of cells, with specified functions, which are up-regulated or down-regulated under the altered cardiovascular loading in pregnancy.

The main focus of this research has been to investigate pregnancy-induced remodeling of each of the heart valves individually. While in a broad sense we have shown that the valves remodel in largely the same manner, these studies have allowed us to also examine valve-specific differences both in leaflet properties as well as remodeling response. It is important to examine each of the valves and the distinctions between them due to differences in their mechanical loading conditions and embryological origin, which may affect their remodeling response.

6.2 Valve-Specific Differences

The valve-specific differences (left-side versus right-side / inflow versus outflow) in leaflet properties were examined in non-pregnant animals (summarized in Table 6.1). This was followed by a two-way ANOVA to determine whether these relationships were conserved in pregnancy.

6.2.1 Left-side Versus Right-side Valve Differences

The action of mechanical forces in vivo is not simply a consequence of the physiological environment, but in fact is vital to connective tissue homeostasis [37]. Changes in hemodynamic loading imposed on the heart valves, particularly when maintained for extended periods of time, lead to gradual remodeling of leaflet tissues and ultimately to macroscopic structural changes. This process can promote healthy tissue maintenance under the dynamic cardiac environment, or can give way to irreversible damage under pathological conditions. Left and right-side heart comparisons provide information about the influence of differences in mechanical (pressure) loading on the structure and remodeling of the heart valve leaflets.

Mechanical Loading During Development

An interesting example of the result of an extreme but physiological alteration in valve hemodynamics occurs during fetal development, as discussed in Chapter 1. During fetal development, the aortic and pulmonary valves are structurally similar, both experiencing the same TVP [21, 38]. Aldous *et al.* also reported no difference in hydrothermal stability (i.e. remodeling rates) between the fetal aortic and pulmonary valves [244]. However, at birth, due to the closing of the ductus arteriosus and foraman ovale, pressures are

Table 6.1 Valve-specific differences in leaflet properties in non-pregnant animals

	Valve-specific comparisons	
	Left-side valves (compared to right-side valves)	Inflow valves (compared to outflow valves)
Leaflet area	↑	↑
Circumferential length	↑	↑
Leaflet thickness	↑	↑
Layer thicknesses	↑ (fibrosa only)	↑ (all layers)
Crimp length	-	↑
Total collagen content	↑	↓
Extractable collagen content	↓	-
sGAG content	↑	-
Elastin content	↓	-
Total cell density	-	↓
aVIC density	-	↓
aVIC proportion	↑	-
Areal stretch	-	↓
Radial extensibility	-	↓
Denaturation temperature	↓	-

Comparisons were made between valves of differing anatomical positions in non-pregnant animals. Column 1 lists the parameters compared. Column 2 compares left-side (aortic and mitral) valves to right right-side (pulmonary and tricuspid) valves to reveal the effects of loading conditions on the remodeling response. Column 2 compares inflow (mitral and tricuspid) valves to outflow (aortic and pulmonary valves) to reveal the effects of embryological origin on the remodeling response. Statistical t-Test comparisons were made between (i) the left and right side groups, and between (ii) the inflow and outflow groups. The presence and direction of statistically significant differences ($p < 0.05$) between groups, are indicated by the arrows (↑ = higher; ↓ = lower).

drastically changes, decreasing in the pulmonary artery and increasing in the aorta, and altering postnatal flow conditions between the left and right side of the heart. The result is an increase in collagen fiber alignment and thickness associated with thickening of aortic valve [21], as well as the development of a difference in remodeling rates (indicated by the ratio of immature to mature crosslinking) between the aortic and pulmonary valves [244]. These findings are in agreement with findings of increased collagen synthesis under elevated pressures in the porcine aortic valve [40], valve growth of the pulmonary autograft under heighted pressures of the aortic position after the Ross procedure [324-326, 345, 346], and gradual development of a tri-layer leaflet structure (including alterations in collagen, GAGs, and elastin) of implanted tissue-engineered heart valves in ovine animals [347].

Mechanical Loading in Adulthood

After development, the left side of the heart has significantly increased blood pressure and transvalvular pressure (TVP) compared to the right side of the heart. In humans, the maximum pressure experienced by the right side of the heart is ~25 mmHg and that experienced by the left side of the heart is a might ~120 mmHg [42]. Thus, the left-side mitral and aortic valves encounter higher tensile stresses in vivo due to TVP. Investigation of differences between left and right-side valves is therefore valuable to uncovering differences in remodeling potential based on the mechanical loading environment.

Current study

Heart-side differences in leaflet properties were evident across many of the experiments performed in this study. Left-side (aortic and mitral) valve leaflets, compared to right-side (pulmonary and tricuspid valves), were larger in size, thicker, contained higher quantities of total collagen and sGAG content and lower quantities of measureable extractable collagen and elastin content, contained higher proportions of cells expressing markers of the activated cell phenotype, and demonstrated lower denaturation temperatures. All of these heart-side differences in valve properties were present in non-pregnant animals, and were also conserved in pregnancy, with the exception of circumferential length. In non-pregnant animals, circumferential length of valve leaflets

was not significantly different between sides of the heart. However, in pregnancy, left-side valves became 13% longer in the circumferential direction compared to right-side valves, even though all valves had enlarged. It is possible that orifice expansion is higher in left-side valves in pregnancy compared to right-side valves, however, previous reports of valve annular diameters range a great deal between studies so it is difficult to obtain a precise measurement for comparison between valves. Valve orifice expansion has been shown to range from approximately 12-23 % in pregnancy, with no obvious differences between valves [157, 168].

The larger leaflet size of left-side valves is likely strongly skewed by the large area of the anterior mitral valve leaflet compared to all other valve leaflets. In fact, in non-pregnant animals, the mitral valve leaflet was 40–102% larger than each of the other valves leaflets, while the aortic valve was significantly smaller than the pulmonary and tricuspid valve leaflets. Yet in pregnant animals, the aortic valve leaflet increased in area by a striking 84%, and was no longer significantly different from the pulmonary and tricuspid valves. That is, the aortic valve increased in size on a much larger scale than any of the other valves in pregnancy. As mentioned in Chapter 5, this increased remodeling response of the aortic valve may be the first strong evidence of valve-specific remodeling, and may explain the lack of valvular regurgitation observed in this valve in human pregnancy [168].

Furthermore, circumferential length increased more in the left-side (aortic and mitral) valves (32–40 %) compared to the right-side (pulmonary and tricuspid) valves (19–21%). This result, combined with the lower denaturation temperature and higher proportion of activated cell phenotypes, indicates that left-side valves may have an increased rate of collagen turnover and a higher potential for remodeling, compared to their right-side counterparts. In fact, there is evidence that the pulmonary valve tissue remodeling ability is much slower compared to that of the aortic valve, based on studies comparing VIC contraction, phenotype, and biosynthesis [2, 3, 42]. That is, aortic VICs possess the ability to produce higher ECM contraction than pulmonary VICs, which has been linked to increased collagen synthesis [3]. This is not surprising considering that left-side valves experience higher TVPs in vivo, which corresponds to increased tension across the leaflet. Further, Aldous et al. showed a trend toward decreasing thermal stability

(associated with increased collagen turnover), with increasing transvalvular pressure (TVP) [101].

Lastly, we showed that the proportion of cells expressing α-SMA (inferring the activated phenotype) was higher in left-side valves compared to right-side valves. Previous studies suggest that VICs undergo remodeling in response to local tissue stress development [2, 20]. There is a great deal of evidence for the existence of a strong correlation between VIC cell stiffness and the stresses imposed on their leaflet tissues. VICs from the left-side (aortic – higher TVP pressure side) of the ovine heart contain more α-SMA (in agreement with the current study) and Hsp47, exhibit higher contractility, and are two times stiffer than those of the right-side (pulmonary – lower TVP pressure) [3, 42]. It is possible that this increased contractile ability, and hence increased remodeling potential, may be responsible for the enhanced remodeling response, in terms of leaflet expansion, at least in the aortic valve.

6.2.2 Inflow Versus Outflow Valve Differences

Architectural similarities between the inflow (mitral and tricuspid) valves, and between the outflow (aortic and pulmonary) valves, are due to their distinct embryological origins. Anatomically, the inflow and outflow valves arise at opposite ends in the developing heart tube and are thought to have derived from different populations of cells [18]. The cellular origins of the inflow valves arise solely from tissues of the endocardial cushions in the developing heart tube, while the outflow valves, like much of the outflow tract (OFT), are thought to be derived both from endocardial cells as well as immigrating neural crest cells [18, 23-25, 314-316]. Furthermore, the cells of the atrioventricular canal, OFT, and valve tissues may be derived from distinctly different heart fields. Much research points to the role of a primary heart field in linear heart tube, inflow valves, and left ventricular development, and a secondary field in later right ventricular, OFT, outflow valves, and atrial formation [6, 7, 11, 26].

Current study

Valve position differences were found throughout the present study. Inflow (mitral and tricuspid) valve leaflets, compared to outflow (aortic and pulmonary) valve leaflets, were significantly larger in area and circumferential length, thicker in the overall leaflet as well

as each layer thickness, contained lower concentrations of total collagen, exhibited higher crimp length (and correspondingly lower percentage of leaflet area occupied by crimp), contained lower cell densities of both total and activated VICs, and were significantly less extensible, particularly in the radial direction. All of these valve position differences in leaflet properties were present in non-pregnant animals, and were maintained in pregnancy.

The higher leaflet size of the inflow valves in this study is not a surprising finding due to the inherent asymmetry of leaflets in these valves, and how we selected the leaflets for study. As noted in the methods of Chapter 5, the larger leaflets of the mitral and tricuspid valves were preferentially selected for the current study based on *in vivo* stresses and to facilitate comparison to previous studies.

The decreased areal stretch of inflow valves compared to outflow valves is likely related to structural-functional differences between the anatomical locations of these valves. Inflow valves are anchored to the papillary muscles at the apex of each ventricle via chordae tendineae, to prevent inversion and prolapse of the valves into the atria upon closure [1]. The leaflet is divided into the rough zone (toward the free edge) and the clear zone (toward the annulus). The chordae tendineae are collagenous cord-like tendons that insert into the ventricular surface of the leaflets in the rough zone. While the collagen network of valve leaflets is mainly circumferentially aligned in the central region and clear zone of the leaflet [255, 264, 293], and the clear zone is, by definition, free of any chordae insertions, extensions of chordae fibers may protrude past the rough zone and into the belly region of the leaflet [348], effectively reinforcing the collagen network in the radial direction. It is possible that specimens excised from the belly of the inflow leaflets for extensibility experiments were affected by these radial collagenous fibers, decreasing both the radial extensibility and overall areal stretch of the leaflets. Moreover, inflow valves were significantly less crimped compared to outflow valves, which would result in decreased extensibility in the circumferential direction of the leaflet, contributing to decreased areal stretch as well. The presence of these chordae tendineae insertions would also tend to increase the thickness of the inflow valve leaflets compared to their chordae-less outflow valve counterparts.

Valve-Specific Observations in Other Studies

According to a study by Dreger *et al.* [338], there exist valve-specific differences in the expression of MMPs and their inhibitors: MMP–2 is present only in aortic and pulmonary valve tissues, and not in tricuspid and mitral; TIMP–1 and –2 are found in all valves while TIMP–3 is found only in tricuspid valves. Interestingly, the distinction in proteolytic enzyme expression profile appears between inflow and outflow valves, rather than the more frequently observed left and right side heart differences. This finding introduces interesting ties to valve position that may be responsible for the differences in collagen content found between inflow and outflow valves in the present study.

Several studies from Merryman *et al.* describe a correlation between VIC phenotype and TVP (discussed in Chapter 5), but also show a potential link between cell phenotype and inflow/outflow position [3, 60]. α-SMA and Hsp47 expression in the outflow valve was consistently higher than in the corresponding inflow valve on the same side of the heart – aortic VIC protein content > mitral VIC protein content, and pulmonary VIC protein content > tricuspid VIC protein content. Hsp47 is a marker of collagen synthesis, and Merryman *et al*. showed a correlation between α-SMA and Hsp47 [3]. Although the mechanism is unclear, this association makes the expression of α-SMA not only an indicator of cell stiffness and contractile potential, but also a reliable marker for collagen synthesis and thus collagen turnover [3, 20, 22, 45]. These findings (collagen synthesis and α-SMA expression) agree with the current study and present compelling evidence for valve-specific differences that likely relate back to the differing embryonic origins of the inflow and outflow valves during development.

Summary

Valve-specific differences in heart valve structure and composition were reported in many parameters in this study, and agree with previously documented data. Interestingly, however, virtually no differences in remodeling response were found in pregnancy between left and right side valves or between inflow and outflow valves. Nonetheless, the wide scope of the current study has provided the opportunity to probe into the influences of valvular mechanical loading environment and embryological origins on bovine valve properties. It is without question that in vivo stresses do in fact impact VIC mechanical

and biosynthetic properties[3]. The left-side interstitial cells are tailored for the elevated stresses imposed by the left-side cardiac loading environment and likely differentially regulate cytoskeletal protein expression [3] and proteolytic enzyme secretion [349] as necessary to maintain tissue homeostasis. All of this points to a higher rate of collagen synthesis and turnover in left side heart valves, which in turn is indicative of a heightened potential for adaptive remodeling. In fact, the current study did not show evidence of an enhanced remodeling response of left-side valves in pregnancy, as would be expected. Rather, the aortic valve alone demonstrated augmented leaflet expansion compared to all other valves (discussed in Chapter 5) – a potentially unique capacity of this left-sided valve, which requires continued investigation.

6.3 Hormones in Pregnancy

The ability of the heart to adapt to pregnancy, a non-disease state, without failure is remarkable. However, distinguishing the roles of hemodynamic stresses and hormonal alterations as triggers to this tissue remodeling is challenging, and beyond the scope of this study. Nevertheless, it does stand as a limitation in our understanding of the valvular remodeling mechanisms at play in pregnancy.

Hormones are regulatory chemicals that are produced by an organism and secreted into the circulation or extracellular tissue fluids to stimulate cells and tissues. Target cells or tissues are equipped with receptors that bind to that specific hormone. Only cells bearing that binding receptor can be targeted for action. Hormones that are secreted into the blood are able to travel throughout the body and distant to the original location of hormone secretion. These hormones are part of the endocrine hormone system. Paracrine hormones on the other hand are diffused into localized tissue fluids and thus act in the nearby tissue surrounding the location of secretion. Autocrine hormones bind to and act on the same cell that produced the hormone in the first place. Hormonal changes govern maternal physiological adaption throughout gestation, beginning to act on the maternal cardiovascular system very early in pregnancy.

Interestingly, the early and late changes in maternal uterine anatomy in pregnancy are probably due to distinctly different mechanisms. Hypertrophy of myocytes early in the first trimester is likely due to rapid stimulation by maternal hormones, including estrogen

and progesterone [151]. However, by the mid-point of the 1st trimester, mechanical distension due to the pressure of expanding reproductive tissues is likely the main antagonist of change. Ectopic pregnancy, which occurs outside of the uterus, is still accompanied by anatomical changes in the uterus similar to those observed in normal early pregnancy [151], thus reducing likelihood of mechanical stimulation as the dominant remodeling trigger.

6.3.1 Relaxin

Relaxin is an important peptide hormone in pregnancy, first discovered by Frederick Hisaw in 1926 [350]. Hisaw's early relaxin research addressed the role of this hormone in pregnancy-induced adaptation of the pelvic girdle of the guinea pig. More specifically, he observed relaxation of the pubic ligament after injection of virgin guinea pigs with serum from pregnant guinea pigs and rabbits. The term describing this pelvic change was referred to as "pubic-symphysis relaxation", which lead to the naming of its founding hormone "relaxin" [351]. The structure of relaxin was established nearly half a century after the discovery of the hormone itself. It is a 2-chain peptide, composed of an A-chain and a B-chain linked together by two disulphide bonds. Relaxin is structurally (but not chemically) very similar to the insulin molecule, displaying identical positioning of the disulphide bonds [188, 192, 351, 352].

The hormone is encoded by seven genes in humans, three relaxin genes (RLN1:3), and four insulin-like genes (INSL3:6) [192]. In humans, three forms of relaxin have been identified to date: H1, H2, and H3, corresponding to genes RLN1, RLN2, and RLN3 respectively. The function of H1 is not well known, and the gene to encode this peptide is not found in most non-primate species [192, 351]. The genes encoding H2 and H3 are found in most mammalian species. H3 is expressed mainly in the brain [353], while H2 and its non-primate ortholog termed "species relaxin" appears to have important function in mammalian pregnancy [351]. H2 is the only circulating form of relaxin and has been observed in human pregnancy. Human-gene-2 relaxin (H2) and "species relaxin" are commonly simply termed "relaxin".

Relaxin hormone is expressed in both pregnant and non-pregnant mammals, both female and male, with roles in reproductive and non-reproductive tissues. Relaxin is primarily

produced by the corpus luteum in human ovaries, where it is secreted into the blood plasma for circulation (endocrine function) [188, 189, 354-357]. Relaxin is also produced by the placenta and decidua where it does not enter the circulation (autocrine or paracrine function) [351, 355, 357]. Therefore relaxin functions as an endocrine hormone in pregnancy, but also as a paracrine and autocrine factor [190, 192].

Relaxin is critical to proper parturition in rats, mice and pigs, but its role in human and primate pregnancy appears to differ. Rats, mice, and pigs show increased concentrations of relaxin in the second half of pregnancy [189, 194, 358]. Relaxin knockout (in non-primates) leads to minimal cervix dilation at delivery while re-injection of the hormone can resolve these issues [351], facilitating delivery by stimulating softening, growth, and extensibility of the lower reproductive tract, particularly the cervix [188, 189, 312, 358]. In humans, however, relaxin does not appear to be necessary for maintenance of the pregnancy or delivery [351]. The timeline for its secretion from the corpus luteum differs between species but has been shown to be increased in the 3rd trimester at least in rats, guinea pigs, and cows, while in humans its expression is higher in the first trimester [354, 359-363]. Higher levels of relaxin have been associated with multiplets and/or ovarian stimulation, both of which often go hand-in-hand [351]. Furthermore, increased levels of relaxin during pregnancy have been linked to premature parturition [351].

There have been many documented physiological effects of relaxin in mammals: Relaxin has been linked to connective tissue remodeling, and specifically collagen remodeling with stimulation of MMPs (involved in collagen degradation), and inhibition of TIMPs (inhibitors of MMPs) [187-192]. Collagen remodeling has been documented in the uterus and cervix of pregnant rats [297], but it is likely that the remodeling of blood vessels, including the aorta, is also triggered by relaxin. Samuel *et al*. found that the mass of pubic symphysis tissue was greatly reduced at parturition in rats, coinciding with an increase in water content. This agrees with previous evidence of altered collagen turnover and demonstrates that there is an overall reduction in collagen content at delivery in rats [312]. Interestingly though, due to the up-regulation of relaxin, these changes occur under "non-normal" conditions such as a disease state, but also pregnancy [189, 192].

6.3.2 Relaxin in the Heart

Relaxin acts throughout the maternal body during pregnancy, particularly in preparation for parturition, but up-regulation of relaxin also has effects on the heart. Chronotropic effects are those that modify the heart rate, while inotropic effects modify the force and speed of muscle contraction. Both of these effects can be observed in mammals due to relaxin expression or injection [188-190, 192, 352, 364]. High affinity binding sites for relaxin have been identified in rat atria less than one day after birth, and at a higher receptor density than in the uterus [189, 365]. Although cell phenotypes associated with relaxin receptors have not been clearly demonstrated, some studies suggest localization on cardiomyocytes [189, 366]. Humans and sheep do not, however, appear to have receptors present in the atria [190]. It might be expected that relaxin receptors would be present in the ventricles and pacemaker cells of the sino-atrial node, but this has yet to be shown conclusively.

The study of relaxin, its natural physiological functions, and potential use as a pharmacological drug is of great interest under a variety of conditions including pregnancy, hypertension, and heart disease. It has been shown to exhibit higher potency than other hormones in rat hearts [189], and contributes to physiological adaptions all through the body. Its production and antifibrotic activity in the heart along with vascular (coronary) vasodilation has been described as a cardioprotective action and has generated a great deal of attention in the medical community [189-191, 360, 366]. It is not yet clear how the administration of relaxin hormone to humans might affect disease state in the heart.

Although the actions of relaxin have been extensively observed, the mechanisms by which it acts are not well understood. Furthermore, cardiovascular effects of relaxin, to a large extent, have not been investigated. While receptors have been identified in some cardiac tissues, their presence in valvular tissues, and thus their role in the remodeling of heart valves in pregnancy and in disease, is completely unknown. And further, relaxin is not the only hormone that may be acting on leaflet remodeling in pregnancy. For example, estrogen [367] and progesterone [368] have been linked to vascular remodeling in pregnancy, while early research points to the role of oxytosin, another pregnancy-

related hormone, in direct triggering of cardiovascular remodeling in mice [369]. Pinpointing the role of hormones on valvular remodeling in pregnancy would greatly clarify our understanding of the mechanisms behind the adaptions reported in this study and is of particular interest for future studies to follow from this work.

6.4 Fetal Microchimerism (FMC)

In recent years, a re-focusing on the interesting phenomenon of feto-maternal cell trafficking has emerged – that is the invasion of fetal cells into the maternal circulation during pregnancy. This occurrence is referred to as microchimerism, defined as the coexistence of two genetically different cell populations which are present in the same organism, organ, or tissue, and generally occurs due to transfusion, transplantation, or pregnancy [370, 371]. In pregnancy, this is referred to more specifically as fetal microchimerism.

The occurrence of this phenomenon in pregnancy has been collectively agreed upon in the scientific community since the 1970's [372], and was even documented as early as 1893 [373, 374]. However, it was only recently found that these fetal cells can persist in the maternal organs and circulation for as long as several decades after delivery [370, 375, 376]. Fetal cell invasion begins very early in pregnancy and continues to increase with gestation [371, 377], including migration to many maternal organs and tissues, including the heart [370]. It is likely that these cells are tolerated in pregnancy due to maternal immune system suppression by the feto-placental unit [371] .

Remarkably, not only do fetal cells migrate into the maternal heart, but they appear to play an essential role in cardiac injury response, zeroing in on the site of damaged tissues (e.g. an infarction) [370, 375]. This ground-breaking study arose from the clinically observed high recovery rate from heart failure (up to 50%) of patients experiencing peripartum cardiomyopathy [378, 379] – higher than any other form of heart failure [380]. The core mechanisms responsible for the protective effects of these fetal cells in the maternal circulation is not yet known [372].

This research, however, raises the question of whether fetal cells invade all of the maternal cardiovascular tissues (aortic, pericardium, heart valves, etc.), and thus whether fetal microchimerism plays a role in their adaptive remodeling in pregnancy. Further, the

persistence of these fetal cells in the maternal body after pregnancy may underlie the more pronounced remodeling observed in subsequent pregnancies (Chapter 2). Like the hormonal influences on the remodeling mechanisms of heart valve tissues in pregnancy, the contribution of fetal microchimerism is unknown and merits further investigation.

6.5 Maternal Health

Lastly, little attention has focused on the relation between pregnancy and the mother's subsequent health. Data are now increasingly linking maternal vascular complications (metabolic and inflammatory) of pregnancy with an increased risk of vascular disease later in life. Sattar et al. depicted an increase in vascular risk factor with pregnancy, both in the healthy populations as well as in complicated pregnancy [212]. Further, studies are showing that there is an increasing risk for maternal cardiovascular disease with every subsequent pregnancy [213-215]. However, this relationship is not well understood nor has it been the focus of much research.

In Chapter 2, we assessed changes in bovine cardiac dimensions between non-pregnant, early, and late pregnant animals. To expand on this study, we also have sufficient data to allow us to assess (i) the effects of subsequent pregnancies, but also (ii) whether remodeling is reversed after pregnancy. In order to perform this analysis, we used four groups of animals: non-pregnant heifers (never pregnant), non-pregnant cows (not present at the time but with a history ≥ 1 pregnancy), pregnant heifers (first pregnancy), pregnant cows (second or subsequent pregnancy). The results of this study are presented in Table 6.2.

To examine the effects of subsequent pregnancies, we compared pregnant heifers (single pregnancy group) to pregnant cows (multiple pregnancy group), and determined that pregnant cows had significantly larger heart dimensions than pregnant heifers. Furthermore, qualitatively, the hearts from pregnant cows were flaccid compared to the firm hearts of the heifer groups. These results indicate that cardiac remodeling is significantly augmented by subsequent pregnancies. To investigate the reversal of remodeling post-pregnancy, we compared non-pregnant heifers (never-pregnant group) to

Table 6.2 Changes in heart dimensions with pregnancy

	Heart dimensions			
	Non-pregnant		Pregnant	
	Heifer	Cow	Heifer	Cow
Mass, kg	2.13 ± 0.16(11)	3.07 ± 0.24**(3)	2.09 ± 0.10(10)	2.92 ± 0.13***(13)
Volume, L	2.24 ± 0.17(11)	3.12 ± 0.19*(3)	2.13 ± 0.12(8)	2.99 ± 0.15***(13)
Transverse Circumference, cm	45.9 ± 1.3(11)	50.58 ± 0.82*(6)	45.05 ± 0.62(10)	51.2 ± 1.1***(13)
Apical Circumference, cm	53.9 ± 1.2(11)	57.7 ± 2.3*(6)	54.7 ± 1.4(10)	59.0 ± 1.2 *(13)

Values are mean values ± SE of heart dimensions for animals in the heifer and cow groups of non-pregnant and pregnant animals. Statistical comparisons were made between heifer and cow groups using t-Test comparisons and p value ranges are indicated as follows: † = $p < 0.1$; * = $p < 0.05$; ** = $p < 0.01$; *** = $p < 0.001$. n values for each parameter are presented in brackets for each pregnancy group.

non-pregnant cows (post-pregnant group), and found that the dimensions of the heart were larger in non-pregnant cows. This means that pregnancy-induced remodeling is not reversed, or at least not fully, after pregnancy. These findings are in agreement with the reports of increased vascular risk of women later in life with single pregnancy, and augmented risk with multi-parity.

6.6 Significance

The fundamental aim of a strong PhD thesis is to make a substantial and original contribution to new knowledge. In that light, this thesis has addressed an area of research that has never been studied outside of our laboratory and a process that was even once thought to be impossible. Using a bovine pregnancy model, we have shown that physiological remodeling of heart valves *does* occur. From an engineering perspective, recall that the first objective of this study was to determine how the mechanical function of heart valve tissues is altered in pregnancy – this research has identified a remarkable biphasic alteration in biaxial leaflet extensibility as well as valve-specific alterations in biaxial viscoelastic creep. This unique mechanical behavior emphasizes two important findings of this work: (1) Leaflet mechanical properties are significantly altered in pregnancy, but at least some of these properties are recovered in a time-dependent manner; (2) While the leaflets from each heart valve remodel in largely the same manner, there are undoubtedly valve-specific differences in remodeling behaviors. This thesis continued beyond simply documenting effects of pregnancy to investigate how the structure and composition of heart valve tissues remodel to accomplish the observed mechanical behaviors. This latter half of the research objective allowed the consideration of the remodeling mechanisms that appear to be at play in pregnancy. Here we report, for the first time, tremendous changes in leaflet geometry, fiber architecture, composition, hydrothermal stability, and cellularity. To reiterate answers to the specific questions posed at the beginning of this document:

A1. Yes, rapid and dramatic changes in physiological hemodynamics imposed by pregnancy result in valve remodeling during pregnancy.

A2. The valves are remodeling through changes in leaflet size, fiber architecture, composition, crosslinking, and cellularity, resulting in changes to leaflet biomechanical

properties. These changes are generally the same across all four valves, but the magnitude of the changes are valve dependent – particularly, the aortic valve appears to display an enhanced remodeling response in terms of leaflet expansion.

A3. The specific remodeling mechanisms at play appear to be complex and interconnected. All the valves expanded in pregnancy, through an increase collagen synthesis, with accompanying changes to the ECM biochemical composition (increased collagen content, decreased elastin and sGAG content) and leaflet structure (increased fibrosa thickness) as well as the structure of the collagen network (crimp loss, crosslink maturation, and reduction in thermal stability).

6.7 Limitations and Future Research

While the current study has gone a long way to establishing evidence of heart valve remodeling, there remain important research areas to explore further in pregnancy.

6.7.1 Tissue Sampling

It is important to note from the present study, that histological analysis of leaflet thickness, layer thickness, and cellular changes were averaged across the entire cross-section of each heart valve leaflet. And furthermore, biaxial mechanical studies were conducted on square specimens excised from the belly region of the leaflet only. Considering the tremendous heterogeneity, particularly of the mitral valve, but also structural differences in all the valves between the belly and the free and fixed edge regions, these methodologies lose data richness around regional changes. Regional leaflet analysis of mechanical, structural, and cellular changes in pregnancy could provide new insight into regional-specific remodeling mechanisms or responses associated with the dissimilar loads experienced by different regions of the valve leaflet.

6.7.2 Collagen Type & Crosslinking Profile

Analysis of alterations in collagen types in pregnancy is recommended for future studies. Evidence shows that Type III collagen can be crosslinked more rapidly than other forms of collagen due to the formation of intermolecular disulfide bonds, and has been shown to be synthesized and assembled more quickly than other forms of collagen during development and injury response [381]. Both Type I and Type III have

both been shown to increase in myxomatous chordae tendineae [382]. In a similar manner, alterations in collagen type in pregnancy may (i) be indicative both of the laying down of new collagen, and (ii) alter the mechanical properties of the leaflet tissues. Furthermore, the current study has investigated only fiber-level changes in the collagen network of leaflet tissues in pregnancy. Transmission electron microscopy (TEM) examination of changes at the collagen fibril-level could provide information regarding collagen fibril formation, assembly, and organization (i.e. fibril diameter and length) – important determinants of tissue function – as well as physical interactions between VICs and the ECM.

We also reported that mature (hydrothermally stable), crosslinked collagen appears to dominate valve tissues – a surprising discovery because we know collagen turnover is occurring. Thus, we propose two possibilities for this finding: (i) valve collagen, in pregnancy, is crosslinked more quickly after synthesis and assembly, and/or (ii) hydrothermally stable immature keto-amine crosslink HLKNL is preferentially formed during collagen synthesis in pregnancy. Both of these hypotheses are worthy of investigation, and author recommends that the latter be explored by determining the specific crosslinking profile using a biochemical technique such as HPLC.

6.7.3 VIC Phenotype

The results of the cellular and phenotypic experiments in Chapter 5 reported a surprising decrease in cell density with no change in in the expression of α-SMA (activated phenotype). The hypothesis for the existence of subpopulations of cells in valve tissues is a thought-provoking (but recent) idea that requires further investigation. However, another possibility exists regarding the lack of change in the activated cell population. Recall that previous studies in humans report that only 2-5% of cells from normal healthy adults exhibit expression of α-SMA [57], while non-pregnant cattle from the present study showed much higher levels of α-SMA expression, ranging from 27.5–52.6%. This may be a species-related difference, demonstrating that normal, healthy adult bovine may possess a population of VICs that are already primed for remodeling, signifying that VIC activation is not needed for remodeling in these valves. Future studies to clarify if (and how) VIC phenotype is altered in pregnancy, could (a) investigate

alternative indicators of cell phenotype (i.e. P4H, Hsp47, MMPs, non-muscle myosin, and various fibrocyte markers which have all been correlated to the activated cell phenotype [45]), and (b) benefit from reverse transcription polymerase chain reaction (RT-PCR) experiments for identification of phenotypic indicator genes expressed by VICs in pregnancy [383] – thus to identify exactly what the cells are doing. In fact, RT-PCR techniques could be used to analyze a whole host of proteins and enzymes that are hypothesized to be altered in pregnancy – particularly those important to valvular ECM turnover, such as alterations in collagen types and/or the regulation of any MMPs responsible for degradation of collagen and/or elastin, as well as their tissue inhibitory metalloproteinases (TIMPs).

6.7.4 Neovascularization

Normal mature heart valves are reported to be essentially avascular, but due to the imbalance of angiogenic factors in pathological settings, the presence of new blood vessels has been observed [20]. Neovascularization is thus thought to have a role in pathological, and more specifically degenerative diseases, in tendon [384], chordae tendineae [385], and heart valves [386]. This finding likely stems from the fact that while the growth and expansion of vasculature is important to repair and remodeling in tissues, it can also result in weakening of the ECM [387, 388]. Neovascularization was not documented in the current study, but identification of the presence or absence of this process could provide important information about the nature of remodeling in pregnancy compared to pathological conditions.

6.7.5 Chordae Tendineae

The present study has shown that the chordae tendineae of the mitral valve remodel alongside the valve leaflet tissues, with an increase in chordae number accompanying leaflet expansion. It is not yet known whether the tricuspid valve experiences remodeling of the chordae tendineae. Considering the clinical finding of limited left-side (high pressure) compared to right-side (low pressure) valve regurgitation in pregnancy [168], it is possible that prevention of left-side regurgitation has greater survival value than prevention on the right-side. Therefore, equivalent remodeling of the chordae in the tricuspid valve may not be present in pregnancy. Regardless, this study

provides the first evidence of such a remodeling process in the chordae of mature valve tissues. Further, a recent study found that decreases in thermal stability in pregnancy were accompanied by increases in mitral valve chordae diameter [389], providing further evidence of chordal remodeling. However, the process by which these changes occur has not been investigated. The continued expression of periostin in adulthood [31] may be related to the alterations in chordae tendineae associated with pregnancy, in previous and current studies. In the pathological setting, regurgitation of the mitral valve has been shown to be more strongly correlated to poor tethering rather than annular enlargement [223]. Thus, an improved understanding of the mechanisms of chordal remodeling – including changes in mechanical properties – under altered loading in pregnancy could be beneficial to clinical treatment of pathological mitral valve regurgitation. Research into pregnancy-induced changes in the chordae tendineae composition, structure, and mechanical properties is ongoing in our laboratory.

6.7.6 Hormonal Influences

Hormonal changes during pregnancy surely contribute to the tissue remodeling that occurs in the heart valve leaflets, but likely in a complex manner that would be difficult to map. Direct contributions of pregnancy hormones (i.e. relaxin, estrogen, progesterone, and oxytocin) to valvular remodeling could be assessed in a broad sense but determining whether valve tissues contain relaxin receptors. Answering this question, while a small piece of the puzzle, would be an important first step in identifying the triggers of valvular remodeling. As a next step, in vitro tissue and cell culture studies could be used to analyze the response of VICs and leaflet tissues to different hormonal (and even mechanical) signals.

6.7.7 Valve-Specific Remodeling

This thesis showed that left-side valves appear to possess an increased potential for remodeling, but we have also observed enhanced leaflet expansion in the aortic valve specifically. Continued research in the area of valve-specific remodeling is recommended, with a focus on how the remodeling mechanisms of the aortic valve differ from the other valves. Furthermore, pairing of data (where possible) between studies (i.e.

crosslink analysis and creep resistance studies) might provide new insight into valve-dependent behaviors.

6.8 Conclusions

Taken together, these studies provide irrefutable evidence of heart valve remodeling. The ability of the heart to adapt to pregnancy, a non-disease state, without failure is remarkable. This study has captured physiological remodeling of tissues that up until this point were thought incapable of remodeling. Understanding the valvular adaptations to pregnancy may be fundamental both to developing interventions and treatments for valve disease and heart failure, as well as improving the prognosis of the mother later in life by recognizing the implications of pregnancies on long-term vascular risk.

Appendices

APPENDIX 1 JUSTIFICATION OF THE BOVINE MODEL

Comparison of Non-Pregnant Animals in Current Study to Other Animal Models

For these studies, we used a bovine model, which closely parallels many essential features of human pregnancy. A preliminary investigation of the rationality of the bovine model to examine structural and biochemical changes in the mitral valve anterior leaflet in pregnancy as compared to non-pregnant animals, was performed in Chapter 2 [248], and is expanded upon here to include the aortic, pulmonary, and tricuspid valves. Close agreement was found between the measures of leaflet mechanical extensibility, collagen thermal denaturation, crosslinking, and fiber architecture, leaflet and layer dimensions, and biochemical extracellular matrix content, for non-pregnant animals in our study, compared to other animal models. These findings support the validity of the bovine model for heart valve studies, and thereby as a means to examine structural and biochemical changes in the mitral valve anterior leaflet in pregnancy.

Mechanical Extensibility

Biaxial mechanical extensibility data from this study was compared to previous studies in the aortic [39, 295, 296] and mitral [216, 233-236, 295] valve leaflets, revealing strong similarities between peak areal stretch, circumferential extensibility, and radial extensibility, with differences between the studies largely attributed to the choice of reference state between in vitro biaxial testing of leaflet tissues and in vivo or in situ testing of intact valves [248]. In all cases, including the present study, radial extensibility was greater than circumferential extensibility: ratio of radial to circumferential extensibility (λ_R/λ_C) from previous studies on human, ovine, and porcine models ranged from 1.06–1.36 in the aortic valve and 1.03–2.01 in the mitral valve, compared with a λ_R/λ_C ratio of 1.32 and 1.22 in the aortic and mitral valve leaflets respectively of non-pregnant animals in the current study. Areal stretch in the present study was 2.45 and 2.37 in the aortic and mitral valve leaflets respectively. This indicated that the average increase in area from the unloaded state to peak equibiaxial loading conditions (60-N/m) was 145% in the aortic valve and 137% in the mitral valve. Areal stretch ranges a fair amount between studies on other species, calculated based on measurements of radial and circumferential stretch ratios and green strains. The aortic areal stretch ranges from 1.93–

3.27 in porcine [295, 296] and 1.96 in humans [39]. Mitral valve areal stretch ranges from 1.10–2.80 in porcine [216, 233-235, 295] and 2.01 in ovine [236] valves. The results of these studies indicate that our measures of areal stretch in bovine aortic and mitral valve leaflets were in the same range of those reported for other species.

Thermal Stability and Crosslinking

The denaturation temperature and load relaxation time observed in our non-pregnant control group for the aortic (T_d = 68.7 ± 0.4 °C, $t_{1/2}$ = 8.0 ± 2.5 h), mitral (T_d = 68.6 ± 0.2 °C, $t_{1/2}$ = 8.6 ± 1.8 h), pulmonary (T_d = 70.5 ± 0.2 °C, $t_{1/2}$ = 8.5 ± 2.4 h), and tricuspid valves (T_d = 69.8 ± 0.2 °C, $t_{1/2}$ = 5.6 ± 0.9 h), were higher than those described by Aldous *et al.* for adult bovine steer aortic (T_d = 67.8 ± 0.2 °C, $t_{1/2}$ = 4.9 ± 0.4 h), mitral (T_d = 67.1 ± 0.2 °C, $t_{1/2}$ = 3.2 ± 0.5 h), pulmonary (T_d = 69.8 ± 0.2 °C, $t_{1/2}$ = 4.6 ± 0.4 h), and tricuspid valves (T_d = 68.5 ± 0.3 °C, $t_{1/2}$ = 3.0 ± 0.4 h) [101]. However, as suggested previously by Wells *et al.*, since the age of the cattle are similar (12-30 months in the present study vs. 24-30 months in the previous study), these differences are likely associated with sex differences between the two studies [248], and may be related to our use of a 3-hour isotherm compared to the longer 5-hour isotherm used by Aldous *et al.*

SALS NOI and Fiber Direction

Chapter 3 outlines the first study to characterize the collagen fiber network in the bovine mitral valve. We saw close agreement between the results of SALS experiments obtained for our non-pregnant animals compared to other animal models: NOI was only slightly higher in the current study (43.8 ± 0.5 %) than has been previously reported for porcine mitral [264], aortic [49, 257, 265], and pulmonary [257] valve leaflets. Preferred fiber direction (1.8 ± 1.1º) ran along the circumferential axis of the valve leaflet, which is in agreement with previous studies in porcine [49, 254, 255, 257, 264, 265], canine [266], and murine models [267].

Collagen Crimp

Expanding further on the characterization of the collagen fiber network to include the aortic, pulmonary, and tricuspid valves as well as the mitral valve (Chapters 3-5),

histological measures of collagen crimp were taken using polarized light microscopy. The measures of crimp length in non-pregnant animals in the present study in the mitral (22.9 ± 1.2 μm), aortic valves (3.7 ± 0.5 μm), pulmonary (15.4 ± 1.2 μm), and tricuspid valves (6.1 ± 0.6 μm), were similar to those reported for porcine heart valve leaflets under polarized light microscopy of circumferential tissue sections: native and zero pressure-fixed aortic and pulmonary valves (10–17.8 μm) [46, 257, 268-270], and more recently, the mitral valve leaflet (15 μm) [46]. Similar reports of collagen crimp length have also been reported in other cardiovascular tissues including porcine mitral valve chordae (11.3–14.8 μm) [271], and bovine pericardium (17.7–40.6 μm, mean = 26.6 μm) [85, 272-275], which is often used to construct heart valve bioprostheses. No direct comparisons of the tricuspid valve could be performed between species due to a lack of data in the heart valve literature. Joyce *et al.* also reported 40–60% leaflet area occupied by crimp in the porcine aortic and pulmonary valve leaflets [257], compared to somewhat higher values in the present study: 94.2 ± 1.0 % (aortic), 40.2 ± 6.0 % (mitral), 85.5 ± 3.2 % (pulmonary), and 58.2 ± 9.9 % (tricuspid). While these differences in magnitude are likely species and gender related, relative differences between valves in other species (decreased crimp length and increased % crimp in aortic compared to mitral valves) are conserved in the bovine model.

Leaflet and Layer Dimensions

The structure of the bovine valve leaflet was similar between our studies (mitral valve leaflet dimensions reported in Chapter 2 and 3 were taken from an independent group of animals than those dimensions reported in Chapter 4 and 5) and also showed close agreement to those in other species. Bovine aortic valve leaflet thickness measured in non-pregnant animals in the current study (0.730 ± 0.067 mm) very closely matched to thickness measurements reported in human (0.25–1.30 mm) [276] and porcine (0.60 mm) [44] aortic valves. Bovine mitral valve leaflet thickness in non-pregnant animals (1.17 ± 0.08 mm) very closely compared to thickness measurements reported in human [183, 276], ovine [186, 219], and porcine [44, 211, 258, 277] mitral valves. Further, Kunzelman *et al.* [277] reported similar measurements and proportions of leaflet layer thickness in porcine anterior mitral valve leaflets.

Biochemistry

The biochemical makeup of human heart valves has been shown to be composed of approximately 50–70 % collagen (collagen content varies a great deal between studies), 10 % elastin, and the remaining 10–30 % of proteoglycans, glycosaminoglycans, and endothelium by dry weight [210, 277, 279]. Total collagen content as assessed by biochemical measurement of hydroxyproline across all heart valves in the current study (43–60 % dry wt.) was similar to results of previous studies in the human mitral valve (50–67 % dry wt.) [54, 183, 210, 279, 390], ovine mitral valve (59 % dry wt.) [186], human aortic valve (55 % dry wt.) [390], human tricuspid valve (58 % dry wt.) [390], somewhat higher than that of the porcine aortic valve (46% dry wt.) [391], and lower than that of the of bovine pericardial tissue [391]. Water content in valve tissues of NP animals in the present study in aortic (87.8 ± 0.3 %) and mitral (81.4 ± 0.7 %) valves also correlated very well to previous reports in the porcine aortic valve (87 %) [391], human mitral valve (80–87%) [54, 183, 210, 279, 392], as well as in bovine pericardium (72 %) [391].

Biochemical measurements taken using Biocolor Assays (Sircol – extractable collagen; Fastin – elastin; Blyscan – sGAG) are presented in Table A1 in units of percentage of dry weight (reported in the results of the current study) as well as μg/mg wet weight (as per the protocol of Biocolor) – this conversion is included strictly for comparison of non-pregnant animals in the current study to previous studies. Extractable (pepsin-soluble) collagen has been documented previously in the porcine aortic valve (3.0 % dry wt.) [393], porcine pulmonary valve (3.8 % dry wt.) [394], and human aortic and pulmonary valves (34.5 μg/mg wet wt.) [395]. These quantities are somewhat higher than our measures of extractable collagen in bovine heart valve leaflets (0.6–2.6 % dry wt. or 1.1–3.0 μg/mg wet wt.), particularly in the human studies. While differences between dry weight measures of collagen can likely be attributed to species and gender variation, the large discrepancies between wet weight measures are more likely influenced by differences in tissue hydration at the time of measurement. For this reason, more confidence is placed on biochemical compositional measures normalized to dry weight. Elastin content reported in the human mitral (9–10 % dry wt.) [210, 390], aortic (12 %

Table A1 Wet and dry weight units of biochemical measures

		Extracellular Matrix Content, Non-pregnant animals			
		Aortic Valve	Mitral Valve	Pulmonary Valve	Tricuspid Valve
Extractable collagen	% dry wt.	1.1 ± 0.1	0.6 ± 0.1	2.6 ± 0.6	1.9 ± 0.2
	µg/mg wet wt.	1.3 ± 0.1	1.1 ± 0.2	3.0 ± 0.7	2.3 ± 0.3
Elastin	% dry wt.	10.0 ± 0.7	6.2 ± 0.6	13.8 ± 0.7	11.5 ± 1.1
	µg/mg wet wt.	12.1 ± 0.8	11.8 ± 1.1	15.9 ± 0.8	14.1 ± 1.3
sGAG	% dry wt.	3.3 ± 0.4	3.3 ± 0.5	2.3 ± 0.2	1.3 ± 0.2
	µg/mg wet wt.	4.0 ± 0.5	6.4 ± 1.0	2.7 ± 0.2	1.7 ± 0.2

Values are mean values ± SE of biochemical extracellular matrix measures from Biocolor Assays for animals in the non-pregnant (NP) groups: extractable collagen content (Sircol Assay), elastin content (Fastin Assay), and sGAG content (Blyscan Assay). Each parameter is presented in units of percentage of dry weight (% dry wt.) as well as microgram of protein of interest per milligram of wet weight (µg/mg wet wt.).

dry wt.) [390], and tricuspid valves (11 % dry wt.) [390] was very close to bovine elastin content in the present study (6–14 % dry wt.), while elastin content in the porcine aortic (3 % dry wt.) [393] and pulmonary valves (3 % dry wt.) [394] was significantly lower. Lastly, GAG content in previous studies is most commonly measured via two different experimental protocols, but with varying results: (i) Blyscan Assay of sulfated GAGs (chondroitin sulfates, keratin sulfates, dermatan sulfates, heparins and heparin sulfates), and (ii) hexosamine or hexuronic acid assays of all GAGs (sGAGs from (i) in addition to hyaluronate) – GAGs are composed of disaccharide building blocks each containing one amino sugar and one uronic acid, each component contributing approximately half of the total weight of the total protein. Glycosaminoglycans of heart valves have been shown most recently to be comprised mainly of chondroitin/dermatan sulfates (63-75 %) and hyaluronic acid (25-37 %) in human mitral valves [392, 396, 397] and porcine aortic valves [398], while older studies found human aortic, mitral, and tricuspid valves contained higher proportions of hyaluronic acid, from 50–65 % [396, 399, 400]. It is evident that the distribution of GAG classes is not well understood and likely also differs across species [398].

sGAG concentrations are documented in porcine aortic (3.2 % dry wt.) [393] and pulmonary valves (0.45 % dry wt.) [394], as well as human mitral (1.9 % dry wt.) [210], and aortic and pulmonary valves (3.9 μg/mg wet wt.) [395] – similar to non-pregnant animals in the current study (1.3–3.3 % dry wt.). Hexosamine analysis of total GAG content is documented in porcine aortic valves (3.5–3.7 % dry wt.) [398, 401]. GAG content determined by hexuronic acid measurement has been shown in the porcine aortic valve (1.2–3.2 % dry wt.) [402, 403], and human mitral valve (0.9–2.0 % dry wt.) [54, 183, 210, 279]. Combined analysis of uronic acid and hexosamine content in all valves of the bovine heart by Kanke et al. reported total GAG contents of 3.1 %, 3.2 %, 2.3 %, and 2.7 % in the aortic, mitral, pulmonary, and tricuspid valve leaflets respectively [404]. These indicators of total GAG content are only slightly higher than those for sGAGs by Blyscan Assay, indicating that non-sulfated GAG hyaluronan is not present in large quantities in these valve tissues. Therefore, the current study provides an accurate indication of the majority of the populations of GAG present in our heart valve tissues.

APPENDIX 2 TRICUSPID VALVE MECHANICAL EXTENSIBILITY DATA

Mechanical extensibility data for the tricuspid valve was omitted from Figure 5.2 (Chapter 5) due to a lack of significant changes through gestation. The complete figure for all four heart valves is included on the following page (Fig. A2).

Figure A2 Biaxial mechanical properties (all valves including the tricuspid)

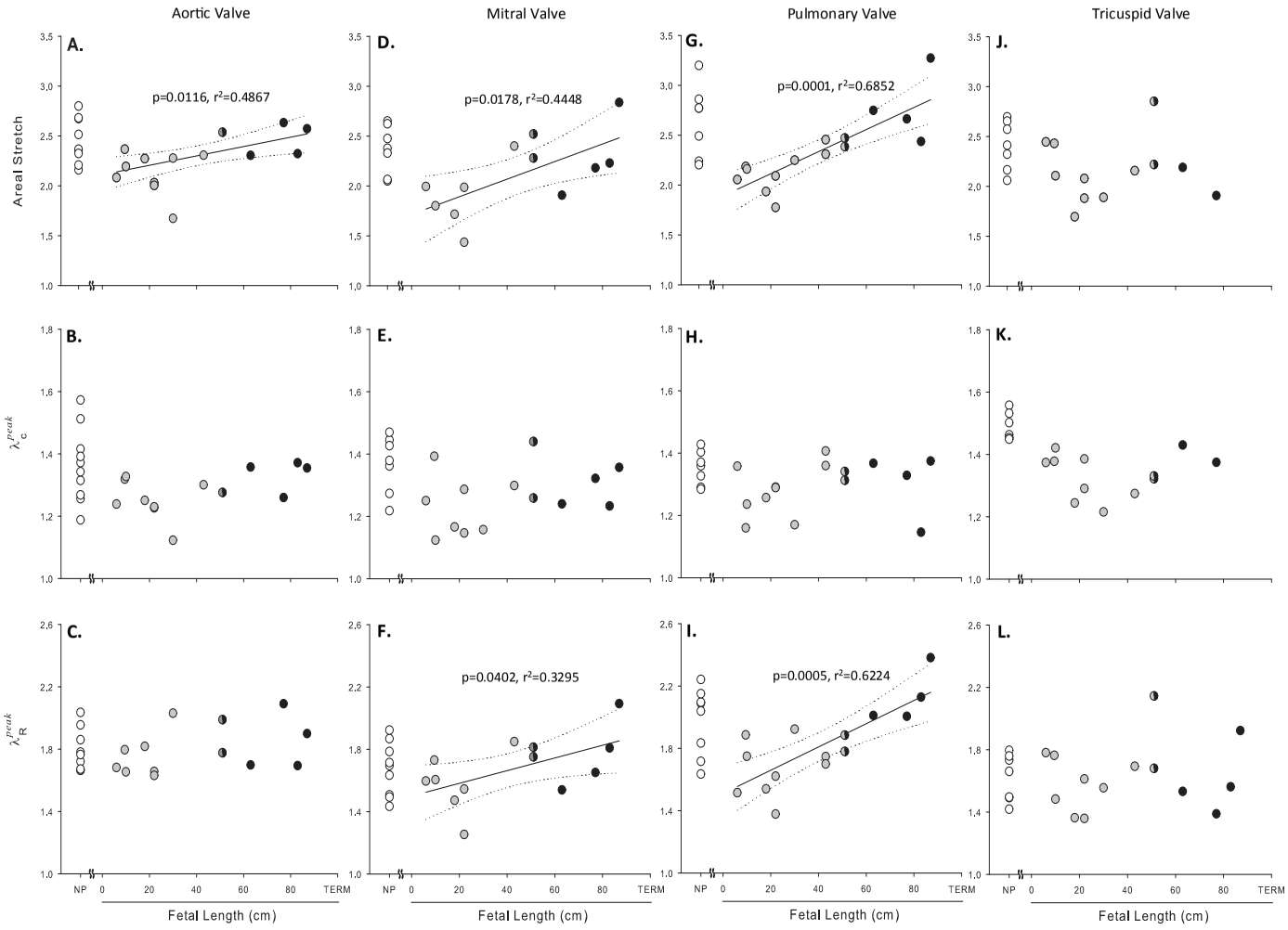

Biaxial mechanical properties of the aortic (A-C), mitral (D-F), pulmonary (G-I), and tricuspid (J-L) valve leaflets: peak values at 60-N/m equibiaxial tension. Peak areal stretch, λ_C^{peak}, and λ_C^{peak}, as a function of fetal crown-to-rump length (~100 cm term) along with measurements from NP heifers (open circles). Pregnant groups are shaded based on gestation: EP (0-169 days of gestation; shaded circles), MP (170-192 days; ½ shaded circles), and LP (193-270 days of gestation; filled circles). Regression lines with 95% confidence intervals are shown for the fetal data where significant.

REFERENCES

1. Saladin KS (2007) Anatomy & physiology : the unity of form and function, 4 ed. McGraw-Hill, New York, NY

2. Sacks MS, Yoganathan AP (2007) Heart valve function: a biomechanical perspective. Philos Trans R Soc Lond, B, Biol Sci 362:1369–1391.

3. Merryman W, Youn I, Lukoff H, et al. (2006) Correlation between heart valve interstitial cell stiffness and transvalvular pressure: implications for collagen biosynthesis. Am J Physiol Heart Circ Physiol 290:H224–H231.

4. Carlson BM (2014) Cardiovascular System. In: Human Embryology and Developmental Biology, 5 ed. Elsevier Health Sciences, Philadelphia, p 520

5. Kirby ML (2007) Cardiac development. Oxford University Press

6. Waldo KL, Kumiski DH, Wallis KT, et al. (2001) Conotruncal myocardium arises from a secondary heart field. Development 128:3179–3188.

7. Harvey RP, Lai D, Elliott D, et al. (2002) Homeodomain factor Nkx2-5 in heart development and disease. Cold Spring Harb Symp Quant Biol 67:107–114.

8. Pashmforoush M, Lu JT, Chen H, et al. (2004) Nkx2-5 pathways and congenital heart disease; loss of ventricular myocyte lineage specification leads to progressive cardiomyopathy and complete heart block. Cell 117:373–386.

9. Abu-Issa R, Kirby ML (2007) Heart field: from mesoderm to heart tube. Annu Rev Cell Dev Biol 23:45–68.

10. Lyons I, Parsons LM, Hartley L, et al. (1995) Myogenic and morphogenetic defects in the heart tubes of murine embryos lacking the homeo box gene Nkx2-5. Genes Dev 9:1654–1666.

11. Mjaatvedt CH, Nakaoka T, Moreno-Rodriguez R, et al. (2001) The outflow tract of the heart is recruited from a novel heart-forming field. Dev Biol 238:97–109.

12. Moorman AFM, Christoffels VM, Anderson RH, van den Hoff MJB (2007) The heart-forming fields: one or multiple? Philos Trans R Soc Lond, B, Biol Sci 362:1257–1265.

13. Tanaka M, Chen Z, Bartunkova S, et al. (1999) The cardiac homeobox gene Csx/Nkx2.5 lies genetically upstream of multiple genes essential for heart development. Development 126:1269–1280.

14. Tanaka M, Schinke M, Liao HS, et al. (2001) Nkx2.5 and Nkx2.6, homologs of Drosophila tinman, are required for development of the pharynx. Mol Cell Biol 21:4391–4398.

15. Yamagishi H, Yamagishi C, Nakagawa O, et al. (2001) The combinatorial activities of Nkx2.5 and dHAND are essential for cardiac ventricle formation. Dev Biol 239:190–203.

16. Leong FT, Freeman LJ, Keavney BD (2009) Fresh fields and pathways new: recent genetic insights into cardiac malformation. Heart 95:442–447.

17. Srivastava D (2006) Making or breaking the heart: from lineage determination to morphogenesis. Cell 126:1037–1048.

18. Armstrong EJ (2004) Heart Valve Development: Endothelial Cell Signaling and Differentiation. Circ Res 95:459–470.

19. Yeung F Cardiac Embryology, 2007 ed. University Health Network

20. Liu AC, Joag VR, Gotlieb AI (2007) The emerging role of valve interstitial cell phenotypes in regulating heart valve pathobiology. Am J Pathol 171:1407–1418.

21. Aikawa E, Whittaker P, Farber M, et al. (2006) Human semilunar cardiac valve remodeling by activated cells from fetus to adult: implications for postnatal adaptation, pathology, and tissue engineering. Circulation 113:1344–1352.

22. Taylor PM, Batten P, Brand NJ, et al. (2003) The cardiac valve interstitial cell. Int J Biochem Cell Biol 35:113–118.

23. Person AD, Klewer SE, Runyan RB (2005) Cell biology of cardiac cushion development. Int Rev Cytol 243:287–335.

24. Kirby ML, Gale TF, Stewart DE (1983) Neural crest cells contribute to normal aorticopulmonary septation. Science 220:1059–1061.

25. Jiang X, Rowitch DH, Soriano P, et al. (2000) Fate of the mammalian cardiac neural crest. Development 127:1607–1616.

26. Jain R, Engleka KA, Rentschler SL, et al. (2011) Cardiac neural crest orchestrates remodeling and functional maturation of mouse semilunar valves. J Clin Invest 121:422–430.

27. Jain R, Rentschler S, Epstein JA (2010) Notch and cardiac outflow tract development. Ann N Y Acad Sci 1188:184–190.

28. Carlson BM (2014) Human Embryology and Developmental Biology, 5 ed. Elsevier Health Sciences, Philidelphia

29. Dickinson MG, Vesely I (2012) Structural changes of rat mitral valve chordae tendineae during postnatal development. J Heart Valve Dis 21:433–439.

30. Oosthoek PW, Wenink AC, Vrolijk BC, et al. (1998) Development of the atrioventricular valve tension apparatus in the human heart. Anat Embryol 198:317–329.

31. Norris RA, Moreno-Rodriguez RA, Sugi Y, et al. (2008) Periostin regulates atrioventricular valve maturation. Dev Biol 316:200–213.

32. Lincoln J, Alfieri CM, Yutzey KE (2004) Development of heart valve leaflets and supporting apparatus in chicken and mouse embryos. Dev Dyn 230:239–250.

33. Gray H, Williams PL, Bannister LH (1995) Gray's anatomy : the anatomical basis of medicine and surgery, 38 ed. xx–2092 p.

34. Hinton R, Lincoln J, Deutsch G, et al. (2006) Extracellular matrix remodeling and organization in developing and diseased aortic valves. Circ Res 98:1431–1438.

35. Sochman J, Peregrin JH (2007) Catheter-based modification of heart valve diseases: from experimental to clinical application. ASAIO J 53:609–616.

36. Stradins P, Lacis R, Ozolanta I, et al. (2004) Comparison of biomechanical and structural properties between human aortic and pulmonary valve*1. European Journal of Cardio-Thoracic Surgery 26:634–639.

37. Chiquet M, Renedo AS, Huber F, Flück M (2003) How do fibroblasts translate mechanical signals into changes in extracellular matrix production? Matrix Biol 22:73–80.

38. Rabkin-Aikawa E, Aikawa M, Farber M, Kratz JR (2004) Clinical pulmonary autograft valves: pathologic evidence of adaptive remodeling in the aortic site. J Thorac Cardiovasc Surg 128:552–561.

39. Christie GW, Barratt-Boyes BG (1995) Mechanical properties of porcine pulmonary valve leaflets: how do they differ from aortic leaflets? Ann Thorac Surg 60:S195–9.

40. Xing Y, He Z, Warnock JN, et al. (2004) Effects of constant static pressure on the biological properties of porcine aortic valve leaflets. Annals of Biomedical Engineering 32:555–562.

41. Butcher JT, (null), Penrod AM, et al. (2004) Unique morphology and focal adhesion development of valvular endothelial cells in static and fluid flow environments. Arterioscler Thromb Vasc Biol 24:1429–1434.

42. Merryman WD, Liao J, Parekh A, et al. (2007) Differences in tissue-remodeling potential of aortic and pulmonary heart valve interstitial cells. Tissue Eng 13:2281–2289.

43. Lloyd-Jones D, Adams RJ, Brown TM, Carnethon M (2010) Heart disease and stroke statistics—2010 update A report from the American Heart Association. Circulation

44. Stephens EH, de Jonge N, McNeill MP, et al. (2010) Age-related changes in material behavior of porcine mitral and aortic valves and correlation to matrix composition. Tissue Eng Part A 16:867–878.

45. Stephens E, Grande-Allen K (2007) Age-related changes in collagen synthesis and turnover in porcine heart valves. J Heart Valve Dis 16:672–682.

46. Kreuz JM, Erskine KN, Blancas AA, Grande-Allen KJ (2013) Age and Regional Dependence of Collagen Crimp in Heart Valves. In: Mechanics of Biological Systems and Materials. Springer International Publishing, Cham, pp 15–23

47. Rabkin E, Aikawa M, Stone J, et al. (2001) Activated interstitial myofibroblasts express catabolic enzymes and mediate matrix remodeling in myxomatous heart valves. Circulation 104:2525–2532.

48. Flanagan TC, Pandit A (2003) Living artificial heart valve alternatives: a review. Eur Cell Mater 6:28–45– discussion 45.

49. Sacks MS, Smith DB, Hiester ED (1998) The aortic valve microstructure: effects of transvalvular pressure. J Biomed Mater Res 41:131–141.

50. Gloeckner DC, Billiar KL, Sacks MS (1999) Effects of mechanical fatigue on the bending properties of the porcine bioprosthetic heart valve. ASAIO J 45:59–63.

51. Messier R, Bass B, Aly H, et al. (1994) Dual structural and functional phenotypes of the porcine aortic valve interstitial population: characteristics of the leaflet myofibroblast. J Surg Res 57:1–21.

52. Kruithof BPT, Krawitz SA, Gaussin V (2007) Atrioventricular valve development during late embryonic and postnatal stages involves condensation and extracellular matrix remodeling. Dev Biol 302:208–217.

53. May-Newman K, Yin FC (1995) Biaxial mechanical behavior of excised porcine mitral valve leaflets. Am J Physiol 269:H1319–27.

54. Grande-Allen KJ, Griffin BP, Ratliff NB, et al. (2003) Glycosaminoglycan profiles of myxomatous mitral leaflets and chordae parallel the severity of mechanical alterations. J Am Coll Cardiol 42:271–277.

55. Christov AM, Liu L, Lowe S, et al. (1999) Laser-induced fluorescence (LIF) recognition of the structural composition of porcine heart valves. Photochem Photobiol 69:382–389.

56. Stella JA, Sacks MS (2007) On the biaxial mechanical properties of the layers of the aortic valve leaflet. Journal of biomechanical engineering 129:757–766.

57. Schoen FJ (2008) Evolving Concepts of Cardiac Valve Dynamics: The Continuum of Development, Functional Structure, Pathobiology, and Tissue Engineering. Circulation 118:1864–1880.

58. Vesely I (1998) The role of elastin in aortic valve mechanics. J Biomech 31:115–123.

59. David H, Boughner DR, Vesely I, Gerosa G (1994) The pulmonary valve. Is it mechanically suitable for use as an aortic valve replacement? ASAIO J 40:206–212.

60. Merryman WD (2007) Mechanobiology of the Aortic Valve Interstitial Cell. University of Pittsburgh 1–196.

61. Blevins TL, Carroll JL, Raza AM, Grande-Allen KJ (2006) Phenotypic characterization of isolated valvular interstitial cell subpopulations. J Heart Valve Dis 15:815–822.

62. Butcher J, Nerem R (2004) Porcine Aortic Valve Interstitial Cells in Three-Dimensional Culture: Comparison of Phenotype with Aortic Smooth Muscle Cells. J Heart Valve Dis 13:478–85– discussion 485–6.

63. Dahl KN, Ribeiro AJS, Lammerding J (2008) Nuclear shape, mechanics, and mechanotransduction. Circ Res 102:1307–1318.

64. Benton JA, Fairbanks BD, Anseth KS (2009) Characterization of valvular interstitial cell function in three dimensional matrix metalloproteinase degradable PEG hydrogels. Biomaterials 30:6593–6603.

65. Huang H, Liao J, Sacks M (2007) In-situ deformation of the aortic valve interstitial cell nucleus under diastolic loading. J Biomech Eng 129:880–889.

66. Cushing MC, Liao J-T, Anseth KS (2005) Activation of valvular interstitial cells is mediated by transforming growth factor-beta1 interactions with matrix molecules. Matrix Biol 24:428–437.

67. Durbin AD, Gotlieb AI (2002) Advances towards understanding heart valve response to injury. Cardiovasc Pathol 11:69–77.

68. Walker G, Masters K, Shah D, et al. (2004) Valvular myofibroblast activation by transforming growth factor-beta: implications for pathological extracellular matrix remodeling in heart valve disease. Circ Res 95:253–260.

69. Butcher JT, Nerem RM (2006) Valvular endothelial cells regulate the phenotype of interstitial cells in co-culture: effects of steady shear stress. Tissue Eng 12:905–915.

70. Stamenkovic I (2003) Extracellular matrix remodelling: the role of matrix metalloproteinases. J Pathol 200:448–464.

71. Flanagan TC, Black A, O rsquo Brien M, et al. (2006) Reference models for mitral valve tissue engineering based on valve cell phenotype and extracellular matrix analysis. Cells Tissues Organs (Print) 183:12–23.

72. Konduri S, Xing Y, Warnock JN, et al. (2005) Normal physiological conditions maintain the biological characteristics of porcine aortic heart valves: an ex vivo organ culture study. Annals of Biomedical Engineering 33:1158–1166.

73. Manasek FJ (1976) Macromolecules of the extracellular compartment of embryonic and mature hearts. Circ Res 38:331–337.

74. Wells S, Sacks M (2002) Effects of fixation pressure on the biaxial mechanical behavior of porcine bioprosthetic heart valves with long-term cyclic loading. Biomaterials 23:2389–2399.

75. Gupta V, Barzilla JE, Mendez JS, et al. (2009) Abundance and location of proteoglycans and hyaluronan within normal and myxomatous mitral valves. Cardiovasc Pathol 18:191–197.

76. Galbraith CG, Sheetz MP (1998) Forces on adhesive contacts affect cell function. Curr Opin Cell Biol 10:566–571.

77. Wells SM, Langille BL, Lee JM, Adamson SL (1999) Determinants of mechanical properties in the developing ovine thoracic aorta. Am J Physiol 277:H1385–91.

78. Gosline J, Lillie M, Carrington E, et al. (2002) Elastic proteins: biological roles and mechanical properties. Philosophical Transactions of the Royal Society B: Biological Sciences 357:121–132.

79. (2011) Hooke's law. In: britannica.com. http://www.britannica.com/EBchecked/topic/271336/Hookes-law. Accessed 4 Jan 2013

80. Fung (2007) Biomechanics - Mechanical Properties Of Living Tissues, 2E. 568.

81. Ward IM, Sweeney J (2004) An introduction to the mechanical properties of solid polymers.

82. Thornton GM, Shrive NG, Frank CB (2003) Healing ligaments have decreased cyclic modulus compared to normal ligaments and immobilization further compromises healing ligament response to cyclic loading. J Orthop Res 21:716–722.

83. Thornton GM, Shrive NG, Frank CB (2002) Ligament creep recruits fibres at low stresses and can lead to modulus-reducing fibre damage at higher creep stresses: a study in rabbit medial collateral ligament model. J Orthop Res 20:967–974.

84. Thornton GM, Oliynyk A, Frank CB, Shrive NG (1997) Ligament creep cannot be predicted from stress relaxation at low stress: a biomechanical study of the rabbit medial collateral ligament. J Orthop Res 15:652–656.

85. Sellaro TL, Hildebrand D, Lu Q, et al. (2007) Effects of collagen fiber orientation on the response of biologically derived soft tissue biomaterials to cyclic loading. J Biomed Mater Res A 80A:194–205.

86. Purslow P, Wess T, Hukins D (1998) Collagen orientation and molecular spacing during creep and stress-relaxation in soft connective tissues. J Exp Biol 201:135–142.

87. Walford RL, Carter PK, Schneider RB (1964) Stability of labelled aortic elastic tissue with age and pregnancy in the rat. Archives of pathology

88. Lefevre M, Rucker RB (1980) Aorta elastin turnover in normal and hypercholesterolemic Japanese quail. Biochim Biophys Acta 630:519–529.

89. Mays P, McAnulty R, Campa J, Laurent G (1991) Age-related changes in collagen synthesis and degradation in rat tissues. Importance of degradation of newly synthesized collagen in regulating collagen production. Biochem J 276 (Pt 2):307–313.

90. Bailey AJ, Shimokomaki MS (1971) Age related changes in the reducible cross-links of collagen. FEBS Lett 16:86–88.

91. Danielsen C (1990) Age-related thermal stability and susceptibility to proteolysis of rat bone collagen. Biochem J 272:697–701.

92. Barnard K, Light N, Sims T, Bailey A (1987) Chemistry of the collagen cross-links. Origin and partial characterization of a putative mature cross-link of collagen. Biochem J 244:303–309.

93. Ku C, Johnson P, Batten P, et al. (2006) Collagen synthesis by mesenchymal stem cells and aortic valve interstitial cells in response to mechanical stretch. Cardiovasc Res 71:548–556.

94. Christiansen D, Huang E, Silver F (2000) Assembly of type I collagen: fusion of fibril subunits and the influence of fibril diameter on mechanical properties. Matrix Biol 19:409–420.

95. Humphrey JD (2003) Continuum Biomechanics of Soft Biological Tissues. Proc R Soc Lond A 459:3–46.

96. Humphrey J, Yin F (1987) A new constitutive formulation for characterizing the mechanical behavior of soft tissues. Biophys J 52:563–70.

97. Miles CA, Avery NC, Rodin VV, Bailey AJ (2005) The increase in denaturation temperature following cross-linking of collagen is caused by dehydration of the fibres. J Mol Biol 346:551–556.

98. Avery NC, Bailey AJ (2005) Enzymic and non-enzymic cross-linking mechanisms in relation to turnover of collagen: relevance to aging and exercise. Scand J Med Sci Sports 15:231–240.

99. Avery NC, Bailey AJ (2008) Restraining cross-links responsible for the mechanical properties of collagen fibers: natural and artificial. In: Fratzl P (ed) Collagen: Structure and Mechanics. Springer, pp 81–110

100. Bailey A (2001) Molecular mechanisms of ageing in connective tissues. Mech Ageing Dev 122:735–755.

101. Aldous IG, Veres SP, Jahangir A, Lee JM (2009) Differences in collagen cross-linking between the four valves of the bovine heart: a possible role in adaptation to mechanical fatigue. Am J Physiol Heart Circ Physiol 296:H1898–906.

102. Naimark WA, Waldman SD, Anderson RJ, et al. (1998) Thermomechanical analysis of collagen crosslinking in the developing lamb pericardium. Biorheology 35:1–16.

103. Naimark W, Lee J, Limeback H, Cheung D (1992) Correlation of structure and viscoelastic properties in the pericardia of four mammalian species. Am J Physiol 263:H1095–106.

104. Brüel A, Ortoft G, Oxlund H (1998) Inhibition of cross-links in collagen is associated with reduced stiffness of the aorta in young rats. Atherosclerosis 140:135–145.

105. Robins S (2007) Biochemistry and functional significance of collagen cross-linking. Biochem Soc Trans 35:849–52.

106. Hulmes D (2008) Collagen diversity, synthesis and assembly. Collagen-Structure and Mechanics New York: Springer 15–47.

107. Bailey AJ, Paul RG, Knott L (1998) Mechanisms of maturation and ageing of collagen. Mech Ageing Dev 106:1–56.

108. Cheung D, DiCesare P, Benya P, et al. (1983) The presence of intermolecular disulfide cross-links in type III collagen. J Biol Chem 258:7774–7778.

109. Kivirikko KI, Risteli L (1976) Biosynthesis of collagen and its alterations in pathological states. Med Biol 54:159–186.

110. Lee J, Pereira C, Abdulla D, et al. (1995) A multi-sample denaturation temperature tester for collagenous biomaterials. Med Eng Phys 17:115–121.

111. Bischof JC, He X (2005) Thermal stability of proteins. Ann N Y Acad Sci 1066:12–33.

112. Wells PB, Thomsen S, Jones MA, et al. (2005) Histological evidence for the role of mechanical stress in modulating thermal denaturation of collagen. Biomech Model Mechanobiol 4:201–210.

113. Miles CA, Bailey AJ (2001) Thermally labile domains in the collagen molecule. Micron 32:325–332.

114. Miles C, Ghelashvili M (1999) Polymer-in-a-box mechanism for the thermal stabilization of collagen molecules in fibers. Biophys J 76:3243–3252.

115. Wright NT, Humphrey JD (2002) Denaturation of collagen via heating: an irreversible rate process. Annual review of biomedical engineering 4:109–128.

116. Harris JL, Humphrey JD (2004) Kinetics of thermal damage to a collagenous membrane under biaxial isotonic loading. IEEE transactions on bio-medical engineering 51:371–379.

117. Wells SM, Adamson SL, Langille BL, Lee JM (1998) Thermomechanical analysis of collagen crosslinking in the developing ovine thoracic aorta. Biorheology 35:399–414.

118. Allain JC, Le Lous M, Cohen-Solal, et al. (1980) Isometric tensions developed during the hydrothermal swelling of rat skin. Connect Tissue Res 7:127–133.

119. Le Lous M, Flandin F, Herbage D, Allain J (1982) Influence of collagen denaturation on the chemorheological properties of skin, assessed by differential scanning calorimetry and hydrothermal isometric tension measurement. Biochim Biophys Acta 717:295–300.

120. Lous ML, Allain J-C, Cohen-solal L, Maroteaux P (1983) Hydrothermal Isometric Tension Curves from Different Connective Tissues. Role of Collagen Genetic Types and Noncollagenous Components. Connect Tissue Res 11:199–206.

121. Latif N, Sarathchandra P, Taylor PM, et al. (2005) Localization and pattern of expression of extracellular matrix components in human heart valves. J Heart Valve Dis 14:218–227.

122. Connell PS, Han RI, Grande-Allen KJ (2012) Differentiating the aging of the mitral valve from human and canine myxomatous degeneration. J Vet Cardiol 14:31–45.

123. Snowden J, Swann DA (1980) Effects of glycosaminoglycans and proteoglycan on the in vitro assembly and thermal stability of collagen fibrils - Google Search. Biopolymers

124. Carabello BA (2002) Concentric versus eccentric remodeling. J Card Fail 8:S258–63.

125. Mihl C, Dassen WRM, Kuipers H (2008) Cardiac remodelling: concentric versus eccentric hypertrophy in strength and endurance athletes. Neth Heart J 16:129–133.

126. Lips D (2003) Molecular determinants of myocardial hypertrophy and failure: alternative pathways for beneficial and maladaptive hypertrophy. Eur Heart J 24:883–896.

127. Grossman W (1980) Cardiac hypertrophy: useful adaptation or pathologic process? The American Journal of Medicine

128. Alyono D, Ring WS, Anderson MR, Anderson RW (1984) Left ventricular adaptation to volume overload from large aortocaval fistula. Surgery 96:360–367.

129. Sugimoto M, Ota K, Kajihama A, Nakau K (2011) Volume overload and pressure overload due to left-to-right shunt-induced myocardial injury - Evaluation using a highly sensitive cardiac Troponin-I assay in children with congenital heart disease. Circulation Journal : official journal of the Japanese Circulation Society 75:2213–2219.

130. Cohn JN, Ferrari R, Sharpe N (2000) Cardiac remodeling—concepts and clinical implications: a consensus paper from an international forum on cardiac remodeling. J Am Coll Cardiol 35:569–582. 131. Frick MH, Konttinen A, Sarajas HS (1963) Effects of physical training on circulation at rest and during exercise. Am J Cardiol 12:142–147.

132. Morganroth J, Maron BJ, Henry WL, Epstein SE (1975) Comparative left ventricular dimensions in trained athletes. Ann Intern Med 82:521–524.

133. Pluim BM, Zwinderman AH, van der Laarse A (2000) The athlete's heart a meta-analysis of cardiac structure and function. Circulation

134. Hagberg JM, Goldberg AP, Lakatta L, et al. (1998) Expanded blood volumes contribute to the increased cardiovascular performance of endurance-trained older men. J Appl Physiol 85:484–489.

135. Schannwell CM, Zimmermann T, Schneppenheim M, et al. (2002) Left ventricular hypertrophy and diastolic dysfunction in healthy pregnant women. Cardiology 97:73–78.

136. Hunter S, Robson S (1992) Adaptation of the maternal heart in pregnancy. Br Heart J 68:540–543.

137. Pritchard JA (1965) Changes in the blood volume during pregnancy and delivery. Anesthesiology 26:393–399.

138. Whittaker PG, Macphail S, Lind T (1996) Serial hematologic changes and pregnancy outcome. Obstet Gynecol 88:33–39.

139. Strek M (2005) Critical Illness in Pregnancy. In: Hall J, Schmidt G, Wood L (eds) Principles of Critical Care, Third Edition. McGraw Hill Professional, pp 1593–1614

140. Sullivan JM, Ramanathan KB (1985) Management of medical problems in pregnancy--severe cardiac disease. N Engl J Med 313:304–309.

141. Lapinsky SE, Kruczynski K, Slutsky AS (1995) Critical care in the pregnant patient. Am J Respir Crit Care Med 152:427–455.

142. Rizk NW, Kalassian KG, Gilligan T, et al. (1996) Obstetric complications in pulmonary and critical care medicine. Chest 110:791–809.

143. Torgersen K, Curran C (2006) A systematic approach to the physiologic adaptations of pregnancy. Crit Care Nurs Q 29:2–19.

144. Hart M, Morton M, Hosenpud J, Metcalfe J (1986) Aortic function during normal human pregnancy. Am J Obstet Gynecol 154:887–891.

145. Katz R, Karliner J, Resnik R (1978) Effects of a natural volume overload state (pregnancy) on left ventricular performance in normal human subjects. Circulation 58:434–441.

146. Thornburg K, Jacobson S, Giraud G, Morton M (2000) Hemodynamic changes in pregnancy. Semin Perinatol 24:11–4.

147. Stout KK, Otto CM (2007) Pregnancy in women with valvular heart disease. Heart 93:552–558.

148. Bernstein IM, Ziegler W, Badger GJ (2001) Plasma volume expansion in early pregnancy. Obstet Gynecol 97:669–672.

149. Clapp JF, Little KD, Widness JA (2003) Effect of maternal exercise and fetoplacental growth rate on serum erythropoietin concentrations. Am J Obstet Gynecol 188:1021–1025.

150. Harstad TW, Mason RA, Cox SM (1992) Serum erythropoietin quantitation in pregnancy using an enzyme-linked immunoassay. Am J Perinatol 9:233–235.

151. Cunningham FG, Leveno KJ, Bloom S, et al. (2009) Maternal Physiology. In Williams Obstetrics (electronic resource). New York, NY : McGraw-Hill Medical.

152. Huisman A, Aarnoudse JG, Heuvelmans JH, et al. (1987) Whole blood viscosity during normal pregnancy. Br J Obstet Gynaecol 94:1143–1149.

153. Kaaja R, Greer I (2005) Manifestations of Chronic Disease During Pregnancy. 294:2751–2757.

154. Stein PK, Hagley MT, Cole PL, et al. (1999) Changes in 24-hour heart rate variability during normal pregnancy. Am J Obstet Gynecol 180:978–985.

155. Capeless EL, Clapp JF (1989) Cardiovascular changes in early phase of pregnancy. Am J Obstet Gynecol 161:1449–1453.

156. Mabie WC, DiSessa TG, Crocker LG, et al. (1994) A longitudinal study of cardiac output in normal human pregnancy. Am J Obstet Gynecol 170:849–856.

157. Robson SC, Hunter S, Boys RJ, Dunlop W (1989) Serial study of factors influencing changes in cardiac output during human pregnancy. Am J Physiol 256:H1060–5.

158. Clark SL, Cotton DB, Lee W, et al. (1989) Central hemodynamic assessment of normal term pregnancy. Am J Obstet Gynecol 161:1439–1442.

159. Dobbenga-Rhodes YA, Privé AM (2006) Assessment and evaluation of the woman with cardiac disease during pregnancy. J Perinat Neonatal Nurs 20:295–302.

160. Duvekot JJ, Cheriex EC, Pieters FA, et al. (1993) Early pregnancy changes in hemodynamics and volume homeostasis are consecutive adjustments triggered by a primary fall in systemic vascular tone. Am J Obstet Gynecol 169:1382–1392.

161. Mesa A, Jessurun C, Hernandez A, et al. (1999) Left ventricular diastolic function in normal human pregnancy. Circulation 99:511–517.

162. Mone SM, Sanders SP, Colan SD (1996) Control mechanisms for physiological hypertrophy of pregnancy. Circulation 94:667–672.

163. Heidemann B (2003) Changes in maternal physiology during pregnancy. BJA CEPD Reviews

164. Eghbali M, Wang Y, Toro L, Stefani E (2006) Heart hypertrophy during pregnancy: a better functioning heart? Trends Cardiovasc Med 16:285–291.

165. Simmons LA, Gillin AG, Jeremy RW (2002) Structural and functional changes in left ventricle during normotensive and preeclamptic pregnancy. Am J Physiol Heart Circ Physiol 283:H1627–33.

166. Kametas NA, McAuliffe F, Hancock J, et al. (2001) Maternal left ventricular mass and diastolic function during pregnancy. Ultrasound in obstetrics & gynecology : the official journal of the International Society of Ultrasound in Obstetrics and Gynecology 18:460–466.

167. Steegers EA, Jongsma HW, Eskes TK, et al. (1991) Atrial natriuretic peptide and atrial size during normal pregnancy. Br J Obstet Gynaecol 98:202–206.

168. Campos O, Andrade J, Bocanegra J, et al. (1993) Physiologic multivalvular regurgitation during pregnancy: a longitudinal Doppler echocardiographic study. Int J Cardiol 40:265–72.

169. Page KL, Celia G, Leddy G, et al. (2002) Structural remodeling of rat uterine veins in pregnancy. Am J Obstet Gynecol 187:1647–1652.

170. Clapp MD III, Ford J, Capeless MD (1997) Cardiovascular function before, during, and after the first and subsequent pregnancies. Am J Cardiol 80:1469–1473.

171. Kametas NA, McAuliffe F, Krampl E, et al. (2003) Maternal cardiac function in twin pregnancy. Obstet Gynecol 102:806–815.

172. Edman CD, Toofanian A, MacDonald PC, Gant NF (1981) Placental clearance rate of maternal plasma androstenedione through placental estradiol formation: an indirect method of assessing uteroplacental blood flow. Am J Obstet Gynecol 141:1029–1037.

173. Dhawan V, Brookes ZLS, Kaufman S (2004) Long-term effects of repeated pregnancies (multiparity) on blood pressure regulation. Cardiovasc Res 64:179–186.

174. Dhawan V, Brookes ZLS, Kaufman S (2005) Repeated pregnancies (multiparity) increases venous tone and reduces compliance. 289:R23–R28.

175. Hameed A, Sklansky M (2007) Pregnancy: Maternal and Fetal Heart Disease. Current Problems in Cardiology 32:419–494.

176. Thilen U, Olsson S (1997) Pregnancy and heart disease: a review. Eur J Obstet Gynecol Reprod Biol 75:43–50.

177. McElroy PA, Shroff SG, Weber KT (1989) Pathophysiology of the failing heart. Cardiol Clin 7:25–37.

178. Maurer G (2009) Mitral leaflet in functional regurgitation: passive bystander or active player? Circulation 120:275–277.

179. Opie LH (2006) Controversies in cardiology. Lancet 367:13–14.

180. Francis GS, McDonald K, Chu C, Cohn JN (1995) Pathophysiologic aspects of end-stage heart failure. Am J Cardiol 75:11A–16A.

181. Wilansky S, Reuss CS, Willerson JT (2007) Pregnancy and the Heart. Cardiovascular Medicine 2453–2483.

182. Zuber M, Gautschi N, Oechslin E, et al. (1999) Outcome of pregnancy in women with congenital shunt lesions. Heart 81:271–275.

183. Grande-Allen KJ, Borowski AG, Troughton RW, et al. (2005) Apparently normal mitral valves in patients with heart failure demonstrate biochemical and structural derangements: an extracellular matrix and echocardiographic study. J Am Coll Cardiol 45:54–61.

184. Quick DW, Kunzelman KS, Kneebone JM, Cochran RP (1997) Collagen synthesis is upregulated in mitral valves subjected to altered stress. ASAIO J 43:181–186.

185. Chaput M, Handschumacher MD, Tournoux F, et al. (2008) Mitral leaflet adaptation to ventricular remodeling: occurrence and adequacy in patients with functional mitral regurgitation. Circulation 118:793–794.

186. Kunzelman K, Quick D, Cochran R (1998) Altered collagen concentration in mitral valve leaflets: biochemical and finite element analysis. Ann Thorac Surg 66:S198–205.

187. Goldsmith LT, Weiss G (2009) Relaxin in human pregnancy. Ann N Y Acad Sci 1160:130–135.

188. Bani D (1997) Relaxin: a pleiotropic hormone. Gen Pharmacol 28:13–22.

189. Samuel CS, Parry LJ, Summers RJ (2003) Physiological or pathological--a role for relaxin in the cardiovascular system? Curr Opin Pharmacol 3:152–158.

190. Du X-J, Bathgate RAD, Samuel CS, et al. (2010) Cardiovascular effects of relaxin: from basic science to clinical therapy. Nat Rev Cardiol 7:48–58.

191. Samuel CS (2005) Relaxin: antifibrotic properties and effects in models of disease. Clin Med Res 3:241–249.

192. Samuel CS, Du X-J, Bathgate RAD, Summers RJ (2006) “Relaxin” the stiffened heart and arteries: The therapeutic potential for relaxin in the treatment of cardiovascular disease. Pharmacol Ther 112:529–552.

193. Pinheiro MC, Moraes SG, Battlehner CN, et al. (2004) Histochemical and ultrastructural study of collagen fibers in mouse pubic symphysis during late pregnancy. Micron 35:685–693.

194. Sherwood OD (2004) Relaxin's physiological roles and other diverse actions. Endocr Rev 25:205–234.

195. Pepine CJ, Kerensky RA, Lambert CR, et al. (2006) Some thoughts on the vasculopathy of women with ischemic heart disease. J Am Coll Cardiol 47:S30–5.

196. Teichman SL, Unemori E, Teerlink JR, et al. (2010) Relaxin: review of biology and potential role in treating heart failure. Curr Heart Fail Rep 7:75–82.

197. Grande-Allen KJ, Barber JE, Klatka KM, et al. (2005) Mitral valve stiffening in end-stage heart failure: evidence of an organic contribution to functional mitral regurgitation. J Thorac Cardiovasc Surg 130:783–790.

198. Gerdes AM, Capasso JM (1995) Structural remodeling and mechanical dysfunction of cardiac myocytes in heart failure. J. Mol. Cell. Cardiol.

199. Lester W, Rosenthal A, Granton B, Gotlieb AI (1988) Porcine mitral valve interstitial cells in culture. Lab Invest 59:710–719.

200. Rabkin-Aikawa E, Farber M, Aikawa M, Schoen FJ (2004) Dynamic and reversible changes of interstitial cell phenotype during remodeling of cardiac valves. J Heart Valve Dis 13:841–847.

201. Smith S, Taylor PM, Chester AH, et al. (2007) Force generation of different human cardiac valve interstitial cells: relevance to individual valve function and tissue engineering. J Heart Valve Dis 16:440–446.

202. Balachandran K, Sucosky P, Jo H, Yoganathan AP (2010) Elevated cyclic stretch induces aortic valve calcification in a bone morphogenic protein-dependent manner. Am J Pathol 177:49–57.

203. Desmoulière A (1993) Transforming growth factor-beta 1 induces alpha-smooth muscle actin expression in granulation tissue myofibroblasts and in quiescent and growing cultured fibroblasts. J Cell Biol 122:103–111.

204. Taylor PM, Allen SP, Yacoub MH (2000) Phenotypic and functional characterization of interstitial cells from human heart valves, pericardium and skin. J Heart Valve Dis 9:150–158.

205. Wang J, Zohar R, McCulloch C (2006) Multiple roles of alpha-smooth muscle actin in mechanotransduction. Exp Cell Res 312:205–214.

206. Desmoulière A, Redard M, Darby I, Gabbiani G (1995) Apoptosis mediates the decrease in cellularity during the transition between granulation tissue and scar. Am J Pathol 146:56–66.

207. Schmitt-Gräff A, Desmoulière A, Gabbiani G (1994) Heterogeneity of myofibroblast phenotypic features: an example of fibroblastic cell plasticity. Virchows Arch 425:3–24.

208. (2011) Global status report on noncommunicable diseases 2010. World Health Organization

209. (2006) Statistics Canada 2006. CANSIM Table 102-0561 - Leading causes of death, total population, by age group and sex.

210. Lis Y, Burleigh MC, Parker DJ, et al. (1987) Biochemical characterization of individual normal, floppy and rheumatic human mitral valves. Biochem J 244:597–603.

211. Kunzelman KS, Reimink MS, Cochran RP (1997) Annular dilatation increases stress in the mitral valve and delays coaptation: a finite element computer model. Cardiovasc Surg 5:427–434.

212. Sattar N, Greer IA (2002) Pregnancy complications and maternal cardiovascular risk: opportunities for intervention and screening? 325:157–160.

213. Ness RB, Harris T, Cobb J, et al. (1993) Number of pregnancies and the subsequent risk of cardiovascular disease. N Engl J Med 328:1528–1533.

214. Ness RB, Schotland HM, Flegal KM, Shofer FS (1994) Reproductive history and coronary heart disease risk in women. Epidemiol Rev 16:298–314.

215. Lawlor D, Emberson J, Ebrahim S, et al. (2003) Is the Association Between Parity and Coronary Heart Disease Due to Biological Effects of Pregnancy or Adverse Lifestyle Risk Factors Associated With Child-Rearing?: Findings From the British Women's Heart and Health Study and the British Regional Heart Study. Circulation 107:1260–1264.

216. Sacks MS, He Z, Baijens L, et al. (2002) Surface strains in the anterior leaflet of the functioning mitral valve. Annals of Biomedical Engineering 30:1281–1290.

217. Junker A, Thayssen P, Nielsen B, Andersen PE (1993) The hemodynamic and prognostic significance of echo-Doppler-proven mitral regurgitation in patients with dilated cardiomyopathy. Cardiology 83:14–20.

218. Silbiger JJ, Bazaz R (2009) Contemporary insights into the functional anatomy of the mitral valve. Am Heart J 158:887–895.

219. Dal-Bianco JP, Aikawa E, Bischoff J, et al. (2009) Active adaptation of the tethered mitral valve: insights into a compensatory mechanism for functional mitral regurgitation. Circulation 120:334–342.

220. Robson SC, Dunlop W, Moore M, Hunter S (1987) Combined Doppler and echocardiographic measurement of cardiac output: theory and application in pregnancy. British journal of obstetrics and gynaecology 94:1014–1027.

221. Grande KJ, Cochran RP, Reinhall PG, Kunzelman KS (2000) Mechanisms of aortic valve incompetence: finite element modeling of aortic root dilatation. Ann Thorac Surg 69:1851–1857.

222. Robson SC, Richley D, Boys RJ, Hunter S (1992) Incidence of Doppler regurgitant flow velocities during normal pregnancy. Eur Heart J 13:84–87.

223. Gorman JH, Gorman RC, Jackson BM, et al. (1997) Distortions of the mitral valve in acute ischemic mitral regurgitation. Ann Thorac Surg 64:1026–1031.

224. Muresian H (2009) The clinical anatomy of the mitral valve. Clin Anat 22:85–98.

225. Reynolds M (1953) Measurement of bovine plasma and blood volume during pregnancy and lactation. Am J Physiol 175:118–122.

226. Scheaffer A, Caton J, BAUER M, Reynolds L (2001) Influence of pregnancy on body weight, ruminal characteristics, and visceral organ mass in beef heifers. J Anim Sci 79:2481–2490.

227. Evans HE, Sack WO (1973) Prenatal development of domestic and laboratory mammals: growth curves, external features and selected references. Zentralbl Veterinarmed C 2:11–45.

228. Kunzelman KS, Cochran RP, Chuong C, et al. (1993) Finite element analysis of the mitral valve. J Heart Valve Dis 2:326–340.

229. Waldman SD, Lee JM (2005) Effect of sample geometry on the apparent biaxial mechanical behaviour of planar connective tissues. Biomaterials 26:7504–7513.

230. Grashow JS, Yoganathan AP, Sacks MS (2006) Biaixal stress-stretch behavior of the mitral valve anterior leaflet at physiologic strain rates. Ann Biomed Eng 34:315–325.

231. Robins SP, Bailey AJ (1973) Relative stabilities of the intermediate reducible crosslinks present in collagen fibres. FEBS Lett 33:167–174.

232. Le Lous M, Allain JC, Cohen-Solal L, Maroteaux P (1982) The rate of collagen maturation in rat and human skin. Connect Tissue Res 9:253–262.

233. Liao J, Yang L, Grashow J, Sacks MS (2007) The relation between collagen fibril kinematics and mechanical properties in the mitral valve anterior leaflet. Journal of biomechanical engineering 129:78–87.

234. He Z, Sacks MS, Baijens L, et al. (2003) Effects of papillary muscle position on in-vitro dynamic strain on the porcine mitral valve. J Heart Valve Dis 12:488–494.

235. Chen L, McCulloch AD, May-Newman K (2004) Nonhomogeneous deformation in the anterior leaflet of the mitral valve. Annals of Biomedical Engineering 32:1599–1606.

236. Amini R, Eckert CE, Koomalsingh K, et al. (2012) On the in vivo deformation of the mitral valve anterior leaflet: effects of annular geometry and referential configuration. Annals of Biomedical Engineering 40:1455–1467.

237. Timek TA, Lai DT, Dagum P, et al. (2006) Mitral leaflet remodeling in dilated cardiomyopathy. Circulation 114:I518–23.

238. Sacks MS, Enomoto Y, Graybill JR, et al. (2006) In-vivo dynamic deformation of the mitral valve anterior leaflet. Ann Thorac Surg 82:1369–1377.

239. Ben Driss A, Benessiano J, Poitevin P, et al. (1997) Arterial expansive remodeling induced by high flow rates. Am J Physiol 272:H851–H858.

240. Langille BL (1996) Arterial remodeling: relation to hemodynamics. Can J Physiol Pharmacol 74:834–841.

241. Ritchie J, Warnock JN, Yoganathan AP (2005) Structural characterization of the chordae tendineae in native porcine mitral valves. Ann Thorac Surg 80:189–197.

242. Howlett JG, McKelvie RS, Costigan J, et al. (2010) The 2010 Canadian Cardiovascular Society guidelines for the diagnosis and management of heart failure update: Heart failure in ethnic minority populations, heart failure and pregnancy, disease management, and quality improvement/assurance programs. Can J Cardiol 26:185–202.

243. Gillam LD (2008) Is It Time to Update the Definition of Functional Mitral Regurgitation?: Structural Changes in the Mitral Leaflets With Left Ventricular Dysfunction. Circulation 118:797–799.

244. Aldous IG, Lee JM, Wells SM (2010) Differential changes in the molecular stability of collagen from the pulmonary and aortic valves during the fetal-to-neonatal transition. Annals of Biomedical Engineering 38:3000–3009.

245. David Merryman W, Shadow Huang H-Y, Schoen FJ, Sacks MS (2006) The effects of cellular contraction on aortic valve leaflet flexural stiffness. J Biomech 39:88–96.

246. Lacroix M-C, Guibourdenche J, Frendo J-L, et al. (2002) Placental growth hormones. 19:73–79.

247. Bonventre MV (1974) Sweet peas, copper, pregnancy, and pills: effects on aorta. N Y State J Med 74:633–637.

248. Wells SM, Pierlot CM, Moeller AD (2012) Physiological remodeling of the mitral valve during pregnancy. AJP: Heart and Circulatory Physiology 303:H878–92.

249. Sacks MS (2006) Biomechanics of engineered heart valve tissues. Conference proceedings : Annual International Conference of the IEEE Engineering in Medicine and Biology Society IEEE Engineering in Medicine and Biology Society Conference 1:853–854.

250. Kindahl H, Kornmatitsuk B, Gustafsson H (2004) The cow in endocrine focus before and after calving. Reprod Domest Anim 39:217–221.

251. Longo LD, (null) (1983) Maternal blood volume and cardiac output during pregnancy: a hypothesis of endocrinologic control. Am J Physiol 245:R720–9.

252. Estergreen VL, Frost OL, Gomes WR, et al. (1967) Effect of ovariectomy on pregnancy maintenance and parturition in dairy cows. J Dairy Sci 50:1293–1295.

253. Bergsjø P, Denman DW, Hoffman HJ, Meirik O (1990) Duration of human singleton pregnancy. A population-based study. SOBS 69:197–207.

254. Wells SM, Sellaro T, Sacks MS (2005) Cyclic loading response of bioprosthetic heart valves: effects of fixation stress state on the collagen fiber architecture. Biomaterials 26:2611–2619.

255. Sacks M, Smith D, Hiester E (1997) A small angle light scattering device for planar connective tissue microstructural analysis. Ann Biomed Eng 25:678–89.

256. Sacks MS (2004) Small-angle light scattering methods for soft connective tissue structural analysis. In: Wnek GE, Bowlin GL (eds) Encyclopedia of Biomaterials and Biomedical Engineering, Second Edition. Informa Healthcare USA, Inc, pp 2450–2463

257. Joyce EM, Liao J, Schoen FJ, et al. (2009) Functional collagen fiber architecture of the pulmonary heart valve cusp. Ann Thorac Surg 87:1240–1249.

258. Kasyanov V, Moreno-Rodriguez RA, Kalejs M, et al. (2013) Age-related analysis of structural, biochemical and mechanical properties of the porcine mitral heart valve leaflets. Connect Tissue Res 54:394–402.

259. Gilbert TW, Sacks MS, Grashow JS, et al. (2006) Fiber kinematics of small intestinal submucosa under biaxial and uniaxial stretch. J Biomech Eng 128:890–898.

260. Thevenaz P, Unser M (2007) User-friendly semiautomated assembly of accurate image mosaics in microscopy. Microscopy Research and Technique vol. 7:135–146.

261. Thevenaz P, Ruttimann UE, Unser M (1998) A pyramid approach to subpixel registration based on intensity. Vol 7:27–41.

262. Woessner JF (1984) Determination of hydroxyproline in connective tissues. The methodology of connective tissue research 23:227–234.

263. Keeley FW, Morin JD, Vesely S (1984) Characterization of collagen from normal human sclera. Exp Eye Res 39:533–542.

264. Cochran RP, Kunzelman KS, Chuong CJ, et al. (1991) Nondestructive analysis of mitral valve collagen fiber orientation. ASAIO Trans 37:M447–8.

265. Sacks M, Schoen F (2002) Collagen fiber disruption occurs independent of calcification in clinically explanted bioprosthetic heart valves. J Biomed Mater Res 62:359–371.

266. Hadian M, Corcoran BM, Han RI, et al. (2007) Collagen organization in canine myxomatous mitral valve disease: an x-ray diffraction study. Biophys J 93:2472–2476.

267. Gould RA, Sinha R, Aziz H, et al. (2012) Multi-scale biomechanical remodeling in aging and genetic mutant murine mitral valve leaflets: insights into Marfan syndrome. PLoS One 7:e44639.

268. Fulchiero GJ, Wells SM, Sacks MS (2002) Alterations in collagen fiber crimp morphology with accelerated cyclic loading and transvalvular pressure fixation in porcine aortic valves. In: Proceedings of the Second Joint EMBS/BMES Conference. Houston, TX, USA, pp 1248–1249

269. Hilbert SL, Barrick MK, Ferrans VJ (1990) Porcine aortic valve bioprostheses: a morphologic comparison of the effects of fixation pressure. J Biomed Mater Res 24:773–787.

270. Hilbert SL, Sword LC, Batchelder KF, et al. (1996) Simultaneous assessment of bioprosthetic heart valve biomechanical properties and collagen crimp length. J Biomed Mater Res 31:503–509.

271. Liao J, Vesely I (2003) A structural basis for the size-related mechanical properties of mitral valve chordae tendineae. Journal of biomechanics 36:1125–1133.

272. Sacks MSM (2003) Incorporation of experimentally-derived fiber orientation into a structural constitutive model for planar collagenous tissues. J Biomech Eng 125:280–287.

273. Sun W, (null), Fulchiero G, et al. (2004) Response of heterograft heart valve biomaterials to moderate cyclic loading. Journal of biomedical materials research Part A 69A:658–669.

274. Langdon SE, Chernecky R, Pereira CA, et al. (1999) Biaxial mechanical/structural effects of equibiaxial strain during crosslinking of bovine pericardial xenograft materials. Biomaterials 20:137–153.

275. Hilbert SL, Ferrans VJ, Swanson WM (1986) Optical methods for the nondestructive evaluation of collagen morphology in bioprosthetic heart valves. J Biomed Mater Res 20:1411–1421.

276. Sahasakul Y, Edwards WD, Naessens JM, Tajik AJ (1988) Age-related changes in aortic and mitral valve thickness: implications for two-dimensional echocardiography based on an autopsy study of 200 normal human hearts. Am J Cardiol 62:424–430.

277. Kunzelman KS, Cochran RP, Murphree SS, et al. (1993) Differential collagen distribution in the mitral valve and its influence on biomechanical behaviour. J Heart Valve Dis 2:236–244.

278. Grande-Allen K (2004) Fibrotic vs. myxomatous remodeling of mitral valves. Conference proceedings : Annual International Conference of the IEEE Engineering in Medicine and Biology Society IEEE Engineering in Medicine and Biology Society Conference 5:3737–3740.

279. Cole WG, Chan D, Hickey AJ, Wilcken DE (1984) Collagen composition of normal and myxomatous human mitral heart valves. Biochem J 219:451–460.

280. Driessen NJB, Peters GWM, Huyghe JM, et al. (2003) Remodelling of continuously distributed collagen fibres in soft connective tissues. J Biomech 36:1151–1158.

281. Driessen NJ, Boerboom RA, Huyghe JM, et al. (2003) Computational analyses of mechanically induced collagen fiber remodeling in the aortic heart valve. J Biomech Eng 125:549–557.

282. McCarthy KP, Ring L, Rana BS (2010) Anatomy of the mitral valve: understanding the mitral valve complex in mitral regurgitation. Eur J Echocardiogr 11:i3–9.

283. Grande-Allen KJ, Cochran RP, Reinhall PG, Kunzelman KS (2001) Mechanisms of aortic valve incompetence: Finite-element modeling of Marfan syndrome. J Thorac Cardiovasc Surg 122:946–954.

284. Cannon DJ, Davison PF (1977) Aging, and crosslinking in mammlian collagen. Exp Aging Res 3:87–105.

285. Sims TJ, Avery NC, Bailey AJ (2000) Quantitative determination of collagen crosslinks. Methods Mol Biol 139:11–26.

286. Broom ND (1977) The stress/strain and fatigue behaviour of glutaraldehyde preserved heart-valve tissue. Journal of biomechanics 10:707–724.

287. Billiar KL, Sacks MS (1997) A method to quantify the fiber kinematics of planar tissues under biaxial stretch. Journal of biomechanics 30:753–756.

288. Clark RE, Finke EH (1974) Scanning and light microscopy of human aortic leaflets in stressed and relaxed states. J Thorac Cardiovasc Surg 67:792–804.

289. Sacks MS, Chuong CJ, More R (1994) Collagen fiber architecture of bovine pericardium. ASAIO J 40:M632–7.

290. Driessen NJB, Cox MAJ, Bouten CVC, Baaijens FPT (2008) Remodelling of the angular collagen fiber distribution in cardiovascular tissues. Biomechanics and modeling in mechanobiology 7:93–103.

291. Driessen NJB, Bouten CVC, Baaijens FPT (2005) Improved prediction of the collagen fiber architecture in the aortic heart valve. J Biomech Eng 127:329–336.

292. Chen HH, Schrier RW (2006) Pathophysiology of Volume Overload in Acute Heart Failure Syndromes. The American Journal of Medicine 119:S11–S16.

293. Pierlot CM, Lee JM, Amini R, et al. Pregnancy-Induced Remodeling of Collagen Architecture and Content in the Mitral Valve. Annals of Biomedical Engineering (in press)

294. Le Lous M, Cohen-Solal L, Allain JC, et al. (1985) Age related evolution of stable collagen reticulation in human skin. Connect Tissue Res 13:145–155.

295. Stella JA, Liao J, Sacks MS (2007) Time-dependent biaxial mechanical behavior of the aortic heart valve leaflet. J Biomech 40:3169–3177.

296. Billiar KL, Sacks MS (2000) Biaxial mechanical properties of the natural and glutaraldehyde treated aortic valve cusp--Part I: Experimental results. J Biomech Eng 122:23–30.

297. Zhao L, Samuel CS, Tregear GW, et al. (2000) Collagen studies in late pregnant relaxin null mice. Biol Reprod 63:697–703.

298. Fung YC (1993) Biomechanics: Mechanical Properties of Living Tissues, 2nd ed. Spring-Verlag, New York, NY, P

299. Grashow JS, Sacks MS, Liao J, Yoganathan AP (2006) Planar biaxial creep and stress relaxation of the mitral valve anterior leaflet. Ann Biomed Eng 34:1509–1518.

300. Sacks MS, David Merryman W, Schmidt DE (2009) On the biomechanics of heart valve function. J Biomech 42:1804–1824.

301. Anssari-Benam A, Bader DL, Screen HRC (2011) Anisotropic time-dependant behaviour of the aortic valve. Journal of the Mechanical Behavior of Biomedical Materials 4:1603–1610.

302. Kao KY, Hitt WE, Leslie JG (1976) The intermolecular cross-links in uterine collagens of guinea pig, pig, cow, and human beings. Proc Soc Exp Biol Med 151:385–389.

303. Robins SP (1982) Analysis of the crosslinking components in collagen and elastin. Methods Biochem Anal 28:329–379.

304. Knott L, Bailey AJ (1998) Collagen cross-links in mineralizing tissues: a review of their chemistry, function, and clinical relevance. Bone 22:181–187.

305. Horgan DJ, King NL, Kurth LB, Kuypers R (1990) Collagen crosslinks and their relationship to the thermal properties of calf tendons. Arch Biochem Biophys 281:21–26.

306. Allain JC, Le Lous M, Bazin S, et al. (1978) Isometric tension developed during heating of collagenous tissues. Relationships with collagen cross-linking. Biochim Biophys Acta 533:147–155.

307. Thomas PD, Cotter TA, Li X, et al. (2001) Exercise training attenuates aging-associated increases in collagen and collagen crosslinking of the left but not the right ventricle in the rat. European journal of applied physiology 85:164–169.

308. Lerman TT, Weintraub AY, Sheiner E (2013) Pregnancy outcomes in women with mitral valve prolapse and mitral valve regurgitation. Arch Gynecol Obstet 288:287–291.

309. Traill TA (2012) Valvular heart disease and pregnancy. Cardiol Clin 30:369–381.

310. Roeder HA, Kuller JA, Barker PCA, James AH (2011) Maternal valvular heart disease in pregnancy. Obstetrical & gynecological survey 66:561–571.

311. Reimold SC, Rutherford JD (2003) Clinical practice. Valvular heart disease in pregnancy. N Engl J Med 349:52–59.

312. Samuel C, Coghlan J, Bateman J (1998) Effects of relaxin, pregnancy and parturition on collagen metabolism in the rat pubic symphysis. J Endocrinol 159:117–125.

313. Pierlot CM, Moeller AD, Michael Lee J, Wells SM Biaxial Creep Resistance and Structural Remodeling of the Aortic and Mitral Valves in Pregnancy. ABME (submitted June 2014)

314. Snarr BS, Kern CB, Wessels A (2008) Origin and fate of cardiac mesenchyme. Dev Dyn 237:2804–2819.

315. de Lange F, Moorman A, Anderson R, et al. (2004) Lineage and morphogenetic analysis of the cardiac valves. Circ Res 95:645–654.

316. Hinton RB, Yutzey KE (2011) Heart valve structure and function in development and disease. Annu Rev Physiol 73:29–46.

317. Ramos-Vara JA (2005) Technical aspects of immunohistochemistry. Vet Pathol 42:405–426.

318. Taylor CR, Shi SR, Chen C, et al. (1996) Comparative study of antigen retrieval heating methods: microwave, microwave and pressure cooker, autoclave, and steamer. Biotech Histochem 71:263–270.

319. Pileri SA, Roncador G, Ceccarelli C, et al. (1997) Antigen retrieval techniques in immunohistochemistry: comparison of different methods. J Pathol 183:116–123.

320. Gogoladze G, Dellis SL, Donnino R, et al. (2010) Analysis of the mitral coaptation zone in normal and functional regurgitant valves. Ann Thorac Surg 89:1158–1161.

321. Sohmer B, Hudson C, Atherstone J, et al. (2013) Measuring aortic valve coaptation surface area using three-dimensional transesophageal echocardiography. Can J Anaesth 60:24–31.

322. Saito K, Okura H, Watanabe N, et al. (2012) Influence of chronic tethering of the mitral valve on mitral leaflet size and coaptation in functional mitral regurgitation. JACC Cardiovasc Imaging 5:337–345.

323. Otto CM, Bonow RO (2009) Valvular Heart Disease: A Companion to Braunwald's Heart Disease. Elsevier Health Sciences

324. Solymar L, Südow G, Holmgren D (2000) Increase in size of the pulmonary autograft after the Ross operation in children: growth or dilation? J Thorac Cardiovasc Surg 119:4–9.

325. Schoof PH, Cromme-Dijkhuis AH, Bogers JJ, et al. (1994) Aortic root replacement with pulmonary autograft in children. J Thorac Cardiovasc Surg 107:367–373.

326. Elkins RC, Knott-Craig CJ, Ward KE, et al. (1994) Pulmonary autograft in children: realized growth potential. Ann Thorac Surg 57:1387–93– discussion 1393–4.

327. Werb Z, Banda MJ, McKerrow JH, Sandhaus RA (1982) Elastases and Elastin Degradation. J Invest Dermatol 79:154s–159s.

328. Shapiro SD, Endicott SK, Province MA, et al. (1991) Marked longevity of human lung parenchymal elastic fibers deduced from prevalence of D-aspartate and nuclear weapons-related radiocarbon. J Clin Invest 87:1828–1834.

329. Langille BL (1993) Remodeling of developing and mature arteries: endothelium, smooth muscle, and matrix. J Cardiovasc Pharmacol 21 Suppl 1:S11–7.

330. Starcher B, Percival S (1985) Elastin turnover in the rat uterus. Connect Tissue Res 13:207–215.

331. Woessner JF, Brewer TH (1963) Formation and breakdown of collagen and elastin in the human uterus during pregnancy and post-partum involution. Biochem J 89:75–82.

332. Helbig G, Krzemień S (2004) Clinical significance of elastin turnover--focus on diseases affecting elastic fibres. Wiad Lek 57:360–363.

333. Konova E, Aleksovska T, Atanasova M, et al. (2009) Anti-elastin antibodies and elastin turnover in normal pregnancy and recurrent pregnancy loss. Am J Reprod Immunol 61:167–174.

334. Brennan-Pierce, Pierlot CM, Howie AP, et al. (2012) Pregnancy-induced cardiovascular remodeling is not reversed. Proceedings of 2012 BMES Annual Fall Meeting Biomedical Engineering Society Atlanta, Georgia, October 24-27, 2012 1–1.

335. Visse R, Nagase H (2003) Matrix metalloproteinases and tissue inhibitors of metalloproteinases: structure, function, and biochemistry. Circ Res 92:827–839.

336. Mecham RP, Broekelmann TJ, Fliszar CJ, et al. (1997) Elastin degradation by matrix metalloproteinases. Cleavage site specificity and mechanisms of elastolysis. J Biol Chem 272:18071–18076.

337. Edep ME, Shirani J, Wolf P, Brown DL (2000) Matrix metalloproteinase expression in nonrheumatic aortic stenosis. Cardiovasc Pathol 9:281–286.

338. Dreger SA, (null), Taylor PM, et al. (2002) Profile and localization of matrix metalloproteinases (MMPs) and their tissue inhibitors (TIMPs) in human heart valves. J Heart Valve Dis 11:875–80– discussion 880.

339. Obayashi K, Miyagawa-Tomita S, Matsumoto H, et al. (2011) Effects of transforming growth factor-β3 and matrix metalloproteinase-3 on the pathogenesis of chronic mitral valvular disease in dogs. Am J Vet Res 72:194–202.

340. Simionescu A, Simionescu D, Deac R (1996) Biochemical pathways of tissue degeneration in bioprosthetic cardiac valves. The role of matrix metalloproteinases. ASAIO J 42:M561–7.

341. Scott M, Vesely I (1995) Aortic valve cusp microstructure: The role of elastin. Ann Thorac Surg 60:S391–S394.

342. Meuris B, Flameng W (2004) Antimineralization Treatment. Encyclopedia of Biomaterials and Biomedical Engineering 71–83.

343. Ivan Vesely AB (2005) The Effect of Glycosaminoglycans and Hydration on the Viscoelastic Properties of Aortic Valve Cusps. 3:2979–2980.

344. Doane J, Lee JM, Wells SM (2013) Structural-Mechanical Changes in the Pericardium During Pregnancy. Cardiovascular Engineering and Technology 4:39-52.

345. Calhoon JH, Bolton JW (1995) Ross/Konno procedure for critical aortic stenosis in infancy. Ann Thorac Surg 60:S597–9.

346. Sievers HH, Leyh R, Loose R, et al. (1993) Time course of dimension and function of the autologous pulmonary root in the aortic position. J Thorac Cardiovasc Surg 105:775–780.

347. Rabkin E, Hoerstrup SP, Aikawa M, et al. (2002) Evolution of cell phenotype and extracellular matrix in tissue-engineered heart valves during in-vitro maturation and in-vivo remodeling. J Heart Valve Dis 11:308–314.

348. Ranganathan N, Lam JH, Wigle ED, Silver MD (1970) Morphology of the human mitral valve. II. The value leaflets. Circulation 41:459–467.

349. Balachandran K, Sucosky P, Jo H, Yoganathan AP (2009) Elevated cyclic stretch alters matrix remodeling in aortic valve cusps: implications for degenerative aortic valve disease. Am J Physiol Heart Circ Physiol 296:H756–64.

350. Hisaw FL (1926) Experimental relaxation of the pubic ligament of the guinea pig. Proc Soc Exp Biol Med 23:661–663.

351. Goldsmith LT, Weiss G, Steinetz BG (1995) Relaxin and its role in pregnancy. Endocrinol Metab Clin North Am 24:171–186.

352. Hsu SY, Nakabayashi K, Nishi S, et al. (2002) Activation of orphan receptors by the hormone relaxin. Science 295:671–674.

353. Bathgate RAD, Samuel CS, Burazin TCD, et al. (2003) Relaxin: new peptides, receptors and novel actions. Trends Endocrinol Metab 14:207–213.

354. Hudson P, Haley J, John M, et al. (1983) Structure of a genomic clone encoding biologically active human relaxin. Nature 301:628–631.

355. Hansell DJ, Bryant-Greenwood GD, Greenwood FC (1991) Expression of the human relaxin H1 gene in the decidua, trophoblast, and prostate. J Clin Endocrinol Metab 72:899–904.

356. Hudson P, John M, Crawford R, et al. (1984) Relaxin gene expression in human ovaries and the predicted structure of a human preprorelaxin by analysis of cDNA clones. EMBO J 3:2333–2339.

357. Bogic LV, Mandel M, Bryant-Greenwood GD (1995) Relaxin gene expression in human reproductive tissues by in situ hybridization. J Clin Endocrinol Metab 80:130–137.

358. Sherwood OD, Downing SJ, Guico-Lamm ML, et al. (1993) The physiological effects of relaxin during pregnancy: studies in rats and pigs. Oxf Rev Reprod Biol 15:143–189.

359. Fields MJ, Fields PA, Castro-Hernandez A, Larkin LH (1980) Evidence for relaxin in corpora lutea of late pregnant cows. Endocrinology 107:869–876.

360. Van Der Westhuizen ET, Summers RJ, Halls ML, et al. (2007) Relaxin receptors--new drug targets for multiple disease states. Curr Drug Targets 8:91–104.

361. Golos TG, Weyhenmeyer JA, Sherwood OD (1984) Immunocytochemical localization of relaxin in the ovaries of pregnant rats. Biol Reprod 30:257–261.

362. Anderson ML, Long JA (1978) Localization of relaxin in the pregnant rat. Bioassay of tissue extracts and cell fractionation studies. Biol Reprod 18:110–117.

363. Anderson ML, Long JA, Hayashida T (1975) Immunofluorescence studies on the localization of relaxin in the corpus luteum of the pregnant rat. Biol Reprod 13:499–504.

364. Dschietzig T, Stangl K (2003) Relaxin: a pregnancy hormone as central player of body fluid and circulation homeostasis. Cell Mol Life Sci 60:688–700.

365. Tan YY, Wade JD, Tregear GW, Summers RJ (1999) Quantitative autoradiographic studies of relaxin binding in rat atria, uterus and cerebral cortex: characterization and effects of oestrogen treatment. Br J Pharmacol 127:91–98.

366. Dschietzig T, Richter C, Bartsch C, et al. (2001) The pregnancy hormone relaxin is a player in human heart failure. FASEB J 15:2187–2195.

367. Keyes LE, Moore LG, Walchak SJ, Dempsey EC (1996) Pregnancy-stimulated growth of vascular smooth muscle cells: importance of protein kinase C-dependent synergy between estrogen and platelet-derived growth factor. J Cell Physiol 166:22–32.

368. Kim M, Park HJ, Seol JW, et al. (2013) VEGF-A regulated by progesterone governs uterine angiogenesis and vascular remodelling during pregnancy. EMBO Mol Med 5:1415–1430.

369. Habashi JP, Huso N, Bedja D, et al. (2012) A mechanism and treatment strategy for pregnancy-associated aortic dissection in Marfan syndrome. ASHG Annual Meeting

370. Kara RJ, Bolli P, Karakikes I, et al. (2012) Fetal Cells Traffic to Injured Maternal Myocardium and Undergo Cardiac Differentiation. Circ Res 110:82–93.

371. Fugazzola L, Cirello V, Beck-Peccoz P (2011) Fetal microchimerism as an explanation of disease. Nature Reviews Endocrinology

372. Lee ES, Bou-Gharios G, Seppanen E, et al. (2010) Fetal stem cell microchimerism: natural-born healers or killers? Molecular Human Reproduction 16:869–878.

373. Lapaire O, Holzgreve W, Oosterwijk JC, et al. (2007) Georg Schmorl on trophoblasts in the maternal circulation. Placenta 28:1–5.

374. Schmorl G (1893) Pathologisch-anatomische Untersuchungen über Puerperal-Eklampsie. Verlag Von FCW Vogel, Leipzig

375. Pritchard S, Bianchi DW (2012) Fetal cell microchimerism in the maternal heart: baby gives back. Circ Res 110:3–5.

376. Bianchi DW, Zickwolf GK, Weil GJ, et al. (1996) Male fetal progenitor cells persist in maternal blood for as long as 27 years postpartum. Proc Natl Acad Sci USA 93:705–708.

377. Fujiki Y, Johnson KL, Peter I, et al. (2009) Fetal cells in the pregnant mouse are diverse and express a variety of progenitor and differentiated cell markers. Biol Reprod 81:26–32.

378. Mehta NJ, Mehta RN, Khan IA (2001) Peripartum cardiomyopathy: clinical and therapeutic aspects. Angiology 52:759–762.

379. James PR (2004) A review of peripartum cardiomyopathy. International journal of clinical practice 58:363–365.

380. Felker GM, Thompson RE, Hare JM, et al. (2000) Underlying causes and long-term survival in patients with initially unexplained cardiomyopathy. N Engl J Med 342:1077–1084.

381. Burgeson RE, Nimni ME (1992) Collagen types. Molecular structure and tissue distribution. Clin Orthop Relat Res 250–272.

382. Akhtar S, Meek KM, James V (1999) Immunolocalization of elastin, collagen type I and type III, fibronectin, and vitronectin in extracellular matrix components of normal and myxomatous mitral heart valve chordae tendineae. Cardiovasc Pathol 8:203–211.

383. Gu X, Masters KS (2011) Role of the Rho pathway in regulating valvular interstitial cell phenotype and nodule formation. Am J Physiol Heart Circ Physiol 300:H448–H458.

384. Pufe T, Petersen WJ, Mentlein R, Tillmann BN (2005) The role of vasculature and angiogenesis for the pathogenesis of degenerative tendons disease. Scand J Med Sci Sports 15:211–222.

385. Kimura N, Shukunami C, Hakuno D, et al. (2008) Local tenomodulin absence, angiogenesis, and matrix metalloproteinase activation are associated with the rupture of the chordae tendineae cordis. Circulation 118:1737–1747.

386. Butany J, Gotlieb Al (2001) Native valvular heart disease. In: McManus BM (ed) Atlas of Cardiovascular Pathology for the Clinician, 2nd ed. Current Medicine Inc, Philadelphia, pp 201–215

387. Krishnan L (2008) Interaction of Angiogenic Microvessels with the Extracellular Matrix. ProQuest

388. Yoshioka J, Lee RT (2008) Vascularization as a potential enemy in valvular heart disease. Circulation 118:1694–1696.

389. Wells S, Veres S, Iles P, et al. (2011) Structure and thermal stability of heart valve chordae tendinae: association with physiological loading conditions. Proceedings of the 2011 Annual Biomedical Engineering Society 1–1.

390. Bashey RI, Torii S, Angrist A (1967) Age-related collagen and elastin content of human heart valves. J Gerontol 22:203–208.

391. Liao K, Seifter E, Hoffman D, et al. (1992) Bovine pericardium versus porcine aortic valve: comparison of tissue biological properties as prosthetic valves. Artificial organs 16:361–365.

392. Grande-Allen KJ (2004) Glycosaminoglycans and proteoglycans in normal mitral valve leaflets and chordae: association with regions of tensile and compressive loading. Glycobiology 14:621–633.

393. Balachandran K, Konduri S, Sucosky P, et al. (2006) An ex vivo study of the biological properties of porcine aortic valves in response to circumferential cyclic stretch. Ann Biomed Eng 34:1655–1665.

394. Schenke-Layland K, Vasilevski O, Opitz F, et al. (2003) Impact of decellularization of xenogeneic tissue on extracellular matrix integrity for tissue engineering of heart valves. J Struct Biol 143:201–208.

395. Schenke-Layland K, Stock UA, Nsair A, et al. (2009) Cardiomyopathy is associated with structural remodelling of heart valve extracellular matrix. Eur Heart J 30:2254–2265.

396. Murata K (1981) Acidic glycosaminoglycans in human heart valves. J Mol Cell Cardiol 13:281–292.

397. Dainese L, Polvani G, Barili F, et al. (2007) Fine characterization of mitral valve glycosaminoglycans and their modification with degenerative disease. Clin Chem Lab Med 45:361–366.

398. Simionescu DT, Lovekamp JJ, Vyavahare NR (2003) Glycosaminoglycan-degrading enzymes in porcine aortic heart valves: implications for bioprosthetic heart valve degeneration. J Heart Valve Dis 12:217–225.

399. Baig MM, Daicoff GR, Ayoub EM (1978) Comparative studies of the acid mucopolysaccharide composition of rheumatic and normal heart valves in man. Circ Res 42:271–275.

400. Torii S, Bashey RI, Nakao K (1965) Acid mucopolysaccharide composition of human-heart valve. Biochim Biophys Acta 101:285–291.

401. Eckert CE, Fan R, Mikulis B, et al. (2013) On the biomechanical role of glycosaminoglycans in the aortic heart valve leaflet. Acta Biomaterialia 9:4653–4660.

402. Vyavahare N, Ogle M, Schoen FJ, et al. (1999) Mechanisms of bioprosthetic heart valve failure: fatigue causes collagen denaturation and glycosaminoglycan loss. J Biomed Mater Res 46:44–50.

403. Lovekamp JJ, Simionescu DT, Mercuri JJ, et al. (2006) Stability and function of glycosaminoglycans in porcine bioprosthetic heart valves. Biomaterials 27:1507–1518.

404. Kanke Y, Mori Y, Bashey RI, Angrist AA (1971) Biochemical study of cardiac valvular tissue. Biosynthesis in vitro of hexosamine-containing substances in bovine heart valve. Biochem J 124:207–214.